Development of sterilisation strategies for decellularised peripheral nerve grafts

James Holland

Submitted in accordance with the requirements for the degree of Doctor of Philosophy

The University of Leeds

Faculty of Engineering

July 2019

The candidate confirms that the work submitted is his/her own. The candidate confirms that appropriate credit has been given within the thesis where reference has been made to the work of others.

Abstract

Peripheral nerve injuries represent one of the leading causes of disability globally; due to limitations of current therapies, there is a clear clinical need for a novel peripheral nerve graft . Decellularised porcine peripheral nerves may represent a suitable material; however, they would require terminal sterilisation prior to use.

The main aim of this study was to identify a sterilisation method which minimally impacted upon decellularised nerve extracellular matrix (ECM) structure, biochemical composition, biomechanical properties and biocompatibility. Peracetic acid (PAA) solution 0.1 % (v/v) caused disruption to the structure of the endoneurium and reductions in the intensity of antibody labelling for basement membrane components, particularly collagen IV (with increased severity after a 12 month storage period). Supercritical carbon dioxide ($SCCO_2$) treatment (with an additive solution containing 13.5 - 18.5 % [v/v] PAA and 4.5 - 6 % [v/v] H_2O_2) under standard conditions induced similar effects to the histioarchitecture and significant alterations to tensile mechanical properties; processing of the tissue whilst submerged in phosphate-buffered saline appeared to protect against such effects.

Treatment with gamma radiation (25 – 28 kGy) and E Beam (33 – 37 kGy) mediated retention of the decellularised nerve ECM structure, and changes to the localisation and intensity of labelling for basement membrane components were minimal compared with those observed following treatment with PAA solution or $SCCO_2$ under standard conditions. However, gamma radiation caused the stiffness of the nerves to increase.

Contact culture experiments did not yield evidence of cytotoxicity following any of the sterilisation methods; furthermore, the sterilised nerves did not induce any significant changes in the secretion of key cytokines by a murine macrophage cell line.

These data indicate that E Beam could be an optimal sterilisation method for use with the decellularised nerves, notwithstanding preliminary results indicating that $SCCO_2$ processing under submerged conditions may enable superior basement membrane preservation.

Contents

List of Figures and Tables

Figures

Tables

List of Abbreviations

ANOVA	Analysis of variance
BDNF	Brain-derived neurotrophic factor
BHK	Baby hamster kidney
CO_2	Carbon dioxide
CSPG	Chondroitin sulphate proteoglycan
DAMP	Damage-associated molecular pattern
DNA	Deoxyribonucleic acid
DSC	Differential scanning calorimetry
E Beam	Electron beam
ECM	Extracellular matrix
EDC	1-ethyl-3-(3-dimethylaminopropyl) carbodiimide hydrochloride
EDTA	Ethylenediaminetetraacetic acid
ELISA	Enzyme-linked immunosorbent assay
FBRI	Foreign body-related infection
FGF	Fibroblast growth factor
FTIR	Fourier transform infrared spectroscopy
GAG	Glycosaminoglycan
H & E	Haematoxylin and eosin
H_2O_2	Hydrogen peroxide
HCl	Hydrochloric acid
HIV	Human immunodeficiency virus
HMDI	Hexamethylene di-isocyanate
HRP	Horseradish peroxidase

IL	Interleukin
ISO	International Organisation for Standardisation
kGy	Kilogray
LIF	Leukaemia inhibitory factor
LPS	Lipopolysaccharide
MeV	Megaelectron volt
NaOH	Sodium hydroxide
NBF	Neutral buffered formalin
NGC	Nerve guidance conduit
NGF	Nerve growth factor
PAA	Peracetic acid
PBS	Phosphate buffered saline
PCL	Polycaprolactone
PGA	Polyglycolic acid
PGLA	Poly (lactic-co-glycolic acid)
RNA	Ribonucleic acid
SAL	Sterility assurance level
SASP	Small acid-soluble spore protein
$SCCO_2$	Supercritical carbon dioxide
SD	Standard deviation
SDS	Sodium dodecyl sulphate
SE	Standard error of the mean
SEM	Scanning electron microscopy
SIS	Small intestine submucosa
TEM	Transmission electron microscopy

TGF	Transforming growth factor
TMB	Tetramethylbenzidine
TNF	Tumour necrosis factor
UTS	Ultimate tensile strength

Acknowledgements

I'd like to thank my supervisors Dr Helen Berry, Dr Louise Jennings, Dr Paul Rooney, and Dr Stacy-Paul Wilshaw, for all of their help and guidance over the past four years. Without their input this project would not have been possible, and so for that I'm grateful.

I'd also like to thank the wider laboratory team and research group at iMBE. There are too many to name all individually, but I'd like to single out Gavin Day, Ray Kwan, Aaron Zammit-Wheeler and (in particular) Georgina Webster for the social support during the course of the project, which I believe is an undervalued element of life in academia. I would also like to thank Dr Daniel Thomas for being a font of all knowledge when confronted with any and all requests regarding the practical side of research, and for helping to put ideas into practice.

On a personal level, I would like to thank my fiancé Mary for supporting and encouraging me through the process (and for putting up with me during the most frustrating moments, which is arguably much more of a challenge!). I'd also like to thank my family and all of my friends for their invaluable support during the whole process – hopefully you'll be able to stop asking me that dreaded question "so WHEN exactly will you be finished with this PhD…"

1 Introduction

1.1 General Introduction

Peripheral nervous system injuries are associated with a high socioeconomic burden [11]. The annual cost of surgery and primary care for peripheral nerve injuries is approximately $7 billion in the USA; in the UK, the annual cost of treating of peripheral nerve injuries to the hand alone increased threefold between 1990 and 2000 to a figure in excess of £100 million [12]. Indirect costs, as a result of lost working hours, have been estimated as being up to sixfold greater than the direct treatment-related costs [13]. Peripheral nerve injuries are a major cause of chronic morbidity; using current repair methods, the duration of time between injury and restoration of function may be seven years [14, 15]. Full rehabilitation may never be achieved, negatively impacting the personal and professional activities of patients, and consequently their quality of life, over an extended period of time.

Peripheral nerve injuries typically follow a different pattern to those in some other tissue types, being more commonly the result of acute traumatic injury than chronic diseases related to processes of ageing and regeneration. The relatively young age of the patient demographic and the poor inherent regenerative capacity of the tissue mean that surgical interventions and the implantation of graft material are often required for the repair of all but the smallest defects [16].

Current therapies include the use of autografts and synthetic nerve guidance conduits. However, each method presents significant limitations when considering application across defects of varied size and location.

Processes mediating the removal of whole cells and other potentially immunogenic materials have been developed for use with allogeneic and xenogeneic materials [17]. Such “decellularisation” processes may enable these materials to be implanted and support regeneration in much the same manner as a conventional autograft or allografts.

Decellularised tissues have numerous advantages over conventional graft materials including minimal immunogenicity, the ability to supply large quantities

of graft material and the provision of an extracellular matrix scaffold with similar biomechanical, structural and biochemical properties to native tissue.

Previous research has led to the development of a decellularisation process for porcine peripheral nerves, which has shown initial promise as a material for supporting the growth of infiltrating Schwann cells and neurons [18]. Given these results, and the clear clinical need for novel peripheral nerve grafts, these decellularised nerves may represent a promising alternative material for use in the repair of peripheral nerve defects.

Xenogeneic tissues may harbour a pathogenic bioburden which could pose a serious infection risk to patients following implantation [19]. Therefore, in order for decellularised porcine nerves to be considered as a potential graft material, a suitable terminal sterilisation method must be identified. Such a method should enable international standards for bioburden reduction to be met whilst minimally affecting scaffold properties. The identification of such a method could enable further progression of decellularised nerve grafts towards clinical use.

1.2 Anatomy of the peripheral nervous system

The peripheral nervous system consists of individual nerves facilitating the passage of neural cell structures, known as axons, to the end target innervated organ/tissue [20]. Axons are extensions of neurons originating from cell bodies located close to the regions of the central nervous system (e.g. in dorsal root ganglia) [21]. Neurons function either to mediate the communication of sensory information (sensory/afferent nerve fibre) or facilitate control of a specific function through effectors (motor/efferent nerve fibre). The distribution of such sensors and effectors requires the network of the peripheral nervous system to be present throughout the body, up to and including the extremities of the limbs (Figure 1-1).

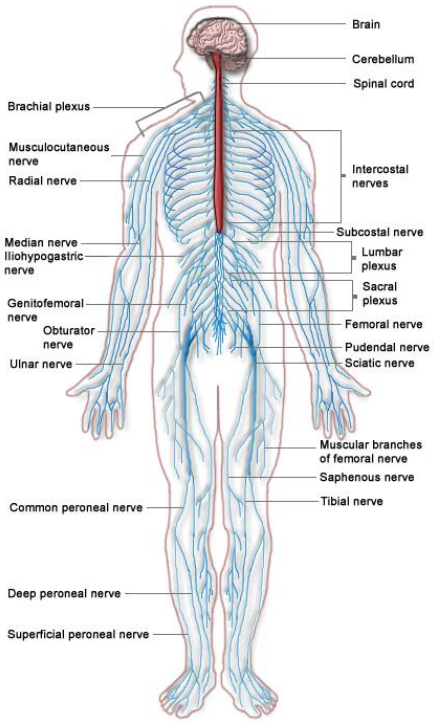

Figure 1-1 Peripheral nervous system

Overview of the major components of the peripheral nervous system in the human anatomy. The central nervous system (brain and spinal cord) is also shown. Adapted from original image (Wikimedia commons [22]).

1.2.1 Cells of the peripheral nervous system

1.2.1.1 Neurons

Neurons are the primary functional cell type of the peripheral nervous system, responsible for conducting sensory or function-activating (e.g. muscular contraction, hormone release) information in the form of electrical impulses [23]. Neurons consist of a cell body located within regions of the central nervous system (e.g. spinal cord), from which the long, thin axons project. The dimensions of peripheral axons vary greatly; the length of axons may be between 1 – 100 cm (or greater), and diameter can vary from 1 – 20 μm [24]. Electrical impulses initiated at the cell body propagate along axons by directional depolarisation of the plasma membrane. This is caused by a transmembrane influx of sodium ions, temporarily creating a positive membrane potential. This membrane potential “propagates” along the axon by the sequential opening of sodium channels stimulated by a local change in voltage becoming greater than the typical resting level (from approximately - 60

millivolts (mV) to approximately – 30 mV). Repolarisation is mediated by the release of potassium ions from the cell, allowing potassium-sodium exchange pumps to remove sodium from the cell and restore the original polarity.

1.2.1.2 Schwann cells

Schwann cells are a glial cell type present on/near the surface of axons, the primary function of which is to coat axons with multiple layers of plasma membrane containing a lipid-rich substance known as myelin [25]. This process is referred to as myelination. Myelin is a highly effective insulator due to a high lipid content, and therefore prohibits effective transmembrane ion exchange of the axon outside of regularly spaced myelin-free sites known as Nodes of Ranvier. Distance between nodes (internode distance) is dictated by the length of individual myelinating Schwann cells, and may vary from around 0.2 – 2 mm [26]. The large variance in internode length is thought to be due to factors such as the length and diameter of the nerve in question, growth and ageing [27]. Myelination maintains the speed of conductivity during propagating action potentials, due to the fact that full length depolarisation requires the opening of fewer ion channels and therefore can occur at a greater rate.

1.2.1.3 Accessory cells of the peripheral nervous system

Perineurial cells are a type of glial cell found within the perineurium and are epithelial-like in their characteristics, with a flattened squamous morphology [28]. Perineurial cells are thought to modulate mechanical stresses and enable homeostasis of the intraperineurial environment via the formation of intercellular tight junctions [29]. Perineurial cells are found attached to the concentric basal lamina layers of the perineurium.

Exterior to the basement membrane the endoneurium is populated by cells exhibiting fibroblastic properties, whose primary function is the production of extracellular matrix (ECM) components [30]. These cells may also have roles in regulating processes associated with the degradation of the nerve following injury (e.g. the infiltration and response of the immune system).

A population of resident macrophages exists within peripheral nerves [31]. Resident neural macrophages are particularly important in the early phase response to injury in peripheral nerve, mediating clearance of cellular and matrix debris resulting from the injury and stimulating the de-differentiation of

Schwann cells. Resident neural macrophages act synergistically with Schwann cells to recruit non-resident macrophages (as well as) from the circulation, through the secretion of cytokines including interleukins (IL)-1, IL-6 and tumour necrosis factor (TNF)-α [32].

The recruitment of a large population of activated macrophages ensures rapid clearance through phagocytosis of the debris resulting from myelin and axonal fragmentation [33]. Following the recruitment of immune cells (primarily macrophages) from circulation, the secretion of IL-10 is upregulated; this limits the duration of the pro-inflammatory response and so enables the process of tissue regeneration to begin (section 1.6) [34, 35]. The level of cytokine secretion and the specific cytokines secreted can have a profound impact upon the host response to an implanted graft material (e.g. decellularised tissue) [36, 37]. Investigation of the host response, in an *in vitro* and/or *in vivo* setting, is therefore a vital step in determining the likely biocompatibility of such materials.

1.2.2 Macroscopic structure of peripheral nerves

Peripheral nerves have a common macroscopic structure, there are three distinct regions: the endoneurium, the perineurium and the epineurium (Figure 1-2).

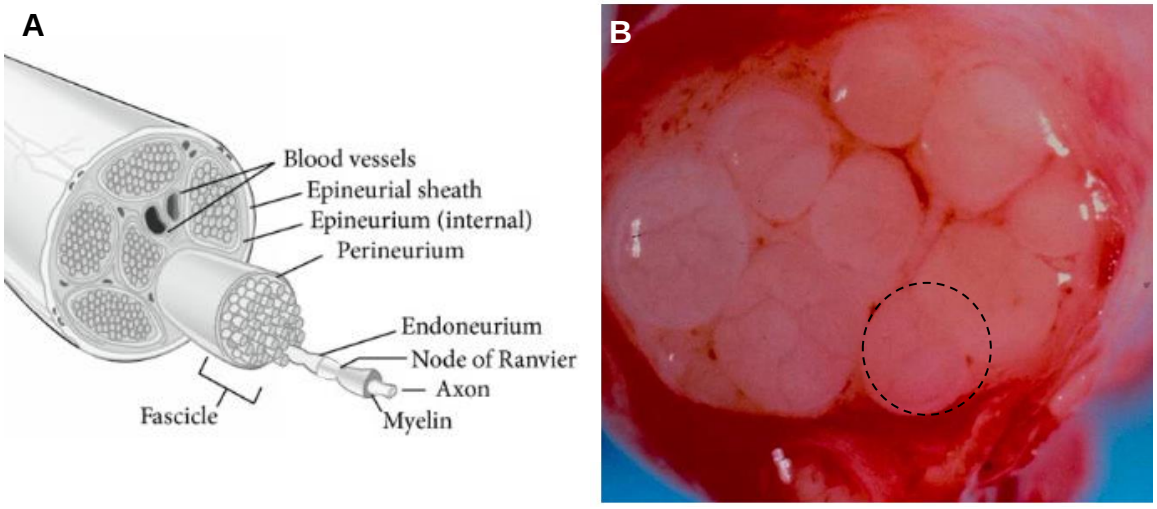

Figure 1-2 Structure and anatomy of peripheral nerve.

Details of peripheral nerve anatomy, including A) Depiction of peripheral nerve showing the concentric layering of the major ECM structures of the epineurium, perineurium and endoneurium, as well as other features including the vasculature (vasa nervorum) and in situ Schwann cells and axons; B) Cross sectional image of human peripheral nerve transected during surgical repair. Individual fascicle indicated by dashed circle. Adapted from Grinsell et al (2014) [2], Ray and Mackinnon (2010) [10].

1.2.2.1 Epineurium

The outermost layer of the nerve containing all endoneurial and perineurial structures, is the epineurium. The epineurium is a sheath-like structure composed primarily of type I and III collagens, and can be divided arbitrarily into the interfascicular epineurium and the outer epineurial sheath of the nerve [38]. There is a gradual rather than delineated transition between the two epineurial regions. In addition to collagenous ECM, adipose tissue is also present in the epineurium, located primarily within the interfascicular region [39]. The adipose tissue within the epineurium may have a crucial role in the regulation of lipid metabolism by Schwann cells located within the endoneurium.

The epineurium defines the nerve from the external environment, insulates it and facilitates the passage of the vasa nervorum [40]. The major vessels of the vasa nervorum are located in the epineurium, and branch to form the minor blood vessels which facilitate blood supply to the interior tissues of the nerve. The epineurium is a major contributor to the mechanical strength of the peripheral nerve tissue as a whole, a function aided by its high type I collagen content [8].

1.2.2.2 Perineurium

The perineurium is located superior to the endoneurium, containing groups of endoneurial tubes known collectively as a bundle or fascicle (Figure 1-2). The perineurium is a concentrically-layered lamellar matrix structure composed primarily of type I and II collagens . Each layer of the perineurium also contains a basal lamina (or basement membrane), which provides attachment sites for the perineurial cells. The primary components of the perinerurial basal lamina are type IV collagen, fibronectin, laminin, and heparan sulphate [41]. The interior structure of peripheral nerves is made up of multiple perineurial tubes connected by a highly-collagenous ECM-region known as the interstitial matrix (or internal epineurium) [42].

The function of the perineurium can be considered to be twofold; the provision of mechanical strength and the regulation and maintenance of the intrafascicular microenvironment [4]. The perineurium provides site-specific mechanical support and protection to the axons and Schwann cells contained within the endoneurial bundles, aiding in the prevention of injury through

mechanisms such as excessive compression. In addition to this, the perineurium also contributes significantly, along with the epineurium, to the determination of the tissue-scale biomechanical properties of peripheral nerve [43].

The perineurium is a crucial structure for the homeostatic regulation of the intrafascicular environment (including the regulation of pressure and concentration of soluble molecules and ions), and therefore ultimately the microenvironment of axons and Schwann cells within individual endoneurial tubules [44]. The perineurium provides a highly effective diffusion barrier, with transport regulated by intercellular tight junctions composed of proteins including as occludins and claudins (Figure 1-3) [4]. Passage of molecules and ions across the perineurium is thought to be mediated by specific trans-membrane transport proteins (e.g. glucose is transported via Glucose transporter-1) and vesicular transit [4].

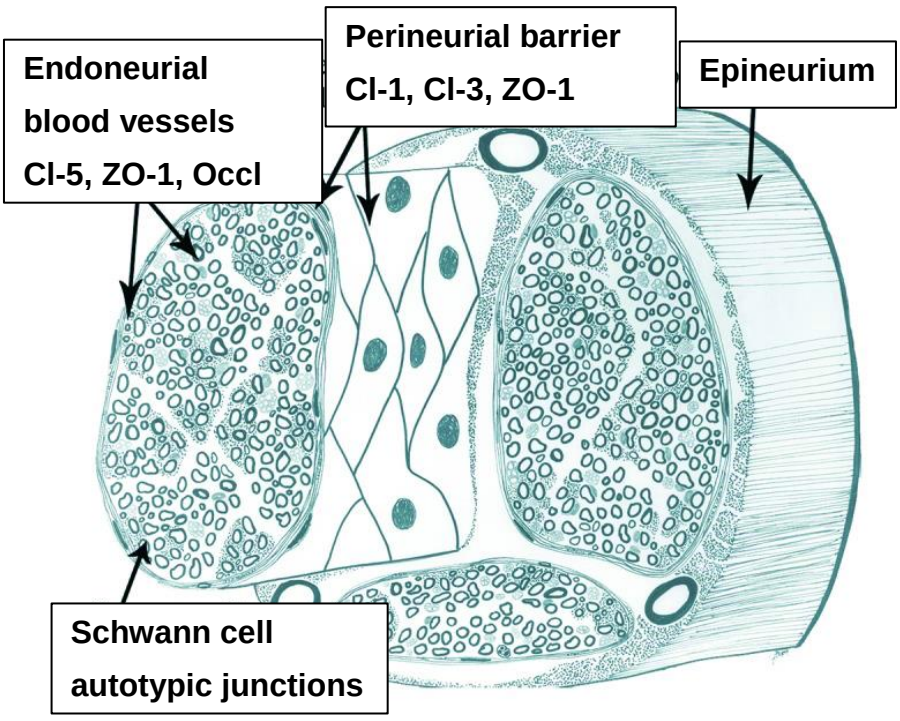

Figure 1-3 Diagram of peripheral nerve tight junctions relative to histoarchitecture

The different levels of peripheral nerve ECM structure are shown, with the epineurium surrounding individual fascicles. The layered lamellar structure of the perineurium is depicted, and inferior to the the network of tubules which form the distinctive structure of the endoneurium. At each level, the types of intercellular tight junction enabling homeostasis of the perinaurial and endoneurial microenvironments are shown. Cl = claudin, ZO = zonula occludens, Occl = occludin. Adapted from Peltonen et al (2013) [4].

1.2.2.3 Endoneurium

The endoneurium is an ECM structure with a honeycomb-like cross section, contained within each fascicle interior to the perineurium. Individual myelinated axons (or multiple axons if unmyelinated), together with Schwann cells and other fibroblastic-type cells, are contained within the tube-like structures of the endoneurium. The majority of the endoneurium is made up of type I and II collagens [45]. Individual endoneurial tubules contain basal lamina with a composition similar to that found in the perineurium, made up of molecules including heparan sulphate, laminin, fibronectin and collagen IV [46].

The endoneurial basal lamina within each tubule provides directional chemotrophic guidance and also facilitates Schwann cell adherence, growth and migration. The endoneurial basal lamina is therefore crucial to successful growth, regeneration and myelination of axons (described in section 1.2.1.2) [47, 48]. The larger vessels of the peripheral nerve vascular network , the vasa nevorum, do not directly access the endoneurium [40]. Instead, a fine capillary network permits individual axons access to the circulation.

1.3 Biochemical composition of peripheral nerve extracellular matrix

The peripheral nerve ECM is made up of numerous different biomolecules, the most abundant of which is type I collagen [49]. Other peripheral nerve ECM components include type II, III, IV and V collagens, glycosaminoglycans (GAGs), elastin, laminin, fibronectin and chondroitin sulphate proteoglycans (CSPGs) [50]. The interaction of cells (e.g. neurons, Schwann cells and immune cells such as macrophages) with peripheral nerve ECM components may influence tissue regeneration following injury, by the promotion or inhibition of processes such as cell growth and migration, the secretion of additional ECM components and remodelling of the ECM.

1.3.1 Collagens

Collagens represent the majority of the biomolecules making up peripheral nerve ECM (approximately 90 %) [49]. Collagens are key structural components of nerve ECM histoarchitecture, including the nerve–specific structures; the

epineurium, perineurium and endoneurium [51]. Collagen is a trimeric molecule, the main functional domain of which is the alpha chain [52]. The combination of alpha chain sub-types determines the overall type of the collagen molecule.

In vivo, fibrillar collagen molecules are assembled in a hierarchical order of increasing size as microfibrils, fibrils and fibres [53]. The tri-helix three-dimensional structure of fibrillar collagen molecules (of which types I, III and V are examples present in the peripheral nerve) within the ECM are crucial for mechanical strength, and therefore important for the support and protection of axons [54].

Type IV collagen is a highly glycosylated network-forming collagen located mainly in the basal lamina of the endoneurium. Due to the structural differences compared with other collagen subtypes at the level of individual molecules, such as retention of a C4 domain at the C-terminus and the lack of the regular glycine residue every third amino acid, type IV collagen molecules do not assemble in a parallel, hierarchical fibrillar pattern [55]. Instead, type IV collagen molecules assemble to form ß-sheets; these are crucial to the function of basement membranes, and in the nerve provide binding sites for the key moieties (e.g. laminins) which in turn enable the cellular processes of Schwann cells and neurons [56].

1.3.2 Elastin

Elastin is known to be present in low concentrations within the peripheral nerve ECM, in each of the epineurium, perineurium and endoneurium [57]. Bundles of elastin fibrils are thought to be most concentrated in the perineurium, as well as the lumen of blood vessels in the vasa nervorum. It is thought that elastin predominantly contributes to the initial biomechanical properties (at low strain levels) of peripheral nerve tissue [58].

1.3.3 Laminins

Laminins are ECM proteins made up of three subunits (α,β,γ), with around 45 differing isoforms possible [50]. Laminins are a crucial component of the basal lamina (both endoneurial and perineurial), with extensive functions related to cell adhesion, growth and migration [47]. Laminins have been linked to an important role in the promotion of axonal regeneration within endoneurial tubes

following injury; however, exact functions differ by sub-type. Laminins are most frequently bound by integrins, which mediate both cell adhesion and the transduction of signals from contact with different ligands [59]. A comparison study showed that the addition of laminin to the surface of a poly-3-hydroxybutyrate scaffold produced the biggest increase in Schwann cell growth and proliferation compared with type I collagen or fibronectin [60]. The importance of differing laminin subtypes to different functions within the nerve have also been examined. In *lama4 -/-* gene knockout mice, Schwann cell function was impaired to a greater degree following a sciatic nerve crush injury compared with wild type animals; for example, the myelin sheath in mutant animals was approximately 15% thinner, and myelination was not consistent between axons and across the length of individual axons [61]. In contrast, axonal growth did not appear to be affected by the mutation. These results suggested that Schwan cell function is influenced by interaction with laminin-8, which contains the laminin-α4 chain, whereas axons interact with the basement membrane through binding to laminin-2. These results were corroborated by a concurrent *in vitro* study, which demonstrated that increased growth of Schwann cells when incubated with a substrate of laminin-2 compared with laminin-8; the opposite was found to be true for neurons.

1.3.4 Fibronectin

Fibronectin, a key component of the basal lamina, is synthesised in nerves by Schwann cells *in vivo* [50]. Fibronectin is a glycoprotein that enables binding of cell surface proteins such as integrins [60]. When included as a supplementary material within a nerve guidance conduit, fibronectin has been shown to stimulate Schwann cell growth and migration. Fibronectin is predominantly located in the endoneurium and perineurium. Fibronectin is associated with axonal regeneration and myelination; for example, the addition of fibronectin to an alginate-based hydrogel conduit improved Schwann cell viability and enabled association with neurons, ultimately leading to improved neuronal regeneration in a rat sciatic nerve defect model [62].

1.3.5 GAGs

GAGs are polysaccharide molecules forming conjugates with proteins to give an overall unit known as a proteoglycan [63]. GAGs may be sulphated (e.g.

heparan sulphate) or non-sulphated (hyaluronic acid). Sulphated GAGs confer a range of functions, which can be broadly subdivided into modulation of cellular processes (e.g. heparin sulphates, chondroitin sulphates) and maintenance of tissue hydration (keratan sulphates, chondroitin sulphates) [64]. Non-sulphated GAGs, which (unlike sulphated GAGs) are only linked to proteins in a non-covalent manner, primarily function to aid in shock absorption (e.g. in articulating joints, where high concentrations of hyaluronic acid are found in the articular cartilage coating the joint surface). GAGs are known to be present in the ECM of peripheral nerve, with hyaluronic acid being the most abundant [58]. However, the specific function of GAGs within peripheral nerve is poorly characterised [65].

Chondroitin sulphate proteoglycans (CSPGs) are a sub-type associated with the Schwann cell basal lamina in the peripheral nerve [50]. CPSGs are upregulated following injury to the nerve and are known to be inhibitory to the process of Schwann cell attachment and axonal regeneration [66]. This is thought to be due to CSPGs binding to laminins in the basement membrane, inhibiting the chemotrophic effect these molecules can exert upon Schwann cells and neurons [67]. The magnitude of this effect is compounded by the increase in concentration of CSPGs within the endoneurium following damage, providing a potential barrier to sprouting neurons and therefore restoration of function [68]. It is thought that these CSPGs are subsequently degraded, permitting the extension of axons and the growth and migration of Schwann cells [69, 70]. Because of this, some nerve grafts (e.g. the Avance® decellularised human nerve graft) derived from native peripheral nerve ECM have been treated with the enzyme chondroitinase to eliminate CSPGs. This may serve to improve function, though to date insufficient evidence exits to conclusively demonstrate the clinical benefit of such treatment [69, 71]. In addition, it is highly likely that that the categorisation of CPSGs as only inhibitory to processes of neuroregeneration is an oversimplification. Rather, it is increasingly thought that CSPGs may have important regulatory functions during neuroregeneration. A previous study utilised transmission electron microscopy to provide evidence that CSPGs may influence the direction and phenotype (e.g. growth cone morphology, cell attachment molecule expression) of extending axons during regeneration [72].

1.4 Biomechanical properties of peripheral nerves

Unlike tissues such as bone, tendon and ligament, the primary function of peripheral nerve tissue is not primarily related to an ability to bear mechanical load. Instead, the mechanical functions of peripheral nerve ECM primarily relate to the protection of the axonal cell bodies travelling within the tissue [73]. The epineurium and perineurium are the ECM structures thought to be primarily responsible for the mechanical properties of peripheral nerve, whilst the endoneurium is thought to have mainly non-mechanical functions (e.g. axonal guidance, the provision of Schwann cell attachment sites). The perineurium, formed from a highly organised, layered lamellar structure of aligned collagen fibrils, surrounds each fascicle and is thought to be the most important contributor to the tensile mechanical properties of peripheral nerve [74].

Peripheral nerves must be able to maintain structure and functional properties when subjected to differing forces. As well as tensile stress, peripheral nerves may also experience compressive and shear stresses [8]. Articulating joints and muscular tension and relaxation may alter the dimensions of the connective tissue channel through which the nerve travels, subjecting the nerve to an increase in compressive stress [73]. Such changes in the magnitude and type of stress experienced at differing locations are reflected by the local structure of the perineurium [75]. Regions of the nerve at sites likely to generate higher levels of tensile and compressive stress (e.g. nerve junctions, nerves close to articulating joints) have a greater number of perineurial layers than areas of nerve fibre found in regions associated with lesser mechanical stress.

The level of strain (and therefore stress) a peripheral nerve is subjected to may also be influenced by the movement of the nerve within its connective tissue sheath; a gliding motion known as excursion [76]. Excursion of the nerve may decrease the overall tensile strain the nerve experiences, but result in an increase in shear stress due to friction between the exterior of the peripheral nerve and the connective tissue it resides within.

The length and distribution of peripheral nerves result in a wide variation in the localised mechanical forces experienced by the tissue [8]. Peripheral nerve tissue must therefore exhibit sufficient extensibility and elasticity to avoid compromising axonal function during movement, whilst also providing protection

from compression and shear forces. The biomechanical properties of peripheral nerves are known to vary with changes in parameters such as the diameter, location, fascicle number and function (sensory/motor etc.) of the nerve [77]. Such localised heterogeneity of properties is particularly crucial when the nerve is present in spaces close to articulating joints, for example within the arm where the median, radial and ulnar nerves travel close to the elbow joint between the humerus and the radius and ulnar. For example, sections of nerve located close to articulating joints may exhibit higher levels of compliance than those in regions experiencing less frequent and lower levels of localised strain.

A 2006 study by Topp and Boyd utilised cadaveric human limbs to facilitate measurement of the strain experienced by peripheral nerves during movement [8]. When the limbs were positioned at different degrees of joint flexion, strains of approximately 5 - 11 % were applied to the nerve trunk (Figure 1-4) . At specific locations, for example where the ulnar nerve passes through the elbow, strain levels of up to 30 % were observed.

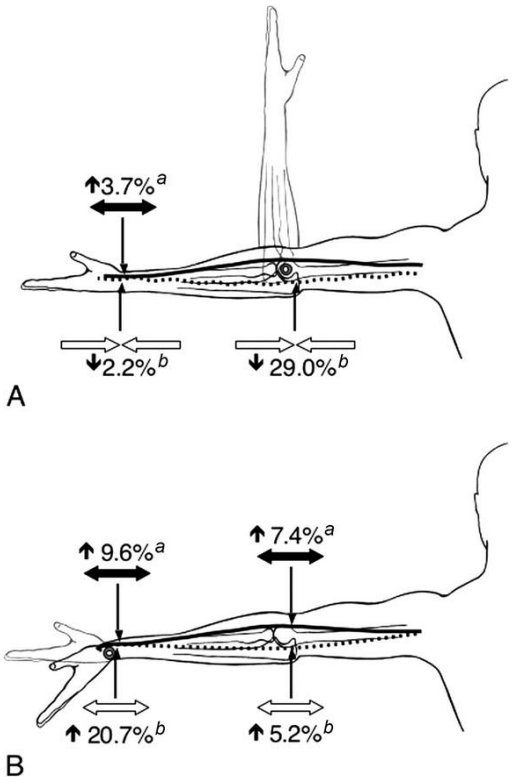

Figure 1-4 Variation in peripheral nerve strain during articulating joint flexion
Variation of localised strain experienced by the median (continuous line) and ulnar (dashed line) nerves during extension of A) the elbow and B) the wrist. Adapted from Topp and Boyd (2006) [8].

The mechanical properties of a tissue are commonly expressed as a curve of stress against strain (Figure 1-5). The mechanical characteristics of collagenous tissues are generally well characterised, particularly for tissues where the primary function is directly related to such properties. For example, the functions of soft musculoskeletal tissues (e.g. tendon, and ligament, such as the maintenance of stability within articulating joints whilst simultaneously facilitating complex movement patterns), are highly dependent on specific mechanical properties, and as a result these properties have been the subject of numerous studies [78]. In contrast, the mechanical functions of peripheral nerve tissue are considered secondary are primarily related to the protection of the key effector cells (especially axons and neurons) from mechanical injury; therefore, these properties are comparatively less studied. However, in common with other soft

tissues, the mechanical properties of peripheral nerve are primarily thought to be mediated by the fibrillar collagens (e.g. collagen I) which represent the majority of the ECM. Therefore, the limited data which do exist regarding peripheral nerve biomechanics can reasonably be compared to data from other such tissues when attempting to understand the underlying processes which determine these properties.

Indeed, a comparison of stress-strain curves for three soft collagenous tissues, tendon, diaphragm, and peripheral nerve, indicates that the basic characteristics are similar (Figure 1-5) [74, 79, 80]. The stress-strain curves for all three tissues (peripheral nerve, tendon and diaphragm) exhibit a toe region, a linear region and a defined point of rupture. The toe region is seen at low levels of strain; this region is characterised by comparatively low rates of increase in stress versus strain (i.e. the relationship between the two is non-linear in this region of the stress-strain curve). Studies investigating the mechanical properties of tendon and peripheral nerve have attributed this to the uncrimping of higher order collagen structure; this has been further corroborated through the use of biophysical analytical techniques [81-83]. For example, a 2018 synchotron x-ray diffraction study of the human ligament; based on observed changes in individual collagen fibre and fibril-level strain and stress when the ligaments were subjected to differing strain rates, the authors concluded that the characteristic regions of the stress-strain curve pertaining to collagenous tissues are primarily determined both by the higher order structure and proteoglycan sidechains forming bridges between tropocollagen molecules (Figure 1-6) [79, 84]. In the toe region the relationship between stress and strain is primarily determined by unfolding of the collagen crimp, loss of molecular-level “kinks” and recruitment of individual collagen molecules, whereas the linear region is predominantly defined by extension of the collagen fibres (mediated both by extension of the triple helices and sliding of the individual tropocollagen molecules past each other), and to a lesser extent isolated instances of fibril rupture. An x-ray diffraction study of rat sciatic nerves during tensile loading revealed differential levels of contribution to the bearing of mechanical load between the different tissue components, with collagen fibril strain correlating linearly with load in the linear region of the tissue-level stress-strain curve [81]. At the point of failure (rupture), the proteoglycan bridges are

debonded from the tropocollagen molecules, causing widespread (macroscopic) loss of fibril integrity (Figure 1-5A and Figure 1-6).

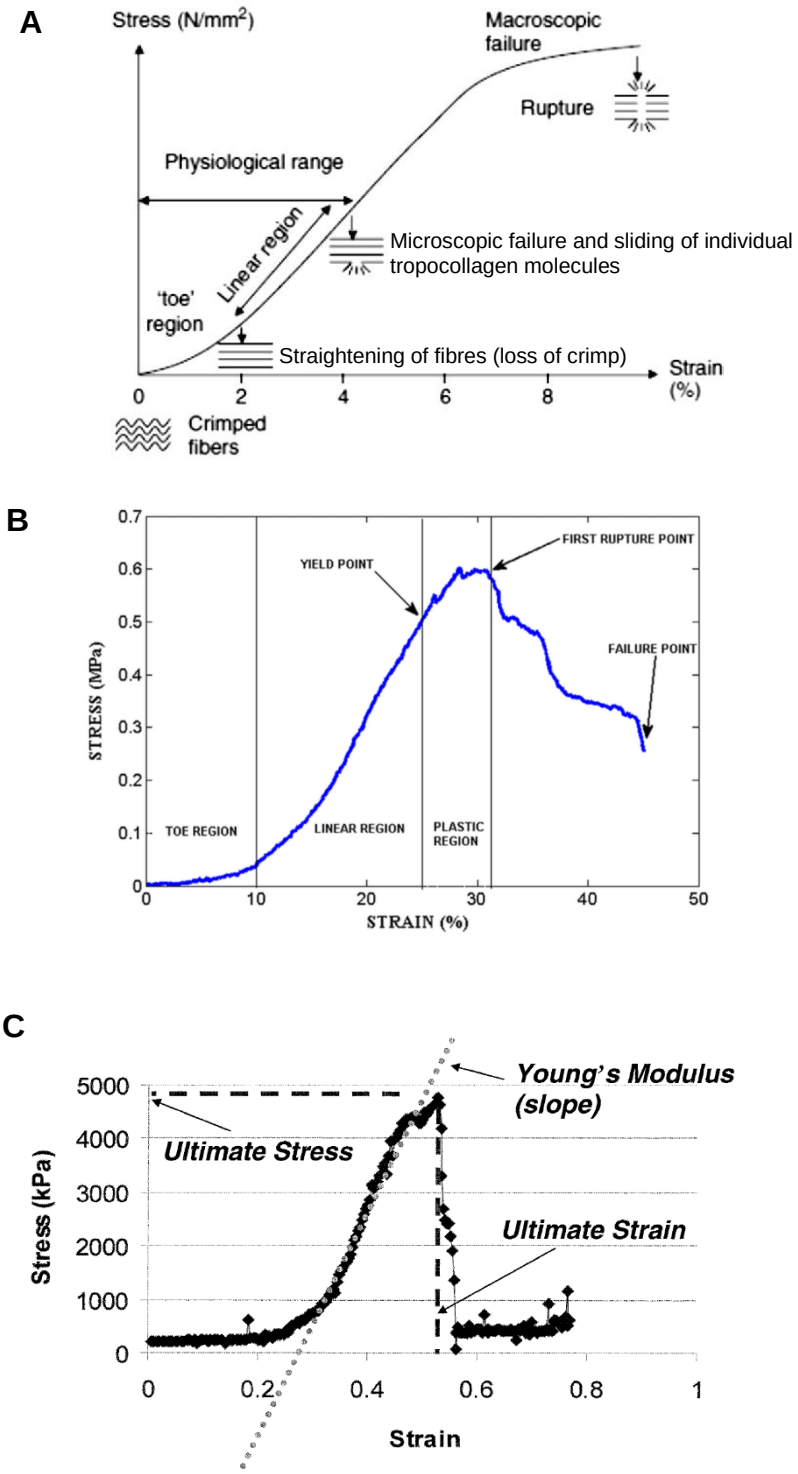

Figure 1-5 Example stress- strain curves for collagenous soft tissues
Example stress-strain curves for (A) human tendon, (B) human diaphragm, and (C) rat sciatic nerve. Adapted from (A) Trumbull et al (2016), (B) Paur et al (2016), and (C) Borschel et al (2003) [74, 79, 80].

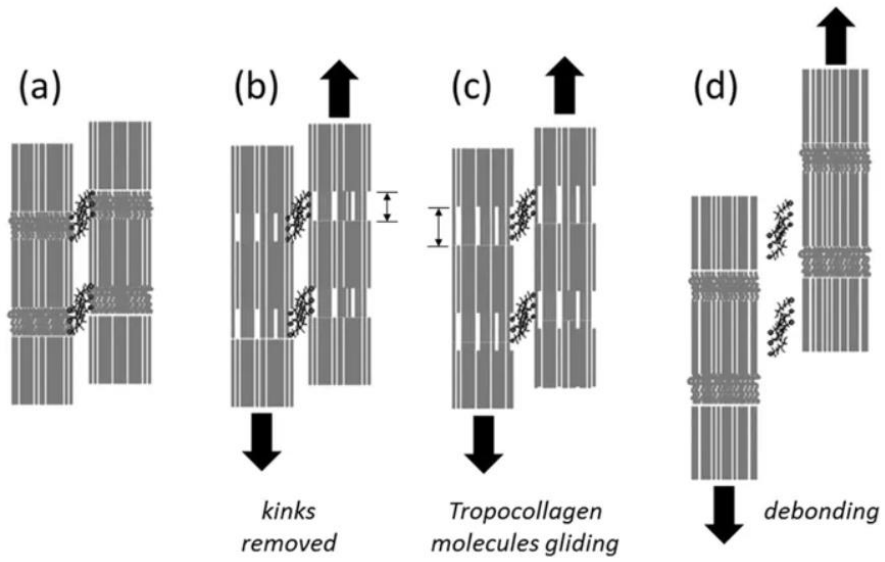

Figure 1-6 Multilevel changes in collagen tissue structures underlying different regions of the characteristic stress-strain curve

Structural changes which act as prmary determinants underlying the stress-strain characteristics of collagenous soft tissues, including changes in collagen fibre and fibril structure, and intermolecular GAG bridges between individual tropocollagen units. The different changes correspond to tissue in the (A) resting state, (B) toe region, (C) linear region and (D) point of rupture (and to a lesser extent the linear region)Adapted from Karunaratne et al (2018) [84].

The difference in the shape of the stress-strain curve (and therefore the differences in the underlying mechanical properties) between tissues and polymeric materials are likely due to three main factors. Biological tissues (such as peripheral nerve) generally exhibit a heterogeneity of structure and composition, with different constituent ECM components and structures contributing to the overall mechanical properties of the tissue (even though fibrillary collagens are often the most important contributing component) [50, 81]. Further, in contrast to synthetic polymeric materials, biological tissues contain a significant fluid component (interstitial fluid) [85]. The flow of this fluid within the tissue is known to affect the tensile mechanical properties of soft tissues, particularly at lower levels of strain as the fluid is forced out of the tissue; this is primarily due to a relative decrease in cross-sectional area as the level of strain is increased. In the context of peripheral nerve, the fluid component within the tissue therefore has the potential to influence the toe region of the curve in particular. Finally, as detailed above, the unique and complex multilevel structure of collagen proteins (at the level of fibres, fibrils,

and interactions between individual tropocollagen units) is fundamentally different to that of polymers, and produces a unique and characteristic stress-strain curve [52, 53]. Because of these three factors, the typical stress-strain curve exhibited by polymers is therefore quite different (for example, the toe region is absent), and is instead primarily reliant on differences in intermolecular branching and chain length and is not governed by the same structural changes [86].

However, these differences also present potential disadvantages when conducting *in vitro* mechanical testing of tissues. Whereas the effect of environmental factors on the mechanical properties of polymers have been well characterised, a tissue sample which has been excised, possibly stored, and then subjected to mechanical testing under non-native like conditions is unlikely to exhibit exactly the same mechanical behaviour as it would *in situ* [85]. For example, in an *in vivo* situation a peripheral nerve is likely under a low level of mechanical tensile strain (compared with the same material when not physically attached at two defined points [i.e. after excision]) at resting state [73, 87, 88]; therefore, unless this exact level of strain (and changing patterns of strain application, which may influence the repeatability of stress-strain values taken from collagenous soft tissues and can be simulated through cyclic preconditioning) can be measured and replicated prior to the initiation of testing, measured tensile testing data may not completely reflect the “true” tensile properties fo the tissue *in* situ (e.g. the measured toe region may be extended slightly due to the additional strain required to achieve the transition to the linear region) [89]. In addition, the exact proportion of fluid within the tissue in an *in vitro* situation is unlikely to be the same as when the tissue is within it’s native homeostatic environment; as fluid flow is thought to contribute to the mechanical properties of soft tissue, change in the relative fluid proportion within the tissue may therefore also alter the measured mechanical properties of the tissue relative to the *in vivo* situation [90].

Cross-referencing of the likely conditions (e.g. strain levels) experienced once the tissue graft is *in situ* (Figure 1-4) with the baseline mechanical properties of native tissue (Figure 1-5) can enable informed consideration of the potential impact of changes to tissue mechanical properties on the function of a tissue (including the function of resident cells within the tissue). Given the

physiologically relevant levels of strain experienced by peripheral nerve tissue, approximately 0 - 30 % (Figure 1-4), changes to tissue mechanical properties influencing the toe region and the initial part of the linear region of the stress-strain curve have the greatest potential to influence axonal function (Figure 1-5). For example, a decrease in the level of strain at which the linear elastic region is entered, or alteration to the gradient of the linear slope, and therefore to the Young's Modulus (also known as the Modulus of Elasticity), would likely cause an increase in the local levels of stress experienced by axons.

Levels of strain and/or stress in excess of physiological parameters can have a multitude of effects upon cells within the peripheral nerve tissue, particularly if the tissue is subjected to such conditions over extended periods of time [91]. Possible effects include changes to the vessel diameter of the vasa nervorum and therefore a decreased supply of blood to cells within the nerve, and a decrease in the number of successfully activated action potentials and compound action potentials (due to multiple causative factors including an increase in distance between Nodes of Ranvier, increased Schwann cell death and a decrease in the number axons travelling within the nerve) [92, 93].

1.5 Clinical background to peripheral nerve injury

Peripheral nerve injuries occur within the population at a frequency of approximately 1 in 1000, with approximately 300,000 new injuries incurred annually in the European Union alone [94]. According to the World Health Organisation, the global incidence rate is thought to vary between 2.25 and 6 million new cases per year [95]. Approximately half of clinically diagnosed peripheral nerve injuries require surgical repair by grafting [96].

The affected demographic are relatively young, with the mean age of incidence being approximately 27 [97]. This may be due to the greater levels of physical activity (associated with work, sports etc.), as well as (in some locations) increased likelihood of injury as a result of excessive consumption of alcohol within this demographic and a consequently increased risk of traumatic injury [97]. By contrast, a 2015 study by Bekelis *et al* found that older patients are more susceptible to incurring peripheral nerve injury as a result of a simple fall, with 39 being the mean age of incidence for this type of injury [98].

Peripheral nerve injuries result in significant disability, significantly affecting quality of life due to effects such as decreased ability to work and engage in leisure pursuits [2]. A 2015 study reviewed quality of life following compressive peripheral nerve injuries to the upper limb [99]. The review found that the outlook for perceived quality of life is highly dependent on the severity and, in particular, the location of a given injury, with more proximal injuries linked to a relatively poor quality of life. For example, a study of 158 patients suffering from upper limb peripheral nerve injuries found that injuries to the brachial plexus a significantly higher score on the DASH matrix (Disabilities of the Arm, Shoulder and Hand; brachial plexus) compared with those to more distal branches such as the ulnar nerve [100].

Patients suffering from longer-lasting physical symptoms as a result of peripheral nerve injury, for example chronic pain and loss of function, were found to have an increased incidence of additional psychosocial comorbidities such as depression and anxiety [100].

The loss of working days and the cost of care and rehabilitation associated with peripheral nerve injuries results in the induction of a significant economic burden. As an example, the cost of surgery and primary care alone resulting from peripheral nerve injury in the USA is approximately $7 billion. The total cost would be much higher when loss of productivity and the cost of social care during the recovery period are added to this figure.

Peripheral nerve damage is typically the result of traumatic injury, through mechanisms such as crushing (compression), laceration and excessive tension (traction) [101]. Injury to the nerves can be the result of (relatively) chronic or acute damage; an often cited example of chronic damage is “Saturday night palsy” (AKA radial nerve palsy), caused by radial nerve compression (often following after heavy alcohol consumption) incurred following an unusual sleeping position and consequent excess local pressure being exerted for long periods of time on the radial nerve [102].

Nerves in the limbs (e.g. the brachial or peroneal nerves) are particularly vulnerable to injuries [97]. The leading cause of peripheral nerve injuries in civilian populations is vehicle accidents; other common causes include bullet wounds, glass fragment/blade-induced laceration, injuries associated with

sports, blunt trauma and accidents during surgical procedures [11, 103]. Peripheral nerve injuries are associated with industries requiring physical activity in higher risk environments, examples of such being the agricultural, forestry and construction sectors [97].

Peripheral nerve injuries are commonly characterised according to one of two accepted grading systems, Seddon's Classification and Sunderland's Classification (Table 1-1) [16]. The first two categories of both classification systems describe injuries in which a degree neuronal function is lost without significant disruption or physical damage to the ECM structure. Sunderland's injury grades III, IV and V describe differing extents of damage resulting from severe compression, traction or laceration of the nerve, according to the depth to which the ECM has been damaged and the extent of the injury (Figure 1-6).

Table 1-1 Grades of Nerve injury according to the classification systems of Seddon and Sunderland [16, 104]

Sunderland's/ Seddons'	Type and severity of injury	Prognosis for recovery
I / Neurapraxia	Some localised demyelination and associated temporary loss of conduction. Axons intact.	Surgery generally not required
II / Axonotmesis	Demyelination combined with some disruption of axons. ECM remains intact.	Slower than Grade I, but surgery not generally required.
III / Axonotmesis	Disruption of axons and the endoneurium, leading to significant, prolonged loss of conductivity.	Surgical intervention may be required, according to the extent of disruption.
IV / Axonotmesis	Disruption to axons, endoneurium and perineurium. No recovery without surgery, slow recovery following surgery.	Surgical intervention required. Recovery very limited with no intervention.
V / Neurotmesis	Total severance of nerve-axons, endoneurium, perineurium and epineurium all disrupted. Most likely grade to require graft material for repair.	No prospect for recovery of function without surgical intervention.
VI / Elements of more than one category	A mixed injury which may require intervention according to the type and severity. Presents elements of more than one grade of injury.	Surgical intervention generally required, with varying extent.

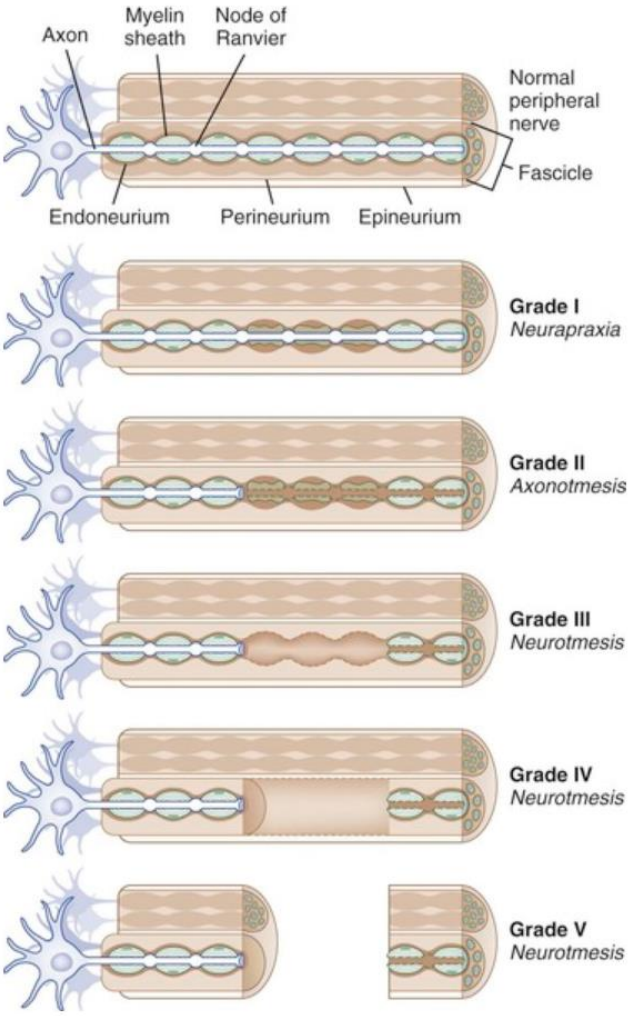

Figure 1-7 Visual representations of traumatic peripheral nerve injury classifications according to Sunderland's and Seddon's scales

Adapted from Tsao et al, 2006 [105].

1.6 Pathophysiology of peripheral nerve injury

The timescale of recovery and degree of functional restoration following peripheral nerve injury is dependent on the type and extent of damage which has been incurred [103]. Sunderland type I injuries recover without surgical intervention, as remyelination occurs independently with time (the axon itself does not suffer significant damage). Higher grades of injury, where the axon is damaged or severed, have longer and more complex processes of regeneration.

Axons which have been severely damaged (typically from Sunderland's Grade II upwards; Figure 1-6) undergo a process known as Wallerian Degeneration

[105, 106]. The segment of the axon distal to the site of injury begins to degenerate within 48 - 72 hours of occurrence. The first stage of Wallerian Degeneration is cytoskeletal destruction mediated by the protease calpain. Calpain activation is mediated by the increased intracellular calcium concentration. The increase in intracellular calcium is driven by a cessation of nuclear intron maturase 2 (Nmat2) signalling, which promotes cell survival through the regulation of transmembrane calcium exchange [70]. Nmat2 is produced in the neuronal cell body, and therefore is no longer able to reach the severed, distal portion of the axon following injury. The decreased local concentration of Nmat2 and associated breakdown products leads to the dis-regulation of calcium signalling and rapid opening of calcium channels post-injury [107]. After a short delay (latent period), rapid degradation of the distal axon is initiated. This axonal degeneration is a result of a combination of factors, which include further protease activity degrading remaining cytoskeletal components, fragmentation of the axon, and increased membrane permeability. The remainder of the intracellular components are destroyed in the period immediately following cytoskeletal degradation and fragmentation (Figure 1-8). Axonal degradation is followed by fragmentation of the myelin sheath, thought to be mediated by polymerisation of actin at key locations (e.g. the Schmid-Lanterman clefts) and subsequent elimination of E-cadherin [108]. Schwann cells de-differentiate and proliferate, whilst pro-inflammatory cytokine signalling (e.g. IL-1β, TNF-α) signalling from both the Schwann cells and activated resident tissue macrophages leads to the recruitment and activation of monocytes from the systemic circulation. Fragmented myelin and cellular debris from the degraded distal portion of the neuron is removed through phagocytosis or selective autophagy, mainly by Schwann cells and macrophages [109].

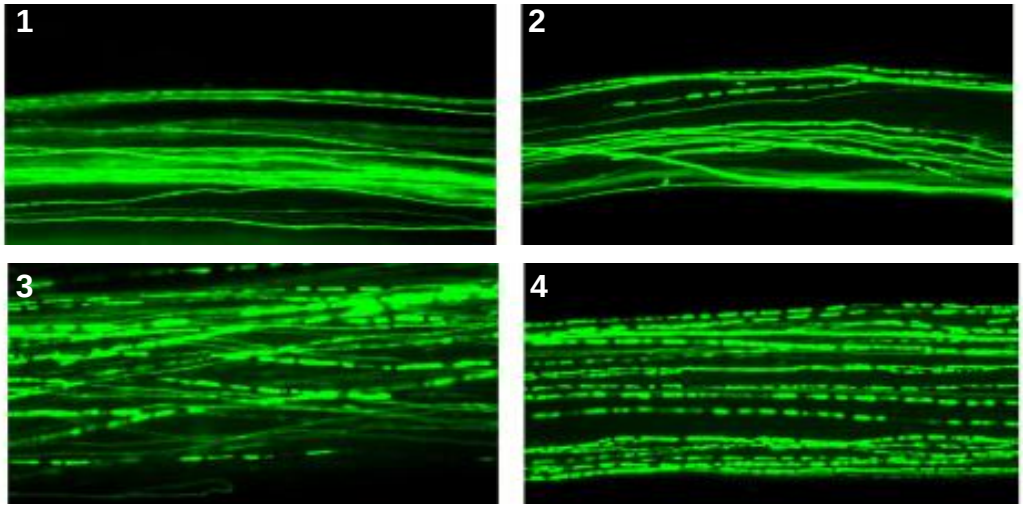

Figure 1-8 The process of Wallerian Degeneration illustrated through fluorescent imaging of neurons in mice expressing yellow fluorescent protein (pseudo-coloured green)

The difference between proximal sections of nerve following crush (1) and severance (3) compared to distal sections (2 following crushing, 4 following severance) can clearly be seen. Fragmentation of the neurons is much more evident in the distal sections. Severance of the nerve also appears to induce a more severe degenerative response in comparison to crushing. Adapted from Beirowski et al (2005) [5].

The proximal stump of the axon retracts following injury, but does not undergo Wallerian Degeneration; instead, regenerative processes begin to occur (Figure 1-9). Schwann cells dedifferentiate and proliferate, then begin to secrete (and stimulate the secretion of) cell-signalling molecules such as nerve growth factor (NGF), leukemia inhibitory factor (LIF), brain-derived neurotrophic factor (BDNF) and fibroblast growth factor (FGF) [48]. These molecules act to promote processes associated with neuroregeneration, such as the formation of a proximal neuronal growth cone and the secretion of chemotrophic factors by Schwann cells to enhance directional guidance of the regenerating axon [110]. The expression of signalling molecules and receptors associated with inhibition of neuroregeneration processes is downregulated simultaneously as expression of receptors associated with the promotion of neuroregeneration is upregulated.

The secretion of key ECM components, such as that of the basal lamina components fibronectin and laminin by Schwann cells, is upregulated following injury [111]. This process provides material for the fabrication of new ECM structures which provide guidance and further chemotrophic stimulation to regenerating axons.

Intracellular signalling through pathways such as the mitogen-activated protein kinase pathway leads to the formation of “sprouts” at the proximal stump of the affected axon, each with an associated “growth cone” (a bulbous formation with multiple extending processes [filopodia], the structure of which is primarily maintained by the cytoskeletal component actin) which mediates interaction with the surrounding ECM environment and is the primary site of growth and elongation [112]. Neuronal sprouts extend distally from the proximal stump, with the purpose of reconnecting with the target innervated organ/tissue and restoring downstream function. Factors influencing the rate and success of downstream target reinnervation include the size of the defect, the proportion of the axonal population severed, the distance from the target organ and the proportion of conserved/remodelled endoneurial tubules available for physical guidance [106]. Greater distance between the injury site and end target is associated with a lesser chance of full functional recovery due to the degradation of distal components, increased distance from cells secreting chemotrophic factors and the increased length of axonal regeneration required. Without the influence of environmental factors (e.g. appropriate physical and chemotrophic guidance), the direction of growth is random in nature [113]. These random growth patterns may lead to the formation of a benign tumour known as a neuroma and these are characterised by hyperexcitable axonal sprouts that can cause chronic neuropathic pain in affected patients [7]. Surgical intervention is often required to reduce the likelihood of neuroma formation and provide an optimal environment to support the reinnervation of downstream targets.

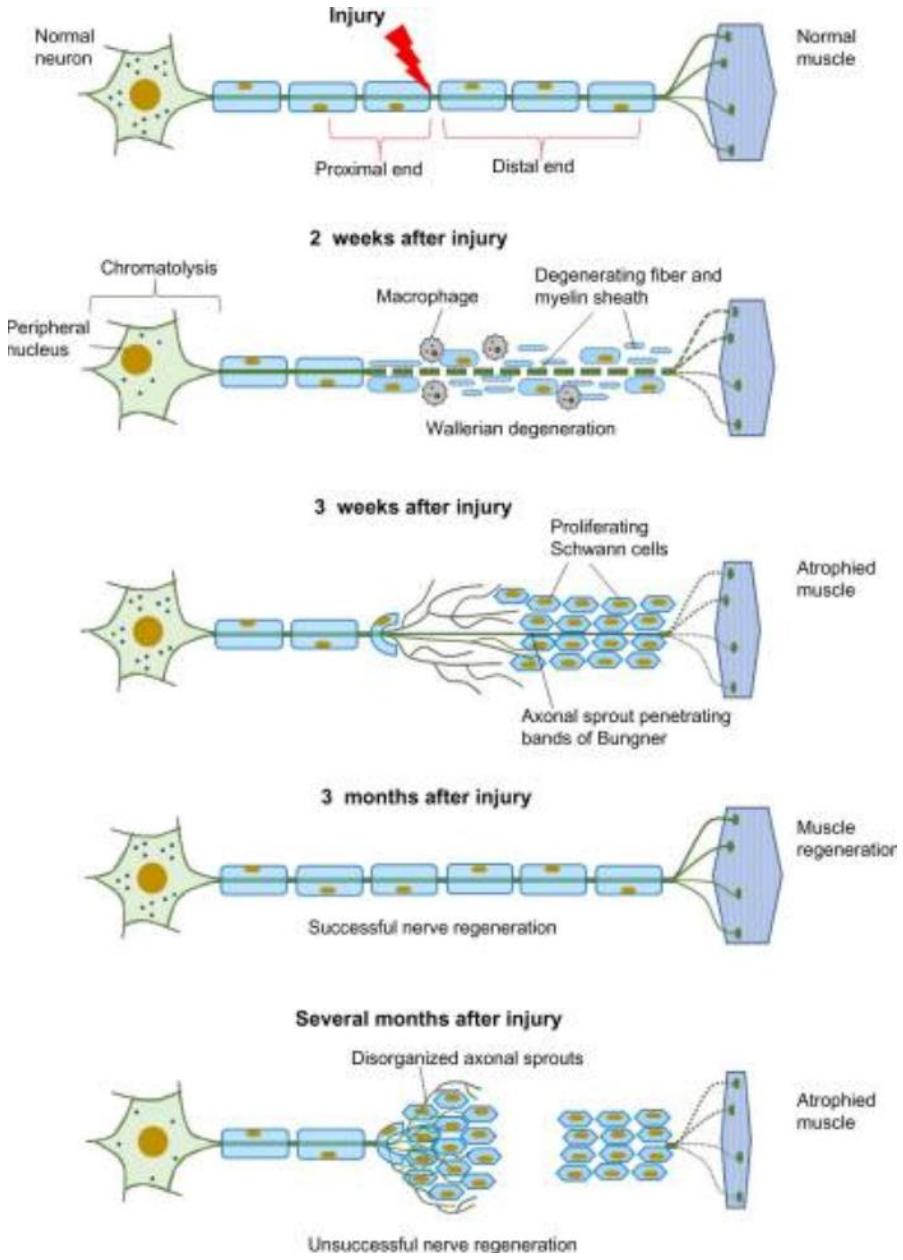

Figure 1-9 Possible outcomes after peripheral nerve injury

Processes underlying degradation and regeneration of a peripheral nerve within three months of incurring an injury of Grade II or higher according to Sunderland's classification scale. Processes depicted are (1) injury), (2) Wallerian Degeneration, (3) Initial regeneration, (4) successful reinnervation and (5) neuroma formation. Adapted from Arslatunali et al (2014) [103].

Strategies for the repair of peripheral nerve injuries vary according to the size of the defect and the functional importance of the nerve [114]. Currently, the vast majority of repairs are carried out using long-established surgical techniques of coaptation and autografting [115]. However, the limitations of such therapies

(particularly over defects of a larger size, including longer length and in nerves of a greater diameter and fascicle number) mean that functional restoration following injury, and consequently patient quality of life, is often severely compromised. Therefore, there is a clear need for an alternative in the form of therapeutic medical devices [116]. In order to become widely adopted, the efficacy and safety of these medical devices must be established and a comparison to current therapies must be determined. Furthermore, the ability of new therapies to provide further advantages, for example in areas such as ease of sourcing and supply, must be demonstrated to strengthen a case for widespread clinical adoption.

1.7.1 Coaptation

Coaptation is defined as repair of peripheral nerve defects by microsurgical suturing of the epineurium at the severed ends of the nerve, sometimes with dissection of surrounding connective tissue to facilitate the repair [117]. Coaptation is extremely effective for restoring function over nerve gap injuries of a lower length (approximately < 8 mm). In some cases direct fascicle to fascicle matching may be possible [118]. Coaptation also avoids the multiple surgical procedures and associated donor site morbidities which are required for allograft procedures.

It has been extensively documented that coaptation repairs placing a strain of greater than 10 % on the surrounding nerve tissue and subsequent increase in tension placed upon the axons residing within the nerve can impair regeneration, [119] decreasing both the speed and size of propagating action potentials [120]. A tension-free repair is the ideal surgical intervention, however larger nerve gaps require additional material to form a graft “bridging” the gap between the proximal and distal nerve endings.

1.7.2 Autografts

The current gold standard treatment for nerve defects too large to be repaired by coaptation is the autograft [121]. Donor tissue is taken from a nerve considered to be of lesser functional importance, such as the sural nerve (Figure 1-10 [122]), and implanted within the defect. The ECM structure of the tissue acts as a scaffold, with the endoneurium in particular providing guidance and support to regenerating axons.

One of the most important limitations of autografting is the induction of donor site morbidity and associated loss of function in the affected nerve (e.g. loss of sensory function on the outside of the foot in the case of the sural nerve) [50]. In addition, complete repair of larger defects may not be possible due to the limited length and diametric range of the available donor tissue; it is not possible to sacrifice a large amount of autologous peripheral nerve tissue without comprising function elsewhere. This is especially true during the repair of defects within a larger diameter nerve and it is not practical for a “like-for-like” match to be obtained. In such situations, it is possible to “cable” several sections of smaller diameter nerve using suture material to create a graft structure with the appropriate dimensions [123]. Significant anatomical variation can also exist between the donor nerve and the site of grafting (e.g. fascicle size and number, epineurial thickness etc.) [114]. This can compromise functional restoration, increasing the likelihood of permanent loss of function. Autografts have also been linked to the occasional formation of neuromas (benign but abnormal growth of nerve tissue) over longer time periods [119].

Figure 1-10 Anatomical location of the sural nerve

Depiction of the peripheral nerve anatomy surrounding the ankle joint, including the location of the sural nerve. Adapted from Citak et al (2007) [111].

1.7.3 Nerve Guidance Conduits

The use of nerve guidance conduits (NGCs) may be needed for nerve gaps which are too large to repair by coaptation [10]. NGCs are tubular structures which are implanted by suturing and give directional guidance to regenerating axons and aid in the maintenance of a pro-regenerative microenvironment (by ensuring localisation of cell signalling molecules is retained). Directional cell-scale guidance is often improved by the inclusion of surface patterning, striations or fibres within the NGC, arranged in a linear fashion, or by producing the conduit material in a single sheet and rolling it to create internal layers [124]. NGCs have been fabricated from a range of materials, both natural (e.g. collagen) and synthetic (e.g. Polyglycolic acid (PGA), Poly (lactic-co-glycolic acid) (PGLA), Polycaprolactone (PCL) [125].

Several NGCs have been fully translated and are currently in clinical use including Neurotube® (PGA; Synovis) and Axoguard™ (Porcine subintestinal mucosa; Axogen Inc) [126]. NGCs can be highly effective when used to facilitate repair over smaller defects. For example, a study using the NeuroGen® (Integra LifeSciences) conduit (composed of type I collagen) demonstrated restoration of function after 12 months in patients with digital nerve gaps of 6 - 18 mm; the majority of patients scoring “good” or “excellent” in sensibility testing (a subjective test measuring restoration of nerve function through the ability to difference in the ability to discriminate between two distinct points of contact in a defined zone on the skin; this was assessed using the established static and moving two point method) [127]. Various strategies have been investigated in an attempt to extend the length of defect over which successful reinnervation is possible, including 3D structures inside the conduit (e.g. striations, “honeycomb” tubular structures mimicking the structure of the native endoneurium, fibres travelling in a linear direction within the conduit), the incorporation of growth factors (e.g. NGF, transforming growth factor-β) and seeding of the conduit with “support cells” e.g. Schwann cells (Figure 1-11) [128].

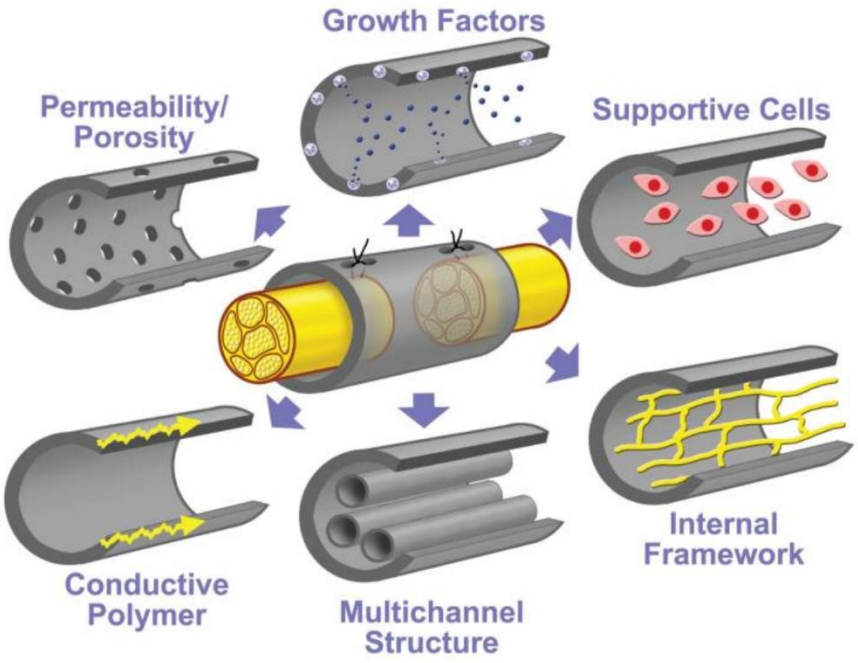

Figure 1-11 NGC modifications to improve directional growth

Examples of modifications to NGC structure/supporting biological components to maximise the capacity to support neuroregeneration. Adapted from Hudson et al (2000) [118].

Despite advances in NGC structure and the incorporation of growth factors/cells within the conudits, the key limitation of NGCs remains that the degree of functional restoration is curtailed when the size of a given defect exceeds a critical value, due to difficulty in supporting the growth of axons [7]. The critical value has often been defined as a length, generally given as 3 cm. However, it is thought the volume of the defect space may be a more important measure [10]. This effect is illustrated diagrammatically below (Figure 1-12).

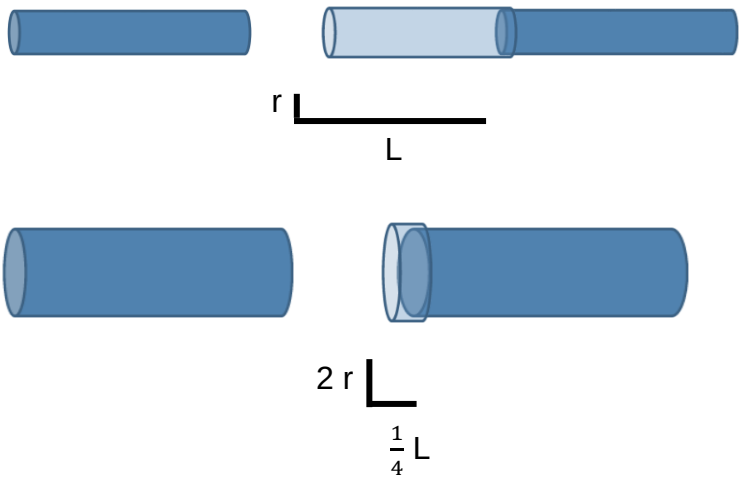

$V = \pi r^2 L$

V = volume

L = length

r = radius

Figure 1-12 Size limitations of nerve guidance conduits
Diagram showing diametric constraints when considering the use of a nerve guidance conduit. In the example given here, the radius (and therefore diameter) of the nerve to be repaired is doubled, the maximum length for effective conduit repair is reduced by a factor of 4. Figure adapted from Moore et al (2009) [7].

The limitations described may be due the lack of neurotrophic cues and nerve-specific ECM architecture [7]. This insufficient physical directional guidance combined with an unfavourable chemical microenvironment for effective stimulation of regeneration means axons are unlikely to re-innervate distal portions of nerve [7]. The inability of nerve conduits to support repair over larger defects has been observed in case studies [7]. One such study examine the implantation of a type I collagen conduit (NeuraGen) into a 7 x 20 mm defect in the median nerve. After a 4 year period the graft was investigated surgically in an attempt to identify the cause of persistent pain. A large neuroma had formed within the conduit, with no evidence of reinnervation across the defect and, consequently, no restoration of function. Histological examination revealed a disorganised structure, consistent with random growth of neuronal sprouts without sufficient directional guidance. Similar results (neuroma formation and

lack of functional restoration) were observed in other larger nerve defects repaired with conduits composed of PGA and type I collagen (GEM neurotube and NeuraGen, respectively). Functional restoration was only achieved in patients who elected to have autologous graft surgery, with the inherent disadvantage of having to sacrifice additional peripheral nerve tissue and the associated donor site morbidities which are incurred because of this.

1.7.4 Decellularised Nerve Grafts

Whilst unprocessed allogeneic and xenogeneic materials can provide an ECM structure to act as a scaffold for tissue regeneration in a similar fashion to an autograft, the potential immunogenicity presents a significant disadvantage [37]. In allogeneic cellular tissues, cells, nucleic acids and some ECM components all present antigens which may be recognised as foreign by the innate and specific immune system resulting in a catastrophic inflammatory cascade and ultimately graft rejection [129]. Xenogeneic cellular tissue present similar issues, in addition to further specific antignes such as Galα(1,3)Gal in porcine tissue.

Decades of research have led to the development of numerous methods for the removal of cells and nucleic acids from tissue, referred to under the umbrella term of decellularisation [17]. Decellularisation significantly reduces the possibility of an adverse host immune response to the graft, and therefore maximises the chance of successful graft integration and subsequently the restoration of function [130]. Numerous methods have been developed to achieve decellularisation of tissues; these include (but are not limited to) the use of chemicals including detergent, weak acids/bases and hypo-/hypertonic buffer solutions, and physical methods such as repetitive freeze-thaw, sonication, pressure and agitation [17]. Physical and chemical methods have been used across different tissues in combination and isolation; different tissue types often require radically different decellularisation protocols.

Decellularisation should remove immunogenic material from a tissue in order to minimise the potential for an adverse immunological response [131]. Whilst there are no officially defined parameters for such a reduction, previous proposals have included the requirement for a total of less than 50 ng of double stranded DNA (more than 200 base pairs in length), and no nuclear material visible when tissue is stained with haematoxylin and eosin (H & E). Incomplete

decellularisation results in residual cellular component debris (e.g. nucleic acids, cytosolic components, phospholipid membrane fragments), collectively referred to as damage-associated molecular patterns (DAMPs) [132, 133]. The immune response to decellularised tissues may be more favourable to graft integration and eventual functional restoration compared with an untreated cellular graft [36, 37, 132, 134]. The exact nature of the immune response to a decellularised tissue graft is likely to vary in response to a range of factors. Given the likely importance of such a response to the process of graft integration and functional restoration, it should be considered and investigated when developing a novel tissue graft.

A suitable decellularisation process for peripheral nerves would allow retention of the ECM histioarchitecture (with endoneurial structure considered to be particularly important) and biochemical composition, providing guidance, mechanical support and chemical stimulation to regenerating axons [135-137].

Previous work on the decellularisation of human peripheral nerves led to the development of a clinical product licensed for use in the USA, the Avance® nerve graft. This has shown promising results (around 75-100 % of patients recovering function depending on the size of the defect and the type of nerve) in the functional regeneration of nerve tissue, and has been successfully applied over a much greater range of defect size than NGCs (up to 7 cm in length). A functional model of a defect in the sciatic nerve of rats showed that in the nerve defect sizes studied (14 and 28 mm), acellular nerves produced through the Avance® process facilitated the growth of a 20 fold greater population of myelinated axons in comparison to a synthetic NGC [138].

The use of xenogeneic tissue as a source material presents potentially significant advantages over human tissue in terms of a consistent supply of high quality tissue [58]. To take advantage of these factors, a collaborative research partnership was formed between the University of Leeds and the University of Sheffield to develop an optimised decellularisation process for use with porcine peripheral nerves [18]. The nerves appear to retain similar structural, biochemical and biomechanical properties to native porcine nerves, and initial *in vitro* and *in vivo* evidence suggests the decellularised nerves support the attachment and growth of rat Schwann cells and neurons [18, 139]. Further

translational research is required for these nerves to progress towards a clinical product.

1.8 Need for effective sterilisation of decellularised grafts

Medical devices (including processed allografts and xenografts) may be contaminated with pathogenic organisms, increasing the risk of foreign-body related infections (FBRIs) [140]. FBRIs are extremely varied in both severity and distribution, and are most commonly introduced during surgical procedures. Surgical staff, equipment and the patients themselves represent possible sources of infection. However, ineffective sterilisation procedures can also lead to pathogens being present on a medical device prior to surgery, providing a potentially significant route of infection [141].

Decellularised scaffolds of allogeneic or xenogeneic origin may contain infectious pathogenic organisms either sourced from the donor or introduced during harvesting and tissue processing [142]. The risk of infection is an important potential cause of severe adverse effects following tissue transplantation procedures [143]. Screening donors/tissue sources prior to harvesting can reduce this risk. However, complete assurance can only be provided by an effective terminal sterilisation procedure.

Estimates for the mortality rate amongst individuals contracting FBRIs vary from 10 - 80 %, determined by factors including distribution of the infection and the specific pathogen present [144]. The identification of a suitable sterilisation method for a given decellularised ECM scaffold is therefore a crucial step in the translational process towards producing a medical device suitable for use in a clinical environment [145]. A terminal sterilisation step, meaning one which can be applied after packaging and thereby eliminate the risk of contamination post-sterilisation, effective across a broad range of pathogenic species must therefore be developed [146].

1.8.1 Accepted standards of sterility for medical devices

The efficacy of a sterilisation procedure is commonly defined by the ability to achieve the accepted sterility assurance level (SAL) for medical devices of 10^{-6}, defined in the international standard ISO 14937 [147]. The attainment of this

value means that less than 1 in 1,000,000 devices sterilised by a given method within a defined set of parameters will contain a surviving viable microorganism [148].

The D-value of population reduction, also known as the decimal reduction value, is another measure of sterilisation efficacy [149]. The D-value can be defined as the time taken for a given dosage of a sterilisation method to achieve a pre-determined reduction in a population of microorganisms, typically a D-$\log_{10}$ ($D_{10,}$ 90 %) reduction in the overall population (Figure 1-13). D-values vary considerably between pathogens for a particular sterilisation method, due in part to differing susceptibilities to specific methods of killing. Establishing D_{10} values for specific sterilisation methods requires the use of standard indicator organisms, for which the relative resistance to different killing mechanisms is well characterised [150]. Standard indicator organisms are highly resistant to most killing (sterilisation) methods, and so represent a “worst case” scenario; commonly used examples include endospores of *Bacillus pumilis* and *Bacillus atrophaeus [151]*.

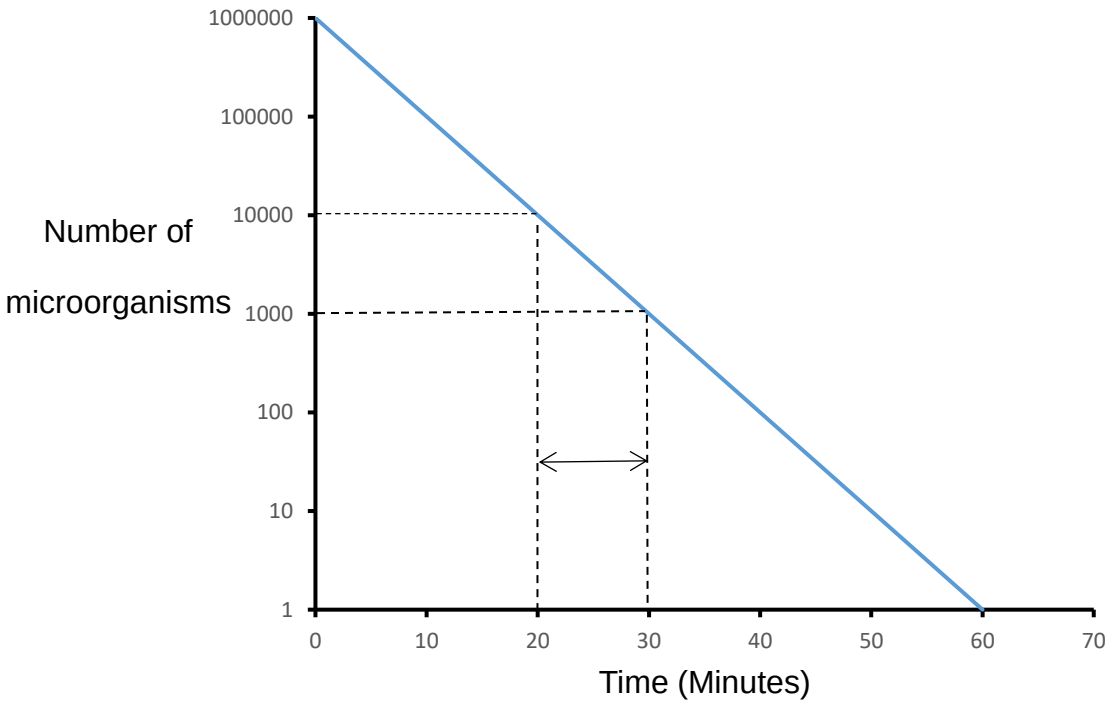

Figure 1-13 Diagram demonstrating the measurement of D-value reduction time

D-value is defined as a the time/dose for a log reduction in a given population of microorganisms (e.g. bacterial spores, bacteria, viruses, fungi) when exposed to a defined sterilisation process.

1.8.2 Common pathogens associated with tissue grafts

Tissue grafts may be contaminated with pathogenic organisms from a variety of different sources [152]. Pathogens may be resident within the tissue (though screening of source tissue for known bacteria and viruses reduces this possibility) or acquired from the environment during processing. To mitigate against the possibility of introducing an FBRI, it is therefore crucial that terminal sterilisation methods are effective across a diverse population of pathogens.

1.8.2.1 Bacteria

Bacteria are prokaryotic unicellular organisms, with a cell wall composed primarily of peptidoglycan located exterior to the membrane [153]. Bacteria can be divided into two classes, Gram-negative and Gram-positive [154]. Gram-positive bacteria have a thicker layer of peptidoglycan within the cell wall than Gram-negative species, whilst the cell wall of Gram-negative bacteria is more permeable to the transport of ions and molecules due to the presence of protein channels known as porins [155].

A population of bacteria may form a three-dimensional polysaccharide matrix known as a biofilm to create a perfect niche for cell survival and proliferation; they are also associated with residual endotoxins within medical devices [156]. Biofilms can increase the difficulty of accessing and eliminating the bacterial cells within, and represent one reason why dose levels of a sterilisation treatment proven to achieve the standard of SAL 10^{-6} (or equivalent) are often exceeded in common practice [141].

Antibiotic compounds are unsuitable for use in the sterilisation of tissue scaffolds, due to a lack of efficacy against other classes of pathogens such as viruses and the recent emergence of resistant strains of several bacteria common to clinical environments (e.g. methicillin-resistant *Staphylococcus aureus;* MRSA) [157].

1.8.2.2 Bacterial endospores

Some bacteria (predominantly Gram-Positive *e.g. Bacillus subitilis, Clostridium difficile*) have the ability to adopt a dormant phenotype known as a spore when subjected to environmental challenges (e.g. lack of sufficient nutrients) [9]. Sporulation can facilitate survival of the population until the environment

becomes favourable, at which point the endospore can reactivate itself to the vegetative (cellular) state.

Bacterial spores are significantly more resistant to external stresses (e.g. radiation) than vegetative cells, and therefore generally require administration of a greater dosage of a given sterilisation treatment to achieve the equivalent reduction in population [158]. Spores have layers of protective extracellular proteins and polysaccharides surrounding the cellular components in the core; for example, the exosporium is a spore coat consisting primarily of components including peptidoglycan and dipicolinic acid [159] (Figure 1-14).

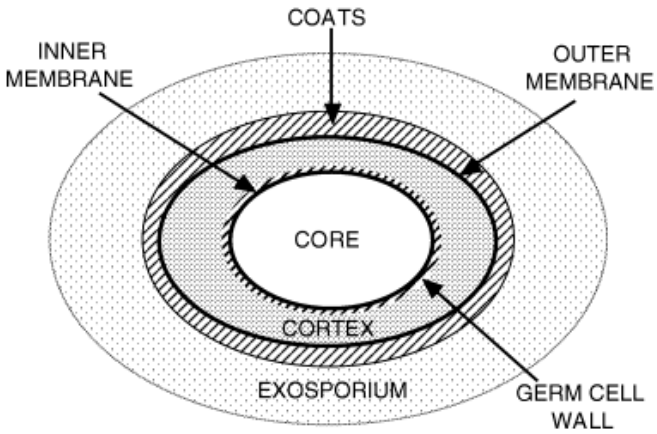

Figure 1-14 Structure of a bacterial endospore

The core region is depicted, containing important components (e.g. nucleic acids) required for germination and transition to cellular form. The coats, membranes and exosporium all protect the core and restrict access of potential sources of damage (e.g. ionising radiation, alkylating agents). Adapted from Setlow (2006 [9]).

These external protective layers can prevent the access of chemical agents to the core, and contain enzymes aiding this function (e.g. superoxide dismutase for the prevention of oxidant action). Pigments within these layers may absorb/block a proportion of ionising radiation [160]. Other mechanisms protect spores against the indirect effects of radiation. Spores have a decreased water content in comparison to the cellular form of the organisms, and therefore a decreased chance of hydroxyl radical formation. Spores also contain small acid-soluble spore proteins (SASPs), which appear to have a protective effect against oxidative damage both from radiation-generated radicals and chemical

agents [161]. SASPs change the shape and structure of DNA helices upon binding, a process which has been strongly implicated in protection against direct radiation damage to DNA.

The ability of bacteria to survive extreme conditions when in the form of endospores means that the efficacy of sterilisation methods against spores is a key factor in the choice of specific method and dosage to be used.

1.8.2.3 Viruses

Viruses are non-cellular organisms, which may exist as single or double stranded RNA or DNA [23]. The nucleic acid components are contained within a protein capsid, and this may be surrounded by a lipid membrane known as an envelope. Viruses function through infiltrating host cells and utilising the intracellular machinery to replicate nucleic acids, synthesise components of the capsid and envelope and ensure the release of replicated viral particles. Viruses are referred to as obligate intracellular parasites, lacking the molecular machinery to carry out these processes independently.

The specific population of pathogens present within a tissue graft of allogeneic or xenogeneic origin may differ significantly from those present on a medical device fabricated from synthetic materials, such as an artificial joint [162]. Of particular concern in grafts originating from porcine tissue are porcine endogenous retroviruses, which are (unlike most human endogenous retroviruses) capable of host infection [163].Tissue allograft sterilisation procedures should consider both the possibility of environmental contamination (as is applicable to all medical device manufacture), in addition to pre-existing pathogenic populations already residing within the tissue. The necessity of donor screening when using human tissue was reinforced by documented cases of HIV transmission through bone allografts [164]. Regardless of the efficacy of such screening programmes, sterilisation processes for tissue-based grafts should be able to produce a reduction in viral population of a similar level to other microbial populations (i.e. in line with the accepted benchmark of SAL 10^{-6}).

1.8.2.4 Fungi

Fungi are eukaryotic organisms which may take either unicellular or multicellular forms [165]. In the context of infections associated with tissue allografts,

multicellular fungi are largely irrelevant. Unicellular ungi have been identified as responsible for approximately 38 % of infections related to tissue allografts, with organisms such as *Candida albicans* and *Aspergillus niger* commonly implicated [166].

Fungi are susceptible to killing via DNA damage by radiation or chemical agents; however, the D_{10} value varies considerably and some fungi are significantly more resistant to killing than a majority of bacterial species [152].

1.8.2.5 Prions

Prions were only formally proposed as a class of infectious agents as recently as 1967 [167]. Prions are thought to possess no nucleic acids but are able to replicate via influencing protein folding within cells. Prions are obligate parasites implicated in diseases including Creuzfeld-Jakob Disease [168] and Gerstmann-Straussler-Scheinker Syndrome [169]. An American study of infections acquired over a three year period as a result of tissue transplants found one case of potential infection with a prion [166]. The possibility of infection means they cannot be discounted when considering the sterilisation of tissue-based scaffolds.

1.8.3 Tissue sterilisation methods

Sterilisation of devices for medical use can be carried out through a number of methods, which can be broadly subdivided according to mechanism of action into heat-based methods, ionising radiations and chemical methods [170]. While some materials, such as stainless steel surgical equipment, may be able to withstand rigorous sterilisation methods such as autoclaving, tissue grafts are much more susceptible to degradation and function-altering damage. The proteinaceous components of the ECM may be damaged by heat (for example, the denaturation temperature of collagen is approximately 66 °C), direct interaction with radiation, and interaction with free radicals or alkylating agents [171-173]. As such, selection of a suitable sterilisation method for use with a decellularised tissue which is sufficiently robust to ensure a sterilising action throughout the graft material, can achieve the accepted sterility benchmark of SAL 10^{-6} whilst retaining the key biological and biomechanical properties of the graft represents a complex challenge.

1.5.3.1. Peracetic Acid

Treatment with peracetic acid (PAA) solution has been used as a sterilisation method across diverse tissue types including dermis [174], anterior cruciate ligament [175] and (most commonly) bone [176].

In solution PAA exists in equilibrium with derivative compounds, acetic acid and hydrogen peroxide (H_2O_2) [177] (Figure 1-14). The mode of killing of PAA is thought to be related to a high level of oxidative activity [178], inducing the denaturation of intracellular and membrane-associated proteins, and critical disruption of the cellular membrane [179]. PAA is eliminated from the scaffold as non-toxic breakdown products including H_2O, O_2 and CO_2. This presents an advantage over some other chemical methods such as ethylene oxide treatment [180].

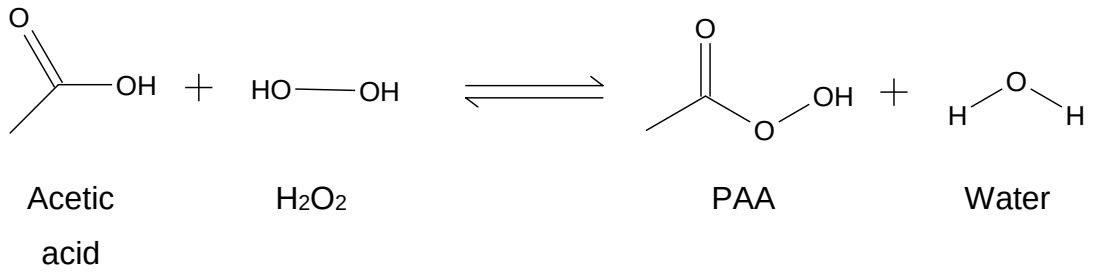

Figure 1-15 Diagram of equilibrium for PAA in solution
PAA exists in equilibrium with acetic acid and H_2O_2 when in solution [165].

Other advantages to the use of PAA include good efficacy against a broad spectrum of pathogenic organisms [181], relatively low cost and requirements for additional equipment, the relatively short duration of the procedure and the fact that it can be carried out at room temperature, eliminating the risk of heat-induced degradation of the ECM proteins.

However, grafts treated with PAA require an aseptic transfer process following treatment to place the tissue within the final packaging . This introduces the possibility that the tissue could be contaminated with a pathogen post-processing, and necessitates the use of additional equipment (e.g. controlled environments such as clean rooms). As such, PAA treatment cannot be considered to be a truly “terminal” sterilisation method.

1.8.3.1 Ethylene Oxide

Ethylene oxide has been extensively used in the sterilisation of surgical equipment, joint replacement components and some tissue allografts such as bone [182]. Ethylene oxide is a highly reactive epoxide gas which causes the addition of adducts to nucleic acids and some amino acids (e.g. cysteine, histidine, valine) through alkylation, altering the metabolic processes of microorganisms and preventing reproduction. Ethylene oxide also has the ability to diffuse effectively through scaffolds enabling it to be a highly penetrative method of sterilisation [183]. When used with medical devices constructed from robust materials (e.g. stainless steel), ethylene oxide treatment may be conducted at temperatures ranging between 100 - 140 °C. Whilst such conditions would normally prohibit the use of a sterilisation method with temperature-sensitive materials such as collagenous tissue grafts, the sterilising activity of ethylene oxide has been validated against a range of pathogens (including bacterial spores such as Bacillus atrophaeus and viruses such as HIV-1) in human musculoskeletal grafts at relatively low temperatures (approximately 30 - 40 °C for 14 hours) [184-186]. In terms of historical clinical use with tissue scaffolds, ethylene oxide treatment has primarily been applied to bone allografts [187].

Ethylene oxide treatment of scaffolds leads to the deposition of residues of both ethylene oxide and associated derivative compounds [188]. Common derivatives include ethylene chlorohydrin and ethylene glycol, which are formed as a result of reactions with chloride ions and water respectively [189]. Accepted levels of ethylene oxide and derivative by-products in medical devices are defined by the international standard ISO 10993-7 [189].

Both ethylene oxide and associated derivative by-products have been linked to the induction of acute toxic effects, as well as causing longer term morbidities (including a possible increased cancer risk as a result of the carcinogenic properties of ethylene oxide) [190]. A 3 year follow-up study of 109 patients who received a freeze-dried, ethylene oxide-treated bone-patella tendon-bone allograft noted that 6.4% experienced a chronic intraarticular inflammatory response, which resolved upon removal of the graft [191]. Although increased cancer risk has not been linked to ethylene oxide-treated tissue grafts, exposure

to ethylene oxide in the workplace has been associated with an increased incidence of mortality as a result of cancer (particularly haematological and lymphatic malignancies), and as such this risk cannot be ruled out on the basis of current evidence [192]. In order to minimise the formation of toxic derivatives, decellularised scaffolds can be lyophilised to reduce the amount of potential reactants present [193]. Lyophilisation may also aid penetration of ethylene oxide into the scaffold, increasing sterilisation efficacy. Due to the inherent toxic properties of ethylene oxide, an effective aeration procedure is required following completion of the sterilisation process to ensure elimination of residual ethylene oxide and any derivative compounds (e.g. ethylene chlorohydrin and ethylene glycol) [194]. The use of gas permeable packaging allows ethylene oxide treatment to be used as a true terminal sterilisation step [146].

1.8.3.2 Gamma Radiation

Gamma irradiation has long been used for sterilisation of food, medical devices and surgical equipment [195], as well as for the direct radiotherapy treatment of tumours [196]. Gamma radiation is an ionising radiation, typically sourced from neutron-beam generated synthetic radioisotopes such as Cobalt-60 (Co^{60}). The decay of such isotopes leads to the emission of high-energy photons known as gamma rays.

Control of the dosage is both of critical importance and difficult to achieve, as the rate of photon emission from the isotope cannot be artificially altered. Altering the length of exposure time, distance from source and configuration of source (e.g. quantity of Co^{60}) are the most effective methods to dictate dose control [197]. The standard accepted dosage for medical device sterilisation is determined by ISO 11137 [198], which specifies the application of 25 kilograys (kGy) to achieve the SAL of 10^{-6}. Sterilisation by gamma irradiation is slow relative to some other methods (e.g. E-Beam) [199]. However, gamma radiation can penetrate materials to a greater depth than other forms of radiation treatment i.e. E-beam and so may be more suitable for the sterilisation of larger tissue grafts.

Gamma rays induce changes to nucleic acids through effects such as double and single strand breaks, crosslinking of nucleic acids and proteins and oxidative damage of component bases [200]. Direct damage to DNA occurs due

to direct energy transfer from photons to nucleic acid chains. Hydroxyl radicals formed by the interaction of gamma radiation and water molecules can cause indirect damage to nucleic acids, which accounts for approximately 90 % of total lesions. Inactivation/death of microorganisms can be caused when DNA repair mechanisms are unable to repair the quantity of lesions formed, or when aberrational repair leads to the presence of mutations at critical points within the nucleic acid sequence [201].

The susceptibility of pathogenic organisms to radiation varies; cellular organisms and spores are more susceptible than viruses, possibly due to the water content within the cell [202, 203]. Data from previous studies indicate that a higher dosage of approximately 30 kGy is required to achieve sufficient inactivation of some viruses, such as HIV [204-206]. Water content is an environmental factor which significantly affects the ability of ionising radiation to induce DNA strand breaks through hydroxyl radical production. However, this effect can be counteracted if compounds with “radical scavenging” properties are present (e.g. ascorbic acid & ethanol) [207]. These compounds have been shown to be radioprotective to bacterial and fungal cells, an effect which increases linearly with increased scavenger concentration.

1.8.3.3 Electron Beam (E beam*)*

E beam sterilisation utilises an electron accelerator to produce beams of electrons equivalent to between 0.3 and 12 megaelectronvolts (MeV) [208]. The principal advantage of E Beam compared with alternative sources of ionising radiation (e.g. Co^{60}) allows greater control of dose intensity possible through manipulating the output of the electron accelerator [194]. Historically, E beam has been used much less frequently than gamma radiation for the purpose of medical device sterilisation, and as such little clinical data is available. The effects of E beam on tissue grafts have been investigated in a laboratory setting, primarily with musculoskeletal tissues (e.g. rabbit tendon, human patella tendon-bone) [209, 210].

The required dosage for sterilisation is determined by ISO-11137 [198] and ISO/ASTM-51649 [211]. Similarly to gamma radiation, the minimum applied dose has generally been considered as 25 kGy (with a beam strength of 10

MeV) [209]. However, higher doses (over 30 kGy) may be required to eliminate more resistant pathogens such as parvovirus or HIV [204].

A major disadvantage of E beam is a lack of penetrance in comparison to gamma radiation; historically, this means has limited the range of medical devices suitable for E beam treatment [212]. However, recent evidence suggests this may be dependent on the energy of the beam applied. A 10 MeV beam may penetrate tissue to a depth of around 6 cm, which would enable the use of E beam for the sterilisation of all sizes of peripheral nerve [213].

1.8.3.4 Supercritical Carbon Dioxide

Supercritical carbon dioxide ($SCCO_2$) is a supercritical fluid, also known as a dense phase gas [3]. This state is formed by maintaining CO_2 above critical values of temperature and pressure, 304.25 Kelvin (K) and 7.58 megapascals (MPa) respectively (Figure 1-16). Supercritical fluids exhibit properties similar to both gases (e.g. excellent diffusibility) and liquids (e.g. solvent-like properties) [175]. Recent research has examined the potential use of $SCCO_2$ for the purpose of tissue sterilisation, due to the potential reduced induction of adverse effects upon soft tissue grafts when other sterilising agents are applied (see 1.8.4) [214].

$SCCO_2$ can achieve a high level of penetration scaffolds due to its diffusibility, viscous properties and ability to be compressed. $SCCO_2$ operates at relatively low temperatures and pressures and presents low toxicity potential in comparison to some other methods such as ethylene oxide. $SCCO_2$ can also be rapidly and effectively eliminated from a scaffold by decreasing the pressure causing transition to a gaseous state and allowing elimination by aeration.

The diffusibility of $SCCO_2$ is thought to enable it to pass through plasma membranes and accumulate at high concentrations within cells [3], leading to cell death through the production of carbonic acid which lowers the intracellular pH, disrupting metabolic processes and the transport of substances (e.g. ions) across the membrane.

$SCCO_2$ is less effective as a sterilising agent against organisms with no membrane/an additional defensive structure such as a cell well; for example, viruses and bacterial spores. This has prevented validation and standardisation as achieving the required SAL of 10^{-6}. Adding small volumes of additional

agents, primarily oxidising agents such as PAA and H_2O_2, may allow a SAL of 10^{-6} to be achieved [215]. There would theoretically be a reduced likelihood of adverse effects on the tissue, due to the fact that such additives are included at significantly lower concentrations than when employed as stand-alone treatments. A study by Qiu *et al* in 2009 found that a combination treatment of $SCCO_2$ and 0.1 % (v/v) PAA solution led to the successful achievement of SAL 10^{-6} for indicator organisms of bacterial spores (Bacillus atrophaeus) and viruses (encephalomyocarditis) in a time of approximately 30 minutes [216]. The authors postulated that the highly diffusive properties of $SCCO_2$ may help to increase the penetration of the PAA into the scaffold and therefore allow it to act upon a greater proportion of the bioburden present.

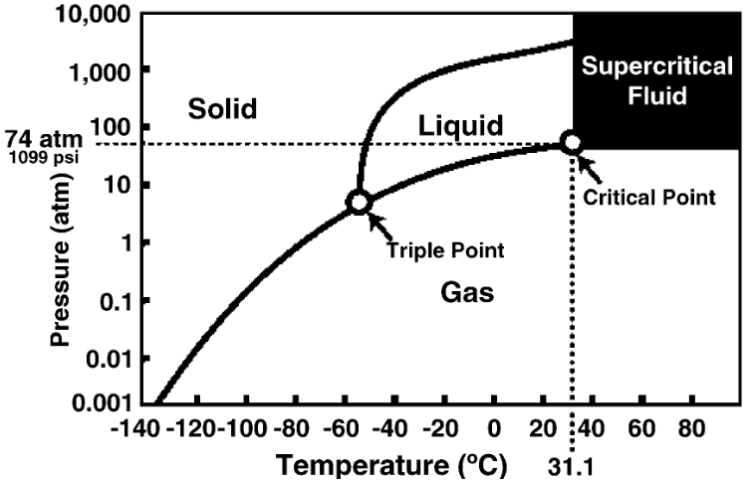

Figure 1-16 Diagram showing phases of CO_2 within different parameters of temperature and pressure

Certain substances can be maintained in a supercritical fluid state when subjected to given conditions of temperature and atmospheric pressure. The "critical point" at which this transformation occurs can be achieved in CO_2 using relatively moderate conditions, minimising the potential for adverse effects on tissue. Image adapted from White et al (2006)[3].

1.8.3.5 H_2O_2 (in isolation or combination with Copper (II) Chloride)

H_2O_2 is extensively used in isolation as an industrial sterilant [217]. H_2O_2 sterilisation is applied across a wide variety of fields including water purification, food chain sterilisation processes and the treatment of surgical equipment and medical devices. Whilst the precise mechanism of action is unclear, the biocidal properties of H_2O_2 are believed to be due to a highly oxidative nature and an

ability to lyse structures such as bacterial cells and spores [218]. The free radicals derived from H_2O_2, particularly hydroxyl radicals, can cause extensive oxidative damage to nucleic acids (through the formation of single base substitutions and crosslinking DNA lesions), proteins and lipid components of cell membranes.

The elimination of H_2O_2 is straightforward, due to its degradation over time into water molecules [219]. Any adverse effects induced by treatment of an ECM scaffold with H_2O_2 (e.g. changes to mechanical properties, microstructural alterations) would likely to be the result of the hydroxyl radicals generated [220]. Previous work has found that at an effective dosage (3 % [v/v]) there was no significant alteration to the trabecular structures of a demineralised bone ECM scaffold [221].

The formation of free radicals can be catalysed by the presence of transition metals [141]. This has been demonstrated by work showing that cells with a greater intracellular iron concentration require the presence of a significantly lower H_2O_2 concentration to be reduced to a specified percentage of the original population size [142].

Recent work within the NHS Blood and Transplant Tissue and Eye services (NHSBT TE) has indicated promise in the use of a solution of copper (II) chloride and H_2O_2 as a novel sterilisation treatment [222]. Both compounds independently have biocidal properties; however, use in combination requires lower concentrations of each and potentially reduce the extent to which changes to scaffold properties are induced.

The addition of copper (II) chloride leads to the presence of (cupric) copper ions within the solution. Copper is a transition metal, meaning it can mediate the formation of hydroxyl radicals from H_2O_2 through Fenton chemistry [223]. Copper ions are known to bind to the DNA base pairing Guanine-Cytosine (G-C); this would mean that radicals formed will be in close proximity to nucleic acid strands and therefore are more likely to induce lesions.

A combination treatment regime of copper (II) chloride and H_2O_2 therefore provides both a potential source of hydroxyl radicals and a potent catalytic agent which would be likely to locate itself in a favourable region for the induction of nucleic acid lesions [222].

1.8.4 Overview of the adverse effects of sterilisation methods on ECM scaffolds

In addition to effectively reducing the bioburden a sterilisation method should minimally affect the properties, and therefore efficacy, of the device being sterilised [170]. This is especially critical for susceptible materials such as ECM-based scaffolds.

It is well documented that sterilisation processes can significantly alter the histoarchitecture (including cell-scale architecture) and mechanical properties of ECM-based scaffolds (e.g. ultimate tensile/compressive strength, Young's Modulus) and therefore the capacity to support recellularisation [224] [173]. The use of different sterilisation techniques, and any observed effects resulting from the application of such methods, have been studied in both cellular and decellularised tissue grafts; however, these studies have focussed on a limited range of tissue types.

Sterilisation techniques requiring the application of high temperatures, such as dry heat, steam or pasteurisation, are clearly inappropriate for use in the treatment of scaffolds derived from ECM. The exposure of ECM-based products to temperatures approaching and in excess of 65 °C would result in extensive denaturation of the pretentious components of the scaffold and consequently a critical loss of function [141].

Radiation-based sterilisation methods, such as gamma irradiation and E beam, can have pronounced effects on the structure of collagen chains [225]. Disrupted ultrastructural features were observed when decellularised murine tracheas and porcine heart valves treated with gamma radiation (10 and 25 kGy respectively) were examined by transmission electron microscopy, predominantly manifesting as a loss of organisation in the collagen fibres [226, 227]. Gouk *et al* (2008) used scanning electron microscopy and haematoxylin and eosin staining to highlight significant alterations to the histoarchitecture of lyophilised Alloderm®, a decellularised human dermis which is currently in clinical use, following gamma radiation (12 kGy; Figure 1-17) [6]. While the porosity of the scaffold appeared to have increased following irradiation, which may aid in cellular infiltration post-implantation, the finer details of the ECM structure were lost. These changes compromised the mechanical properties of

the scaffold, causing a decrease in ultimate tensile strength compared with non-sterilised Alloderm®. Gamma irradiation also increased the susceptibility of the tissue to digestion with proteolytic enzymes (trypsin, pepsin and proteinase K). Gamma irradiation of Alloderm did not appear to negatively impact upon the growth of seeded human fibroblasts over 21 days compared with a non-irradiated control, and, when examined with Masson's Trichrome staining, collagenous ECM appeared to be remodelled and deposited by the fibroblasts in greater quantities on the gamma-irradiated scaffolds. This corresponds with the increase in susceptibility to enzymatic digestion; together, these observations may be indicative of chain scission within the ECM, due to the fact that the gamma irradiation was carried out under dry conditions.

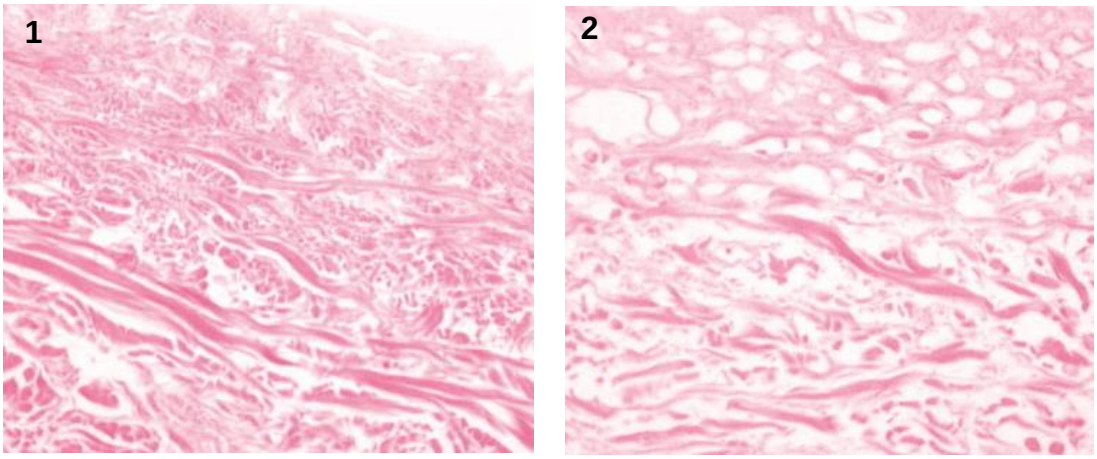

Figure 1-17 Haematoxylin and Eosin-stained samples of AlloDerm™ decellularised dermis

Freeze-dried decellularised dermis and 2) freeze-dried decellularised dermis treated with gamma irradiation at 12 kGy. Alterations are evident following irradiation, with increased porosity and apparent loss of the finer ECM structures. Adapted from Gouk et al (2008) [6].

If tissue is irradiated in a wet state, alterations to the collagen chains are primarily mediated by interaction with hydroxyl radicals generated through radiolysis of water molecules, leading to the formation of cross-links between collagen chains (Figure 1-18) [228]. This can affect the mechanical properties of a tissue; for example, radiation-mediated crosslinking has been associated with increased ultimate strength but also increased stiffness in decellularised tissues such as porcine heart valve (gamma-irradiated at 1 - 100 Gy) [229]. In contrast,

when tissue is irradiated in a dry state (e.g. if the tissue has been lyophilised) the predominant mechanism of action is direct breakage (or scission) of the polypeptide chains. This can lead to a decrease in all mechanical parameters, and produce an altered histoarchitectural structure as described above. E beam treatment also causes the production of free radicals which interact directly with collagens in the tissue, and may affect structural and biomechanical properties [230]. However, if the dose is applied in a consecutive series of lower doses of radiation (e.g. the original dose is applied in 10 equal doses, 2.5 kGy if using the industry standard 25 kGy) then the magnitude of such effects may be reduced [231]. This process is known as fractionation, and can also be applied (less easily) to gamma radiation [232]. Treatment of allograft tendon with 10 doses of 3.4 kGy as opposed to 1 dose of 34 kGy retains effective reduction of the populations of key indicator organisms in allograft tendon, whilst significantly reducing biomechanical changes [213].

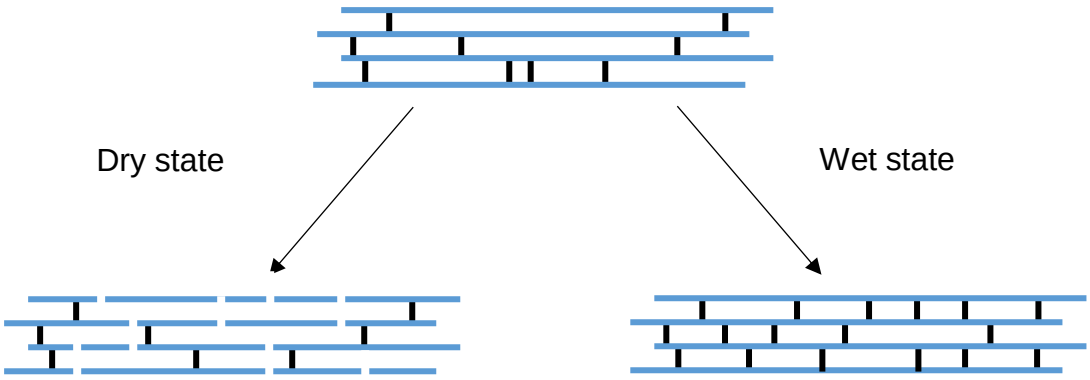

Figure 1-18 Comparison of the effects of irradiation on collagen fibrils under dry and wet conditions

Representation of structural changes to collagen after irradiation in dry or wet state. In dry state irradiation, chain scission is the dominant phenomenon and leads to fragmented collagen chains and degradation to higher order structures. In contrast, Irradiation in a wet state induces the formation of crosslinks between the collagen chains (and therefore maintenance of higher order structure). Adapted from Aquino (2012) [1].

Kajbafzadeh *et al* (2013) demonstrated this phenomenon in decellularised ovine livers treated with gamma radiation (30 kGy) [233]. Livers irradiated in a “wet” state retained an ultimate tensile strength and elastic modulus close to that of native tissue, whereas livers which were lyophilised prior to irradiation were found to have incurred decreases in these parameters of approximately 30 and 50 % respectively. ECM-based scaffolds should therefore be irradiated in a wet state, as the changes caused by dry state irradiation are likely to result in an unsuitable graft material.

Following 12 weeks *in vivo,* the tensile mechanical properties of ovine musculus flexor digitorum superficialis tendons treated with E Beam (34 kGy), including the maximum load at failure and stiffness, were found to have decreased in comparison to a non-irradiated control allograft [234]. However, increased tissue remodelling, cellular activity and vascularisation were also observed, suggesting that over a longer time span the E Beam-treated samples may exhibit better integration into the injury site and therefore superior functionality as a graft material.

The induction of alterations to ECM scaffold properties is not unique to radiation-based sterilisation methods. Commonly used chemical sterilants (e.g. oxidising agents such as PAA, alkylating agents such as ethylene oxide) may also significantly interact with and alter the protein components of ECM-based scaffolds [235].

PAA treatment has been shown to induce alterations to the structure and biomechanical properties of some ECM-based scaffolds, which may be related to an increase in scaffold porosity [236]. Sterilisation of decellularised human patellar tendons with 0.1 % (v/v) PAA appeared to maintain the integrity of individual tissue structures, whilst causing a notable increase in the looseness/porosity of the overall tissue histoarchitecture [237]. Some alterations to the basement membrane component collagen type IV have been observed in decellularised tissues including porcine mitral valves, porcine pulmonary valves, human aorta and porcine bladder, where each tissue was treated with 0.1 % (v/v) PAA as a terminal sterilisation step [238-241]. The exact nature of these changes and the associated implications for cell attachment (and therefore tissue regeneration) remain unclear. Matuska et al (2014) found that sterilisation

with either ethylene oxide or PAA (in 4 % ethanol) caused an approximate 80 % reduction in the compressive modulus of temporomandibular disks [179]. Furthermore, structural disruption was observed to the ultrastructure of sample treated with ethylene oxide, and a reduction in seeded cell viability compared to PAA-treated or gamma irradiated samples.

There is limited knowledge regarding the effects of $SCCO_2$ treatment on ECM structure and composition, due to its relatively recent development as a sterilisation method [19]. However, the inclusion of oxidising agents (e.g. PAA, H_2O_2) as components of an additive solution (to aid in the reduction of viral/bacterial spore populations) raises the possibility of adverse alterations being induced to ECM structure, as well as damage to components of the basement membrane (in particular collagen IV) [242]. Decellularised porcine aortic valves treated with $SCCO_2$ combined with a small volume of additive solution (containing 13.5–18.5 % PAA and 4.5– 6 % H_2O_2 [v/v]) did not appear to sustain damage to the ECM structure upon histological and SEM-based examination [19]. Treatment of decellularised rat lungs with a similar process appeared to mediate superior retention of ECM structure and key components for cell attachment (e.g. laminin) compared with lungs treated with 0.1 % (v/v) PAA solution in 4 % (v/v) ethanol [243]. However, an approximate threefold increase in the Young's Modulus of the decellularised lungs compared with non-sterilised decellularised lungs was recorded at a strain of 30 %; the authors postulated crosslinking of collagens due to the elevated pressures (approximantely 1400 – 1500 pounds per suare inch [PSI]) associated with processing, or dehydration of the tissue during processing, as possible mechanisms underlying this change. When the (limited) published data are taken together, these initial results suggest that $SCCO_2$ processing may be a promising method for achieving effective sterilisation of tissue whilst inducing minimal adverse effects to the ECM relatively to methods such as irradiation or ethylene oxide treatment, and that the use of a small volume of additive solution may limit the occurrence of alterations to basement membrane components which have been described when agents such as PAA are used in isolation.

Ethylene oxide treatment of tissue grafts can also result in the induction of an adverse host immune response following implantation. *In vitro* studies have provided contrasting data regarding the cellular response to ethylene oxide

residuals. Lyophilised human bone containing 2.61 µg/g of ethylene oxide reduced the growth of fibroblasts by 22 % compared with non-treated samples [244]. However, a 2001 study found that ethylene oxide sterilisation of human bone did not alter the secretion of pro-inflammatory cytokines by human peripheral blood monocytes compared with a non-sterilised control [245]. Despite these data, 6.4 % of a patient cohort who underwent implantation of a bone-tendon-bone allograft ACL replacement developed a chronic, intraarticular inflammatory reaction which necessitated the removal of the graft; the cellular populations were found to be predominantly lymphocytic in nature [191]. The authors concluded that the presence of an ethylene oxide breakdown product, ethylene chlorohydrin, within the grafts was the likely cause of the observed immune response. Concerns such as these, alongside worries that lyophilisation may negatively impact mechanical properties, underlie the relative lack of use of ethylene oxide (compared with gamma radiation) amongst tissue banks [173, 182, 188, 191, 192]. The working concentration of chemical sterilisation agents, the length of time for which a scaffold is exposed and the implementation of an appropriate elimination strategy post-treatment are critical determinant parameters when minimising potential alterations to scaffold properties.

Relatively little is known about the potential effects of copper (II) chloride on the properties of ECM-based scaffolds, and therefore this should be considered carefully [246]. High intracellular concentrations of copper are known to be cytotoxic (due to intracellular redox reactions) [247], and therefore effective removal of residual copper (II) chloride would be essential to ensure the prevention of adverse effects on tissue integration or cellular ingrowth capabilities of the graft [248, 249]. Furthermore, copper is known to induce neurodegenerative symptoms in patients suffering disorders such as Wilson’s disease; here, a mutated form of the ATP7B gene prevents removal of copper from the brain, resulting in neurodegeneration and associated symptoms such as parkinsonism and ataxia. While the effect of copper toxicity is less well defined in the PNS than the CNS, this evidence of neurotoxicity indicates that treatment of materials with copper compounds should be carried with caution, and full elimination of the reagent should be ensured, if the material functions to support neurons. A further potential disadvantage of this sterilisation method

would be the requirement for an additional aseptic transfer procedure before final packaging (similar to PAA), increasing the risk of contamination.

The need for the identification of an effective terminal sterilisation process for decellularised porcine peripheral nerves is clear, due to the source of the tissue and the intended application. However, it has been well documented that sterilisation can negatively impact the functional properties of an ECM-derived scaffold; these include (but are not limited to) biocompatibility (including immunogenicity), biomechanical properties, biochemical composition, and histoarchitecture (including retention of ECM structures and components). Due to the possible implications of changes to such properties, the sterilisation method chosen for use with a novel tissue scaffold must be evaluated carefully.

To date, the majority of the literature regarding the sterilisation of tissue scaffolds focusses on the use of historically commonly applied methods (particularly gamma radiation) with musculoskeletal and dermal allografts. Evidence is particularly lacking regarding the effects of sterilisation methods upon tissues containing delicate ECM structures which are thought to be critical to effective function. The endoneurium in peripheral nerve is an example of such a structure; maintenance of the intricate “honeycomb” structure and the integrity of the basement membrane (e.g. retention of key components such as type IV collagen and laminin) is thought to be key to stimulating and supporting neuroregeneration and functional restoration. The material properties of the nerves must be retained to ensure the axons are protected from excessive mechanical forces which may impair growth and function. Furthermore, given its importance in determining the success or otherwise of graft integration following implantation, the effect of sterilisation on the immune response to decellularised tissue grafts has not been widely investigated. A range of potentially suitable sterilisation methods, established and/or more novel, should be identified and the effects on sterilised decellularised nerves should be compared with baseline data from tissue which has not undergone a terminal sterilisation procedure. The identification of a suitable method preserving the key functional properties of the decellularised nerves is essential to enabling clinical translation of the device; retaining such properties would provide an optimal material for supporting the growth of key cell types including neurons and Schwann cells, and the promotion of functional restoration.

1.9 Hypothesis and aims

Project hypothesis

A terminal sterilisation process, novel or established, can be used to treat decellularised porcine peripheral nerves without compromising biological and/or physical properties.

Project aims

1. To optimise and validate the previously developed decellularisation process for porcine peripheral nerves;
2. To characterise the biochemical, biomechanical and biological properties of decellularised porcine peripheral nerves;
3. To identify candidate sterilisation methods with the potential for use with decellularised porcine nerves, and characterise the effects of sterilisation on the structural and biochemical properties of sterilised decellularised porcine nerves.
4. To characterise the material properties of decellularised porcine peripheral nerves treated with identified candidate sterilisation methods.
5. To determine the effect of candidate sterilisation methods on the biocompatibility and immunogenicity of decellularised porcine peripheral nerves.
6. To determine the effects of storage on the properties of sterilised decellularised porcine peripheral nerves.

2 General Methods

This chapter details the general methods used during the course of this study. Specific methods are described in the relevant chapter.

2.1 Chemicals and reagents

For details of chemicals and reagents used in this study, see Appendix A, Table 1.

2.2 Equipment

For details of equipment used in this study, see Appendix A, Table 2.

2.3 Glass/plasticware

For details of glass/plasticware used in this study, see Appendix A, Table 3.

2.4 Consumables

For details of consumables used in this study, see Appendix A, Table 4.

2.5 Antibodies

For details of antibodies used in this study, see Appendix A, Table 5.

2.6 Determination of pH

A Jenway 3020 pH meter was used to determine the pH of solutions. The pH meter was used in conjunction with a temperature probe to allow for variance caused by temperature change. Buffer solutions of pH 4, 7 and 10 were utilised to calibrate the pH meter prior to use. If required, solutions of 1 M hydrochloric acid and 1M sodium hydroxide were used to adjust the pH, added in a drop wise fashion with constant stirring.

2.7 Light microscopy

A Zeiss Axio Imager M2 microscope was used for Köhler, circularly polarised and fluorescent microscopy. An HPX 120 illuminator was used in conjunction with a DAPI filter (450 - 465 nm) for fluorescent imaging. Images were captured using an attached Zeiss Axiocam MRc5.
Zeiss Zen Pro software was used to control the microscope and camera, and process the images captured. An Olympus IX51 Inverted microscope (fitted with an Olympus XC-50 camera) was used for phase contrast microscopy. Cell B software was used to capture images.

2.8 Sterilisation of equipment/reagents and solutions

Dissection equipment was sterilised in a hot air oven (190 °C for four hours). Solutions (and equipment deemed unsuitable for sterilisation by dry heat) were sterilised in an autoclave. Items were subject to a temperature of 121 °C and pressure of 15 PSI for 20 minutes.

2.9 Dissection of porcine peripheral nerve plexus

Porcine hind legs were obtained from a local abattoir (J. C. Penny, Rawdon, Leeds, United Kingdom) within 24 hours of slaughter. The skin was removed, and the major nerve plexus (consisting of the sciatic, tibial and peroneal nerves) of the leg was then extracted by blunt dissection. The plexus was separated into the individual constituent nerves and the superficial connective tissue was removed. The nerves were washed at room temperature (with gentle agitation) in phosphate buffered saline (PBS) for 30 minutes (pH 7.2 -7.4). The nerves were stored for up to six months at - 70 °C prior to use.

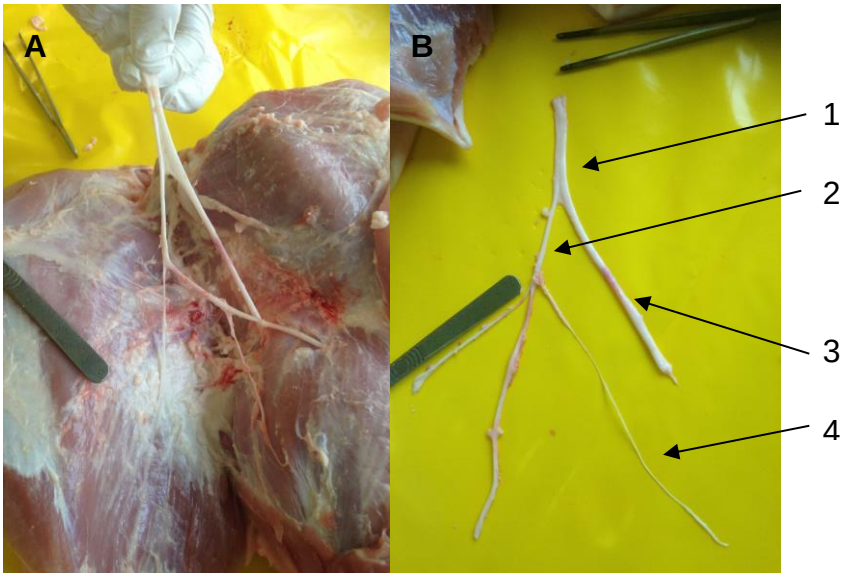

Figure 2-1 Dissection of porcine nerve architecture

Images showing (A) the nerve architecture partially dissected from porcine hind leg and (B) the dissected major nerve architecture. Different levels of anatomical hierarchy can be identified. Most superior is (1) the sciatic nerve, running down to its bifurcation into the branches of (2) the common peroneal nerve and (3) the tibial nerve. The most inferior branch which can be observed is (4) the sural nerve.

2.10 Decellularisation of porcine peripheral nerves

2.10.1 Preparation of solutions for decellularisation

2.10.1.1 Phosphate Buffered Saline (PBS)

Ten PBS tablets were dissolved in 1 L of distilled water using a magnetic stirrer bar. The pH of the solution was adjusted to 7.2 - 7.4 using 6 M sodium hydroxide (NaOH) or 6 M hydrochloric acid (HCl).

2.10.1.2 Disinfection solution

Stock solutions of the antibiotics vancomycin hydrochloride, gentamicin sulphate and polymyxin B were added to 100 ml of PBS and mixed using a magnetic stirrer bar (required concentrations and volumes given in Table 2-1). The pH of the solution was adjusted to 7.2 - 7.4 using 6 M NaOH or 6 M HCl, and the solution made up to 1 L with sterile PBS.

Table 2-1 Reagent concentrations for antibiotic wash solution

Antibiotic	Working Concentration	Stock concentration	Volume of stock
Vancomycin hydrochloride	0.05 $mg.ml^{-1}$	10 $mg.ml^{-1}$	5 ml
Gentamicin sulphate	0.5 $mg.ml^{-1}$	100 $mg.ml^{-1}$	5 ml
Polymyxin B	0.2 $mg.ml^{-1}$	50 $mg.ml^{-1}$	4 ml

Working concentrations, stock concentrations and required volumes of stock solution of antibiotics for 2 L of disinfection solution.

2.10.1.3 EDTA solution (200 mM EDTA)

EDTA solution was produced by dissolving 74.4 g EDTA in 900 ml of distilled water using a magnetic stirrer bar. The pH of the solution was adjusted to 7.2 - 7.4 by the addition of 6 M NaOH or 6 M HCl, and the solution was made up to a final volume of one litre using distilled water.

2.10.1.4 Hypotonic buffer solution (10 mM tris, 2.7 mM EDTA, 10 $KIU.ml^{-1}$ aprotinin)

Hypotonic buffer solution was produced by dissolving 1.21 g trizma base and 1 g EDTA in 900 ml of distilled water using a magnetic stirrer bar. The pH of the solution was adjusted to 8.0 - 8.2 by the addition of 6 M NaOH or 6 M HCl, and the solution was made up to a final volume of one litre using distilled water. Aprotinin (10,000 $KIU.ml^{-1}$) was added immediately before use; 1 ml was added per litre of solution.

2.10.1.5 Hypotonic buffer solution containing 0.1 % (w/v) SDS (10 mM tris, 2.7 mM EDTA, 10 $KIU.ml^{-1}$ aprotinin)

Sodium dodecyl sulphate (SDS; 10 %; w/v; 10 ml) was added aseptically to 990 ml hypotonic buffer solution (produced as described in section 3.2.1.1.4), to give a working concentration of 0.1 % (w/v). Aprotinin (10,000 $KIU.ml^{-1}$) was added immediately before use; 1 ml was added per litre of solution. The solution was mixed by inversion and used immediately.

2.10.1.6 PBS-EDTA solution (2.7 mM EDTA, 10 $KIU.ml^{-1}$ aprotinin)

PBS-EDTA solution was produced by dissolving ten Oxoid PBS tablets and 1 g EDTA in 900 ml of distilled water using a magnetic stirrer bar. The pH of the

solution was adjusted to 7.2 - 7.4 using 6 M NaOH or 6 M HCl, and the solution was made up to a final volume of one litre using distilled water. Aprotinin (10,000 $KIU.ml^{-1}$) was added immediately before use; 1 ml was added per litre of solution.

2.10.1.7 Nuclease solution (50 mM tris, 1 mM $MgCl_2.6H_2O$, 1 $U.ml^{-1}$ Benzonase)

Nuclease buffer solution was produced by dissolving 6.1 g trizma base and 0.203 g magnesium chloride in 100 ml of distilled water using a magnetic stirrer bar. The pH of the solution was adjusted to 7.5 - 7.7 using 6 M NaOH or 6 M HCl, and the solution was made up to a final volume of one litre using distilled water.
Benzonase stock solution (4 µl, stock concentration 250 $U.µl^{-1}$) was added to the solution immediately prior to use, and mixed gently by inversion.

2.10.1.8 Hypertonic buffer solution (50 mM tris, 1.5 M sodium chloride)

Hypertonic buffer solution was produced by dissolving 87.66 g sodium chloride and 6.06 g tris in 900 ml of distilled water, using a magnetic stirrer bar. The pH of the solution was adjusted to 7.5 - 7.7 using 6 M NaOH or 6 M HCl, and the solution was made up to a final volume of one litre using distilled water.

2.10.2 Decellularisation process

The method detailed here illustrates the final iteration of the deceullarisation process, resulting from several rounds of optimisation. With the exception of Chapter 3, which describes the optimisation process, the decellularised tissue used for the work described here was produced according to this method. With the exception of the initial dissection and antibiotic wash steps, all changes of solution were carried out under aseptic conditions in a laminar flow cabinet.
Dissected porcine peripheral nerves (sciatic [Chapter 3 only], tibial and peroneal) were thawed and cut into segments approximately 1.5 - 3 cm in length. All washes (with the exception of the Benzonase step) were with agitation, at a speed of 110 rpm. Nerve segments were washed for 30 minutes in an antibiotic cocktail (0.05 $mg.ml^{-1}$ vancomycin hydrochloride; 0.5 $mg.ml^{-1}$ gentamycin sulphate; 0.2 $mg.ml^{-1}$ polymyxin B) at 37 °C. Each segment was washed using in 200 mM EDTA (pH 7.2 - 7.4) at 4 °C for 24 hours. Nerve segments were subject to washes in a hypotonic buffer (10 mM Tris-HCL; 2.7 mM EDTA; 10 $KIU.ml^{-1}$ aprotinin; pH 8.0

- 8.2) and hypotonic buffer with the addition of SDS at a concentration of 0.1 % (w/v) for 24 hours each at 42 °C. The nerve segments were then subjected to three 30 minute washes in PBS, and incubated in PBS for 16 hours at 42 °C. Each segment was washed using PBS-EDTA solution (2.7 mM EDTA; 10 $KIU.ml^{-1}$ aprotinin; pH 7.2 - 7.5) for 48 - 72 hours at 4 °C, before being incubated in a buffer solution (50 mM Tris; 1 mM $MgCl_2$; pH 7.5 - 7.7) containing Benzonase (1 $U.ml^{-1}$) at 37 °C for two periods of three hours with agitation (50 rpm). Nerve segments were then washed in PBS for 16 hours, then washed in hypertonic buffer (50 mM Tris; 1.5 M NaCl; pH 7.5 - 7.7) for 24 hours (both at 42 °C). A series of three washes in PBS at 42 °C were then carried out for 30 minutes each. Decellularised nerve segments were stored in PBS at 4 °C for up to three months.

2.10.3 Sterilisation of decellularised nerves

A range of sterilisation methods were applied to the decellularised nerve segments during the course of this work; the specific methods and conditions used are described here.

2.10.3.1 PAA

2.10.3.1.1 Solution

2.8 ml of 36 – 40 % (v/v) PAA was added to 800 ml of distilled water and mixed using a magnetic stirrer bar. The pH of the solution was adjusted to 7.2 with 12M HCl, and the volume was adjusted to one litre through the addition of distilled water. The solution was used within one hour of preparation.

2.10.3.1.2 Method

Groups of decellularised nerve segments (n = 30) were incubated in 0.1 % (v/v) PAA solution (pH 7.2 - 7.5) at room temperature for three hours at room temperature with agitation (110 rpm). Each nerve segment was subsequently washed three times in PBS (pH 7.4) at 42 °C for 30 minutes each.

2.10.3.2 Gamma radiation

Groups of decellularised nerve segments (n = 30) were suspended individually in 3 ml PBS (pH 7.4) within polystyrene bijou tubes. The decellularised nerves were gamma irradiated at a dose level of 25 kGy (range 25 - 28 kGy) (Dalton

Nuclear Institute, University of Manchester). The internal temperature of the irradiation chamber did not exceed 35 °C.

2.10.3.3 E Beam

Groups of decellularised nerve segments (n = 30) were suspended individually in 3 ml PBS (pH 7.4) within polystyrene bijou tubes and treated with an E Beam (Synergy Health, STERIS). The administered dose level was approximately 33 - 37 kGy.

2.10.3.4 $SCCO_2$

Decellularised nerve segments (n = 30) were packaged individually in polystyrene tubes and placed in the Nova2200™ $SCCO_2$ reaction chamber (NovaSterilis Inc, NY, USA). NovaKill™ proprietary additive (4 ml; 13.5 - 18.5 % [v/v] PAA and 4.5 - 6 % [v/v] H_2O_2) was added to a cellulose pad within the chamber and 25 ml of water was sprayed into the vessel. CO_2 was injected into the chamber to reach a set pressure of 1,436 PSI and the temperature was held at 35 °C. These conditions were maintained for three hours before the CO_2 was released from the chamber. Sterile PBS (pH 7.4) was then added to the tubes aseptically prior to shipping.

2.10.3.5 Positive control

2.10.3.5.1 Solution

NaOH (40 g) was added to 250 ml of distilled water, and mixed using a magnetic stirrer bar until dissolved.

2.10.3.5.2 Method

Groups of decellularised nerve segments (n = 3) were incubated in 100 ml of 1 M NaOH at room temperature for 12 hours; the nerve segments were subsequently washed three times in PBS for one hour each. Samples were stored in PBS (pH 7.4) at 4 °C.

2.11 Histology

2.11.1 Fixation and processing of native and decellularised tissue samples

Tissue samples for histology were trimmed to 9 - 10 mm using a scalpel and placed inside a histology cassette. All samples were fixed and processed using a Leica TP1020 processor using a predetermined protocol (Table 2-2).

Table 2-2 Tissue processing protocol
List of reagents and incubation times used during the fixation and wax embedding of porcine peripheral nerve segments.

Station	Solution	Duration (hours)
1	10 % (w/v) neutral buffered formalin	1
2	70 % (v/v) alcohol	1
3	90 % (v/v) alcohol	1
4	100 % (v/v) alcohol	0.5
5	100 % (v/v) alcohol	1
6	100 % (v/v) alcohol	1
7	100 % (v/v) alcohol	1
8	Xylene; 100 % (v/v)	1
9	Xylene; 100 % (v/v)	1
10	Xylene; 100 % (v/v)	1
11	Molten wax	1
12	Molten wax	1

2.11.2 Microtomy

Paraffin wax embedded samples were sectioned using a Leica RM2255 microtome at a thickness of 5 µm. The sections were floated onto glass slides. The temperature of the water bath was held at 30 °C as opposed to the conventional 56 °C, due to an observed loss of tissue integrity at higher temperatures. Slides were dried overnight at room temperature.

2.11.3 Dewaxing and rehydration

Samples were immersed in two changes of xylene for ten minutes each for dewaxing and rehydrated by three successive washes in 100 % (v/v) ethanol and a single wash in 70 % (v/v) ethanol (three, two, two and two minutes in length respectively), and immersion for three minutes in running water.

2.11.4 Dehydration and mounting

Sections were immersed in 70 % (v/v) ethanol (five seconds), before successive immersions in 100 % (v/v) ethanol for periods of two minutes each. Sections were then immersed twice in xylene for ten minutes each, and mounted using Distyrene Plasticiser Xylene (DPX) mountant. All sections were allowed to air dry overnight in a fume cabinet.

2.11.5 Haematoxylin and eosin staining

Dewaxed rehydrated sections were immersed in Mayer's haematoxylin for one minute and rinsed in tap water until running clear. Sections were then immersed consecutively in Scott's tap water and eosin for three minutes each. Sections were dehydrated, mounted and visualised using Köhler illumination.

2.11.6 DAPI staining

Sections were stained with DAPI (4',6-diamino-2-phenylinole) to reveal the presence and distribution of double stranded DNA. DAPI working solution (concentration 0.1 $\mu g.ml^{-1}$) was made up immediately prior to use by addition of 20 µl DAPI dye to 200 ml PBS. Dewaxed, rehydrated sections were immersed in DAPI working solution for ten minutes in darkness. The sections were subsequently washed three times in PBS in darkness, then mounted using DAKO fluorescent mounting medium. The slides were allowed to dry at room temperature overnight in darkness, and stored at 4 °C prior to imaging. Sections were viewed and imaged using a DAPI filter and fluorescent illumination.

2.11.7 Sirius red and Miller's Elastin

2.11.7.1 Solutions

5 % (w/v) potassium permanganate: 15 g of potassium permanganate was added to 300 ml of distilled water and mixed using a magnetic stirrer bar. The solution was filtered before use.

1 % (w/v) oxalic acid: 1 g of oxalic acid was added to 100 ml of distilled water and mixed using a magnetic stirrer bar. The solution was used immediately.

Weigerts haematoxylin: Equal volumes of solution A and solution B were mixed by gentle agitation and used immediately.

1% acid alcohol (1% concentrated Hydrochloric Acid in 70% Ethanol): 5ml of concentrated HCl was added to 495 ml of 70 % (v/v) ethanol.

0.1 % (w/v) Sirius red: 0.1 g Sirius red was added to 100 ml of aqueous saturated picric acid solution and mixed using a magnetic stirrer bar. The solution was filtered before use.

2.11.7.2 Methods

Tissue sections were stained for the presence of collagen and elastin using Sirius red and Miller's stain. Dewaxed, rehydrated sections were immersed in 5 % (w/v) potassium permanganate for five minutes and washed in distilled water. Tissue sections were then immersed in 1 % (w/v) oxalic acid for two minutes and washed in distilled water for two separate periods of one and four minutes respectively. Sections were immersed sequentially for periods of one minute in 70 % (v/v) and 95 % (v/v) ethanol, and then subjected to treatment with Miller's stain for one hour. Each section was rinsed in 95 % (v/v) ethanol until running clear, then in 70 % (v/v) ethanol for one minute and running tap water for two minutes. Sections were stained in Weigert's haematoxylin for ten minutes, then washed in water and 1 % (v/v) acid alcohol for one minute each, and rinsed in distilled water for 30 seconds. Sections were immersed in 0.1 % (w/v) picrosirius red for one hour, before excess stain was removed by rinsing with distilled water. Sections were dried by blotting, dehydrated and mounted. Sections were visualised using both Köhler and circularly polarised illumination.

2.11.8 Immunohistochemistry

Immunohistochemistry was used to locate the presence of specific ECM components in sections of porcine peripheral nerves.

2.11.8.1 Solutions

PBS: PBS was made up as described in 2.10.1.1.

H_2O_2 solution (3 %; v/v): 20 ml of H_2O_2 solution (30 %; v/v) was added to 180 ml of PBS. The solution was mixed gently and used immediately.

10x TBS: 24 g of Trizma base and 88 g of NaCl were dissolved in 700 ml of distilled water, and mixed using a magnetic stirrer bar. The pH of the solution was adjusted to 7.6 with 12 M HCl, and the volume was adjusted to one litre through the addition of distilled water.
1x TBS (20 mM Tris, 150 mM NaCl): 100 ml of 10x TBS was added to 900 ml of distilled water, and mixed using a magnetic stirrer bar.
TBS containing 0.05 % (w/v) Tween 20 (TBS-T): 500 µl of Tween 20 was added to one litre of TBS and mixed using a magnetic stirrer bar. The pH of the solution was adjusted to 7.6 using 6 M NaOH or 6 M HCl.
BSA solution (5 %; w/v BSA): 2.5 g bovine serum albumin was dissolved in 50 ml PBS using a magnetic stirrer bar. The solution was passed through a 0.2 µm filter into a sterile collection container in a class II cabinet.
Antibody diluent (TBS, 0.1 % (w/v) BSA, 0.1 % (w/v) sodium azide): 6 ml sodium azide (1%) , 300 µl 5 % (w/v) bovine serum albumin and 40 ml TBS were mixed together using a magnetic stirrer bar. The pH of the solution was adjusted to 7.6 using 6 M NaOH or 6 M HCl, and the volume made up to 60 ml with TBS.
Scott's tap water substitute (1x): 50 ml of Scott's tap water 10x solution was added to 450 ml of distilled water.

2.11.8.2 Horseradish peroxidase (HRP) Method

Sections of porcine liver were included as a positive control, negative (diluent) and isotype controls were also carried out. Reagents from the Ultravision One immunohistochemistry kit were used for immunohistochemistry. Dewaxed, rehydrated sections were subjected to antigen retrieval by incubation in proteinase K solution (DAKO) for 20 minutes at room temperature. Each section was immersed in 3 % (v/v) hydrogen peroxide in PBS for ten minutes, and rinsed under running tap water for three minutes. The sections were then washed twice using Tris-buffered saline (TBS; pH 7.6) with gentle agitation for ten minutes. Each section was drawn around using an ImmEdge hydrophobic marker pen. Sections were blocked by application of 25 µl of endogenous enzyme block and incubated at room temperature for ten minutes. Sections were subjected to two further washes of ten minutes each in TBS with gentle agitation. Sections were incubated in primary antibody (diluted to working concentration using antibody diluent (TBS, 0.1 %; w/v BSA, 0.1 %; w/v sodium azide; pH 7.6) for 60 minutes at room temperature. Each section was washed twice using Tris-buffered saline

containing 0.05 % (w/v) Tween 20 (TBST) with gentle agitation, followed by two additional ten minutes washes in TBS. HRP polymer was then added and the sections incubated for 30 minutes in the dark. Each section was washed using two ten minute washes in each of TBST and TBS respectively. Substrate DAB chromagen was added in aliquots of 25 - 50 µl per section, and the sections were incubated for ten minutes at room temperature. The sections were each washed four times in distilled water, then incubated in haematoxylin for ten seconds. Sections were rinsed in tap water until excess stain was removed, and immersed in Scott's tap water for ten minutes. Each section was rinsed in tap water for three minutes, dehydrated and mounted. Sections were visualised using Köhler illumination.

2.11.8.3 Immunofluorescent Method

Initial processing (including antigen retrieval and incubation with the primary antibody) were conducted as described in section 2.11.8.2. Fluorescent secondary antibodies, diluted to an appropriate concentration in antibody diluent, were added to each section. Sections were then incubated in a humidified chamber in conditions of darkness for 30 minutes at room temperature. Each section was washed for two ten minute periods in each of TBST and TBS respectively, all under conditions of darkness. The sections were incubated in DAPI working solution for one minute. Each section was rinsed in PBS three times in darkness, and mounted using fluorescent mounting medium. Sections were visualised and imaged using a DAPI filter and fluorescent illumination.

2.12 Cytotoxicity testing

2.12.1 Cell culture media

Baby hamster kidney (BHK) cells were cultured in Glasgows Modified Eagles Medium (GMEM), containing 5 % (v/v) foetal bovine serum (FBS), 10 % (v/v) tryptone phosphate broth (TPB), 100 $\mu g.ml^{-1}$ penicillin-streptomycin and 2 mM L-glutamine.

L929 cells were cultured in Dulbecco's Modified Eagle Medium (DMEM), containing 10 % (v/v) FBS, 100 $\mu g.ml^{-1}$ penicillin-streptomycin and 2 mM L-glutamine.

2.12.2 Resurrection and culture cells from cryostorage

Vials of cells were removed from cryostorage in liquid nitrogen. The cell pellets were thawed rapidly in a water bath at 37 °C and transferred in a class II environment to individual sterile universal tubes. Culture media (10 ml) was added drop wise to each universal, before centrifugation at 150 x g for ten minutes. The supernatant was discarded, the cells resuspended in 5 ml of specific culture medium and transferred into a T75 flask. The cells were incubated at 37 °C in an atmosphere of 8 % (v/v) CO_2 in air. The culture medium was changed 24 hours after revival, then every 48 - 72 hours. Cells were passaged once they were observed to be 80 % confluent.

2.12.3 Cell passaging

Upon reaching 80 % confluence, the medium was aspirated from the culture flask, and the cell layer washed twice in PBS (without magnesium or calcium). The PBS was discarded and 3 ml trypsin/EDTA was added, and the flask incubated for five minutes at 37 °C with 8 % (v/v) CO_2 in air. The cells were carefully dislodged by tapping and 10 ml of culture medium was added. The total volume present in the flask was transferred to a universal tube and centrifuged at 150 g for ten minutes. The supernatant was discarded, and the cells suspended in 1 ml of medium. The cells were counted and viability determined with Trypan blue. Cell suspension and Trypan Blue (20 µl each) were mixed, and 10 µl was added to a haemocytometer. The number of viable cells per grid was then determined, and the total number of cells ml^{-1} calculated using the equation below:

$$Number\ of\ viable\ cells.mL^{-1} = \frac{number\ of\ viable\ cells}{n}\ x\ 10^4\ x\ Dilution\ factor$$

The cell suspension was then diluted as appropriate and seeded to a T 75 flask and incubated at 37 °C in an atmosphere of 8 % (v/v) CO_2 in air.

2.12.4 Contact cytotoxicity assay

This assay was carried out using two distinct cell types (BHK and L929 cells). Triplicate samples of decellularised peripheral nerve (5 mm^2) were dissected, placed in to individual wells of a six well plate and secured using Steri-Strips. A positive control was provided by the addition of a droplet of cyanoacrylate to a separate culture well on each plate. A Steri-Strip was added to another well, to act as a negative control. Each well was seeded with cells a density of 5 x 10^6

cells in 2 ml of media. The plates were incubated at 37 °C, in an atmosphere of 8 % (v/v) CO_2 in air, for hours. After 48 hours in culture, the cells in each well were observed using phase contrast microscopy and images captured digitally. Any changes in cell morphology were noted. The medium was aspirated from each well, and the plates washed twice in PBS (without calcium or magnesium) and the cell layer fixed for ten minutes using 10 % (v/v) Neutral Buffered Formalin (NBF). After the NBF was removed, Giemsa stain was added to each well and the plates were incubated for a further five minutes. The plates were washed in gently running tap water. Stained cell sheets were viewed using Köhler illumination and images captured digitally.

2.13 Uniaxial tensile testing

Samples of peripheral nerve from each test group were subject to uniaxial tensile testing to failure using an Instron 3365 machine equipped with a 5 kN load cell. Segments of peripheral nerve were cut to approximately 30 mm in length, and the width and thickness of each determined using callipers and a thickness gauge. The nerve segments were mounted in indented grips, using a baseplate to ensure a gauge length of 10 mm was maintained (Figure 2-2). Paper towel was used to prevent slippage of the tissue during testing. The grips were then attached to the Instron housing in a tension free manner and subject to a single ramp-to-failure tensile test, at a strain-rate of 10 $mm.minute^{-1}$. The maximum load each sample sustained was recorded and used (in conjunction with the measured cross sectional area) to calculate the ultimate tensile strength, and the gradient of the slope in the linear region of the stress-strain curve was used to define the Young's Modulus (Figure 2-3). If the tissue sample was observed to slip within the grip (s) or fail at the grip, the data from the sample was considered void.
It was not possible to shape the nerves into standard sizes for testing, due to the heterogeneity of nerve ECM structure and the differing contributions of the structures in nerve ECM to mechanical properties. Therefore, a method to measure the dimensions of the nerve samples without resizing was developed. However, due to the inherent inaccuracies which these restrictions could introduce to the calculation of cross-sectional area, maximum load and stiffness were also considered during the course of this study, as measures of

mechanical properties which could be determined independent of the physical dimensions of the tissue.

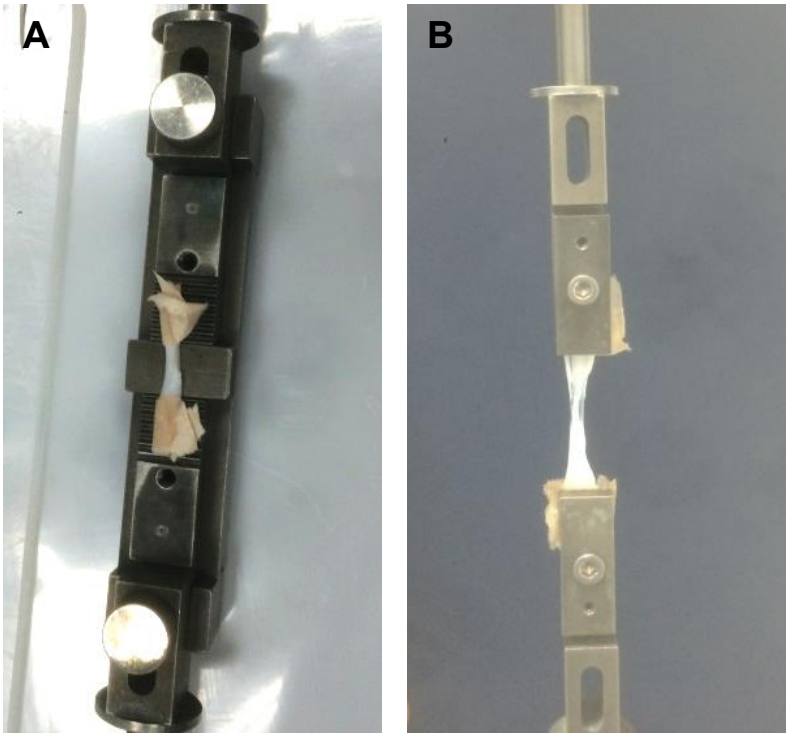

Figure 2-2 Uniaxial tensile testing of peripheral nerves.

Images show (A) peripheral nerve segment in the process of mounting onto tensile grips (mounted on baseplate) and (B) peripheral nerve sample at point of failure during tensile test.

$F = force\ applied$

$A = cross\ sectional\ area$

$L = sample\ length$

$\Delta L = change\ in\ length$

$E = Young's\ Modulus$

$k = stiffness$

$$Stress = \frac{F}{A}$$

$$Strain = \frac{\Delta L}{L}$$

$$E = \frac{F/A}{\Delta L/L} \times 10^{-6}$$

$$k = \frac{F}{\Delta L}$$

Figure 2-3 Formulas used to calculate mechanical properties of peripheral nerve segments.

The formulas displayed were used to calculate stress, strain, Young's Modulus and stiffness of the peripheral nerves.

2.14 Biochemical characterisation

2.14.1 Lyophilisation

The wet weight of peripheral nerve samples was determined by triplicate measurements. Samples were transferred to a freeze dryer (Savant ModulyoD) and lyophilised under constant conditions of -50 °C and 0.15 – 0.2 mbar. Repeated measurements of sample weight were taken at 48 hours, and at 24 hour intervals thereafter until a constant weight was achieved. The dry weight of all samples was determined to allow accurate calculation of biochemical constituents.

2.14.2 Acid hydrolysis

Samples of nerve were lyophilised, diced and placed in vented glass test tubes. A volume of 5 ml of 6 M HCl was added to each tube, and the samples were transferred to a benchtop autoclave to conditions of 121 °C and 15 PSI for four hours. Samples were neutralised by the addition of NaOH at varying concentrations.

2.14.3 Quantification of hydroxyproline content

In vertebrates, the amino acid hydroxyproline is mainly found in collagen (though it is also present in elastin). It occurs at a known frequency in the amnino acid sequence of collagen, and therefore the quantification of hydroxyproline within a tissue sample can be used to produce an accurate estimate of collagen content. Quantification was achieved by a colourimetric assay based on the method of Edward's and O'Brien (1980)[250]. Pyrroles formed by oxidation of hydroxyproline react with p-dimethylaminobenzaldehyde to produce a red chromophore which can be measured spectrophotometrically.

2.14.3.1 Solutions

Assay Buffer: Assay buffer was made up by dissolving 13.3 g citric acid, 32 g sodium acetate hydrate, and 9.1 g sodium hydroxide in 3.2 ml glacial acetic acid and 80 ml propan-1-ol using a magnetic stirrer bar. The solution was then made up to 300 ml using distilled water. The pH was adjusted to 6.0 - 6.5 using 6 M NaOH or 6 M HCl.

Chloramine T: This solution was made up for immediate use. 1.41 g of chloramine T was dissolved in 100 ml distilled water using a magnetic stirrer bar.

Ehrlich's reagent: This solution was made up for immediate use. 7.5 g p-dimethylaminobenzaldehyde was added to 30 ml propan-1-ol and 13.4 ml 60 % (v/v) perchloric acid. A volume of 6.6 ml distilled water was added and the solution was mixed with a magnetic stirrer bar.

2.14.3.2 Assay method

Samples of nerve were lyophilized to give a dry weight of approximately 20 mg, and hydrolysed in 5 ml of 6 M HCl (as described in 2.14.1 and 2.14.2 respectively).

Solutions of known concentrations of trans-4-hydroxy-L-proline (0, 2, 4, 6, 8, 10, 15, 20, 25 and 30 $\mu g.ml^{-1}$) were made up, to be used as the basis of a standard curve. Test solutions were diluted at a ratio of 1:20 in assay buffer.

Aliquots (50 µl) of each known standard/sample was added in triplicate to a clear flat-bottomed 96 well plate. Chloramine T solution (100 µl) was added to each well, and the plate was subjected to gentle agitation for five minutes.

Ehrlich's reagent (100 µl) was added to each well, and the plate was incubated at 60 °C in an orbital incubator shaker (no agitation) for 45 minutes. Measurements of optical density were taken for each well containing a standard and sample, at a wavelength of 570 nm.

A curve of absorbance against concentration was plotted for the known standards, and used as a standard curve. The absorbance values for test samples were used to generate interpolated hydroxyproline concentrations. These values were then used in conjunction with the values of tissue mass and dilution factor to calculate the hydroxyproline content of the tissue samples.

2.14.4 Estimation of collagen content from hydroxyproline content

The collagen content of the tissue samples was estimated by extrapolation from the calculated hydroxyproline content. Values produced by Goll *et al* (1963) are widely used to estimate collagen content, based on the ratio of hydroxyproline residues to other amino acids in the primary structure of collagen [251]. The calculated hydroxyproline content of each sample was multiplied by the given factor of 7.52 to give an accurate estimate of collagen content [252].

2.14.5 Quantification of denatured collagen content

Denatured collagen content was determined by a colourimetric assay of solubilised enzyme digestion products. This was enabled by enzymatic digestion with α-chymotrypsin, which selectively digests denatured collagen molecules.

2.14.5.1 Solutions

α-chymotrypsin digest buffer: 1.21 g Trizma base and 0.15 g calcium chloride were dissolved in 100 ml of distilled water using a magnetic stirrer bar. The pH of the solution was adjusted to 7.8 using 6 M NaOH or 6 M HCl.

α-chymotrypsin working solution: Lyophilised α-chymotrypsin was dissolved in the digest buffer using a magnetic stirrer bar, to give a working concentration of 5 $mg.ml^{-1}$.

2.14.5.2 Assay Method

Samples of nerve were diced and lyophilised (as described in 2.14.1) to give a dry weight of approximately 20 - 30 mg. α-chymotrypsin working solution (5 ml) was added to each sample, and the samples were incubated in a water bath for 24 hours at 30 °C. The digested samples were centrifuged at 600 g for ten minutes, and the supernatant (4 ml) was transferred to a sterile glass tube. HCl (4 ml; 6 M) was added to each tube, and the samples were hydrolysed and neutralised as described in section 2.14.2.

The neutralised samples were then subjected to colourimetric assay with P-dimethylaminobenaldehyde as described in section 2.14.3.2 and the denatured collagen content estimated as described in section 2.14.4.

2.14.6 Quantification of GAG content

Sulphated GAG concentration in tissue samples can be calculated from solubilised enzymatic digestion products. A colourimetric assay was used, based on the method described by Farndale et al (1982) [253]. The assay reaction is based upon the metachromasy which is induced when 1,9-dimethylmethylene (dimethylene blue, DMB) interacts with GAGs under acidic conditions.

2.14.6.1 Solutions

Papain digest buffer: 0.788 g L-cysteine hydrochloride and 1.8612 g disodium EDTA were disosolved in 1 L of distilled water using a magnetic stirrer bar. The pH of the solution was adjusted to 6.0 using 6 M NaOH or 6 M HCl.

Papain working solution: Lyophilised papain was dissolved in the digest buffer to give a working concentration of 800 $kU.ml^{-1}$.

0.1 M sodium di-hydrogen orthophosphate: 3.45 g sodium di-hydrogen orthophosphate was dissolved in 250 ml distilled water using a magnetic stirrer bar.

0.1 M di-sodium hydrogen orthophosphate: 3.55 g di-sodium hydrogen orthophosphate was dissolved in 250 ml distilled water using a magnetic stirrer bar.

Assay buffer: 137 ml of 0.1 M sodium di-hydrogen orthophosphate and 63 ml of 0.1 M d-sodium hydrogen orthophosphate were mixed using a magnetic stirrer bar. The pH of the solution was adjusted to 6.8 using 6 M NaOH or 6 M HCl.

DMB Dye solution: 16 mg of DMB was dissolved in 5 ml ethanol and 2 ml formic acid using a magnetic stirrer bar. 2 g of sodium formate was added, and distilled water was added to give a total volume of 1 L. The pH of the solution was adjusted to 3 by the addition of formic acid.

2.14.6.2 Assay Method

Samples of nerve were lyophilised (as described in section 2.14.1) to give a dry weight of approximately 50 mg. Papain working solution (5 ml) was added to each sample. The samples were incubated at 60 °C in an orbital incubator shaker for 36 hours.

Solutions of known concentrations of chondroitin sulphate B (0, 3.125, 6.25, 12.5, 25, 50, 100, 150, 200 $\mu g.ml^{-1}$) were made up in assay buffer, to be used as the basis of a standard curve. Test solutions were assayed neat. Each known standard/sample was added in triplicate 40 µl aliquots to a clear flat-bottomed 96 well plate. DMB dye solution (250 µl) was added to each well, and the plate was subject to gentle agitation for two minutes. Measurements of optical density at a wavelength of 525 nm were taken for each well, using a spectrophotometer.

A standard curve of absorbance against concentration was plotted for the known standards. GAG concentrations were interpolated using the standard curves from average absorbance values. The final GAG concentration was calculated by factoring in tissue mass and any dilution factor.

2.14.7 Quantification of fat content

A colourimetric assay for the quantification of fat in tissue was carried out, based on a protocol developed by Stern and Shapiro (1953)[254]. The assay relies on a reaction between hydroxylamine and esters of fatty acids in solution. The hydroxamic acids formed by this reaction can be quantified by comparison of optical density following reaction with iron (III) chloride.

2.14.7.1 Solutions

Hydroxylamine hydrochloride (2 M): 1.39 g hydroxylamine hydrochloride was added to 10 ml of distilled water and mixed by inversion.

Iron (III) chloride in trichloroacetic acid: 500 mg iron (III) chloride and 3.75 g trichloroacetic acid were added to 5 ml distilled water and mixed by inversion.

2.14.7.2 Assay Method

Samples of nerve were lyophilised (as described in 2.14.1) to give a dry weight of approximately 30 mg. The samples were immersed in 600 µl of ethanol and incubated at 42 °C for 4 hours with agitation. Porcine lard was dissolved in 600 µl of ethanol to give a range of standards of known concentrations (0, 39, 78, 156, 312.5, 625, 1250, 2500 $\mu g.ml^{-1}$). Hydroxylamine hydrochloride and 3.5 M NaOH (100 µl each) were added to each standard/sample. The standards and samples were incubated for 20 minutes at room temperature, before 100 µl each of 4 m HCL and iron (III) chloride were added. Aliquots of each standard or sample (250 µl) were added in triplicate to a clear, flat-bottomed 96 well plate. Measurements of optical density at a wavelength of 540 nm were taken for each well, using a spectrophotometer. A curve of absorbance against concentration was plotted for the known standards, and used as a standard curve. The absorbance values for test samples were used to generate interpolated fat concentrations. These values were then used in conjunction with the values of tissue mass and dilution factor to calculate the fat content of the tissue samples.

2.15 Statistical analysis

Means were compared using the statistical analysis software GraphPad Prism 7. Confidence limits at 95 % ($\alpha = 0.05$) were calculated with a minimum of n=3 using the equation shown (Figure 2-4). The distribution of the data was determined using a Shapiro-Wilk test. If the data were found to follow Gaussian distribution, the difference between two means was determined using a student's t-test, and three (or more) means by one-way analysis of variance (ANOVA; if one independent variable) or two-way ANOVA (if two independent variables). If the data were not found to follow Gaussian distribution, the

difference between two means was determined using a Mann-U Whitney test, and three (or more) means by Kruskal-Wallis. The location of significant differences was determined by Tukey's Honestly Significant Difference test (parametric data) or Dunn's test (non-parametric data). The minimum significant difference (MSD) between two means was defined as p = 0.05. Data was displayed as ± 95 % confidence limits. Linear regression analyses of standard curves, via calculation of the coefficient of determination (r^2), was used to determine the strength of a liner relationship between x and y (with 0 = no relationship and 1 = perfect relationship) and therefore the accuracy of interpolating unknown values via such a regression.

$$\boldsymbol{M = \frac{\sum x}{n}}$$

$$\boldsymbol{St\ Dev = \sqrt{\frac{\sum x^2}{n-1}}}$$

$$\boldsymbol{SEM = \frac{St\ Dev}{\sqrt{n}}}$$

$$\boldsymbol{95\ \%\ confidence\ limits = M \pm t\ x\ SE}$$

$$\boldsymbol{MSD = Q\ (a[k, v])x\ SE}$$

$n = sample\ size$

$M = mean$

$ST\ dev = standard\ deviation$

$SE = standard\ error$

$t = critical\ value$

$MS_w = Mean\ square\ width$

$MSD\ =\ Minimum\ significant\ difference$

$Q\ =\ critical\ value\alpha\ =\ p\ =\ 0.05$

$k\ =\ number\ of\ groups$

$v\ =\ degrees\ of\ freedom\ (n-1)$

Figure 2-4 Selected equations applied for statistical calculations

3 Decellularisation and characterisation of porcine peripheral nerves

3.1 Introduction

3.1.1 Decellularised tissues in regenerative medicine

Decellularised tissues have great potential for use as scaffolds in tissue engineering applications. A major advantage of the use of decellularised tissues in comparison to synthetic graft materials is the inherent similarity to native tissue. The retention of the ECM microarchitecture, biomechanical properties, biochemical composition and chemotrophic cues ensures a native-like microenvironment [255]. A native-like ECM microenvironment can promote cellular infiltration and the retention of tissue-specific phenotypic characteristics [17]. The environmental niche provided by decellularised tissue can also induce the expression of such characteristics in undifferentiated stem cells; this has been demonstrated in adipose-derived stem cells and bone marrow-derived stem cells seeded to segments of decellularised adipose and tendon respectively [256, 257]. The provision of an optimal environment for the promotion of cell infiltration, growth and function is key to facilitating tissue regeneration.

Decellularisation protocols typically mediate the removal of cells and nucleic acids from the tissue, and may be tailored to remove other unwanted ECM components or cellular debris (e.g. the xenoantigen alpha-1,3-galactose) which may stimulate an adverse immune response [36]. It can be hypothesised that the removal of these major sources of foreign antigens from the tissue maximises the chance of successful graft integration and restoration of function [130].

The widely used criteria for the removal of immunogenic material are based upon data presented by Crapo et al (2011) [131]. The guidelines proposed include a total of less than 50 ng of double stranded DNA (dsDNA) per mg of tissue (dry weight), no fragments of DNA greater than 200 base pairs in length, and no nuclei visible when tissue is stained with haematoxylin and eosin (H & E). These criteria are based upon evidence suggesting that the extent of the

host immune response can be directly linked to the concentration of DNA present in a scaffold [258]. Although the presence of residual DNA in decellularised tissues is associated with an adverse immune response, in isolation DNA is only thought to induce some localised calcification [259]. Gilbert et al (2012) found quantifiable levels of DNA in eight commercially available ECM-based scaffolds [260]. Histological examination of scaffolds derived from porcine intestinal submucosa and porcine urinary bladder basement membrane and mucosa also revealed visible nuclear remnants and whole nuclei. Individual studies into each scaffold showed good clinical efficacy, indicating that the degree of host response induced by such materials is not sufficient to negatively affect function of the scaffold. Instead, it is thought that the proposed relationship between the measured DNA content and host response to decellularised material is primarily due to the relative levels of other cellular debris [134]. If DNA is retained following decellularisation, it is highly likely that other debris such as membrane phospholipids (together with associated integral proteins/glycoproteins) are also retained [260]. Membrane fragments, cytoplasmic proteins and other cellular debris represent a source of important foreign antigens (e.g. alpha 1,3-galactose, major histocompatibility complex I) [261]. It may be beneficial, depending on the tissue type and donor source, to demonstrate the elimination of specific antigens during the development of a novel decellularisation process (e.g. alpha 1,3-galactose in porcine aortic valves) [262]. The criteria presented by Crapo et al therefore represent a guideline rather than a required standard for decellularisation, and parameters such as percentage DNA reduction are instead used as predictive indicators of the likely host response [263].

3.1.2 Methods of decellularisation

Since decellularisation was first proposed as a potential method for producing alternative graft materials, research has focused on the identification of an optimal method for the lysis and removal of cells and other immunogenic material. Such decellularisation techniques can be classified into the distinct sub-categories of physical, chemical and enzymatic methods. It is common for decellularisation protocols to utilise a number of techniques in combination to maximise the removal of immunogenic material whilst minimising alterations to the properties of the scaffold.

3.1.2.1 Chemical methods

3.1.2.1.1 Detergents

Detergents are surfactants, with a hydrophilic head region and a hydrophobic tail. Detergents are powerful agents of decellularisation, able to integrate within the phospholipid bi-layer of the cell membrane [264]. This process eventually induces the formation of micelles and ultimately leads to cell lysis. Detergents are also able to mediate the detachment of nucleic acids from ECM proteins following cell lysis, reducing the potential immunogenicity of the scaffold. The concentration of detergent used is key to enabling these beneficial effects without causing significant disruption to the biochemical composition, structure and material properties of the ECM [265]. Ferng et al (2017) demonstrated that the use of SDS at a concentration of 3 % (v/v) to decellularise porcine hearts resulted in no measurable decrease in Young's Modulus [266]. However, the use of SDS at concentrations of 5 % and 10 % caused reductions in Young's Modulus of approximately 20 % and 90 % respectively; reductions of such a magnitude would have negative implications for the functionality of the tissue. Scanning electron microscopy was used by Oliveira et al (2013) to demonstrate superior retention of ECM structures murine small intestine was decellularised with Triton-X at a concentration of 0.1 % (v/v) as opposed to 0.3 % or 0.6 % [267].

Detergents can be classified according into three categories: ionic, non-ionic and zwitterionic.

Ionic detergents are those in which the head group is either positively or negatively charged (cationic or anionic respectively). They are effective decellularisation agents, acting by disrupting non-covalent protein-protein, protein-lipid and lipid-lipid interactions [268]. However, the concentration of detergent used is proportional to the level of disruption/damage to, and/or denaturation of, ECM proteins. For example, SDS is an anionic detergent which is highly effective at disrupting membranes and facilitating the removal of both phospholipid and protein components, but is also known to significantly reduce the collagen and GAG content of decellularised scaffolds if used at high concentrations or for extended periods of time [269]. Protein denaturation is

mediated through single molecules of SDS binding to hydrophobic regions of a protein between alpha helices [270]. This provides a “nucleation site” enabling further SDS molecules to bind, a process which leads to micelle formation, the disruption of non-covalent linkages and unfolding of the tertiary structure. The ability of SDS to unfold higher-order protein structures, enabling denaturation of cellular proteins and ECM components, is further evidenced by its application in a range of protein identification assays [271]. One example is SDS polyacrylamide gel electrophoresis (SDS-PAGE), in which SDS is used to solubilise and unfold proteins and thereby enable identification according to size.

Non-ionic detergents, such as Triton X-100, have no overall charge at the head region (which is therefore hydrophilic) [272]. Non-ionic detergents do not disrupt protein-protein interactions, and therefore induce lower levels of denaturation relative to ionic detergents. However, studies comparing decellularisation protocols for rat aortic valves and porcine carotid arteries indicated that treatment with Triton X-100, even at relatively high concentrations (e.g. 5 – 10 %), is inferior in terms of nuclei and DNA removal compared to treatment with SDS [273, 274]. A combination treatment of 0.05 % trypsin and 5 % Triton X-100 was able to sufficiently eliminate nuclei in the rat aortic valves, but lead to widespread disruption of the ECM ultrastructure. Dense tissues such as bone, cartilage, blood vessel and kidney may be able to withstand more robust SDS-based protocols than more delicate tissues such as cornea, and may require such protocols due to the increased difficulty of cell and nucleic acid removal [17]. The use of concentration Triton X-100 may be more appropriate for more delicate tissues such as cornea [275].

Zwitterionic detergents have a net neutral charge, effectively disrupt protein-protein interactions and exhibit properties of both ionic and non-ionic detergents [265]. They are less potent as agents of decellularisation in relative terms, and are mainly employed in thinner/ more delicate tissues where the use of ionic or non-ionic detergents may cause significant disruption to the ECM integrity [276, 277]. The most commonly used zwitterionic detergent in decellularisation processes is 3-[(3-Cholamidopropyl)dimethylammonio]-1-propanesulfonate (CHAPS). CHAPS has been used to successfully decellularise lung tissue from several species including rat, pig and human,

whilst preserving ECM structures and mechanical properties better than SDS [277, 278]. However, Ferng et al (2017) showed that intact nuclei were still present in porcine heart tissue after treatment with CHAPS, indicating incomplete decellularisation [266].

Failure to sufficiently eliminate detergents from tissue can lead to post-production degradation of the ECM, and cytotoxic effects following implantation [279].

3.1.2.1.2 Buffer solutions

Hypotonic and hypertonic buffer solutions are commonly used in decellularisation protocols to alter osmotic pressure [17]. Whilst treatment with such buffer solutions in isolation is typically sufficient to cause cell lysis, they are commonly used in combination with other decellularisation agents (e.g. detergents) to increase efficacy and ensure the removal of cellular debris. Hypertonic buffer solutions are also employed for their ability to dissociate any DNA-protein complexes remaining within the tissue [280].

3.1.2.1.3 Other chemical agents

Low concentrations of PAA have been successfully used to decellularise tissues such as subintestinal mucosa and bladder through oxidation of membrane components and denaturation of intracellular nucleic acids. However, mass spectrometric data from murine lungs treated with PAA suggested that denaturation/degradation of major ECM components including collagens type I, IV and VI and laminin had occurred, the most likely mechanism for which is oxidative damage [242]. Syed *et al* were able to successfully decellularise porcine small intestinal submucosa using a 12 hour incubation in 0.1 % (v/v) PAA, but the treatment induced significant increases in Young's Modulus and yield stress, and a significant decrease in the failure strain, compared to untreated tissue [281]. PAA can also be used in conjunction with other reagents to aid in decellularisation; Rosario *et al* (2008) found that treatment of porcine bladder with 0.1 % (v/v) SDS followed by 0.1 % (v/v) PAA enabled the production of a fully decellularised matrix with no apparent adverse effects to the mechanical properties, structure or the attachment and growth of primary stromal cells [282].

Compounds capable of chelating metal ions (in particular ethylenediaminetetraacetic acid (EDTA)) are commonly used in decellularisation processes (in combination with other reagents e.g. detergents) [283]. Chelating agents enable the disruption of interactions between cell adhesion molecules and the ECM by chelating ions (e.g. Mg^{2+}, Ca^{+}) necessary for adhesions through key cell attachment molecules such as integrins [284]. The process of decellularisation carries an inherent risk of scaffold damage due to the activity of proteolytic lysosomal enzymes, which are released upon cell lysis [17, 285, 286]. The chelation of metal ions inhibits the activity the activity of matrix metalloproteases (MMP's), thereby limiting enzymatic damage to the matrix following cell lysis [287]. For similar reasons the small polypeptide aprotinin is often added to solutions of decellularisation agents in order to competitively inhibit serine proteases, preventing degradation of the ECM [288].

3.1.2.2 Enzymatic methods

The primary advantage of the use of enzymes in decellularisation is the specificity of their site of action, and they are therefore most commonly employed to mediate highly targeted destruction and/or removal of undesirable tissue components [17]. Nucleases are commonly used to degrade nucleic acids, which often remain following cell lysis by chemical or physical methods. Endonucleases (such as Benzonase) are considered to be superior for this function as they are able to cleave nucleotide sequences from within, in comparison to exonucleases which systemically remove nucleotides from the ends [289].

Proteases, such as trypsin, have been considered for use as the sole agent of decellularisation [17]. However, the relatively high enzyme concentration and long incubation time required to mediate a full cell removal will also typically cause a significant reduction in the concentrations of ECM components such as collagen and elastin, and lead to a major alteration in the mechanical properties of the scaffold in particular [290, 291]. Treatment with a lower concentration of trypsin has been successfully employed as an initial decellularisation step, to mediate detachment of cells and better diffusion of reagents in tissues with relatively dense ECM [292]. The addition of tryspin treatment to decellularisation protocols based on treatment with other reagents such as EDTA, SDS or Triton

X-100 led to more complete decellularisation in harder tissues such as human auricular cartilage, porcine trachea and porcine articular cartilage [293].

3.1.2.3 Physical methods

The repetitive application of freeze-thaw cycles in solution is an effective mechanism of cell lysis and mediates increased tissue porosity, enabling better diffusion of reagents [294]. Freeze-thaw can be carried out by snap freezing tissue in liquid nitrogen (to minimise the formation of large ice crystals) or by controlled rate freezing to minus 20 °C, followed by a controlled thawing process [295]. Whilst freeze-thaw has been successfully applied in the decellularisation of tissues such as cartilage, liver and lung, ice crystal formation may induce adverse alterations to the microarchitecture and mechanical properties of the resulting scaffolds [296]. The suitability of freeze-thaw is therefore highly dependent upon the degree to which such alterations may affect the capacity of a given decellularised tissue to effectively support regeneration. Tissues for which the main function is mechanical in nature (e.g. cartilage, tendon) are thought to be able to best withstand this process [17].

Physical methods are typically used as an element of a decellularisation process rather than in isolation. Similarly to the application of freeze-thaw, processes such as agitation and sonication are commonly employed to increase the rate of diffusion of chemical/enzymatic agents through the tissue and to aid the passage of cellular debris out of the tissue [17]. The intensity of such processes must be adjusted according to tissue type, as excessive agitation speed/sonication frequency can lead to disruption of the ECM microarchitecture (with potentially negative implications for cell infiltration and migration). For example, a study by Montoya and McFetridge (2009) found that rotary agitation at 100 rpm gave a two-fold greater yield of soluble hydroxyproline in comparison to a convective flow technique when decellularising human umbilical veins [297]. This indicated that a greater degradation of the key structural ECM component collagen was induced by the rotary agitation, and that better preservation of the collagenous ECM could be achieved through the application of the convective flow method.

3.1.3 Application of Leeds decellularisation process to porcine peripheral nerves

A collaborative partnership between the University of Leeds and the University of Sheffield resulted in the development of a decellularisation process for use with porcine peripheral nerves [58]. The key reagents are EDTA, SDS, hypotonic buffer solution, hypertonic buffer solution and Benzonase (Table 3-1). This process was adapted from the patented Leeds decellularisation protocol [298], which has been adapted for use with a multitude of tissue types including dermis, heart valve, amnion, meniscus, tendon and cartilage [299-304].

Table 3-1 Decellularisation process for porcine peripheral nerves, prior to optimisation

Step	Time (hours)	Temperature
Freeze	24	- 80
Thaw	1	37
Dissection of fascia/fat	2	N/A
Antibiotic wash solution	0.5	37
200 mM EDTA solution	24	4
Hypotonic buffer	24	42
0.1 % (w/v) SDS in hypotonic	24	42
Hypotonic buffer	24	42
PBS-EDTA	48-56	4
Hypotonic buffer	24	42
PBS	24	42
Benzonase (x 2)	3	37
PBS (x 3)	0.5	42
Benzonase (x 2)	3	42
PBS (x3)	0.5	42
Hypertonic buffer	24	42
PBS	48-56	4
Storage (PBS)	6 weeks	4

Each of the decellularisation steps is shown, in chronological order. For details of the solutions used, refer to section 2.10.1.

3.2 Aims and Objectives

3.2.1 Aim:

The aim of the work detailed in this chapter was to optimise and validate a previously developed decellularisation process for porcine peripheral nerves, reducing the time required for processing whilst maintaining the efficacy in terms of cell removal and preserving the structure of regions key for axonal function (e.g. the endoneurium).

3.2.2 Objectives:

i. To determine the effect of varying the number of cycles of 0.1 % (w/v) SDS treatment on decellularised nerve histoarchitecture and the efficacy of decellularisation, through staining with H&E.
ii. To determine the effect of different agitation speeds on decellularised nerve histoarchitecture and the efficacy of decellularisation, through staining with H&E.
iii. To validate the successful elimination of cells and DNA from different nerve branches (sciatic, tibial and peroneal) following optimisation of the decellularisation process, through staining with H&E and DAPI respectively.
iv. To confirm that the major structures of the peripheral nerve histoarchitecture were preserved following decellularisation, through staining with H&E.
v. To confirm that the optimised decellularisation process sufficiently reduced the DNA content of peripheral nerves.

3.3 Methods and Experimental approach

For details of the generic decellularisation protocol which was used in this study, see section 2.10. This work package had the objective of optimising a previously developed decellularisation protocol. The desired protocol would minimise structural damage to the histoarchitecture of the nerves (particularly the endoneurium), whilst ensuring that the nerves met widely accepted criteria defining successfully decellularised tissue.

In order to minimise damage induced as a result of the protocol and reduce the duration of the decellularisation process from 14 days to 10 days, two hypotonic buffer steps were removed from the protocol (together with the corresponding PBS wash steps). The decellularisation protocol was then further optimised to ensure effective cell and nucleic acid removal while enabling structural retention.

3.3.1 Optimisation of decellularisation process

Three principal factors potentially affecting the efficacy of decellularisation were identified. Two of these represented possible causes of structural disruption to the peripheral nerve ECM, these being the use of the detergent SDS and the speed of the orbital shakers used to agitate the nerves in solution.

In addition, the anatomical differences between the differing nerve branches used meant it was necessary to determine the efficacy of the decellularisation process in each.

This process is outlined in Figure 3-1.

3.3.1.1 Number of SDS incubation cycles

The generic Leeds decellularisation protocol stipulates the incubation of tissues in a hypotonic buffer solution containing SDS at a concentration of 0.1 % (w/v); however, the optimal length and number of such incubations varies widely between tissues. Therefore, two separate groups of nerves were subject to decellularisation processes inclusive of either one or two cycles of incubation in hypotonic buffer containing SDS. The results were analysed histologically by staining with H & E and DAPI.

3.3.1.2 Agitation speed

The optimal agitation speed varies between tissue types, as harder/more dense tissues may require greater agitation speed to ensure complete permeation of reagents, whilst such speeds may result in adverse changes to the structure of softer tissues. As peripheral nerve is a relatively delicate tissue it was thought that a lower speed may be appropriate. To confirm this, two groups were subject to identical decellularisation processes, but during each step were agitated either at 240 rpm or 120 rpm. The results were analysed histologically by staining with H & E and DAPI.

3.3.1.3 Differing branches of the porcine nerve plexus

Due to the previously observed morphological differences between nerve branches in the porcine leg, the efficacy of the decellularisation process may vary depending on the origin of a particular nerve segment. Therefore, segments of the sciatic, tibial and peroneal nerves were subject to the optimised decellularisation process, and the results analysed histologically by staining with H & E and DAPI.

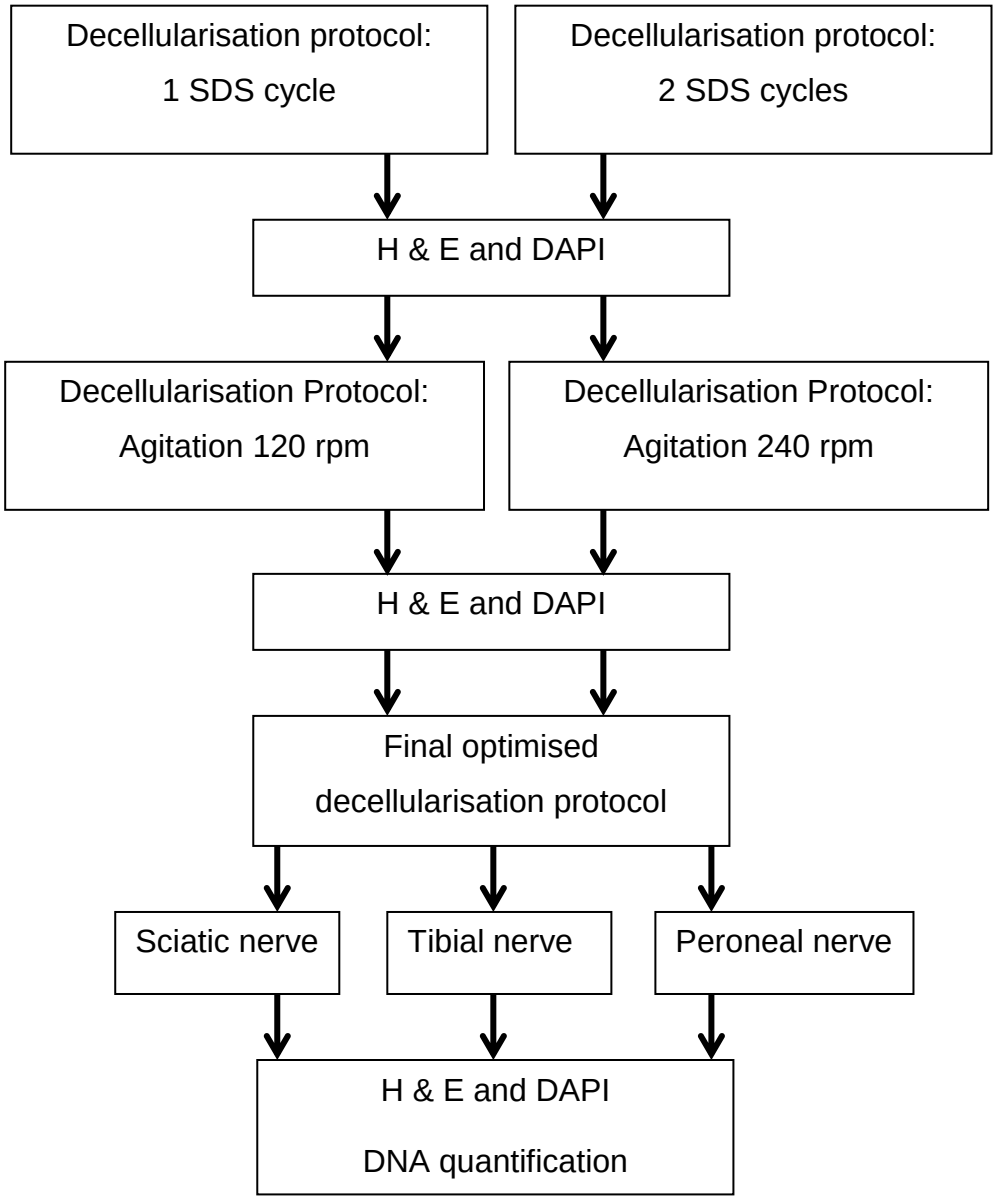

Figure 3-1 Schematic of the experimental approach taken during optimisation of the decellularisation protocol

This was carried out in three separate stages, independently varying the incubation time in 0.1 % (w/v) SDS, the speed of agitation and the specific nerve branch used respectively. Histological examination was used as the primary means of evaluating the effects of each change on the efficacy of cell removal and the preservation of ECM morphology.

3.3.1.4 Histological analysis of tissue treated with optimised decellularisation process

Nerves treated with the final optimised decellularisation process were subjected to histological analysis. H & E staining was used to analyse the degree of cell

removal and the preservation of matrix structures. DAPI staining was used to determine whether DNA (and/or nuclei) was removed.

3.3.1.5 DNA isolation and quantification

Quantification of wet and dry weight DNA content was used as a method of validating the efficacy of the optimised decellularisation process. Samples of native (25 - 50 mg; n = 6) and decellularised (100 - 250 mg; n = 6) peripheral nerve tissue were diced using a scalpel and placed into sterile Eppendorf tubes in preparation for DNA isolation using the DNeasy kit (Qiagen). Samples of native and decellularised nerves for dry weight quantification (n = 6) were lyophilised to a constant weight. Buffer ATL (360 µL) and proteinase K (40 µL) were added to each sample, mixed and incubated for three hours at 56 °C. Each sample was vortexed every 30 minutes. Samples were subject to 15 seconds of vortexing before 400 µL Buffer AL and 400 µL ethanol (100 %; v/v) were added to each, mixing by vortex after each addition. An aliquot of each sample (600 µL) was added to a DNeasy spin column and centrifuged at 6000 x g for one minute. The flow-through was discarded. This step was repeated until all of the original solution had been filtered by the spin column. The spin columns were transferred to fresh collection tubes, and 500 µL Buffer AW1 was added. The spin columns were centrifuged at 6000 x g for one minute and the collection tube was discarded. The spin columns were transferred to fresh collection tubes and 500 µL Buffer AW2 was added, before centrifugation at 16,000 x g for five minutes. The spin columns were placed in sterile 1.5 ml microfuge tubes, and 200 µL Buffer AE was added to the membrane at the base of the columns. The columns were incubated at room temperature for one minute and then centrifuged at 6000 x g for one minute. The eluted DNA contained was stored at - 20 °C until quantification. Total DNA in each isolated sample (2 µL aliquots) was quantified by measuring absorbance at 260 nm in triplicate with a Nanodrop 1000 spectrophotometer; Buffer AE was used as a blank. The DNA content of samples was calculated by interpolating the sample values against a standard curve of absorbance vs calf thymus DNA, and normalising the resulting values according to the sample mass.

3.4 Results

3.4.1 Variation of SDS cycles

Early attempts to decellularise porcine peripheral nerves resulted in alterations to the histoarchitecture. It may be hypothesised that SDS is at least partially responsible for this effect. Accordingly the number of cycles of SDS treatment used was varied between one and two cycles.

H & E staining showed that treatment of nerves with a decellularisation protocol incorporating two cycles of 0.1 % (w/v) SDS led to severe disruption to the major ECM structures of the nerve, including the epineurium, perineurium and especially to the endoneurium (Figure 3-2). Nerves treated with one cycle of SDS appeared to better retain these structures.

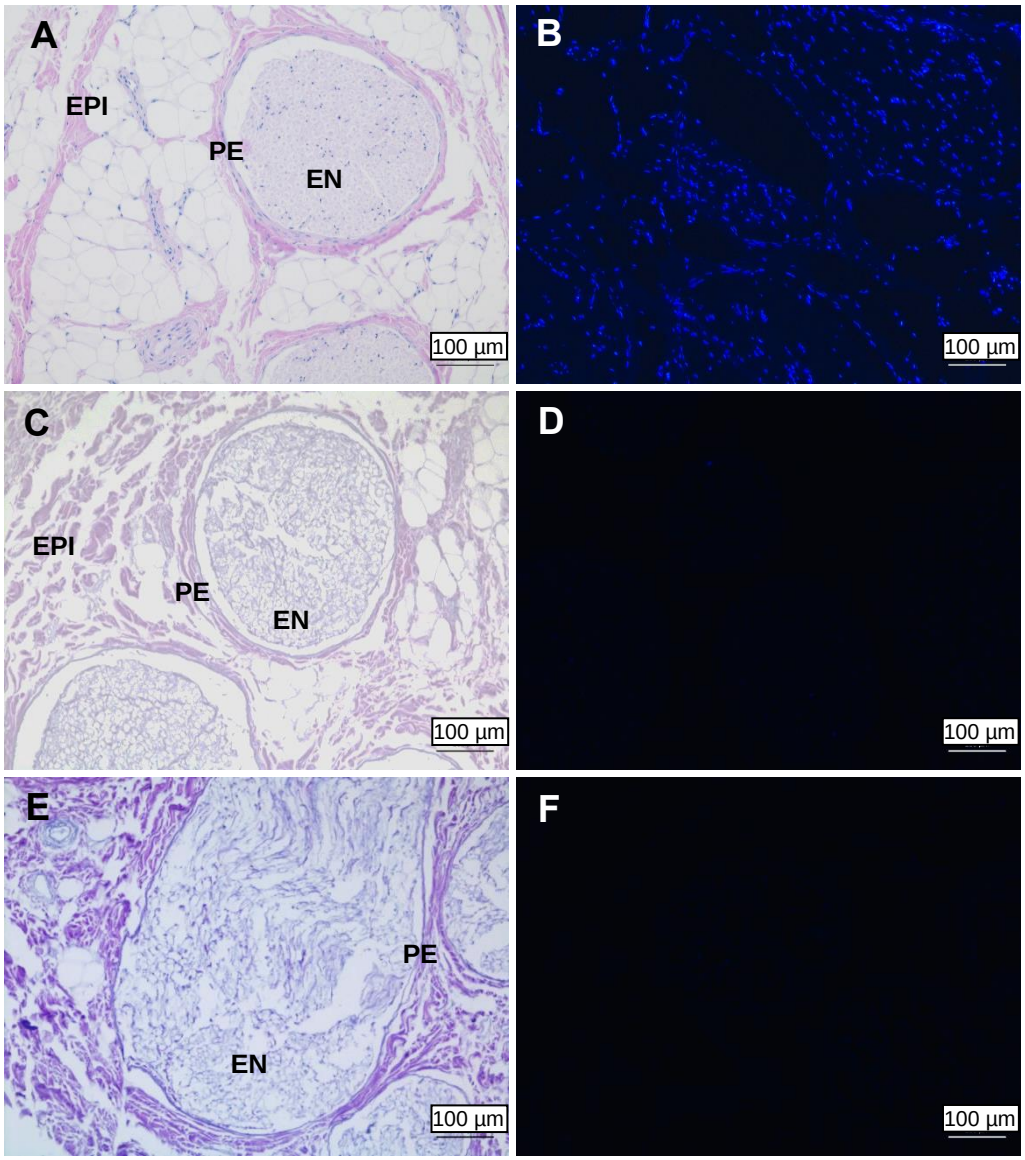

Figure 3-2 Representative images of sections stained with haematoxylin and eosin/DAPI

Sections of native (A and B) and sections of decellularised nerve following treatment with protocols incorporating (C and D) one SDS cycle and (E and F) two SDS cycles (both with agitation at 240 rpm), stained with (A, C and E) haematoxylin and eosin and (B, D and F) DAPI. ECM regions marked as EN (endoneurium), PE (perineurium) and EPI (epineurium). Images were acquired under Köhler illumination using a x10 objective. Scale bars = 100 µm.

3.4.2 Variation of agitation speed

It was proposed that the mechanical forces experienced by the nerves during agitation could be causing alterations to ECM histoarchitecture, particularly in the endoneurium. Therefore, two further groups of nerves were treated with a decellularisation protocol incorporating one cycle of SDS; in one group, the agitation speed was reduced from 240 rpm (as used previously) to 120 rpm. Both protocols appeared to successfully mediate the removal of cells from the tissue, whilst reducing the agitation to 120 rpm appeared to enable better retention of ECM histoarchitecture (Figure 3-3).

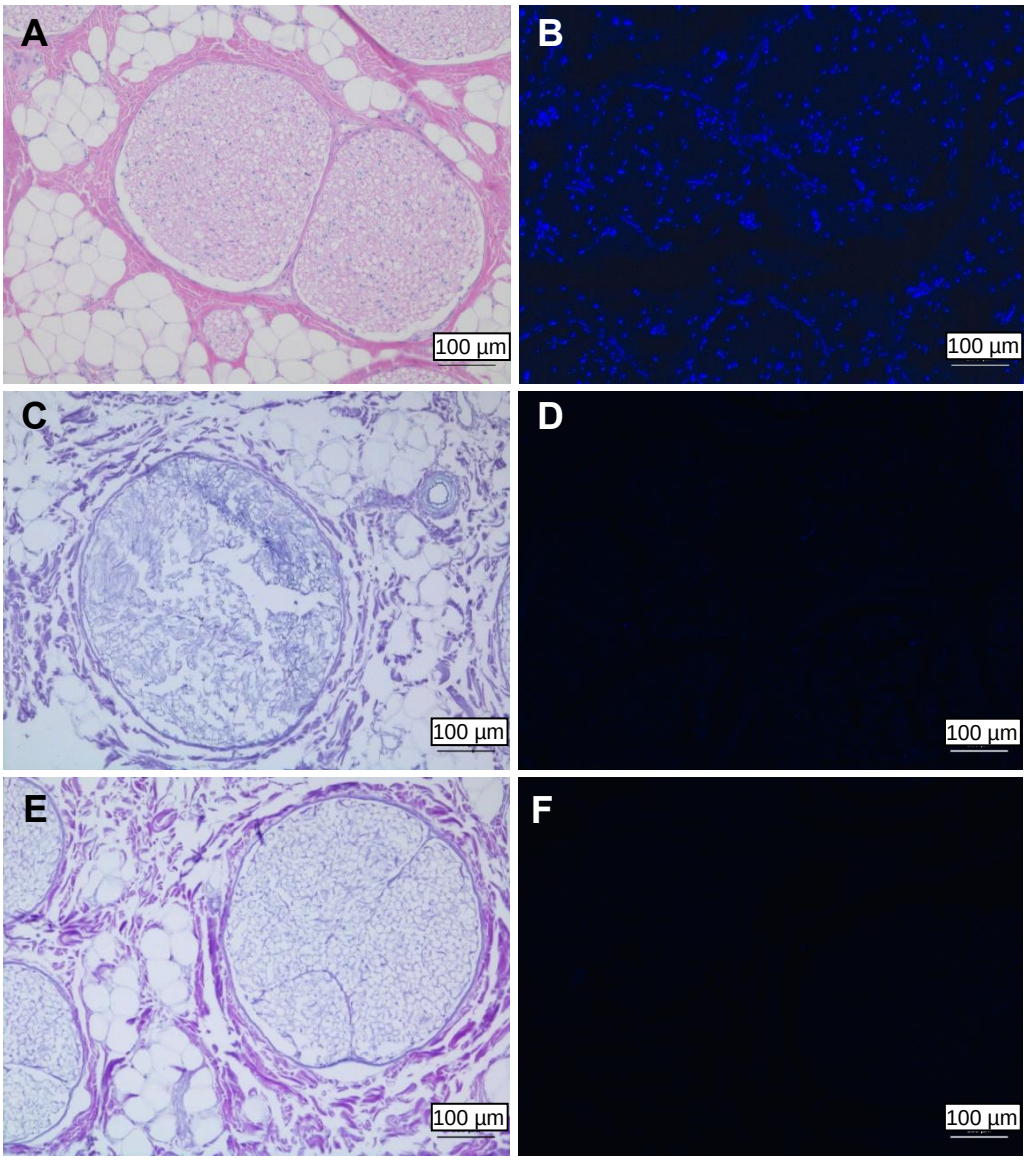

Figure 3-3 Representative images of sections stained with haematoxylin and eosin/DAPI

Sections of native nerve (A and B) and sections of decellularised nerve following treatment with decellularisation protocols incorporating one SDS cycle with agitation at 240 rpm (C and D) and 120 rpm (E and F). Sections stained with haematoxylin and eosin (A, C and E) and DAPI (B, D and F). Images were acquired under Köhler illumination using a x10 objective. Scale bars = 100 µm.

3.4.3 Comparison of decellularisation efficacy in sciatic, peroneal and tibial

The degree to which cell nuclei were successfully removed from tissue was observed to vary between individual samples following decellularisation. It was thought that this may be due to the thicker sciatic nerve requiring a more vigorous decellularisation process than the branches which are derived from it, the common peroneal and tibial nerves.

Segments of each nerve were therefore subject to decellularisation by the previously established protocol (one SDS cycle, agitation at 120 rpm), and sections taken and analysed histologically.

DAPI staining showed the presence of DNA in the endoneurium of sections of sciatic nerve, whereas no obvious staining was visible in sections of the peroneal and tibial nerves (Figure 3-4). Similarly, there were visible cell nuclei in sections of sciatic nerve stained with H & E, but none in either the sciatic nerve or tibial nerve. As a consequence of this, and the ECM structural damage likely to be induced by a more vigorous decellularisation protocol, the sciatic nerve was no longer included in the study.

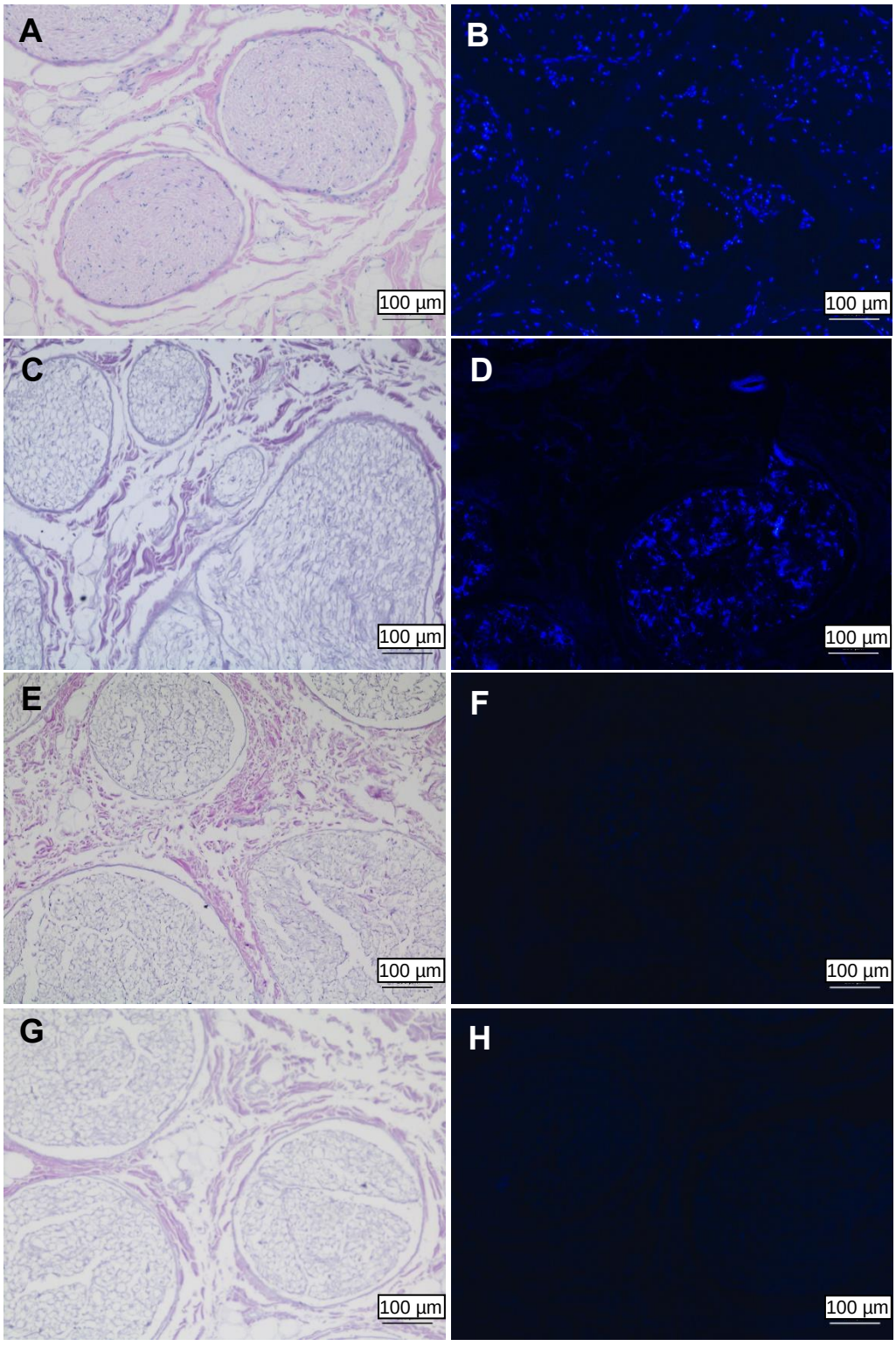

Figure 3-4 Representative images of sections stained with haematoxylin and eosin/DAPI

Sections of native peroneal nerve (A and B), and sections of sciatic (C and D), tibial (E and F) and peroneal (G and H) nerve following treatment with a decellularisation protocol incorporating one SDS cycle and agitation at 120 rpm. Sections stained with haematoxylin and eosin (A, C, E and G) and DAPI (B, D, F and H). Images were acquired under Brightfield illumination using a x10 objective. Scale bars = 100 µm.

3.4.4 Final optimised decellularisation protocol

The optimisation process detailed above yielded a shortened decellularisation protocol for use with peroneal and tibial porcine peripheral nerves (Table 3-2).

Table 3-2 Final optimised decellularisation protocol for porcine peripheral nerves

Step	Time (hours)	Temperature (°C)
Freeze	24	- 80
Thaw	1	37
Dissection of fascia/fat	2	N/A
Antibiotic wash solution	0.5	37
200 mM EDTA solution	24	4
Hypotonic buffer	24	42
0.1 % (w/v) SDS in hypotonic buffer	24	42
PBS (x 3)	0.5	42
PBS	24	42
PBS-EDTA	48-56	4
PBS (x 3)	0.5	42
Benzonase (x 2)	3	37
PBS	24	42
Hypertonic buffer	24	42
PBS (x 3)	0.5	42
PBS	24	42
Storage (PBS)	6 weeks	4

Each of the decellularisation steps is shown, in chronological order. For details of the solutions used, refer to section 2.10.1.

3.4.5 Histological evaluation of decellularisation efficacy and ECM histoarchitecture retention by comparison with native porcine peripheral nerves

H & E staining of native porcine peripheral nerve sections revealed the structure of the peripheral nerve ECM (Figure 3-5). An external layer of thick dense epineurium was evident, whilst deeper into the tissue the structure of the epineurium was less organised and appeared to contain globular fatty regions (Arrow, Figure 3-5 C). The dense ring-like structures of the perineurium surrounding each individual fascicle were evident. Both H & E and DAPI stained sections showed a dense cellular population within the perineurium, particularly in comparison to the epineurial tissue exterior to it. Each fascicle contained a honeycomb-like structure of endoneurial tubes. Haematoxylin staining revealed the presence of cells (morphologically Schwann cells) within the individual endoneurial tubes.

The major ECM structures of the decellularised peripheral nerves (decellularisation protocol incorporating one SDS cycle, with agitation at 120 rpm) appeared similar to that of native nerves following the application of the decellularisation protocol, with some slight disruption to the endoneurium of the decellularised tissue being the only obvious difference. H & E and DAPI staining of native tissue showed a relatively dense cell population within the endoneurium, consistent with the function of the endoneurium in providing an environment for neurons and Schwann cells to attach. Other regions which appeared to have a notable cellular population included the perineurium and the blood vessels travelling within the epineurium (the vasa nervorum). In contrast, the looser collagenous tissue of the epineurium appeared to contain a relatively sparsely distributed cellular population. Sections taken from samples of decellularised tissue showed no visible cell nuclei/nucleic acids.

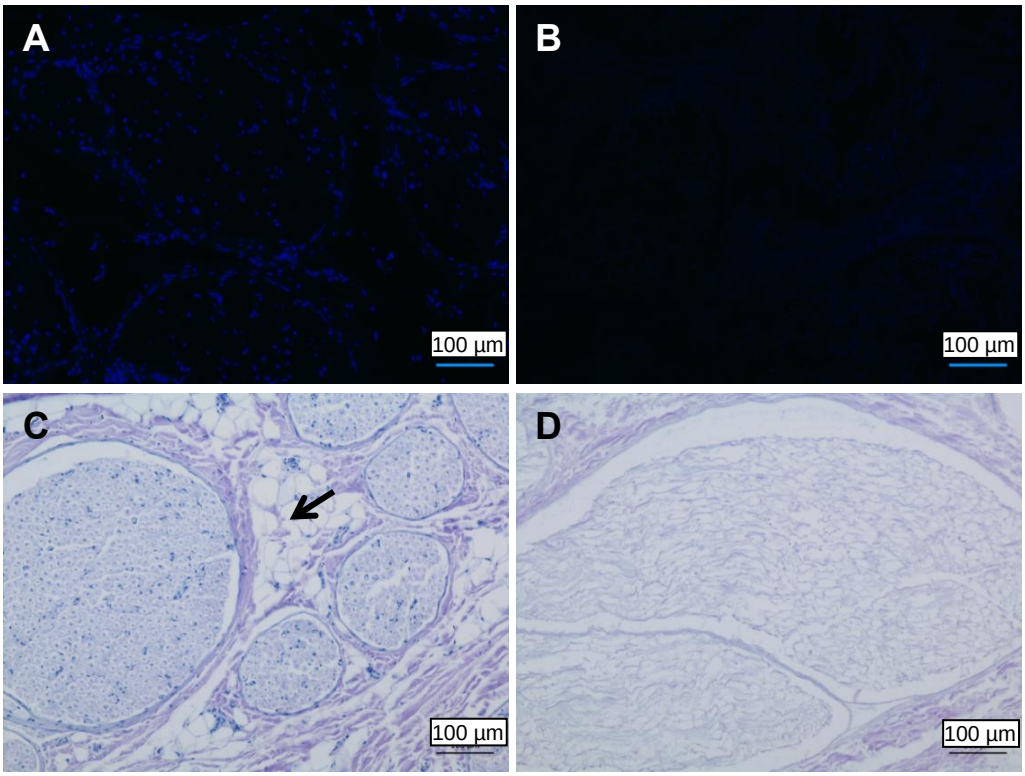

Figure 3-5 Representative images of sections stained with haematoxylin and eosin/DAPI

Sections of native (A and C) and decellularised (B and D) porcine peripheral nerves stained using DAPI (A and B) and haematoxylin and eosin (C and D). Arrow indicates suspected fatty globular tissue within the epineurium. Images were acquired under Köhler illumination using a x10 objective. Scale bars = 100 µm.

3.4.6 DNA content of native and decellularised porcine peripheral nerves

Isolation of total DNA from both wet and lyophilised tissue samples was used to determine the completeness and reproducibility of the decellularisation process. The wet-weight DNA content of native porcine peripheral nerves was found to be 63.01 (+/- 17.25) $ng.mg^{-1}$, whereas the DNA content of decellularised nerves was 13.64 (+/- 6.54) $ng.mg^{-1}$, representing a reduction of 79 %; Figure 3-6). The DNA content of lyophilised native nerves was 169.42 (+/- 29.26) $ng.mg^{-1}$, whereas freeze-dried decellularised nerves had a DNA content of 14.93 (+/- 6.34) $ng.mg^{-1}$, representing a reduction of 91 % (w/w; Figure 3-6).

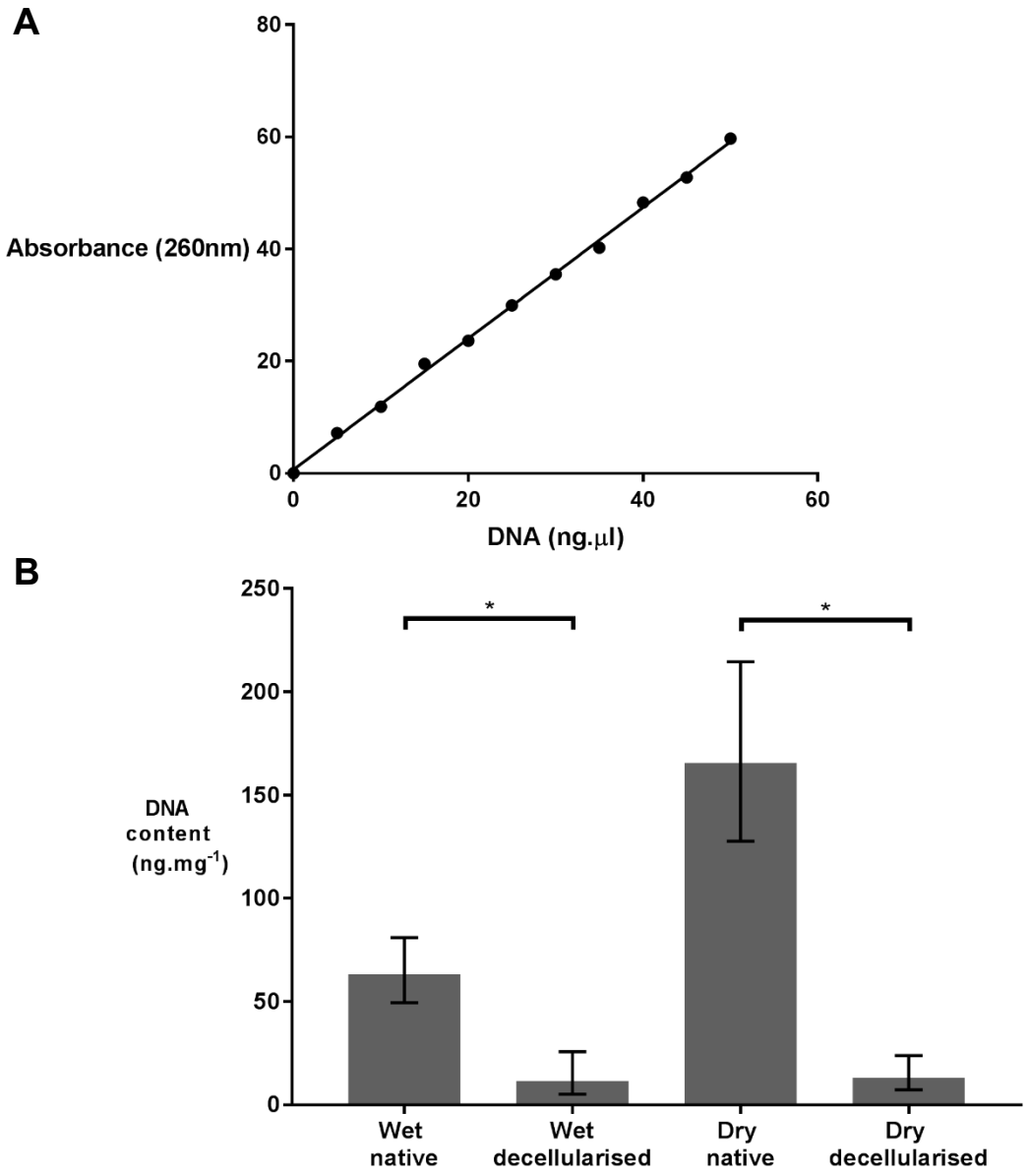

Figure 3-6 DNA content of native and decellularised porcine peripheral nerves

(A) Standard curve of DNA concentration against absorbance at 260 nm and (B) DNA content of wet-weight and lyophilised native and decellularised nerves. Data shown as mean (n=6) +/- 95 % confidence interval. Statistical analysis was by Student's T-test, * denotes groups which are significantly different.

3.5 Discussion

Low concentration SDS, in combination with hypotonic and hypertonic buffers and nuclease enzymes, was utilised to decellularise porcine peripheral nerves. The number of cycles in SDS and the speed of agitation were varied during an optimisation process. The decellularisation protocol developed includes a PAA incubation as a disinfection / sterilisation step, however due to previously observed adverse effects this was not applied here [175, 240]. The ability to remove cells was evaluated histologically in different peripheral nerve branches. Cell removal in the finalised protocol was confirmed using histological staining and DNA quantification.

Histological analysis indicated that in comparison to native tissue the nerve ECM structure was broadly retained following decellularisation. However, alterations to the histoarchitecture were observed in the endoneurium. In particular, the structure of individual tubules appeared to be less defined. The implications of this structural change for the ability of the graft to support neuroregeneration remain unclear. Alteration of the structure of the ECM (e.g. disorganisation, increased density (loss of porosity), loss of components) has been shown to negatively impact upon the ability of cells to infiltrate tissue and compromise biomechanical properties in a diverse range of decellularised tissues, including tendon, heart, liver and lung [305-308]. The primary function of the endoneurium is the provision of an optimal microenvironment for the Schwann cells and axons residing within it. Infiltration of regenerating axons and proliferating Schwann cells is key to the successful repair of peripheral nerves; one of the key advantages of the use of autografts or decellularised allografts over NGCs is the provision of a microscale architecture which can stimulate and guide this process [116]. Therefore, any alterations affecting the structure of the scaffold or key cell attachment motifs would potentially negatively impact on the efficacy of the graft [111]. Treating biological ECM-based scaffolds with ionic detergents such as SDS at higher concentrations is known to affect histoarchitecture and biomechanical properties. This occurs primarily through the disruption of non-covalent linkages and the denaturation of ECM proteins such as collagens, altering their tertiary conformational structure [309]. A study of porcine aortic heart valves found a significant reduction in

thermal stability and extensive disruption to collagen structures following treatment with 1 % (w/v) SDS, indicating that the use of SDS at this concentration is damaging to the scaffold. The collagenous ECM is critical to facilitating the function of the axons travelling within the nerve, maintaining an optimal microenvironment and protecting them from mechanical stress. Other commonly used detergents in decellularisation processes include the non-ionic Triton X-100, the key functional reagent in the production of the Avance® nerve graft. Histology shows changes to the structure of the endoneurial tubes in the Avance® graft similar to those seen here [310]. SDS has been chosen over Triton X-100 in this study due to superior efficacy in the removal of nuclei from tissue (following cell lysis). In addition, SDS has previously been shown to induce significantly less alteration to the mechanical properties of soft tissues than Triton X-100 [311].

Whilst the gross morphology of the decellularised nerve ECM appeared to be preserved following agitation at the higher speed of 240 rpm, the fine structure of the endoneurium appeared to be damaged. Because high agitation forces may have a damaging effect on soft tissue scaffolds, agitation is typically used to enhance the perfusion of solutions through tissues rather than as a primary mechanism of decellularisation [312].

The microanatomy of the porcine nerve plexus varies significantly between the separate major branches, in both porcine and human tissue [58, 313]. The peroneal and tibial nerves represent distal branches of the sciatic nerve, and as such are of a lesser diameter. A 2012 study by Gustafson *et al* found that the average diameter of the human tibial and peroneal nerves was 23 % and 49 % less than that of the sciatic nerve, respectively [313]. Additionally, the ECM making up the outer epineurium of the sciatic nerve is extensive, and surrounds the “true” epineurium of the individual bunches of fascicles which give rise to the peroneal and tibial nerves. This additional connective tissue can alternatively be defined as a distinct region of the ECM, the “paraneurium” [314]. Due to the highly collagenous, sheath-like nature of this structure, it may inhibit the diffusion of reagents into the tissue. This has been identified as a possible cause of failure in the application of local nerve block, necessitating the use of ultrasound guidance to ensure full block of the descending fascicles; with regard to decellularisation, this could prevent effective cell lysis being achieved in the

deeper regions of the tissue. In addition, there is a greater proportion of fascicular tissue relative to outer epineurium / “paraneurium” in the peroneal and tibial nerves than in the sciatic nerve. An decellularised graft produced from these nerves would therefore contain a greater proportion of tissue capable of supporting and guiding infiltrating axons and neurons.

During this study, decellularised nerve segments were produced from porcine peripheral nerves. The only decellularised nerve graft currently commercially available (limited to USA) is the Avance® nerve graft, produced from cadaveric human peripheral nerves [138]. The case for the use of porcine peripheral nerves as an alternative source of graft material is supported by a number of considerations. Xenogeneic tissue (derived from the food supply chain) can be more easily sourced in greater quantities than cadaveric human tissue, increasing the possible production rate (and potentially the overall availability) of decellularised grafts [315]. The tissue is taken from relatively young animals (approximately 6 months for porcine tissue), eliminating the risk of inferior quality tissue being used for the production of grafts (due to the typically older, in relative terms, human donor population) [316]. Furthermore, the tissue is sourced from an inbred strain (Large White Pig), ensuring maximal consistency in terms of the tissue used as the starting material prior to decellularisation. The use of xenogeneic tissue could also reduce the cost of graft production by eliminating the ethical regulatory framework and increased complexity of processing and storing tissue which is required when using human tissue.

In order to be approved for clinical use, decellularised tissue scaffolds must pose no increased risk of harm to the patient in comparison to current therapies, whilst providing a measurable clinical benefit. Minimising the potential for the induction of an adverse host immune response is particularly important for scaffolds derived from xenogeneic tissue, and the post-processing DNA content of a scaffold is one quantitative measure which is commonly used in this context [317]. Fragments of double-stranded DNA sourced from lysed cells in processed tissue grafts, malignant cells or intracellular pathogens are recognised following phagocytosis by intracellular sensor proteins including toll-like receptor 9 (TLR-9), absent in melanoma 2 (AIM2) and gamma-interferon-inducible-protein 16 (IFI16) [318]. These sensor proteins reside within in the cytosol and/or endosome membranes of innate immune system monocytes

such as macrophages and dendritic cells. Binding of dsDNA by sensor proteins leads to downstream stimulation of signalling pathways via mediators including myeloid differentiation adaptor protein 8 (MyD8), the apoptosis-associated Speck-like Protein Containing a Card-caspase 1 complex (ASC-Casp1) and stimulator of interferon genes (STING) [319]. A pro-inflammatory response is initiated in response to activation of these pathways, characterised by the induction of type 1 phenotype in activated macrophages and increased secretion of immunomodulatory cytokines such as IFN-β, IL-1β and IL-6.

Previously, a threshold value of less than 50 ng double stranded DNA per mg (dry weight) of tissue was commonly referenced as the accepted upper limit for a decellularised tissue [17]. Other studies have used different metrics for the determination of sufficient DNA removal; for example, a reduction of greater than 90 % (w/w) of the original native DNA content was specified in a study attempting to decellularised small diameter sections of vasculature [320]. Many decellularised tissue products which are currently successfully used in clinical settings (e.g. Oasis™ and Restore™, both derived from porcine small intestine submucosa) have been found to contain trace amounts of DNA [260]. Based on these findings, the degree to which these small quantities of DNA may induce an adverse response is likely to be negligible. The two cycles of treatment with Benzonase employed during the decellularisation process here appeared to ensure both of the thresholds defined above were achieved, and therefore decellularisation of the porcine nerves can be considered to have been sufficient.

4 Characterisation of the structure, cytocompatiblity, mechanical and biochemical properties of decellularised porcine peripheral nerves

4.1 Introduction

Physical and chemical methods of decellularising tissues are known to disrupt the structure and composition of the ECM. Changes are possible from the level of whole tissue histoarchitecture down to the ultrastructural alterations and the degradation/removal of ECM components.

The key functional reagent in the optimised decellularisation protocol for porcine peripheral nerves, SDS, is an ionic detergent which can disrupt the conformation of and/or denature ECM proteins. The protocol also includes physical processing methods including a freeze-thaw cycle and agitation, both of which may induce structural disruption to the ECM.

Basement membrane components in the endoneurium and perineurium, including collagen IV, laminin and fibronectin, are thought to be key to enabling the attachment of perineurial cells, Schwann cells and neurons [42, 321]. Therefore retention of such components in a decellularised nerve graft is likely to aid cell infiltration and, ultimately, the reinnervation of downstream target sites. Preserving the higher order structure of collagen I molecules, which make up approximately 90 % (w/w) of peripheral nerve ECM, is crucial to maintaining the major ECM structures (the epineurium, perineurium and endoneurium) which provide physical guidance and support to infiltrating cells and determine the mechanical properties of the tissue [38, 73, 82].

Efficacy of the porcine peripheral nerve decellularisation protocol has been established in terms of cell and nucleic acid removal. Characterisation of the collagenous histoarchitecture, distribution of basement membrane components, mechanical properties and biochemical composition of the nerves before and after decellularisation would enable the retention of properties considered key to graft function to be assessed.

4.2 Aims and Objectives

4.2.1 Aim

The aim of this chapter was to characterise the properties of native and decellularised porcine peripheral nerves, to provide a baseline dataset for the determination of the effects of sterilisation treatments on decellularised porcine peripheral nerves.

4.2.2 Objectives

i. To determine the effect of decellularisation on the distribution and structure of collagens, elastin and specific basement membrane proteins within peripheral nerve ECM, through staining with Sirius Red and Miller's Elastin and antibody labelling.
ii. To determine the biocompatibility of the decellularised nerves, through contact culture using two distinct cell types.
iii. To determine the effects of decellularisation on the mechanical properties of peripheral nerves, through slow strain rate to failure uniaxial tensile testing.
iv. To determine the effects of decellularisation on the biochemical composition of peripheral nerves, through quantification of collagen, denatured collagen, GAGs and fat.

4.3 Materials and Methods

4.3.1 Histological analysis

Processing and sectioning of tissue was carried out as described in section 2.11. Staining of sections with Sirius Red & Miller's Stain was carried out as described in 2.11.7.

4.3.2 Antibody labelling for collagen IV, laminin and fibronectin

Processing and sectioning of tissue was carried out as described in section 2.11. Labelling of sections with specific antibodies for collagen IV, laminin and fibronectin was carried out as described in section 2.11.8.

4.3.3 Contact cytotoxicity assay of sterilised nerves

Decellularised nerves were subject to contact cytotoxicity testing, as described in section 2.12.

4.3.4 Uniaxial tensile testing

Samples of decellularised nerve were subject to uniaxial tensile testing, as described in section 2.13.

4.3.5 Quantification of collagen content

The amount of collagen in the decellularised nerves was quantified as described in section 2.14.

4.3.6 Quantification of denatured collagen content

The amount of denatured collagen in the decellularised nerves was quantified as described in section 2.14.5.

4.3.7 Quantification of fat content

The amount of fat in the decellularised nerves was quantified as described in section 2.14.7.

4.4 Results

4.4.1 Sirius Red and Millers Elastin

Sirius Red/Miller's staining was used to define the distribution of collagen and elastin with the ECM of native and decellularised nerves (Figure 4-1). Sirius red staining of porcine peripheral nerve sections showed collagen was present in all three major structures of the ECM. Collagen was highly ordered in the perineurium enveloping each fascicle, and the layered lamellar structure previously described was evident. Sirius red-stained sections showed a greater intensity of staining in these regions when viewed under polarised light, whilst much less intense staining was evident in the endoneurial tubes. Outside of the blood vessels, bundles of elastin fibres were not evident within any of the major structures of the ECM.

The major collagen structures of the ECM were evident in sections stained with Sirius red following decellularisation, however collagen structures appeared to be slightly more disorganised and less tightly packed than in native tissue. When viewed under polarised light collagen present in the perineurium appeared to have a highly organised structure, whereas in the epineurium the collagen appears to be less organised, but consist of larger fibrils. The staining of the perineurium and epineurium also appears to be less intense following decellularisation, possibly indicating damage to or loss of collagen within the ECM. Miller's Elastin stained sections showed the majority of elastin to be present in the lumen of vessels of the vasa nevorum (indicated with arrows in Figure 4-1 A, C and E); the distribution and intensity of staining for elastin did not appear to be altered following decellularisation.

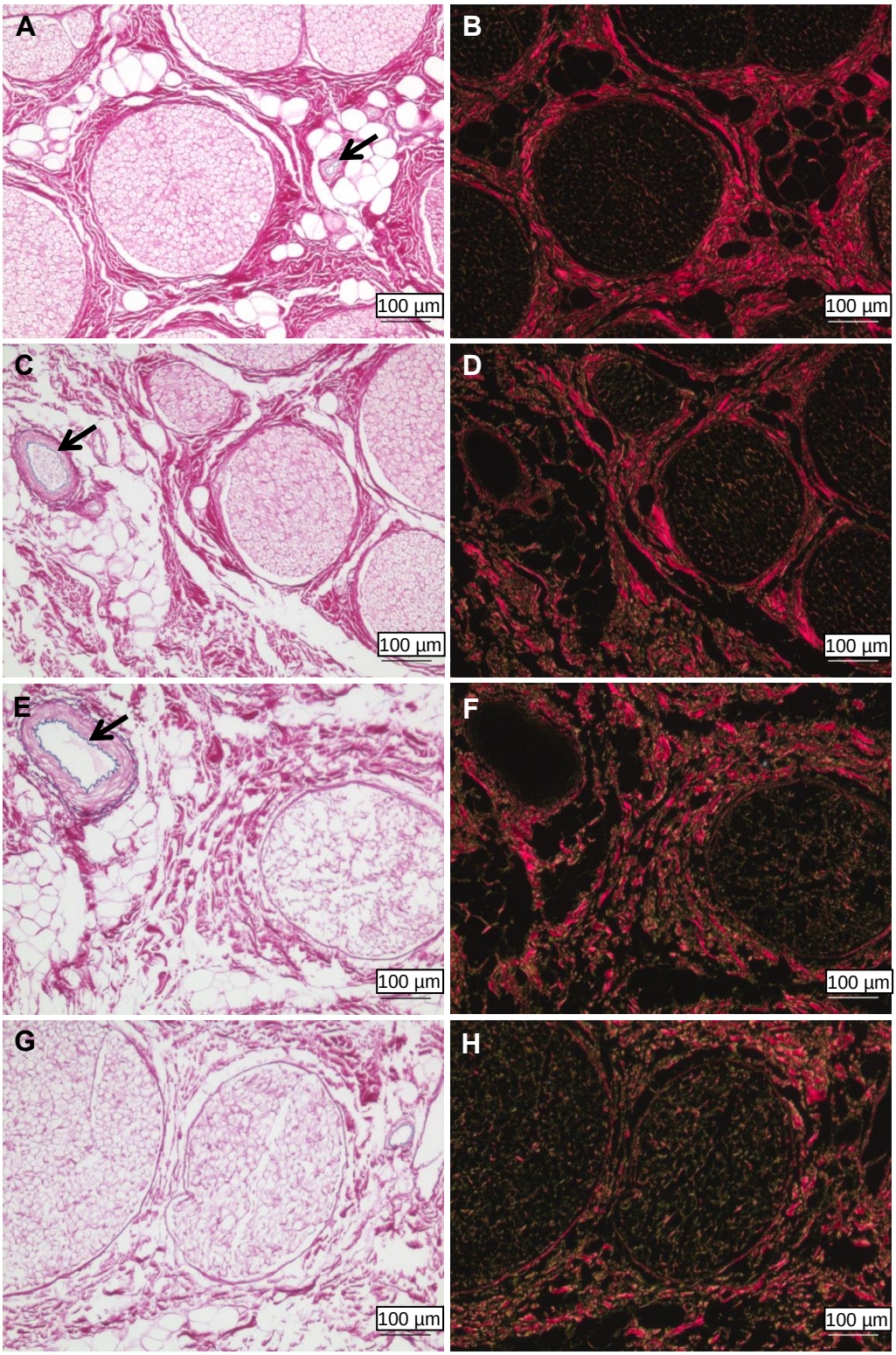

Figure 4-1 Representative images of sections of decellularised nerve stained with Sirius red / Miller's elastin stain

Images of native (A - D) and decellularised (E - H) porcine peripheral nerve under (A, C, E, G) Köhler or (B, D, F, H) circularly polarised illumination. The greatest concentration of elastin is in the lumen of blood vessels of the vasa nevorum (indicated by arrows). Images were acquired using a x10 objective, scale bars = 100 µm.

4.4.2 Immunohistochemical labelling of collagen IV

Sections of native and decellularised peripheral nerve were labelled with monoclonal antibodies against collagen IV. Collagen IV was present in the fascicular structures, the perineurium and the endoneurium (Figure 4-2 C). Staining was particularly intense in the perineurium (black arrows, Figure 4-2 C and D). Labelling intensity was reduced following decellularisation. In the epineurium, labelling was mainly limited to the vasa nervorum. Intense labelling was seen in the smooth muscle and luminal regions of the positive control, porcine femoral artery. No positive labelling was observed in the negative control.

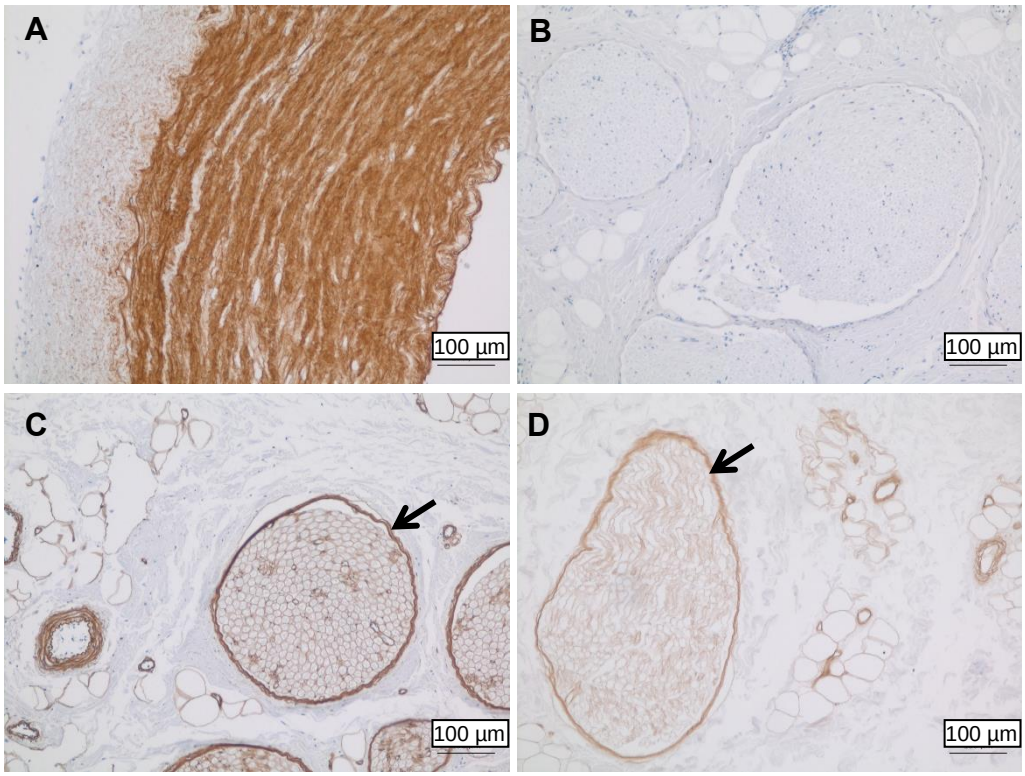

Figure 4-2 Representative images of sections labelled with monoclonal antibodies against collagen IV

Images of (A) porcine femoral artery positive control, (B) native porcine peripheral nerve isotype control, (C) native porcine peripheral nerve and (D) decellularised porcine peripheral nerve, immunohistochemically labelled for the presence of collagen IV. Arrows indicate intense collagen IV staining in the perineurium. Images were acquired under Köhler illumination using a x10 objective. Scale bars = 100 µm.

4.4.3 Immunohistochemical labelling of laminin

Sections of native and decellularised peripheral nerve were labelled with specific antibodies to demonstrate the presence of laminin. Labelling revealed the presence of laminin in the perineurium and endoneurium of native and decellularised porcine peripheral nerves (Figure 4-3). The signal appeared to be slightly reduced, but increased in area in the decellularised nerves. The signal remained localised within the perineurium and endoneurium. Specific labelling was observed in the lumenal and smooth muscle regions of the positive control, porcine femoral artery, whilst no labelling was seen in the negative control.

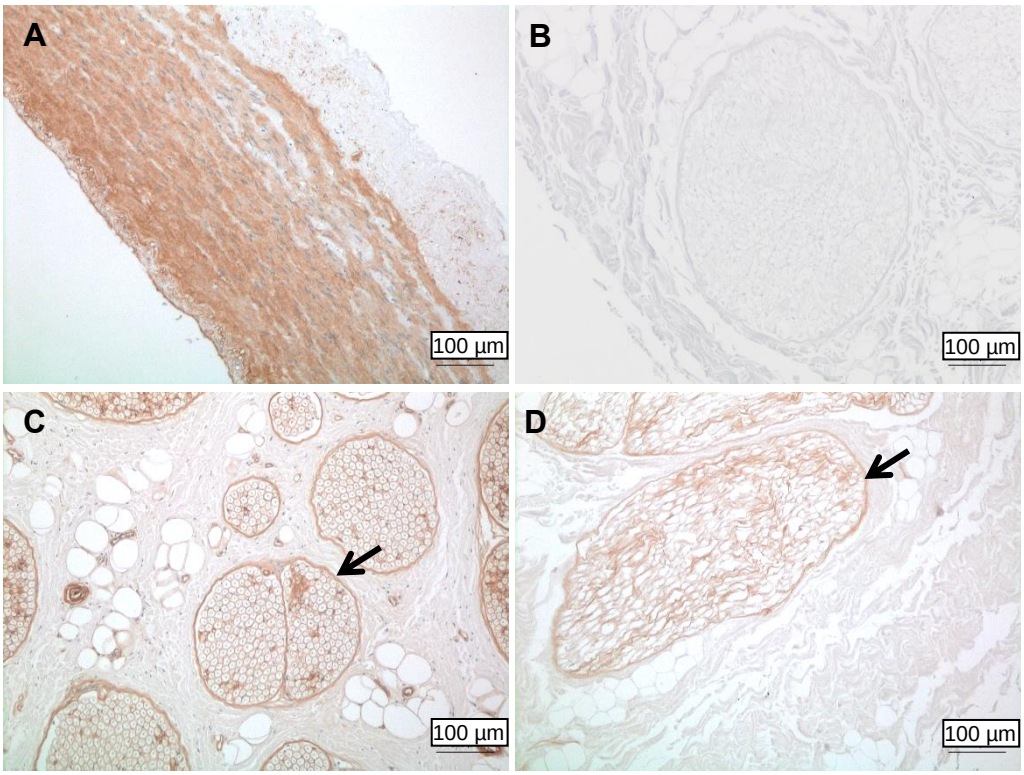

Figure 4-3 Representative images of sections labelled with a monoclonal antibody against laminin and counterstained with haematoxylin

Images of (A) porcine femoral artery positive control, (B) native porcine peripheral nerve isotype control, (C) native porcine peripheral nerve and (D) decellularised porcine peripheral nerve. Laminin was predominantly found in the endoneurium and perineurium, indicated by black arrows. Images were acquired under Köhler illumination using a x10 objective. Scale bars = 100 µm.

4.4.4 Immunofluorescent labelling of fibronectin

Sections of native and decellularised peripheral nerve were labelled with specific primary and fluorescently-tagged secondary antibodies, to demonstrate the presence of laminin. Fibronectin was found to be most prevalent in the perineurium, whilst less intense labelling was evident in the endoneurium (Figure 4-4). Intense labelling for fibronectin was seen throughout the porcine femoral artery positive control. DAPI staining for nuclei but not antibody labelling was observed in the negative control.

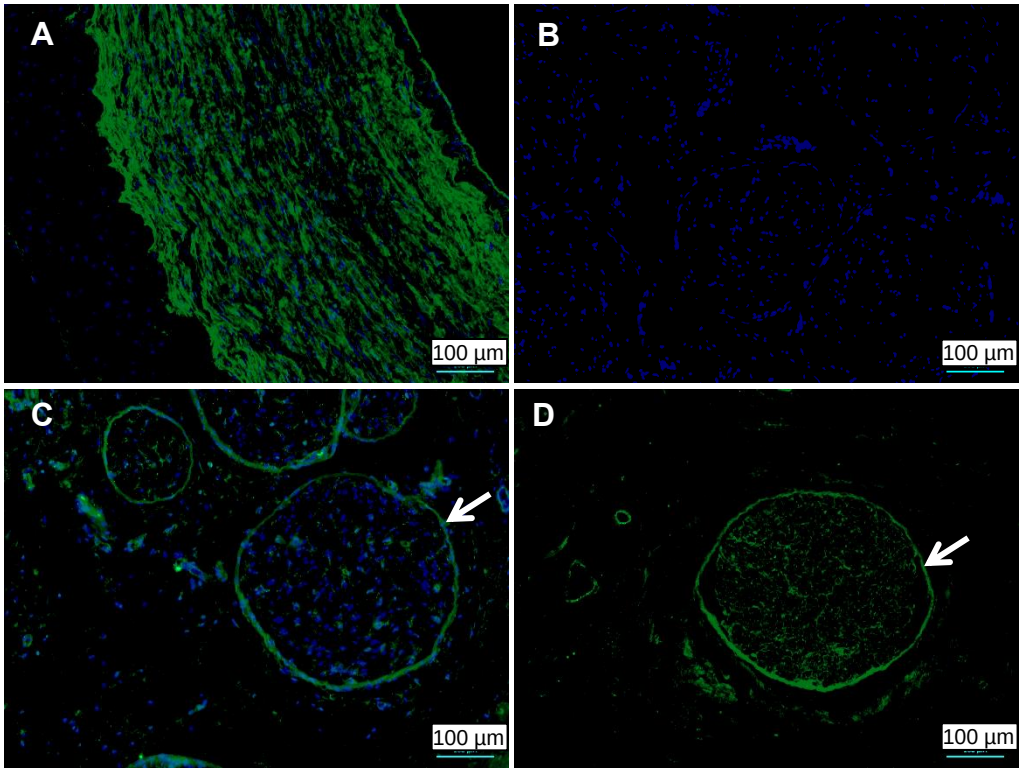

Figure 4-4 Representative images of sections labelled with a monoclonal antibody against fibronectin and counterstained with DAPI

Images show (A) porcine femoral artery positive control, (B) native porcine peripheral nerve negative control, (C) native porcine peripheral nerve and (D) decellularised porcine peripheral nerve. Fibronectin labelling was intense in the lamellar structured perineurium, indicated by white arrows. Images were acquired using a x10 objective. Scale bars = 100 µm.

4.4.5 Contact cytotoxicity of decellularised nerves

The *in vitro* biocompatibility of decellularised porcine peripheral nerves was assessed by contact culture studies using two distinct cell lines, BHK and L929. Cyanoacrylate contact adhesive was used as a positive control and a commercially available surgical closure strip (Steri-Strip) as a negative control.

Cells incubated with the positive control were sparsely distributed and displayed a rounded morphology indicative of cell death (Figure 4-5 A & B).

Cells incubated with the negative control and test samples (segments of decellularised porcine peripheral nerve) appeared to grow up to and in contact with the samples. The cells appeared to display normal morphological characteristics. L929 cells displayed an elongated morphology and less dense population, whilst BHK cells displayed a rounded morphology and denser population.

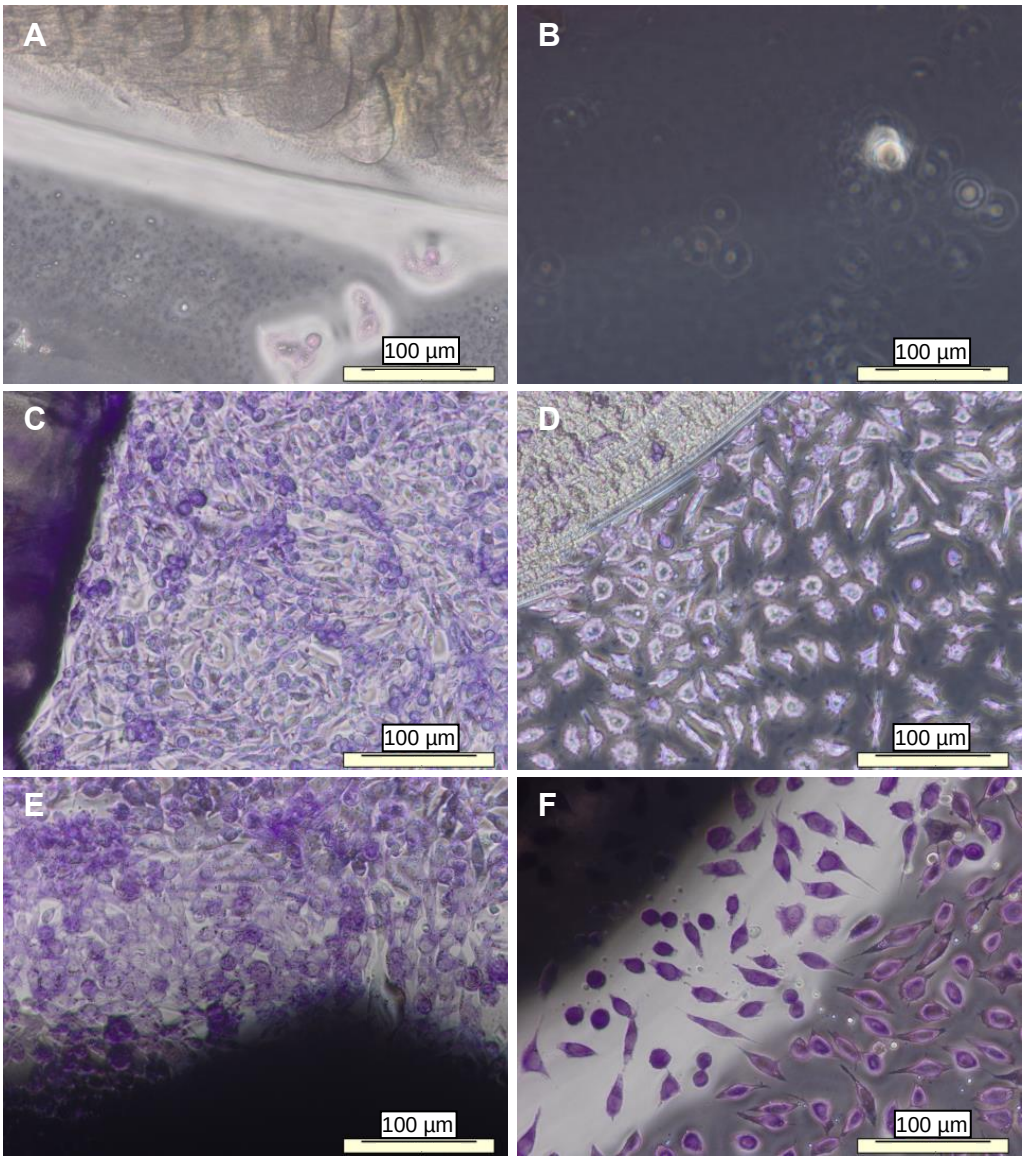

Figure 4-5 Representative images of Giemsa-stained BHK and L929 cells cultured for 48 hours with decellularised porcine peripheral nerves

Images show (A) BHK cells cultured with cyanoacrylate positive control, (B) L929 cells cultured with cyanoacrylate positive control, (C) BHK cells cultured with Steri-Strip negative control, (D) L929 cells cultured with Steri-strip negative control, (E) BHK cells cultured with a segment of decellularised porcine peripheral nerve and (F) L929 cells cultured with a segment of decellularised porcine peripheral nerve. Images were acquired under Brightfield illumination using a x10 objective. Scale bars = 100 µm.

4.4.6 Uniaxial Tensile Testing

Samples of native and decellularised porcine peripheral nerves were subject to uniaxial tensile testing. The UTS of decellularised nerves was found to be 10.37 (+/- 1.16) MPa, whereas that of native tissue was found to be 11.82 (+/- 2.29) MPa (Figure 4-6A). The Young's Modulus of native porcine peripheral nerve was found to be 27.33 (+/- 4.56) MPa, whereas the Young's Modulus of decellularised peripheral nerves was 25.73 (+/- 7.30) MPa (Figure 4-6 B). Statistical analysis by a student's T-test revealed no significant differences between the mechanical properties of native and decellularised nerves.

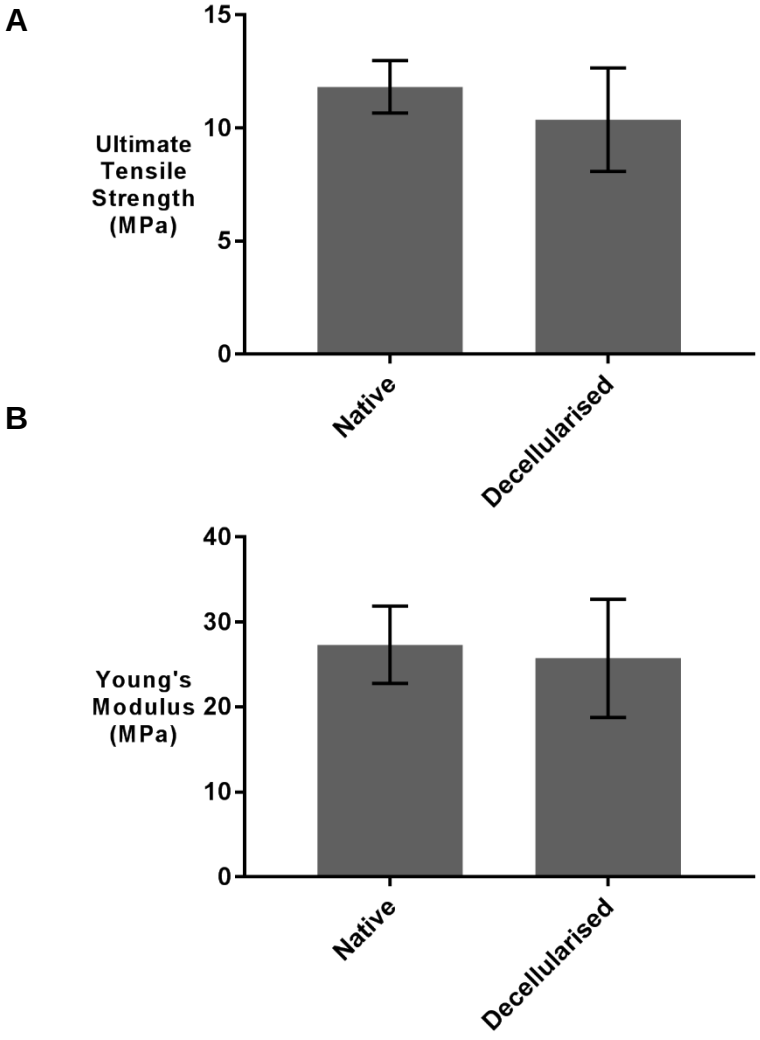

Figure 4-6 Ultimate Tensile Strength and Young's Modulus of native and decellularised porcine peripheral nerve

(A) Ultimate Tensile Strength and (B) Young's Modulus of native and decellularised porcine peripheral nerves. Data shown as mean (n = 6) +/- 95 % confidence interval, n = 6. Statistical analysis was by student's T-test. * denotes groups which are significantly different.

The maximum load at failure sustained by native nerves was 53.13 N (+/- 15.15), whereas for decellularised nerves it was 59.69 N (+/- 29.84) (Figure 4-7A). The stiffness of native nerves was 15.39 $N.mm^{-1}$ (+/- 3.42), whereas for decellularised nerves it was 14.92 (+/- 6.02) $N.mm^{-1}$ (Figure 4-7B). No significant differences were found between the values.

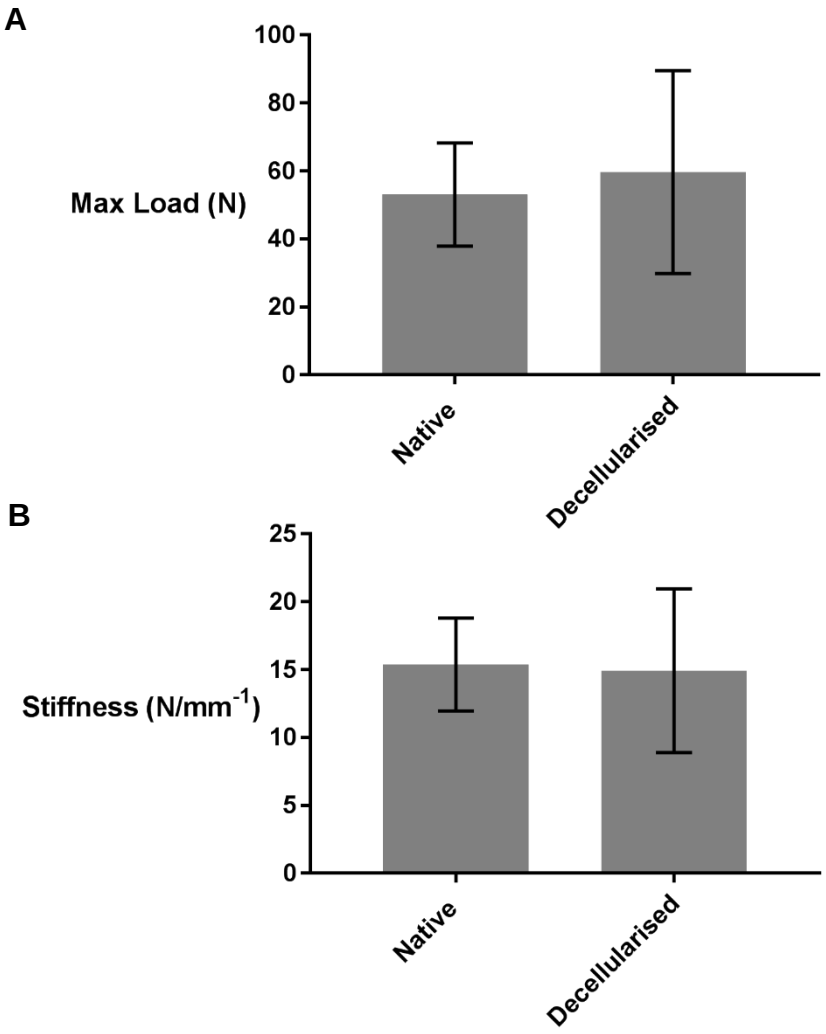

Figure 4-7 Maximum load at failure and stiffness of native and decellularised porcine peripheral nerves

(A) Maximum load at failure and (B) Stiffness of native and decellularised porcine peripheral nerves. Data shown as mean (n = 6) +/- 95 % confidence interval, n = 6. Statistical analysis was by student's T-test. * denotes groups which are significantly different.

Energy to break values were 8.08 MJ/m^3 for native peripheral nerves and 7.31 MJ/m^3 for decellularised peripheral nerves. No significant differences were identified between the values.

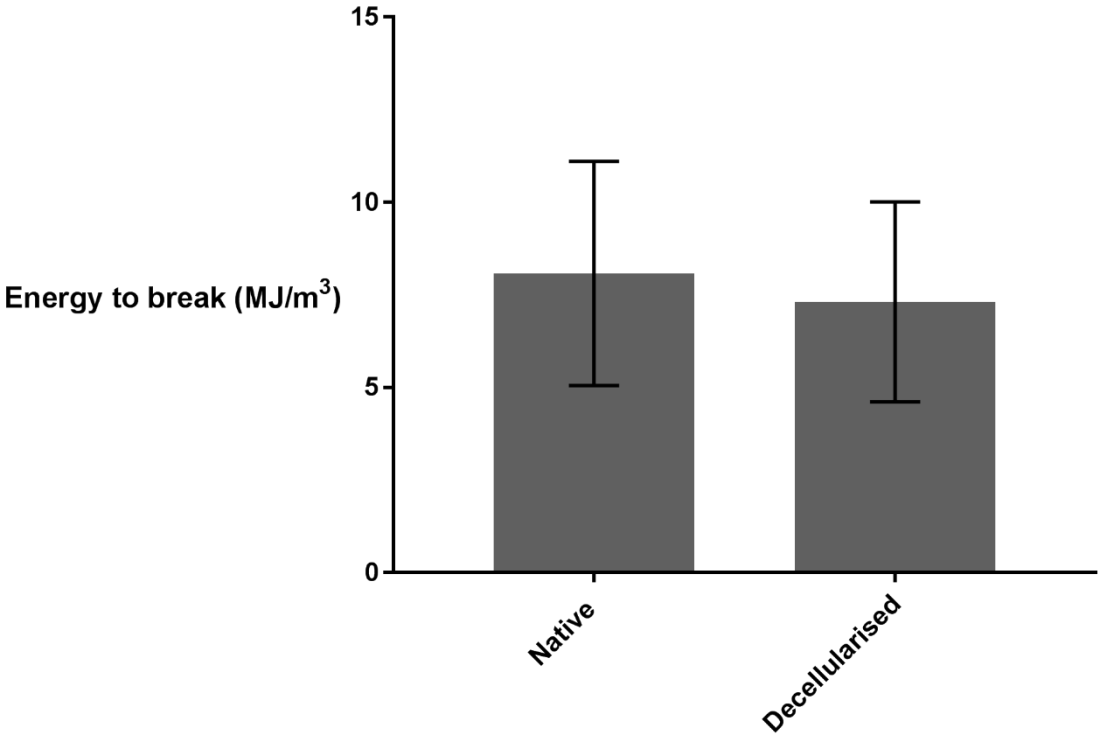

Figure 4-8 Energy to break values for native and decellularised porcine peripheral nerves

Energy to break values for native and decellularised porcine peripheral nerves. Data shown as mean (n = 6) +/- 95 % confidence interval, n = 6. Statistical analysis was by student's T-test. * denotes groups which are significantly different.

4.4.7 Quantification of peripheral nerve collagen content

The hydroxyproline content of native porcine peripheral nerve was 28.98 (+/- 5.03) µg.mg^{-1}, significantly less than decellularised porcine peripheral nerve which had a hydroxyproline content of 39.29 (+/- 5.80) µg.mg^{-1} ($p < 0.05$) (Figure 4-9). These values were then used to estimate collagen content by using the previously determined conversion factor (7.52) [252]. The collagen content of native porcine peripheral nerve was therefore estimated to be 217.92 (+/- 37.79) µg.mg^{-1}, numerically lower than decellularised porcine peripheral nerve which had a collagen content of 295.50 (+/- 43.64) µg.mg^{-1} ($p < 0.05$) .

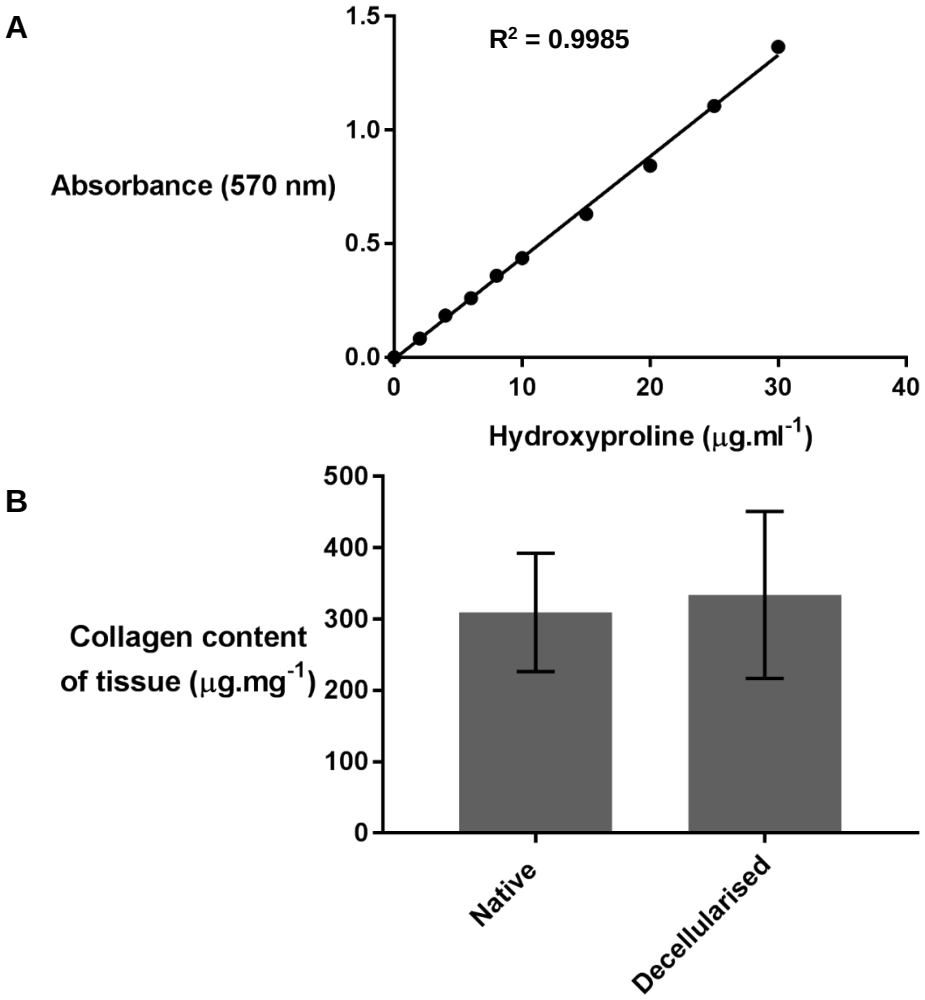

Figure 4-9 Collagen content of native and decellularised porcine peripheral nerves

(A) standard curve of hydroxyproline content against absorbance at 570 nm and (B) estimated collagen content of native and decellularised porcine peripheral nerves. Data shown as mean (n = 6) +/- 95 % confidence interval. Statistical analysis was by student's T-test. * denotes significant difference compared to native samples.

4.4.8 Quantification of denatured collagen content

The denatured collagen content of native and decellularised nerves was determined by digestion of samples with α-chymotrypsin enzyme. Acid hydrolysis was then carried out on the digested samples, and the hydroxyproline content was determined. The hydroxyproline content of the digested collagen fraction was 0.71 (+/- 0.04) $\mu g.mg^{-1}$ and 0.97 (+/- 0.004) $\mu g.mg^{-1}$ for native and decellularised nerves respectively. These values were used to calculate the denatured collagen content using a previously described conversion factor (7.52) [252]. No significant difference was found between the denatured collagen content of native and decellularised nerves, which were determined to be 5.32 (+/- 2.26) and 7.32 (+/- 2.62) $\mu g.mg^{-1}$ respectively (Figure 4-10).

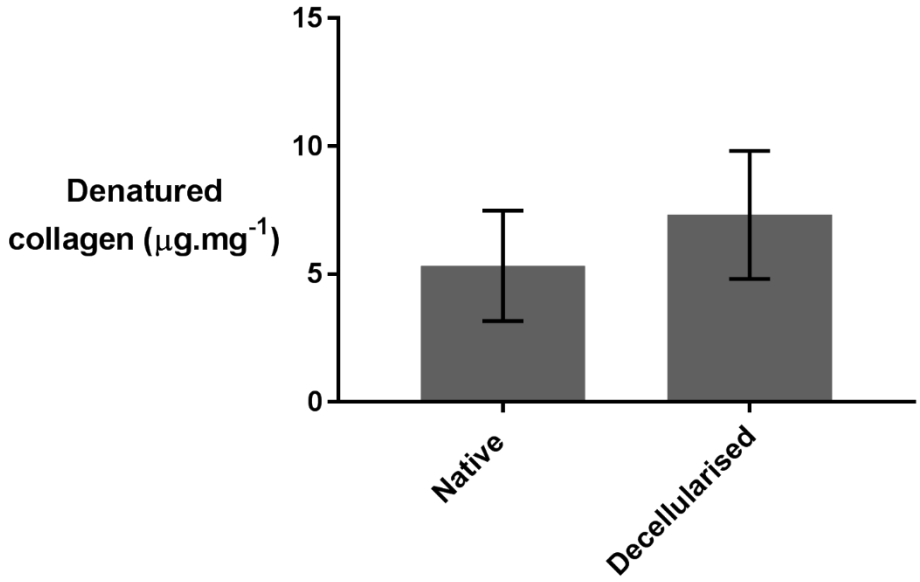

Figure 4-10 Denatured collagen content of native and decellularised porcine peripheral nerves

Estimated denatured collagen content of native and decellularised porcine peripheral nerves. Data shown as mean (n = 6) +/- 95 % confidence interval. Statistical analysis was by student's T-test. * denotes groups which are significantly different.

4.4.9 Quantification of GAG content

Native and decellularised nerves were digested with papain enzyme. The GAG content of the digest was then quantified using a colourimetric assay utilising 1,9-dimethylmethylene blue as an indicator. Native and decellularised peripheral nerves were found to have a GAG content of 11.03 (+/- 10.81) and 13.19 (+/- 12.54) $\mu g.mg^{-1}$ respectively (Figure 4-11). Statistical analysis by students T-test indicated there was no significant difference between the groups.

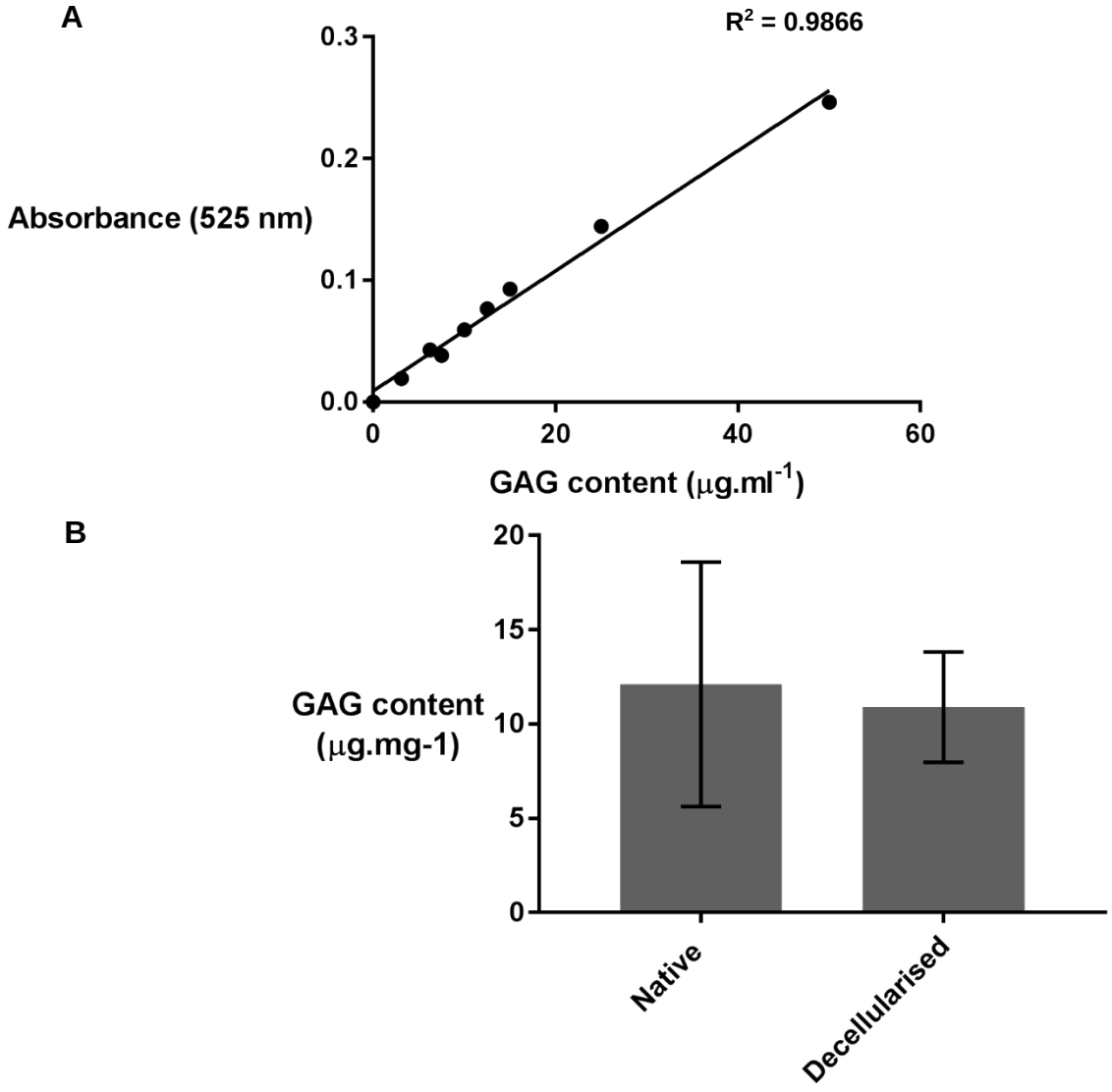

Figure 4-11 GAG content of native and decellularised porcine peripheral nerves

(A) Standard curve of absorbance at 525 nm against GAG content and (B) GAG content of native and decellularised porcine peripheral nerves. Data shown as mean (n = 6) +/- 95 % confidence interval. Statistical analysis was by student's T-test. * denotes groups which are significantly different.

4.4.10 Quantification of fat content

The fat content of native and decellularised nerves was determined by subjecting tissue samples to an extraction process in a known volume of ethanol. The fat concentration of the extracts was then quantified and used to calculate the fat content of the nerves. Native and decellularised nerves were found to have a fat content of 471 (+/- 131) and 511 (+/- 116) µg.mg^{-1} respectively (Figure 4-11). Statistical analysis by students T-test indicated there was no significant difference between the groups.

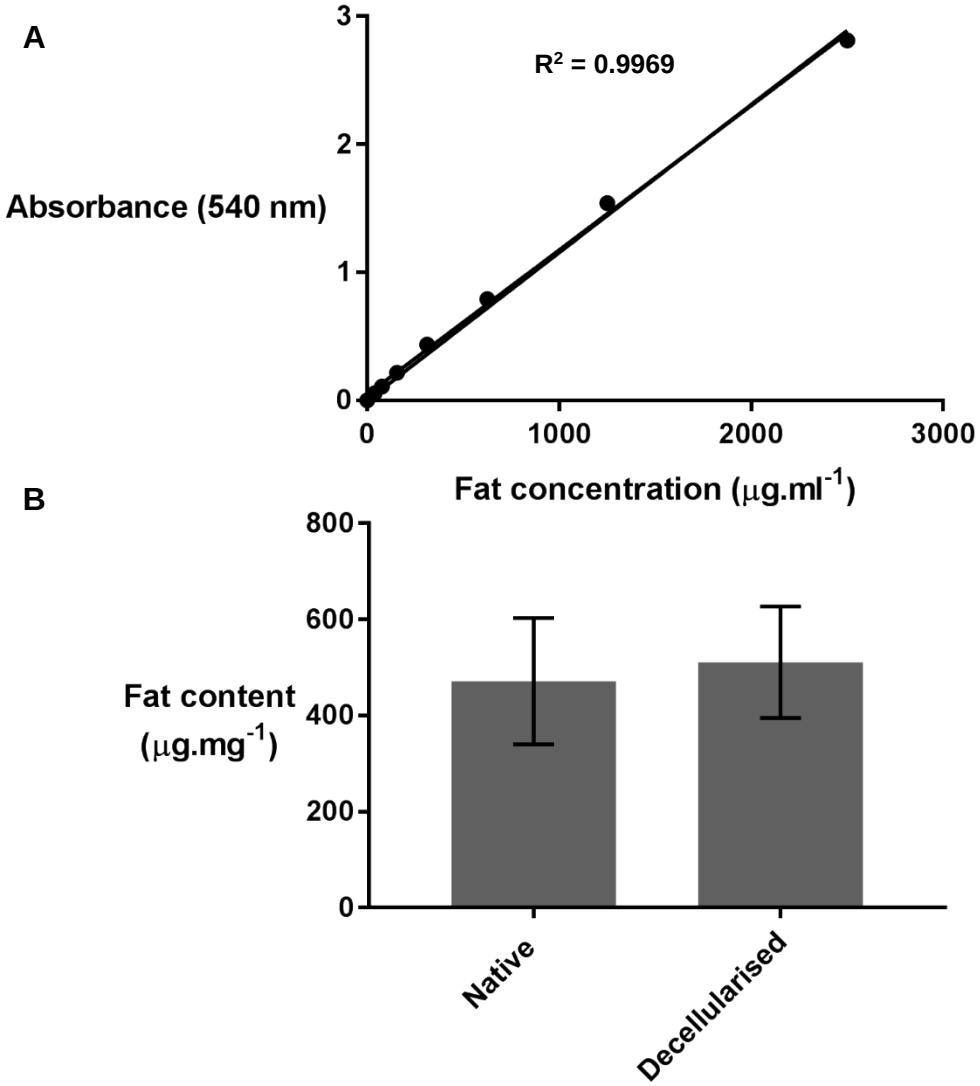

Figure 4-12 Fat content of native and decellularised porcine peripheral nerves

Chart shows fat content of native and decellularised porcine peripheral nerves. Data shown as mean (n = 6) +/- 95 % confidence interval. Statistical analysis was by Mann-U Whitney test. * denotes groups which are significantly different.

4.5 Discussion

The histoarchitecture, biochemical composition and material properties of the porcine peripheral nerves were generally well preserved following decellularisation. The decellularised nerves appeared to be biocompatible, with no apparent cytotoxicity evident during contact culture with two distinct cell types.

The structure of the epineurium appeared to be slightly “looser” following decellularisation. Degradation of the histoarchitecture during decellularisation may be caused by mechanical, chemical or enzymatic treatments, either in isolation or combination [17]. Depending on the compatibility of a tissue with different treatments and the role of tissue structure in facilitating function and/or recellularisation, a degree of structural disruption may be acceptable to ensure full decellularisation. Azhim et al (2013) observed an increase in the porosity and collagen fibre “looseness” of porcine aorta ECM following decellularisation with SDS at a concentration of 2 % (v/v) compared to 0.1 % (v/v) [322]. The use of sonication at 1750 Hz, in place of reciprocal shaking at 30 rpm, caused much higher levels of structural disruption during decellularisation with 2 % (v/v) SDS solution. However, H & E staining revealed the presence of whole nuclei in samples treated with reciprocal shaking, and a 3-fold greater DNA content than in sonicated samples.

Koch et al (2013) decellularised porcine ureters using 1 % (v/v) SDS and lyophilised the resulting scaffold, increasing the porosity of the ECM but retaining the gross morphological features [323]. The structural changes did not impede cell infiltration during subcutaneous implantation in a Wistar rat model. After 30 days, cells were observed growing throughout the scaffold from the exterior to the lumen. In contrast cell growth in decellularised ureters with a tighter “native-like” structure, induced through the use of cross-linking agents (including genipin and 1-ethyl-(3-dimethylaminopropyl)carbodiimide hydrochloride), was limited to the outer region. The structural disruption did not appear to result in any changes to the mechanical properties of the nerves following decellularisation.

Some structural disruption and increase in ECM porosity may therefore be beneficial in decellularised grafts. During decellularisation, increased structural

looseness or porosity may enable increased solution access and egress from the tissue, thereby ensuring maximal removal of cellular material [324]. Following implantation, increased porosity and looseness may enable faster cell infiltration and graft integration. The histoarchitectural disruption observed in the present study was primarily limited to the epineurium. As the structure of individual endoneurial tubules did not appear to be significantly altered, these changes are unlikely to have serious implications for the ability of the decellularised nerves to facilitate the attachment and growth of Schwann cells and regenerating axons.

Increased disruption to the collagenous ECM may also explain the observed reductions in basement membrane component antibody labelling after decellularisation. This was particularly evident in the perineurium. The tightly packed lamellar basement membrane layers of the native perineurium were evident when labelled for key components such as laminin and collagen IV, but were less distinct following decellularisation [58]. Given the larger-scale structural alterations seen in the (primarily collagenous) epineurium, and the fact that basement membrane labelling remained localised, it is likely that disruption to underlying constituent collagen I networks (rather than the basement membrane) was the primary causative factor. Scanning electron microscopy imaging of a porcine urinary bladder ECM scaffold revealed the induction of structural disruption within the collagen fibre network following treatment with 0.1 % (v/v) SDS [325]. SDS-treatment of porcine urinary bladder ECM also led to reductions in collagen IV and laminin antibody labelling intensity [269]. Human urothelial cells cultured on the SDS-treated urinary bladder ECM displayed abnormal morphological characteristics and reduced growth compared to an untreated control.

Similar changes to the basement membrane have been seen in porcine pulmonary heart valves, porcine dermis, and human pulmonary and aortic valves decellularised using variations of the patented Leeds protocol (the common key reagents being 0.1 % SDS, hypotonic and hypertonic buffer solutions, Benzonase) [240, 326, 327]. The observed reduction in antibody labelling intensity for laminin and collagen IV did not seem to affect cell ingrowth to the decellularised human aortic valve ECM during subcutaneous implantation in C3H mice, which was higher than in the cellular tissue control. Laminin and

collagen IV facilitate the attachment of Schwann cells and axons in the endoneurium and perineurial cells in the perineurium [47, 56, 328]. Whilst the cell ingrowth in human aortic valves decellularised using a similar protocol is encouraging, the extent to which the observed changes to the basement membrane would negatively affect the infiltration of site-specific cells (thereby slowing and/or impeding the process of neuroregeneration following scaffold implantation) remains unclear.

The levels of collagen and denatured collagen did not appear to change following decellularisation, indicating minimal loss of the collagenous ECM. This is consistent with data from other tissue types decellularised with SDS including porcine superflexor tendon, porcine anterior cruciate ligament, and human aortic and pulmonary valves [327, 329, 330]. The native and decellularised nerves contained a high proportion of fat, making up approximately 50 % of the dry mass. The majority of fatty tissue in native peripheral nerve is located in the epineurium, commonly referred to as interfascicular adipose tissue [331]. The distribution of interfascicular adipose tissue is variable; as with the collagenous components of the epineurium, interfascicular adipose tissue is present in greater relative quantities in larger, multifascicular nerve branches such as the sciatic nerve [104]. The main function of interfascicular adipose tissue is thought to be the protection of fascicles from compressive mechanical forces [332]. The nerve branches used in the present study, the peroneal and the tibial, descend from the sciatic nerve and are relatively large and multifascicular compared to more distal branches (e.g. the sural nerve) [58]. Therefore, the relatively high proportion of fat seen here in the native and decellularised nerves is to be expected. This is consistent with the large areas of suspected globular adipose tissue observed in sections stained with H & E, which are likely to be important for the maintenance of tissue histoarchitecture in the decellularised nerves.

The distribution and quantity of GAGs in peripheral nerve is not well characterised. Data from the present study indicates that that the GAG content of porcine peripheral nerve ECM is highly variable, and is relatively low compared to other tissues such as articular cartilage [304]. Decellularised porcine peripheral nerves with a slightly higher GAG content were able to support the growth of site-specific cells in an *in vivo* rat model [139]. In light of

this, the low measured GAG content of decellularised nerves seen in the present study is not of concern in terms of potential axonal growth inhibition.

The structural and biological properties of the porcine peripheral nerves were well conserved following decellularisation. The identification of a robust terminal sterilisation process which induces the minimum possible additional changes to these properties is crucial to facilitating translation of the decellularised nerves towards use as a clinical product.

5 The effects of sterilisation on the ECM structure, composition and basement membrane integrity of decellularised nerves

5.1 Introduction

There is a requirement for the terminal sterilisation of medical devices intended for *in vivo* implantation or use (e.g. artificial joint replacements, surgical equipment); this includes decellularised xenogeneic scaffolds [333, 334]. Sterilisation methods which may be suitable for use with decellularised porcine peripheral nerves include treatment with PAA solution, gamma radiation, E Beam, supercritical CO_2, and ethylene oxide [19, 179, 209].

The potential for sterilisation methods to disrupt the structure and biochemical composition of the ECM in decellularised tissue grafts has been widely documented (section 1.8.4) [6, 170, 242, 243, 335]. Furthermore, data in the literature indicate that the extent and severity of such disruption varies according to the specific method (and conditions) used and the individual tissue type being treated.

For example, sterilisation with ionising radiations, such as gamma radiation and E Beam, has been shown to induce extensive structural disruption to the ECM when carried out under dry conditions but not if the tissue is hydrated (a hydrated state being taken as tissue graft which has not undergone an artificial process to remove water from the ECM) [336]. Modulation of the total dose applied (usually quantified in kGy), the dose rate (kGy/h), and the use of dose fractionation, can all influence the extent of disruption to the ECM [1].

Treatment of decellularised tissue grafts with PAA solution has been associated with disruption to the structure and composition of the ECM (especially the basement membrane) in tissues including porcine heart valve, porcine arteries and decellularised porcine dermis [240, 243, 326, 337]. These effects vary according to the concentration of PAA solution and total treatment time [173, 179]. A study in which the same decellularisation process was applied to both porcine and human dermis found that antibody labelling for collagen IV was lost in the porcine dermis treated with 0.1% (v/v) PAA, but retained in the human

dermis for which the PAA sterilisation step was omitted [326]. There is limited knowledge regarding the effects of supercritical CO_2 treatment on ECM structure and composition, due to its relatively recent development as a sterilisation method [19]. However, the inclusion of oxidising agents (e.g. PAA, H_2O_2) as additives to aid in viral/spore killing raises the possibility of associated effects to ECM components being induced.

Prior to treatment with ethylene oxide, decellularised tissue grafts must be dehydrated to enable full diffusion of the gas [193]. This is typically achieved through lyophilisation; however, the ice crystals which form during this process have been shown to induce structural disruption in decellularised soft tissues such as porcine arteries and bovine pericardium [338, 339]. In contrast, hard tissues may be able to better withstand lyophilisation (without negative effects to structural or mechanical properties); historically, lyophilisation followed by ethylene oxide treatment has been widely applied to human bone allografts in tissue banking [187]. Because nerve is a soft tissue with delicate ECM structures (particularly in the endoneurium), and therefore likely to be susceptible to ice crystal-induced ECM damage, the use of alternative dehydration techniques (e.g. desiccation) should be considered. It is also important to demonstrate that the dehydrated tissue can be fully rehydrated without compromising functional properties (e.g. structural and material properties) after processing but prior to implantation, to ensure usability in a clinical situation.

5.2 Aims and objectives

The aim of the work described in this chapter was to characterise the effects of sterilisation methods (PAA solution, gamma radiation, E Beam and supercritical CO_2 treatment) on the structure and composition of decellularised nerve ECM. Alterations were identified by comparison with the baseline dataset described in Chapter 4.

Objectives

i. To determine the effects of methods for dehydrating tissue on decellularised nerve ECM, through staining of histological sections with H & E.
ii. To determine the effects of sterilisation on decellularised nerve ECM structure through staining of histological sections with H & E and Sirius Red with Miller's Elastin.
iii. To determine the effects of sterilisation on the distribution of collagen type IV, laminin and fibronectin within the ECM structure through antibody labelling of histological sections.
iv. To determine the effects of sterilisation on the biochemical composition of decellularised nerves, through quantification of collagen and denatured collagen.
v. To determine the effects of a novel submerged supercritical CO_2 treatment on the retention of basement membrane integrity in decellularised nerves.

5.3 Materials and Methods

5.3.1 Decellularisation of porcine peripheral nerves

Porcine peripheral nerves were dissected, divided into segments of approximately 3 cm in length and decellularised (n = 30 segments per group) using the optimised process as described in section 2.10. Removal of cells and preservation of ECM was assessed using staining with H & E and DAPI and through quantification of DNA content, as described in sections 2.11 and 3.3.1.5.

5.3.2 Optimisation of dehydration process for ethylene oxide treatment

Decellularised nerves (n = 5 per group) were dehydrated using two different processes.

One group of decellularised nerves were frozen to -80 °C, placed in bijous, transferred to a freeze dryer (Savant ModulyoD) and lyophilised at a temperature of -50 °C and a pressure of 0.15 – 0.2 mbar.

A second group of decellularised nerves were placed in bijous and transferred to a glass desiccator with 500 g of silica beads (Figure 5-1).

Figure 5-1 Desiccator used to dehydrate decellularised nerves

The interface between the two halves of the dessicator was sealed with petroleum jelly, to ensure an effective seal was maintained as fully as possible.

Each decellularised nerve segment was weighed once every 24 hours. The dehydration processes were continued until a constant mass was maintained for at least 48 hours. Following dehydration 4 ml of PBS was added to each tube. The dehydrated nerves were incubated in the PBS at 4 °C for up to seven days to allow complete rehydration of the tissue. The results were analysed histologically.

A group of decellularised nerves were frozen once and thawed, as a control for the effects of ice crystal formation during lyophilisation.

The effects were determined by histological staining (H & E).

5.3.3 Sterilisation of decellularised nerves

Groups of decellularised nerves were treated using the following sterilisation methods: PAA (n = 30), gamma radiation, E-beam (n = 30) and supercritical CO_2 (n = 30 for main group; n = 6 for a preliminary study of a novel submerged $SCCO_2$ processing method). The specific conditions used are described in section 2.10.3. The effects of each sterilisation method on the ECM were determined by histological staining (n = 6 per group), antibody labelling (n = 6 per group) and quantification of collagen and denatured collagen content (n = 6 per group). Sodium hydroxide-treated nerves (produced as described in section 2.10.3.5) (n = 3) were used as a positive control.

5.3.3.1 Novel supercritical CO_2 sterilisation method for the processing of tissue under submerged conditions

Decellularised nerves (n = 6) were subjected to a novel supercritical CO_2 process. The conditions (temperature, pressure, cycle length) within the reaction chamber were maintained as described in section 2.10.3.4, but the individual nerve segments were submerged in 3 ml of PBS (pH 7.4) during the treatment cycle. This eliminated the requirement for aseptic addition of sterile PBS following processing. The effects of this process were determined by histological staining (n = 6) and antibody labeling (n = 6).

5.3.4 Histological staining

Formalin-fixed paraffin-embedded sections of decellularised nerves sterilised using different methods were stained using H & E and Sirius Red & Miller's Stain. For each treatment group, sections were taken from segments originating from the peroneal and tibial nerves (n = 3 from each). All sections were viewed microscopically and compared to non-sterilised samples and nerves treated using 1 M NaOH. Any differences were noted.

Processing and sectioning of tissue was carried out as described in sections 2.11.1 and 2.11.2. Staining of sections with H & E and Sirius Red & Miller's Stain was carried out as described in sections 2.11.5 and 2.11.7.

5.3.5 Antibody labelling

Processing and sectioning of tissue was carried out as described in sections 2.11.1 and 2.11.2. Labelling of sections with specific antibodies for collagen IV, laminin and fibronectin was carried out as described in section 2.11.8.

5.3.6 Quantification of collagen and denatured collagen content

The amount of collagen and denatured collagen in the sterilised nerve segments (n = 6 for each group in each assay) was quantified as described in section 2.14.

5.4 Results

5.4.1 Histological characterisation of the effects of different dehydration protocols on decellularised nerves

Dehydration of decellularised tissues is key to enabling the effective application of gaseous sterilisation treatments such as ethylene oxide. H & E staining was used as an initial assessment of the effects of different dehydration protocols upon decellularised nerve histoarchitecture (Figure 5-2).

In isolation, one cycle of freeze-thaw did not result in any gross structural changes in the ECM of decellularised nerves (Figure 5-2 A & B). However, extensive structural disruption was observed when decellularised nerves were frozen and subsequently lyophilised (Figure 5-2 C & D). Disruption to the histioarchitecture was particularly evident in the endoneurium, with the original structure of packed, well-defined tubules almost completely lost. Areas of structural disruption were also seen in the epineurium surrounding the fascicles, with the fascicles appearing to be more detached from the surrounding ECM.

All ECM structures were well-conserved when decellularised nerves were desiccated at room temperature (Figure 5-2 E). However, the structures appeared to be more compact following desiccation and rehydration (Figure 5-2 F, G & H). The original gross histological characteristics of the decellularised nerves, with a loose network of collagenous structures in the epineurium and a defined tighter region of perineurium surrounding each fascicle, did not appear to be restored after incubation in PBS over time points up to six days; this indicated that full rehydration of the tissue was not achieved.

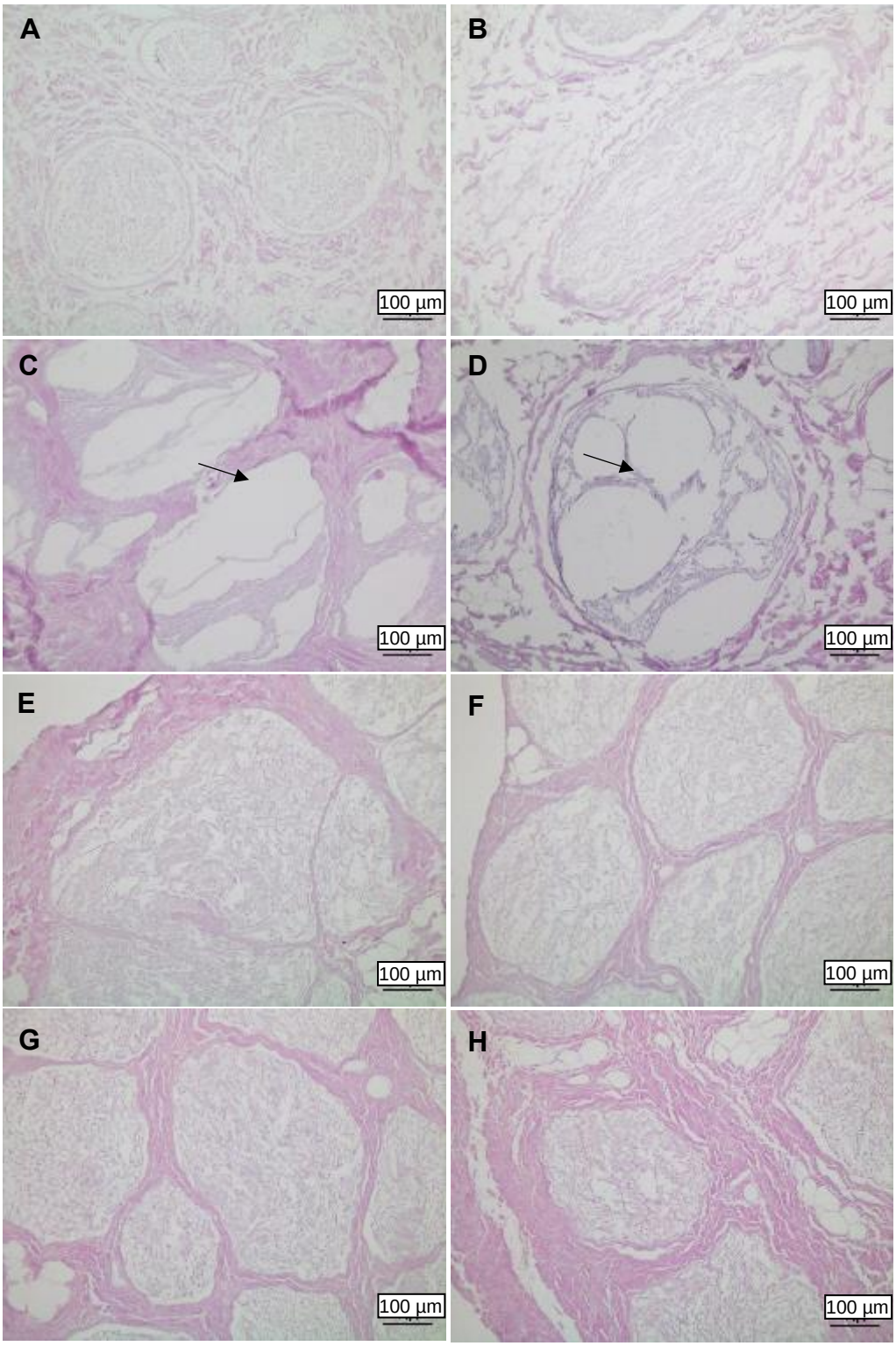
A
100 µm
B
100 µm
C
100 µm
D
100 µm
E
100 µm
F
100 µm
G
100 µm
H
100 µm

Figure 5-2 Representative images of sections stained with H & E (previous page)

H & E-stained sections of (A and B) decellularised nerves frozen to - 80 °C and thawed in PBS, (C and D) decellularised nerves frozen to – 80 °C and lyophilised for 72 hours, before being rehydrated in PBS for 7 days, and decellularised nerves desiccated for 72 hours before being rehydrated in PBS for (E) 0 days, (F) 2 days, (G) 4 days and (H) 6 days. Arrows indicate areas of structural disruption. Images were acquired using Köhler illumination and a x10 objective, scale bars = 100 µm.

5.4.2 Histological analysis of changes to ECM structure.

H & E staining was used to assess the effects of sterilisation treatments upon decellularised nerve histoarchitecture, including the key ECM structures of the epineurium, perineurium and endoneurium (Figure 5-3). Some disruption to both the overall integrity of the endoneurium within each fascicle, as well as the structure of individual tubules, was evident in decellularised nerves treated with PAA and supercritical CO_2. However, none of the sterilisation treatments caused obvious damage to the structures making up the perineurium and epineurium. By contrast, considerable structural changes were observed in the epineurium and perineurium of samples in the positive control group, decellularised nerve denatured through treatment with NaOH. All major ECM structures appeared well conserved following treatment with both gamma radiation and E Beam.

Increased spacing was observed between the perineurium and endoneurium in Figure 5-3 A and Figure 5-3 F. This is likely representive of artefacts introduced during sectioning.

Sirius Red/Miller's Elastin stain was used to define the distribution and structure of collagen and elastin (Figure 5-4). As observed following H & E staining, structural disruption was most evident in the endoneurium of decellularised nerves treated with PAA and supercritical CO_2 when compared to non-sterilised samples. No differences in collagen fibre organisation were evident when sections were viewed under polarised light. The collagen making up the walls of the individual endoneurial tubules appeared to be less dense/thick than in the perineurium and epineurium; however, no differences were discernible between samples in this regard.

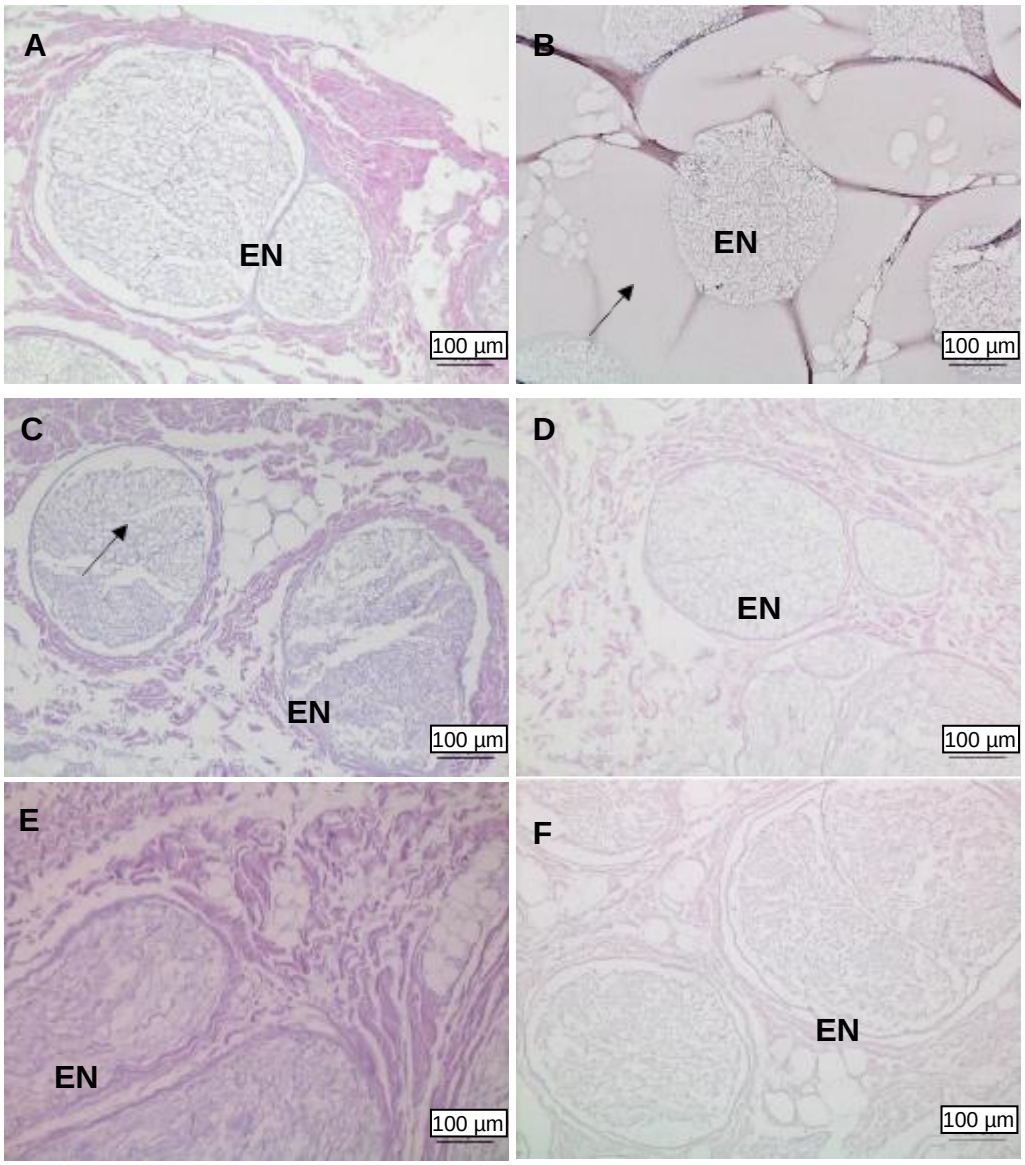

Figure 5-3 Representative images of sterilised decellularised nerve sections stained with H & E

H & E-stained sections of decellularised nerve treated with (A) no sterilisation process, (B) NaOH (positive control), (C) PAA, (D) gamma radiation, (E) E Beam and (F) supercritical CO_2. There was some evidence of disruption to decellularised nerves treated PAA and supercritical CO_2, predominantly located in the endoneurium (EN). Arrows indicate areas of structural disruption. Images were acquired using Köhler illumination and a x10 objective, scale bars = 100 µm.

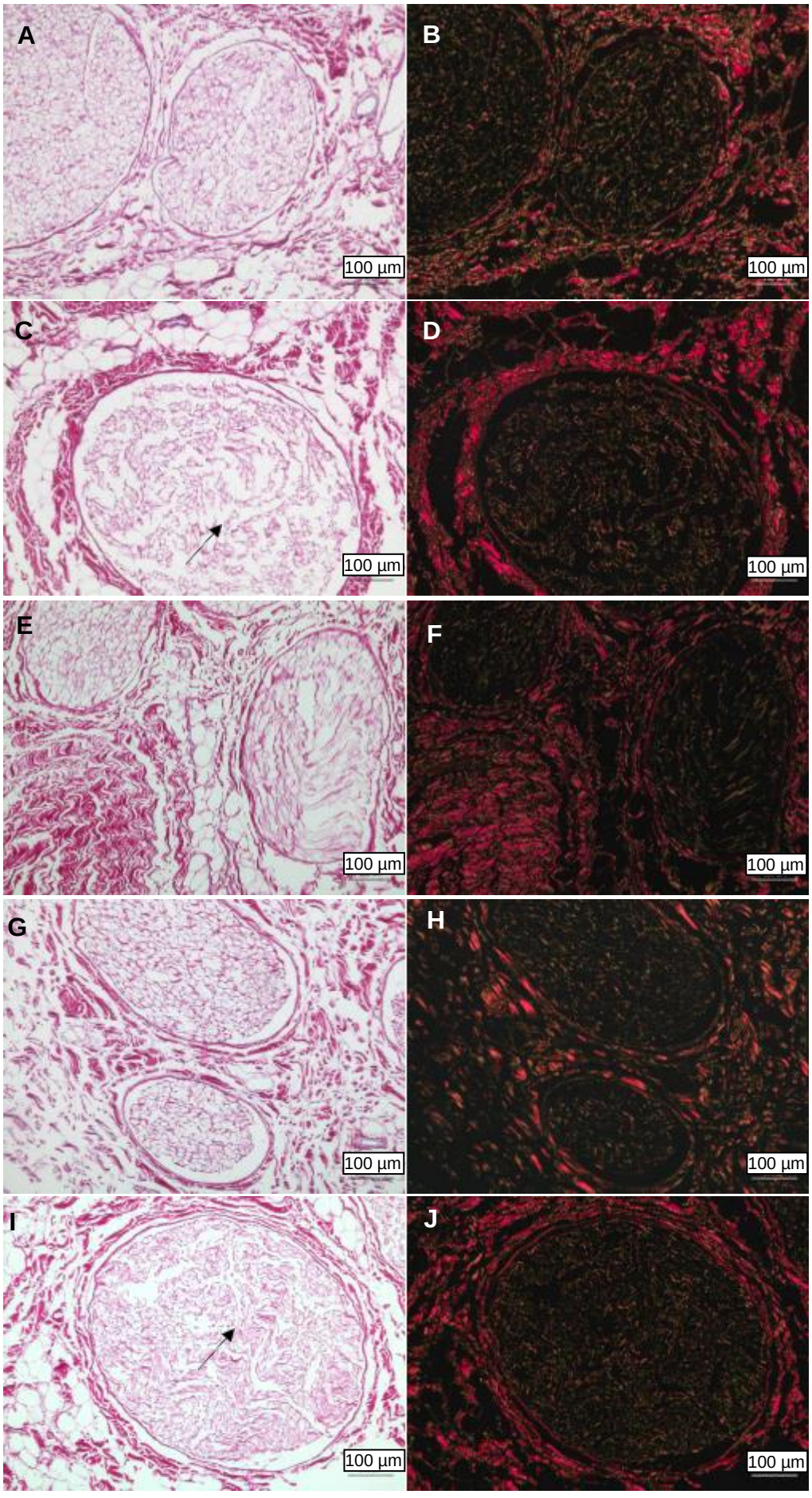
A
100 µm
B
100 µm
C
100 µm
D
100 µm
E
100 µm
F
100 µm
G
100 µm
H
100 µm
I
100 µm
J
100 µm

Figure 5-4 Representative images of decellularised sterilised nerve sections stained with Sirius Red/Miller's Elastin (previous page)

Sirius Red/Miller's-stained decellularised nerve treated with (A and B) no sterilisation process, (C and D) PAA, (E and F) gamma radiation, (G and H) E Beam and (I and J) supercritical CO_2. Some evidence of structural changes were evident, particularly to the endoneurium (indicated by arrows). Images were acquired under Köhler illumination (A, C, E, G, I) and Polarised light conditions (B, D, F, H, J) and using a x10 objective, scale bars = 100 µm.

5.4.3 Immunohistochemical labelling of collagen IV

Sections of decellularised nerves from each sterilisation group were labelled with a monoclonal antibody against collagen type IV to identify if each sterilisation method affected the distribution of collagen IV (Figure 5-5). Specificity of labelling was confirmed through the inclusion of a native porcine artery positive control (Figure 5-5 G). As expected, in non-sterilised nerves collagen IV labelling was predominantly located in the endoneurium and perineurium (Figure 5-5 A); positive labelling appeared to retained in these regions in decellularised nerves treated with gamma radiation and E Beam (Figure 5-5 C, D). The intensity of labelling in irradiated samples was slightly reduced compared with non-sterilised decellularised nerve Figure 5-5 C & D)

No positive labelling for collagen IV was seen in decellularised nerves treated with PAA or supercritical CO_2 (Figure 5-5 B & E, respectively).

Figure 5-5 Representative images of decellularised sterilised nerve sections labelled with monoclonal antibodies against collagen IV (next page)

Collagen IV-labelled decellularised nerves treated with (A) no sterilisation process, (B) PAA, (C) gamma radiation, (D) E Beam and (E) supercritical CO_2. An isotype control (F) and a porcine artery positive control (G) were included. The endoneurium (EN) is labelled for reference. Arrows indicate the basement membrane region of the perineurium (PE). Images were acquired using Köhler illumination and a x10 objective, scale bars = 100 µm.

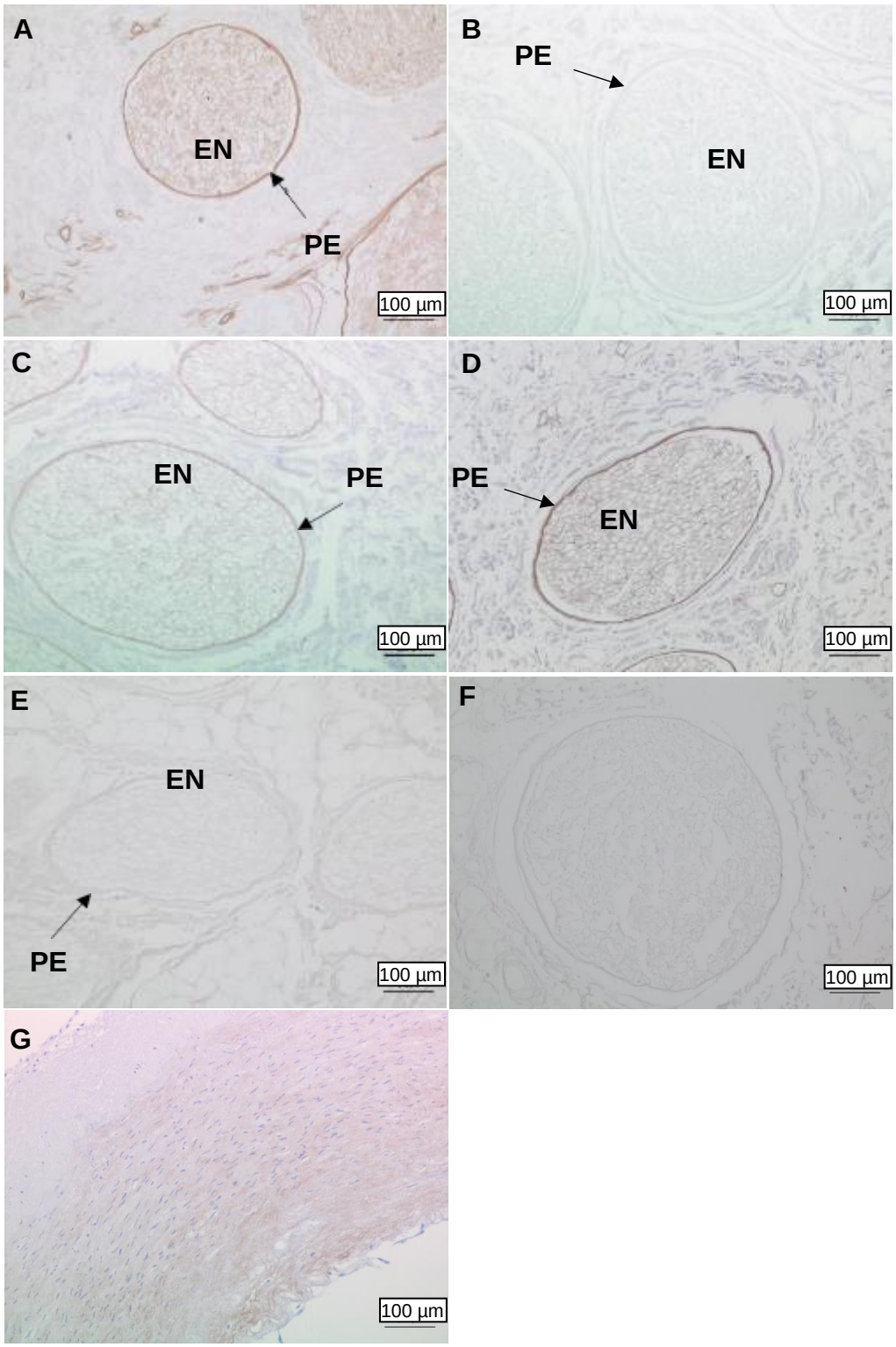
A
EN
PE
100 µm
B
PE
EN
100 µm
C
EN
PE
100 µm
D
PE
EN
100 µm
E
EN
PE
100 µm
F
100 µm
G
100 µm

5.4.4 Immunohistochemical labelling of laminin

Sections of decellularised nerves from each sterilisation group were labelled with a monoclonal antibody against laminin to identify if each sterilisation method affected the distribution of laminin within the ECM (Figure 5-6). The specificity of labelling for laminin was confirmed using a native porcine artery positive control (Figure 5-6 G).

Strong labelling was observed in decellularised nerves treated with PAA, gamma radiation and E Beam (Figure 5-6 B, C and D); as in non-sterilised nerves Figure 5-6 A), laminin labelling was primarily confined to the perineurium and endoneurium. This suggested that laminin was retained in the basement membrane following these treatments.

However, labelling was much reduced in intensity following treatment with supercritical CO_2 (Figure 5-6 E). The localisation of the labelling was also less defined, with weak labelling appearing to be widely distributed throughout the tissue rather than limited to the endoneurium and perineurium.

Increased spacing was observed between the perineurium and endoneurium in Figure 5-6 D and Figure 5-6 F. This is likely representive of an artefact introduced during sectioning.

Figure 5-6 Representative image of of decellularised nerve sections labelled with monoclonal antibodies against laminin (next page)

Laminin-labelled decellularised nerves treated with (A) no sterilisation process, (B) PAA, (C) gamma radiation, (D) E Beam and (E) supercritical CO_2, immunohistochemically labelled for the presence of laminin. An isotype control (F) and a porcine artery positive control (G) were included. Images were acquired under Köhler illumination and a x10 objective, scale bars = 100 µm.

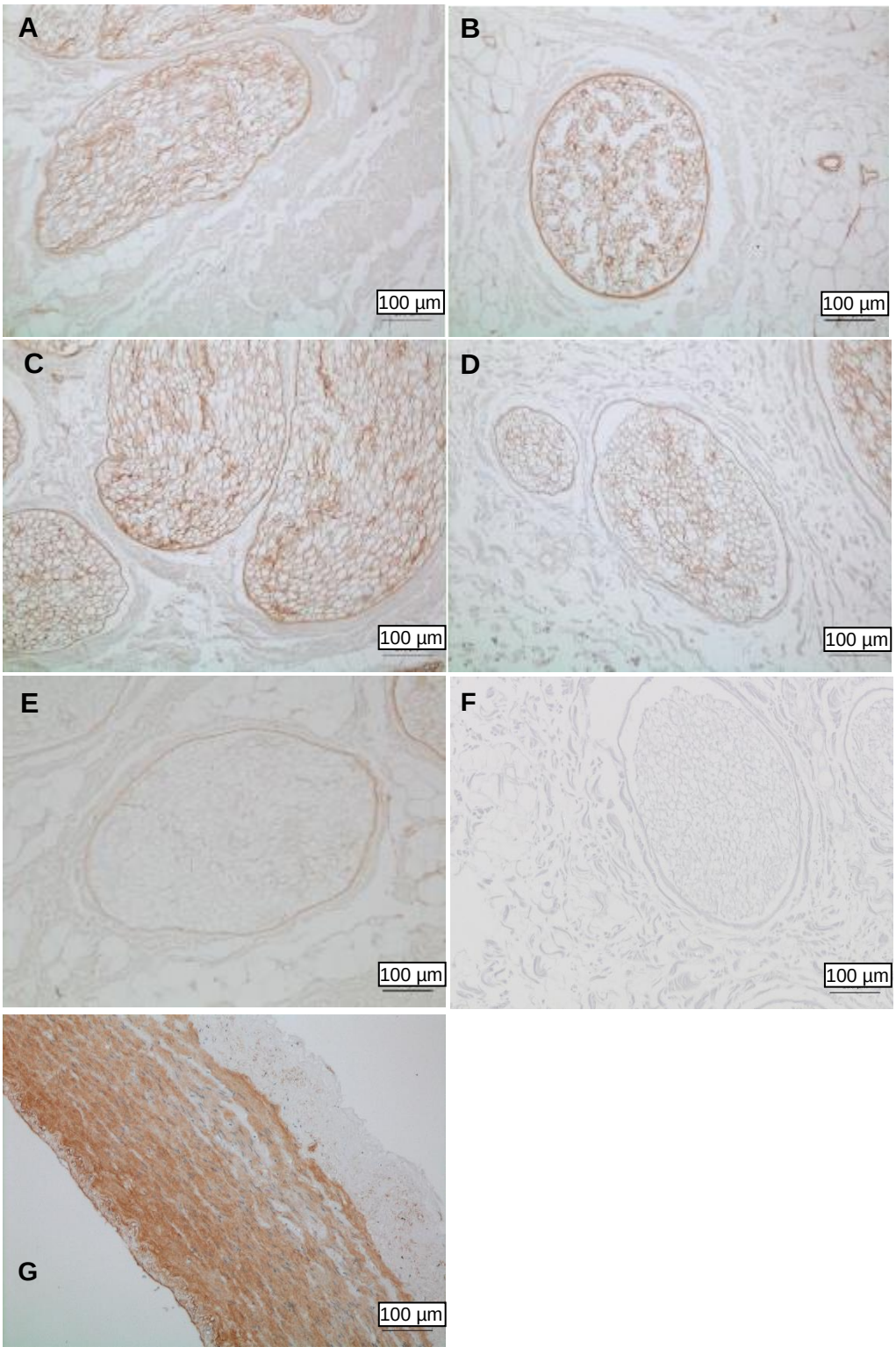
A
100 µm
B
100 µm
C
100 µm
D
100 µm
E
100 µm
F
100 µm
G
100 µm

5.4.5 Immunofluorescent labelling of fibronectin

Sections of decellularised nerves from each sterilisation group were labelled with a monoclonal antibody against fibronectin to identify if each sterilisation method affected the distribution of fibronectin within the ECM. The primary monoclonal antibody was visualised using a fluorescently-tagged secondary antibody. A native porcine artery positive control was included to confirm specificity of labelling (Figure 5-7 G).

Some degree of labelling for fibronectin appeared to be retained following each of the sterilisation treatments (Figure 5-7). The distribution and intensity of fibronectin labelling in nerves treated with PAA, gamma radiation and E Beam (Figure 5-7 B, C and D, respectively) was similar to that observed in non-sterilised nerves (Figure Figure 5-7 A). Fibronectin labelling was intense in the perineurium, but weaker and less consistent in the endoneurium.

The distribution of fibronectin appeared to be altered in decellularised nerves treated with supercritical CO_2 when compared to non-sterilised samples (Figure 5-7E). Fibronectin labelling was reduced in intensity in the perineurium and appeared to be almost completely absent in the endoneurium.

Increased spacing was observed between the perineurium and endoneurium in Figure 5-7 F. This is likely representive of an artefact introduced during sectioning.

Figure 5-7 Representative images of decellularised sterilised nerve sections labelled with a monoclonal antibody against fibronectin and counterstained with DAPI (next page)

Fibronectin-labelled decellularised nerves treated with (A) no sterilisation process, (B) PAA, (C) gamma radiation, (D) E Beam and (E) supercritical CO_2, immunofluorescently labelled for the presence of fibronectin. An isotype control (F) and a porcine artery positive control (G) were included. Fibronectin labelling intensity was well conserved in nerves treated with PAA, gamma radiation and E Beam. Labelling was predominantly localised to the perineurium. The intensity of labelling appeared to be reduced after treatment of decellularised nerves with supercritical CO_2. The endoneurium (EN) and perineurium (PE, arrow) are labelled on the first image for reference. Images were acquired at a wavelength of 488 nm using a x10 objective, scale bars = 100 µm.

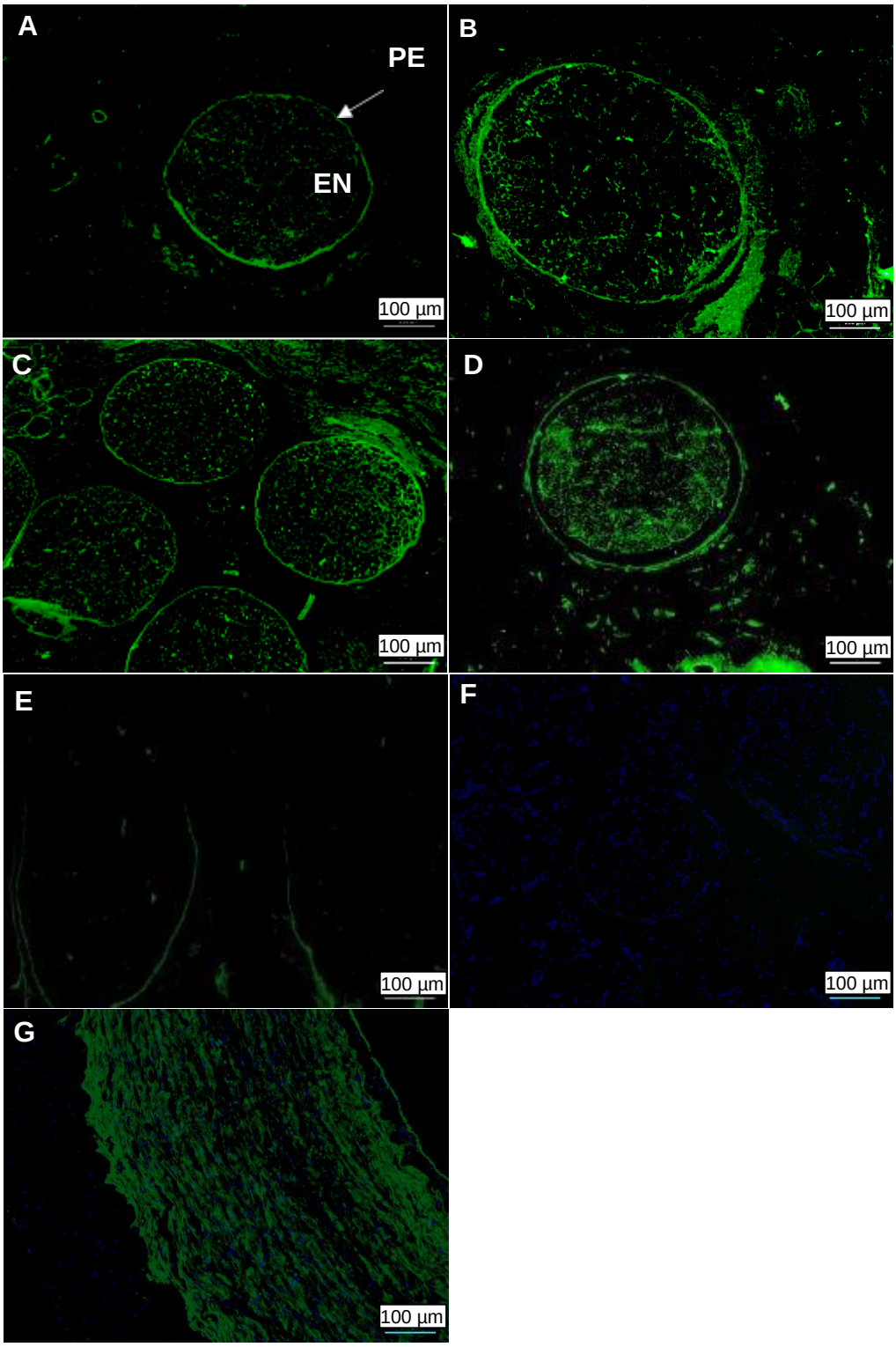
A
PE
EN
100 µm
B
100 µm
C
100 µm
D
100 µm
E
100 µm
F
100 µm
G
100 µm

5.4.6 Quantification of collagen and denatured collagen content

In order to quantify the collagen and denatured collagen content, tissues were assayed for hydroxyproline content with or without prior α-chymotrypsin digest. The assay protocol produced a linear relationship between absorbance at 570 nm and hydroxyproline concentration (Figure 5-8).

No significant differences were found between the collagen content or denatured collagen content of decellularised nerves in any of the treatment groups (Figure 5-9). The exception to this was the NaOH positive control group, which had a significantly increased denatured collagen content in comparison to all other treatment groups.

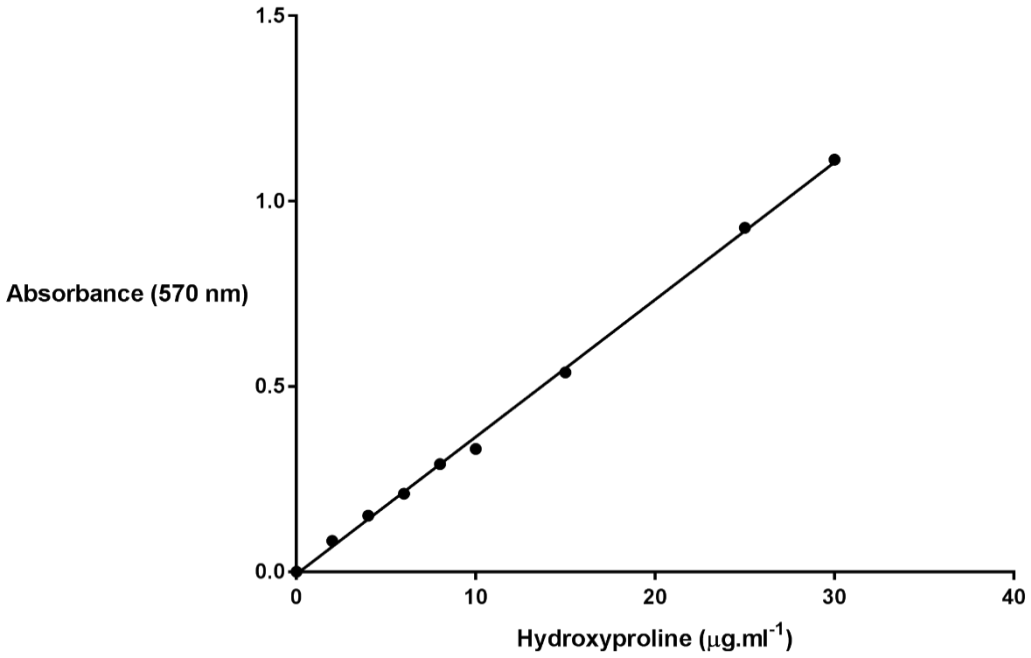

Figure 5-8 Standard curve for the interpolation of hydroxyproline content

Relationship between absorbance at 570 nm and trans-4-hydroxy- L-proline concentration (n = 3), used for the interpolation of hydroxyproline content from hydrolysed and neutralised samples. Samples were either tissue segments or α-chymotrypsin digest supernatants.

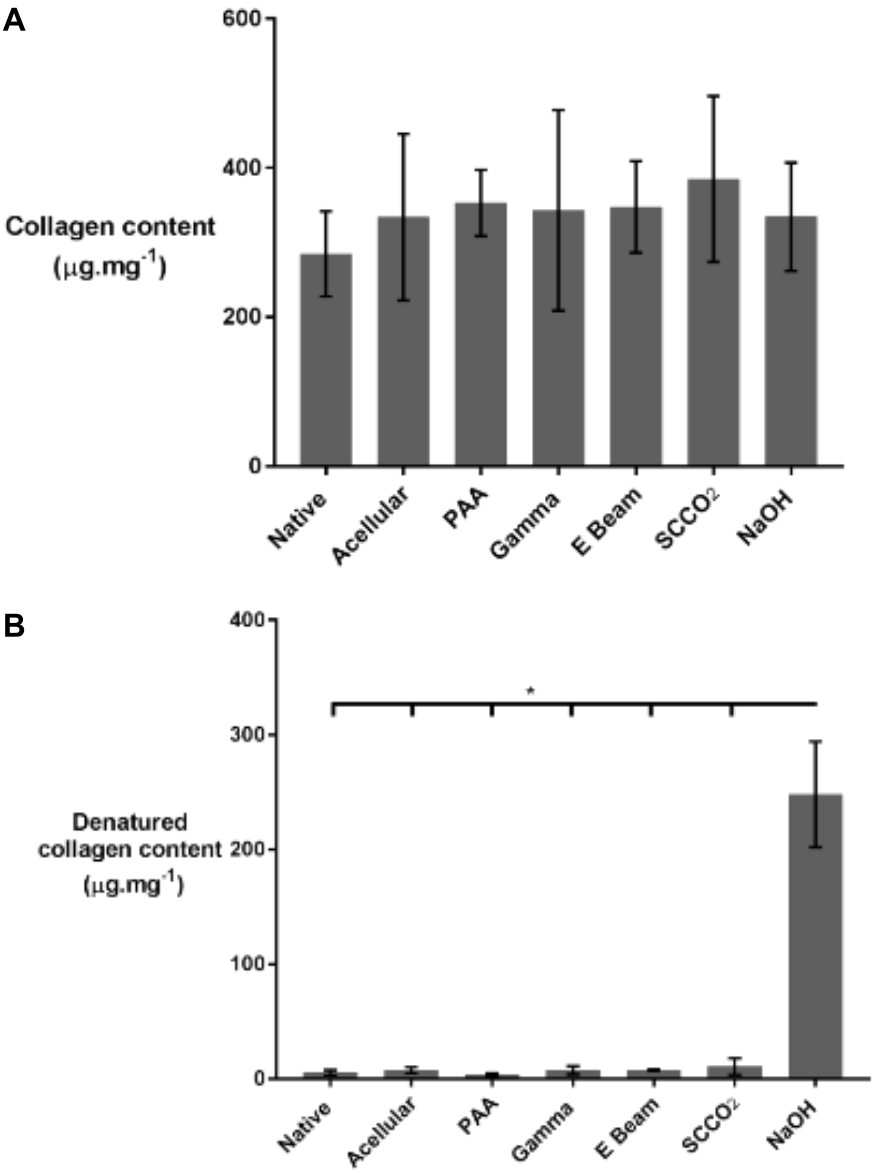

Figure 5-9 Collagen and denatured collagen content of native, decellularised and sterilised porcine peripheral nerves

(A) Collagen content and (B) denatured collagen content of native peripheral nerves, decellularised peripheral nerves from all treatment groups. Data shown as mean +/- 95 % confidence interval, n = 6. Statistical analysis was by (A) one-way ANOVA or (B) Kurskal-Wallis. * denotes groups which are significantly different ($p<0.05$).

5.4.7 Comparison of basement membrane composition in decellularised nerves treated with standard and submerged supercritical CO_2 processes

Decellularised nerves were treated with supercritical CO_2 under two different conditions, 1) in air (section 2.10.3.4) or 2) submerged in PBS (section 5.3.3.1). Sections of decellularised nerves from both treatment groups were labelled with monoclonal antibodies against collagen IV, laminin and fibronectin to establish the distribution of each component throughout the ECM following sterilisation (Figure 5-10).

Collagen IV distribution patterns were retained when decellularised nerves were treated with supercritical CO_2 under submerged conditions (compared with non-sterilised decellularised nerves, verified through comparison with a native porcine artery positive control; Figure 5-5 G), with collagen IV appearing highly localised to the endoneurium and perineurium; however, positive labelling for collagen IV was completely absent in samples treated under the standard conditions (Figure 5-10 A & B).

Laminin labelling was reduced in intensity (compared with non-sterilised decellularised nerve [Figure 5-10A]; specificity confirmed through comparison with native porcine artery positive control [Figure 5-6 G]) and seemed to be diffuse throughout the tissue (rather than primarily located in the basement membrane regions of the endoneurium and perineurium) in decellularised nerves treated under the standard conditions (Figure 5-10 C). In decellularised nerves treated under submerged conditions, the intensity and localisation of staining appeared to be close to that seen in the untreated (non-sterilised) decellularised nerves (Figure 5-10 D). A reduction in the intensity of fluorescent labelling for fibronectin was observed in decellularised nerves treated under the standard protocol (Figure 5-10 E) compared with non-sterilised decellularised nerves, where positive labelling for fibronectin was evident in the basement membrane regions of the perineurium and endonerium (Figure 5-7 A; specificity was confirmed by labelling of a native porcine artery positive control [Figure 5-7 G]). Coverage was incomplete, even in the perineurial region. In contrast, fibronectin seemed to be retained throughout the perineurium of decellularised nerves treated under the submerged process, with some weaker labelling also present in the endoneurium (Figure 5-F).

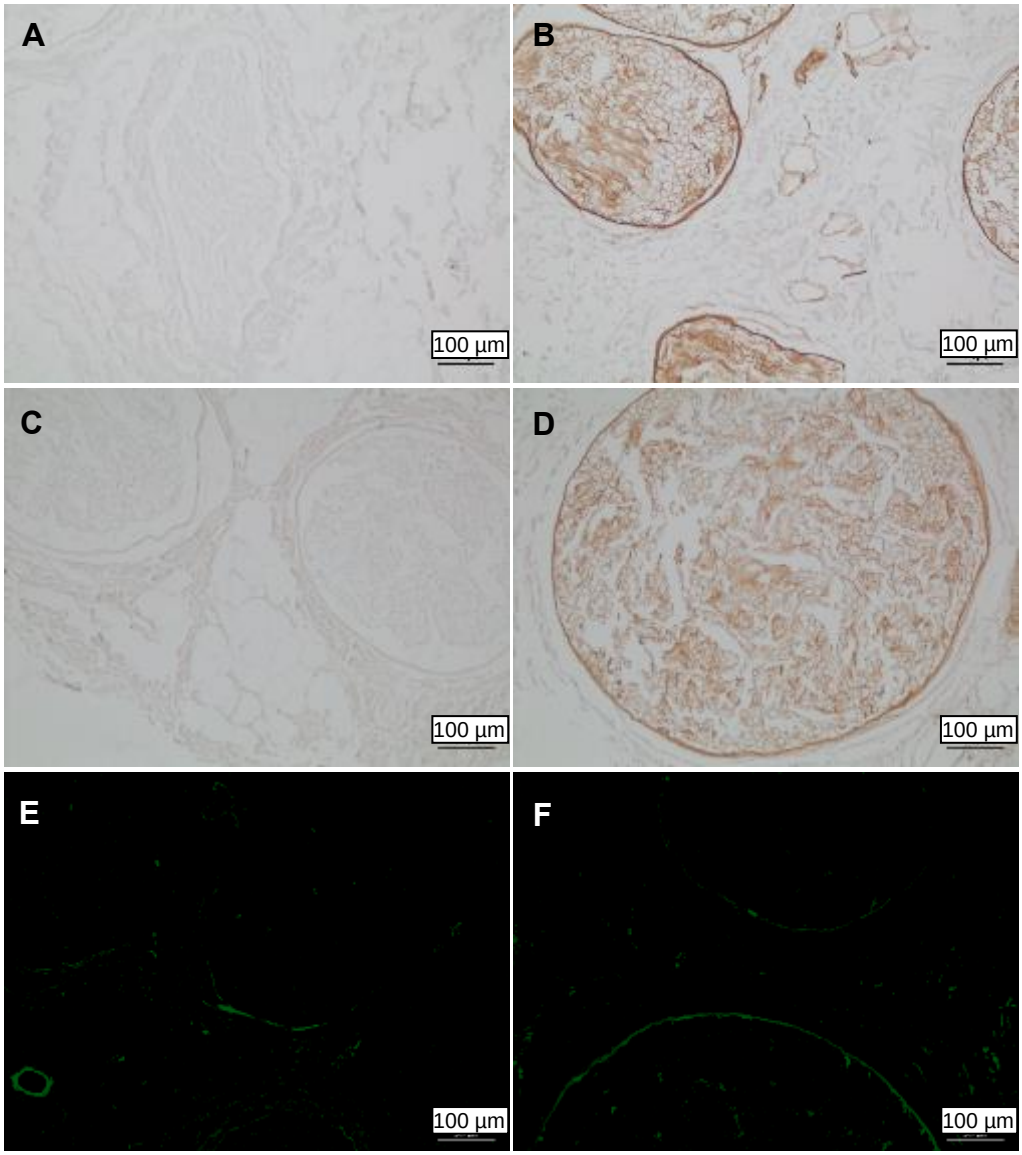

Figure 5-10 Images of sections of decellularised nerves labelled with monoclonal antibodies against collagen IV, laminin and fibronectin

Collagen IV, laminin and fibronectin-labelled decellularised nerves treated with (A, C and E) the standard published supercritical CO_2 protocol and (B, D and F) the submerged supercritical CO_2 protocol, immunohistochemically labelled for the presence of (A and B) collagen IV, (C and D) laminin and (E and F) fibronectin. Images of collagen IV and laminin were acquired using Köhler illumination, and images of fibronectin were acquired at a wavelength of 488 nm, using a x10 objective. Scale bars = 100 µm.

5.5 Discussion

Through staining with H & E and Sirius Red/Miller's, the sterilisation treatments used in this study were shown not to cause extensive damage to the histoarchitecture of the decellularised nerves; quantitative biochemical assays revealed no alterations to the collagen/denatured collagen content. Antibody labelling revealed some changes to the intensity and distribution of collagen IV in the endoneurium and perineurium of nerves treated with PAA or supercritical CO_2 (standard process); similar changes were seen when supercritical CO_2-treated nerves were labelled for laminin and fibronectin.

The only decellularised nerve graft currently in clinical use, the Avance® nerve graft, is sterilised using gamma radiation [137]. While little information is given in the literature about the specific conditions used during irradiation, the nerves appeared to retain positive antibody labelling for laminin following irradiation and did not appear to sustain any obvious structural alterations to the ECM when examined histologically [340]. The published data do not distinguish between the effects of decellularisation and the effects of sterilisation, and it is possible that, given the possible alterations which may occur following gamma irradiation of a tissue graft (e.g. the potential for the induction of chain scission/crosslinking of collagens within the ECM), another sterilisation method may be more suitable for use with decellularised peripheral nerve tissue [1, 172, 341]. A decision was made during the present study to consider the use of several different sterilisation methods (both well established and relatively novel, for use with the decellularised porcine nerves), and to extensively characterise the effects of such methods upon a range of key biological and physical parameters identified as potentially affecting the ability of the grafts to support cell growth and migration and facilitate maximal functional restoration.

For a decellularised tissue graft to be effectively sterilised through ethylene oxide treatment, it must first be dehydrated to enable full diffusion of the gas through the ECM [342]. The formation of ice crystals during the process of lypohilisation may induce structural disruption in decellularised tissue grafts, with soft tissues such as artery being more susceptible than harder tissues such as bone (which is widely used in surgical procedures) [338, 343]. However, a single freeze-thaw cycle has been successfully employed (with no histological

evidence of resulting structural degradation) as a first step in the decellularisation process for tissues such as porcine nerves (including in the current study) and arteries, to “open” the ECM structure and enable better penetration and egress of decellularisation reagents and associated cellular debris [18, 344]. While the process of freezing in isolation did not appear to damage the histoarchitecture of decellularised nerves, extensive structural disruption was evident following rehydration of lyophilised nerves. The loss of structural integrity was evident at all levels of the ECM including the endoneurium, perineurium and epineurium. Such changes are likely to inhibit the mechanical support and physical guidance of regenerating axons, and so it is unlikely nerves treated in this manner would be suitable for use as a graft material.

The process of lyophilisation is mediated through subjecting a given material dissolved in water/containing water (e.g. active biologics in solution, decellularised tissue grafts) to specific environmental conditions of low temperature and pressure in order to induce sublimation (i.e. the change in state of frozen water directly to vapour) [338, 345]. The application of this process to biological materials is widely practised, as the controlled conditions and low temperatures generally enable superior preservation of functional properties compared with other drying processes (e.g. heat-mediated; biological materials are liable to degradation if exposed to excessive heat and/or conditions which may enable facilitate microbial growth and thereby enzymatic digestion) [323, 346]. Because of these advantages, lyophilisation is widely used as a preservation method for biological materials in the food and pharmaceutical industries. As materials must be frozen prior to (and during) lyophilisation, the possible consequences of ice crystal evolution within the tissue should be considered. The thermodynamics of ice crystal formation favours the formation of irregular structures under slower and variable rates of freezing [345]. In the present study, the freezing process alone did not appear to affect the histoarchitecture of the decellularised nerves; therefore, temperature variation within the freeze dryer may have been responsible. In a study of decellularised porcine arteries, initial controlled rate freezing to -40 °C (the rate of which was increased using a pre-cooled shelf) followed by an increase in temperature to 0 °C induced minimal structural disruption compared

to controlled rate freezing to -10 °C [338]. Rapid cooling followed by maintenance of a stable temperature promotes the formation of ice crystals with a more uniform and stable structure, decreasing the likelihood of structural disruption. The freeze dryer used during the present study did not allow for controlled-rate freezing or precise control of internal temperature, and as a result irregular ice crystal structures are likely to have formed and likely induced the observed structural disruption.

In contrast to the lyophilised nerves, structural disruption was minimal after the desiccation of decellularised nerves, likely because the chamber was maintained at room temperature throughout the process. However, the ECM structure appeared to remain “tight” and did not fully rehydrate after incubation in PBS, even after a duration of seven days. A possible explanation for this finding is the relatively high proportion of fat in the decellularised nerves, as demonstrated in section 4.4.10. Meyer *et al* (2013) examined the rate and extent of rehydration in different dehydrated porcine tissues including fat, muscle, lung, cartilage and tendon [347]. Fat was the only tissue not to significantly increase in mass after 60 minutes of rehydration, remaining at approximately 80 % of the original mass. The hydrophobicity of fat was postulated as the most likely reason for this effect, and it is probable that the fatty tissue in the decellularised nerves inhibits full rehydration in a similar manner. Due the role of fat in protecting axons from compressive mechanical forces in the decellularised nerves and the potential impact of removal agents on the ECM, extraction of fat from the tissue using ethanol or acetone could negatively impact upon the ability of the decellularised nerves to support neuroregeneration [348]. Ethylene oxide treatment requires prior dehydration of tissue-based scaffolds, to allow access of the gas throughout the ECM and enable egress (through aeration) of residual toxic breakdown products remaining within the ECM post-processing [184, 185, 342]. Such toxic breakdown products are thought to be retained in higher quantities in fatty tissue; a 35% increase in fibroblast growth was observed when the cells were incubated with lyophilised, ethylene oxide-treated human femoral bone chips which were defatted prior to processing versus those which were not defatted [244]. Until suitable dehydration and rehydration processes for decellularised nerves can be identified, and concerns surrounding the fat content of the nerves

and the resultant potential for the retention of toxic by-products have been addressed, ethylene oxide treatment cannot be considered for use as a sterilisation method with the decellularised nerves.

Some evidence of structural disruption was seen in decellularised nerves treated with 0.1 % (v/v) PAA solution, which was primarily characterised by a loss of definition in the tubular structures of the endoneurium. Structural disruption has been demonstrated in other decellularised soft tissues treated with PAA, including murine lung and porcine small intestine submucosa [173, 242]. In the present study disruption was almost exclusively located in the endoneurium, with no obvious alterations to the perineurium or epineurium. Existing evidence is inconclusive as to whether retention of endoneurial tubule structure is required for a graft to facilitate reinnervation; this is due to the potential for restriction of axonal growth direction resulting in forced rerouting and the potential for compromised functional recovery resulting from this [349]. Some misdirection of regenerating axons was observed in a simple model of rat sciatic nerve laceration, repaired through coaptation and measured through electromyography. However, kinematic analysis of movement patterns did not reveal any negative implications for functional recovery resulting from this (compared to untreated control animals). Macrophages and Schwann cells mediate some remodelling of the endoneurial tubules through the release of MMPs and secretion of new ECM components, which could correct the minor structural disruption seen here in PAA-treated nerves [350].

A 2018 study compared axonal reinnervation of distal pathways following repair of a rat sciatic defect with either a chitosan/PGLA guidance conduit or an autograft [135]. The conduit facilitated superior improvements in motor function and directional accuracy of axonal growth in a 3 mm defect but not in a 6 mm defect. It is recognised that in larger defects regenerating axons benefit from aligned physical and chemotrophic cues to stimulate and guide growth [7]. ECM-based grafts, including autografts and cellular or decellularised allografts and xenografts, fulfil both of these requirements with intact endoneurial tubules composed of key cell attachment molecules including collagen IV, laminin and fibronectin [18].

In vitro studies have shown that synthetic guidance conduits with a linear, aligned topography (whether in the form of striations on the inner surface of the conduit, channels or a mesh of aligned fibres) are able to promote more directed neurite growth across greater distances than those with a simple topography [351]. Preliminary *in vivo* results indicated that the implantation of a multichannel PLGA nerve conduit into a rat sciatic defect model corresponded with a downstream muscle composition being closer to that found in native control tissue animals (a higher proportion of type I to type II muscle fibres) after 12 week *in situ* [352]. In animals where the defect was repaired with a single lumen PGLA conduit, the ratio was closer to 1:1. The authors suggested that this was indicative of a more organised growth of axons across the defect, leading to a higher rate of functional reinnervation at the effector site (distal to the defect). However, the small sample sizes used in this study meant that no differences were detected across other functional parameters including direction of axon growth and the amplitude of compound muscle action potentials, and, when examined histologically; furthermore, both conduits were found to support the growth of significantly fewer myelinated axons across the defect site compared with an autograft repair. Given the relative importance of physical and chemotrophic guidance, it is unlikely that a significantly disrupted endoneurium (such as that observed in decellularised nerves treated with PAA) would facilitate axonal regeneration across large defects. Decellularised nerves sterilised with gamma radiation, E Beam and supercritical CO_2 appeared to retain the fine “honeycomb” structure of the endoneurial tubules and are therefore likely to provide physical guidance for regenerating axons in a similar manner to an autograft, the current gold standard therapy in defects considered too large for repair by coaptation [115].

Cell attachment motifs in the basement membrane are crucial for the attachment, growth and function of cells including Schwann cells, neurons and perineurial cells [42]. In the peripheral nerve, laminin and fibronectin are thought to be the main mediators of interaction between key cell types (axons and Schwann cells) and the ECM [50]. The relative importance of differing subtypes of such components should also be considered; for example, laminin-8 is thought to primarily promote Schwann cell growth and function (e.g. myelination), whereas laminin-2 is associated with axonal growth. These

interactions have been demonstrated *in vitro* and in an *in vivo* murine gene knockout model [61]. In the present study, reductions in the intensity of antibody labelling for basement membrane components (in particular collagen IV) were seen in decellularised nerves treated with PAA and supercritical CO_2. A loss of positive staining for collagen IV following PAA treatment has been demonstrated in decellularised porcine mitral valves and porcine & human decellularised arteries. [239]. Collagen IV provides a scaffold for the attachment of other basement membrane components such as laminin, fibronectin, nidogen, and perlecan [353]. It is unlikely that the collagen IV has been fully denatured or degraded in decellularised nerves treated with PAA solution, due to the preservation of positive labelling for laminin and fibronectin and the fact that collagen IV forms a scaffold structure in the basement membrane onto which these components are bound [60, 328]. Instead, changes to the conformation and/or surface chemistry of the collagen IV molecule may have altered the specific target epitope of the CIV-22 antibody and thereby reduced the incidence of high affinity binding events.

It is likely that a similar chemical mechanism is responsible for the changes seen in decellularised nerves treated with supercritical CO_2, where laminin and fibronectin labelling intensities were also diminished. Supercritical CO_2 is thought to diffuse through the membrane/wall of bacterial cells/endospores, and thereafter dissolve within the cytoplasm. This would increase levels of carbonic acid, and thereby lower the intracellular pH to cytotoxic levels [215, 216]. However, such a mechanism would not be effective against non-cellular pathogens. Therefore the incorporation of the NovaKill™ additive solution, containing the oxidising agents PAA and H_2O_2, is necessary for effective elimination of viral bioburden during supercritical CO_2 processing [216].

The effects of oxidising agents such as PAA and H_2O_2 on ECM proteins at a molecular level, and the resultant implications for cell binding, have not been fully elucidated. Finnegan *et al* (2010) showed that oxidising agents react with a range of amino acids in solution including glycine, cysteine, methionine, lysine, histidine and tryptophan, leading to degradation and the formation of oxidation products [180]. PAA was noticeably more potent than H_2O_2, which required a higher ratio of oxidative agent to amino acid for the reaction to occur. The primary mechanisms for the alteration of amino acids are thought to be

dependent on the side chain type; for example, aliphatic amino acids are susceptible to hydrogen abstraction whereas aromatic amino acids undergo hydrogen addition [354]. Fourier transform infrared spectroscopy (FTIR) analysis of decellularised temporomandibular discs revealed changes in surface chemistry as a result of treatment with 0.2 % (v/v) PAA solution in 4 % (v/v) ethanol [179]. The predominant site of damage was aliphatic side chains; it was postulated that this would not adversely affect cell attachment due to the non-aliphatic composition of the common cell attachment motif RGD (arginine-glycine-aspartic acid). This theory was supported by the results of an *in vitro* cell seeding experiment conducted during the same study. When seeded with human umbilical cord Wharton's Jelly matrix cells, decellularised temporomandibular discs treated with the PAA-ethanol solution supported an approximately fivefold greater surface area of cell coverage compared to those sterilised with either gamma radiation (dry state) or ethylene oxide. These data suggest that the changes to basement membrane components induced through treatment with oxidising agents may not impede cell attachment.
A study into the ability of oxidising agents to degrade proteins found that bovine serum albumin (BSA) was fully degraded by PAA solution [180]. H_2O_2 in a vapourised form mediated full degradation of BSA, whereas H_2O_2 in solution did not. These findings are consistent with the different redox potentials of each reagent, at 1.81 volts (V) compared to 1.76 V for PAA and H_2O_2 respectively [355, 356]. PAA is also known to disrupt disulphide bonds, which are crucial to the maintenance of tertiary and quaternary structure (and therefore the conformation) of collagen IV [357-359].

Mass spectrometric analysis of decellularised murine lungs revealed a significant increase in residual ECM components following PAA treatment but not after gamma radiation [242]. The relative increase was largest for sub-chains associated with collagen types I, IV and VI, laminin, and fibronectin. The increased level of “free” ECM components was attributed to the solubilisation of the ECM components during PAA treatment, which could provide an explanation for the non-specific distribution of laminin seen in sample treated with supercritical CO_2 under standard (non-submerged) conditions.

Histological examination of impacted human allograft bone chips sterilised with $SCCO_2$ in the absence of an additive solution and implanted as part of an ACL

repair procedure found evidence of “creeping” integration into the surrounding cancellous bone, with a marked improvement in tissue remodelling and organisation in biopsies taken 10 months versus those taken at 7 months [360]. This provides the first evidence of the effective use of $SCCO_2$-treated tissue in a clinical setting; however, evidence suggests to that addition of supplementary agents (e.g. oxidising agents) is likely necessary to achieve a sufficient reduction in viral and/or bacterial spore populations to meet the criteria of SAL 10^{-6}, and so the effects of $SCCO_2$ sterilisation in combination with such agents must be considered here [215].

These effects of oxidising agents (especially PAA) including the solubilisation of ECM components, the induction of changes to the conformation of proteins, and alterations to the chemistry of amino acid side chains, have the potential to affect the availability and function of cell attachment motifs and chemoattractants within the basement membrane of decellularised nerves, and therefore could negatively impact on cell ingrowth and neuroregeneration.

The increased severity of basement membrane degradation in decellularised nerves treated with the standard $SCCO_2$ process (i.e., with the tissue segments directly exposed to the $SCCO_2$ and NovaKill™ reagent rather than being submerged in a PBS solution during processing) compared to those treated with the 0.1% (v/v) PAA solution may be due to higher local concentrations of oxidising agents. The NovaKill™ reagent contains PAA at a concentration of 13.5 – 18.5 % (v/v) and H_2O_2 at 4.5 – 6 % (v/v). As the decellularised nerves were not submerged in buffer solution (e.g. PBS) during the $SCCO_2$ treatment cycle under standard conditions, it is possible that the concentration of PAA in direct contact with the ECM components was significantly higher than the 0.1 % (v/v) in the PAA treatment solution. The documented effects of oxidising agents on proteins and the similarities in labelling patterns between decellularised nerves treated with PAA solution and the $SCCO_2$ process (under standard conditions) suggest oxidation of basement membrane components (and solubilisation following the aseptic addition of PBS) is the likely mechanism of damage in these non-submerged conditions.

The retention of localised basement membrane labelling seen in decellularised nerves treated with supercritical CO_2 while submerged in PBS provides further

evidence suggesting that the supercritical fluid is not responsible for the damage observed under standard processing conditions. A similar result was seen in decellularised rat lungs treated with a NovaKill™-based process [243]. In this study, which represents the only published work to examine similar parameters within a decellularised tissue graft, the tissue was not subjected to the proprietary submerged $SCCO_2$ processing method; instead, the lungs were filled with a small volume of PBS to prevent collapse of the airways during processing. However, antibody labelling revealed preservation of laminin labelling after processing, indicating that a similar protective effect may have been provided by the PBS. The lungs were not labelled for collagen IV or fibronectin, and the only other study investiagitn the use of $SCCO_2$ processing as a terminal sterilisation step for decellularised tissues (decellularised porcine aortic valves) did not investigate the retention of specific ECM components [19]. The protective effect of the PBS solution may be multifactorial, preventing the local concentration of oxidising agents from becoming too high and ensuring the elution of any residual reagents following the processing cycle. The retention and distribution of collagen IV, laminin and fibronectin following treatment with supercritical CO_2 under submerged conditions was superior to all other sterilisation treatments. Comparison of the relative levels of active (i.e. non-degraded) PAA and H_2O_2 and characterisation of oxidation products in the decellularised nerves treated with the standard and submerged supercritical processes would provide further evidence to support the proposed mechanism of degradation and the protective effect of PBS solution.

The implications of the observed changes to the basement membrane for the support of neuroregeneration are not known. The importance of fibronectin and (especially) laminin for the growth and migration of Schwann cells and regenerating axons has been widely demonstrated [42]. Laminin and fibronectin act as chemoattractants for Schwann cells and facilitate direct binding of regenerating axons, while the expression of both molecules is upregulated in Schwann cells following injury [361]. Cell interaction with laminin and fibronectin appears to be dependent upon specific components or regions within these ligands: the $\alpha 2$, $\alpha 4$ and $\gamma 1$ laminin sub-chains (contained within the isoforms laminin 2 and laminin 8) and the “V region” of fibronectin are regarded as particularly important [42, 61]. The effects of the changes seen following PAA

and supercritical CO_2 treatment therefore may be dependent on the extent and nature of oxidative damage. The reduction of specific labelling for fibronectin and the loss of localisation in labelling for laminin seen following treatment with the standard supercritical CO_2 process implies a greater level of basement membrane degradation compared to PAA treatment. If the oxidising agents used in this study have caused changes to the localisation, surface chemistry and/or conformation of key binding sites then cellular interaction (and associated process such as Schwann cell growth, ECM remodelling, and axon attachment) may be impeded. Additionally, such alterations could cause the ECM components (or fragments thereof) to be recognised as DAMPs, leading to activation of the innate immune system and potentially compromising the integration of the graft [132, 133]. Conversely, if the specific target epitopes of the antibodies used to label fibronectin and laminin have been affected but the key cell attachment motifs have not, then the ability of the decellularised nerves to support site-specific cells and effectively promote neuroregeneration may not have been compromised.

The role of collagen IV in neuroregeneration is less well characterised than for laminin or fibronectin. Beyond the primary function as a supporting scaffold for the other basement membrane components, *in vitro* studies with rat cells have indicated that collagen IV may have an additional role in cell interaction [321]. Axons interact with collagen IV through α1β1 integrin, while Schwann cells interact with collagen IV through the integrins α1β1 and α2β1 and the G-protein coupled receptor GPR126 [362-364]. Downstream signalling through adenosine 3’-5’-cyclic monophosphate (cAMP) induces the Schwann cells to differentiate and adopt pro-myelinating characteristics; genetic knockout studies altering the conformation of GPR126 prevented the expression of myelin basic protein [365]. The degree of similarity between human and rat Schwann cells and associated myelination processes remains unclear, but specific interaction with collagen IV may well be of importance. Therefore, changes such as those seen after treatment with PAA solution and the standard supercritical CO_2 process preventing antibody binding may also disrupt cell-matrix interactions such as that mediated by GPR126.

Treatment with sterilisation methods incorporating oxidising agents (specifically 0.1% (v/v) PAA in solution and supercritical CO_2 processing incorporating an

additive solution containing low concentration PAA and H_2O_2) appeared to have induce some disruption to the structure of the endoneurial tubules in the decellularised nerves, as well as causing a loss of specific antibody labelling for basement membrane components associated with cell attachment (laminin, fibronectin). Conducting supercritical CO_2 treatment under submerged conditions appeared to prevent such alterations, suggesting that the local concentration of oxidising agents in the tissue during and after treatment may be an important factor in determining the extent of oxidative damage incurred to ECM components. The results of the histological staining and antibody labelling detailed here suggest that treatment of the decellularised nerves with $SCCO_2$ under submerged conditions, gamma radiation, and E Beam mediate superior preservation of peripheral nerve histoarchitectural features and key cell attachment molecules compared with either PAA in solution or $SCCO_2$ processing under standard conditions, and therefore may present a superior material for the promotion and guidance axonal and Schwann cell growth and function when implanted into a defect site.

6 Physical properties of sterilised decellularised nerves

6.1 Introduction

The importance of retaining material properties for the function of decellularised grafts varies by tissue type. Peripheral nerves, unlike musculoskeletal tissues (such as cartilage, tendon, ligament and bone), do not primarily function to provide strength, structure and biomechanical stability [8]. The mechanical function of peripheral nerve ECM is to provide protection for cells residing within the tissue from external tensile and compressive forces. Unique challenges are posed by the length of axons and the potential induction of degenerative injury in the event of exposure to excessive mechanical forces. In particular, peripheral nerves must provide protection from such forces in regions close to articulating joints, where rapid and frequent changes to tensile and compressive stress may be encountered.

Terminal sterilisation methods may alter the material properties of decellularised tissue grafts [179]. Ionising radiations, such as gamma radiation and E Beam, can induce crosslinking or chain scission in the structurally important collagen molecules which make up the majority of the ECM [1]. Treatment with oxidising agents such as PAA or H_2O_2 can cause oxidative degradation and solubilisation of ECM components [242]. Insufficient rehydration of dried decellularised tissues can lead to an increase in stiffness [339]. Changes to the mechanical properties of the decellularised nerves could impede the growth and function of axons; for example, collagen [73, 366].

The structure of collagen within the ECM, including the folding of individual tropocollagen units and interaction between separate units, is crucial to tissue structure and function [367]. The non-covalent (e.g. hydrogen bonds, ionic bonds) and covalent (e.g. disulphide linkages, trivalent pyridinoline and pyrole crosslinks) bonds which contribute to the higher order structure of collagens are susceptible to disruption by decellularisation and sterilisation methods [145, 368]. Disruption of inter and intra-molecular bonds in collagen can lead to full or partial unfolding of higher order structure, potentially affecting the mechanical properties and capacity to support cells of a decellularised tissue.

Differential scanning calorimetry (DSC) enables quantitative analysis of changes in protein bonding patterns [369]. DSC enables the denaturation temperature of collagen to be determined; this represents the temperature at which the higher order structure of the collagen molecule unfolds. A decrease in the denaturation temperature indicates non-covalent and/or covalent bonds have been disrupted and therefore less thermal energy is required to disrupt the remaining bonds. An increase in the denaturation temperature may indicate an increase in inter and/or intra-molecular crosslinking, such as that which may be induced by ionising radiation in the presence of water molecules.

Disruption of inter and/or intra-molecular bonds may also be detected by differences in susceptibility to enzymatic digestion by collagenase A [370]. Samples of tissue are digested for a given time period, after which the hydroxyproline content of the digest solution is quantified and extrapolated to give digested collagen content. A greater proportion of digested collagen per tissue mass is likely to be indicative of disruption to inter and/or intra-molecular crosslinks enabling more rapid digestion.

As the material properties of the decellularised nerves are likely to affect the growth and function of cells *in vivo,* quantification of changes following sterilisation is important to identify methods capable of preserving such properties.

6.2 Aims and Objectives

6.2.1 Aims

The aim of this chapter was to characterise the effects of sterilisation methods on the physical properties of decellularised nerves.

6.2.2 Objectives

i. To determine the effects of sterilisation on the mechanical properties of decellularised nerves through uniaxial tensile testing.
ii. To determine the effects of desiccation on the mechanical properties of decellularised nerves through uniaxial tensile testing.
iii. To determine the effect of sterilisation on the denaturation temperature of collagen in the ECM of decellularised nerves, though DSC.
iv. To determine the effect of sterilisation on the collagenase susceptibility of decellularised nerves.

6.3 Materials and Methods

6.3.1 Decellularisation and sterilisation

Porcine peripheral nerves were dissected, decellularised and sterilised as described in sections 2.9 and 2.10.

6.3.2 Production of controls representing crosslinking and denaturation of collagens in decellularised nerve

Two control treatments were produced as extreme examples for the denaturation or crosslinking of collagens in the ECM. One group of decellularised nerves (n = 6) were denatured through treatment with NaOH, as described in section 2.10.3.5.

A further group (n = 6) of decellularised nerves were incubated in 10 % (v/v) NBF for 120 hours. The samples were washed three times in PBS for one hour each time, before a further PBS wash overnight.

Samples from both control groups were stored in PBS at 4 °C until use.

6.3.3 Uniaxial tensile testing

Samples of native, decellularised, and decellularised nerves from each sterilisation treatment group (n = 6 per group) were subject to uniaxial tensile testing, as described in section 2.13. Briefly, samples of nerve were mounted onto an Instron 3365 machine using clamps and grips which were specifically designed for use with soft tissue. The samples of nerve were subjected to a single ramp-to-failure tensile test at a strain-rate of 10 mm.minute^{-1}. The maximum load each sample sustained was used (in conjunction with the measured cross sectional area) to calculate the ultimate tensile strength, and the gradient of the slope in the linear region of the stress-strain curve was used to define the Young's Modulus. Full details of how these values were calculated is given in section 2.13.

As it was not possible to shape the nerves into standard sizes for testing, due to the heterogeneity of nerve ECM structure and the differing contributions of the structures in nerve ECM to mechanical properties. Therefore, a method to measure the dimensions of the nerve samples without resizing was developed. However, due to the inherent inaccuracies which these restrictions could

introduce to the calculation of cross-sectional area, maximum load and stiffness were also considered during the course of this study, as measures of mechanical properties which could be determined independent of the physical dimensions of the tissue.

6.3.4 DSC analysis of sterilised nerves

Samples of native, decellularised and sterilised decellularised nerves (n = 6 per group) were dissected to give individual segments of 2 – 5 mg (wet weight). Samples were then transferred to individual 1.5 ml eppendorfs containing 1 ml of PBS and shipped in an icepack-cooled container to the Department of Materials Science, University of Cambridge.

The thermal stability of each sample was determined using a Q2000 differential scanning calorimeter. Samples were hermetically sealed into aluminium containers. The temperature was increased at a constant rate of 4 °C.min-1, from 15 - 130 °C. Heat flow through each sample was measured and normalised against the mass of the sample to give a value defined in Watts per gram (W/g). The denaturation temperature was taken as the point of maximum heat flow through the sample.

6.3.5 Collagenase susceptibility assay

The collagenase susceptibility of the nerves (native, non-sterilised decellularised, and treated with either PAA, gamma radiation, E Beam, $SCCO_2$ or NaOH; n = 6 per group) was determined by a colourimetric assay of solubilised enzyme digestion products. This was enabled by enzymatic digestion with collagenase A.

6.3.5.1 Solutions

Collagenase A digest buffer

6.055 g Tris-HCl and 3.7 g calcium chloride were dissolved in 900 ml of distilled water using a magnetic stirrer bar. The pH of the solution was adjusted to 8 using 6 M NaOH or 6 M HCl.

Collagenase A working solution

Lyophilised Collagenase A was dissolved in the digest buffer (pre-warmed to 37 °C) using a magnetic stirrer bar, to give a working concentration of 1 $mg.ml^{-1}$.

6.3.5.2 Assay Method

Samples of nerve were lyophilised (as described in 2.14.1) in a sterile 1.5 ml eppendorf to give a dry weight of approximately 10 – 20 mg. Collagenase A working solution (600 µl) was added to each sample, and the samples were incubated in a water bath for three hours at 37 °C. The digested samples were centrifuged at 15,500 x g for ten minutes, and 25 µl of supernatant was transferred to a fresh sterile screw top 2 ml Eppendorf complete with O-ring seal. HCl (12 M; 25 µl) was added to each tube. Each tube was then sealed autoclaved (121 °C, 18 PSI) for one hour to enable hydrolysis.

After hydrolysis, 450 µl of chloramine T (see section 2.14.3.1) was added to each tube. The tubes were transferred to a water bath and incubated at 65 °C for 20 minutes. 500 µl of Ehrlichs solution (see 2.14.3.1) was added to each tube, after which the samples were transferred back to the water bath for a further 20 minute incubation at 65 °C. 200 µl aliquots of each sample were added in triplicate to a 96 well plate, together with known standards. Measurements of optical density were taken for each well containing a standard and sample, at a wavelength of 570 nm.

A curve of absorbance against concentration was plotted for the known standards, and used as a standard curve. The absorbance values for test samples were used to generate interpolated hydroxyproline concentrations. These values were then used in conjunction with the values of tissue mass and dilution factor to calculate the hydroxyproline content of the tissue samples. The total mass of digested collagen was then calculated using a conversion factor of 7.52, as described in 2.14.4.

6.4 Results

6.4.1 Uniaxial tensile testing of sterilised nerves

Six samples from each different treatment group were subject to uniaxial tensile testing. The data from each sample was plotted as a stress-strain curve, to enable analysis of the effects of the sterilisation treatments on the mechanical properties of decellularised nerves (Figure 6-1).

The UTS of decellularised nerves treated with PAA (7.63 +/- 2.28 MPa) was significantly reduced in comparison to native peripheral nerves (11.82 +/- 1.16 MPa), but not untreated decellularised nerves (10.37 +/- 2.29 MPa; Figure 6-2 A). The UTS of decellularised nerves treated with $SCCO_2$ (14.91 +/- 4.78 MPa) was increased in comparison to untreated decellularised nerves (10.37 +/- 2.29 MPa) and decellularised nerves treated with PAA, gamma, E Beam (7.63 +/- 2.28 MPa, 10.52 +/- 1.51 MPa, and 10.74 +/- 2.75 MPa, respectively).

The maximum load of decellularised nerves treated with $SCCO_2$ (113.3 +/- 29.2 N) was increased compared to native peripheral nerves (53.13 +/- 15.5 N), untreated decellularised nerves (59.69 +/- 29.84 N) and decellularised nerves treated with PAA and gamma radiation (62.53 +/- 12.88 N and 69.23 +/- 20.75 N; Figure 6-2 B).

The Young's Modulus of decellularised nerves treated with $SCCO_2$ was increased compared to native and untreated decellularised nerves and those treated with PAA and E Beam (Figure 6-3 A). The Young's Modulus of decellularised nerves treated with gamma radiation was greater than that of decellularised nerves treated with PAA.

The stiffness of decellularised nerves treated with $SCCO_2$ (45.77 +/- 14.29 MPa) was greater than that of native peripheral nerves (27.33 +/- 4.56 MPa), untreated decellularised nerves (25.73 +/- 7.295 MPa) and decellularised nerves treated with PAA or E Beam (17.68 +/- 3.58 MPa and 24.73 +/- 6.94 MPa, respectively; Figure 6-3 B). The stiffness of decellularised nerves treated with gamma radiation (24.37 +/- 7.55 N/mm^{-1}) was greater than that of native peripheral nerves (15.39 +/- 3.42 N/mm^{-1}), untreated decellularised nerves (14.12 +/- 6.02 N/mm^{-1}) and decellularised nerves treated with PAA (15.2 +/- 2.99 N/mm^{-1}).

No differences were seen between native nerves, non-sterilise decellularised nerves or decellularised nerves treated with any of the candidate sterilisation methods in terms of energy to break (Figure 6-4).

NaOH-treated decellularised nerves displayed consistently degraded mechanical properties compared with all other treatment groups; by comparison, NBF-treated decellularised nerves only showed significant differences compared with $SCCO_2$ in terms of UTS and Young's Modulus, as well as compared with E Beam-treated, PAA-treated, non-sterilised and native nerves in terms of stiffness and nerves from all groups except those treated with gamma radiation, E Beam or $SCCO_2$ in terms of energy to break values.

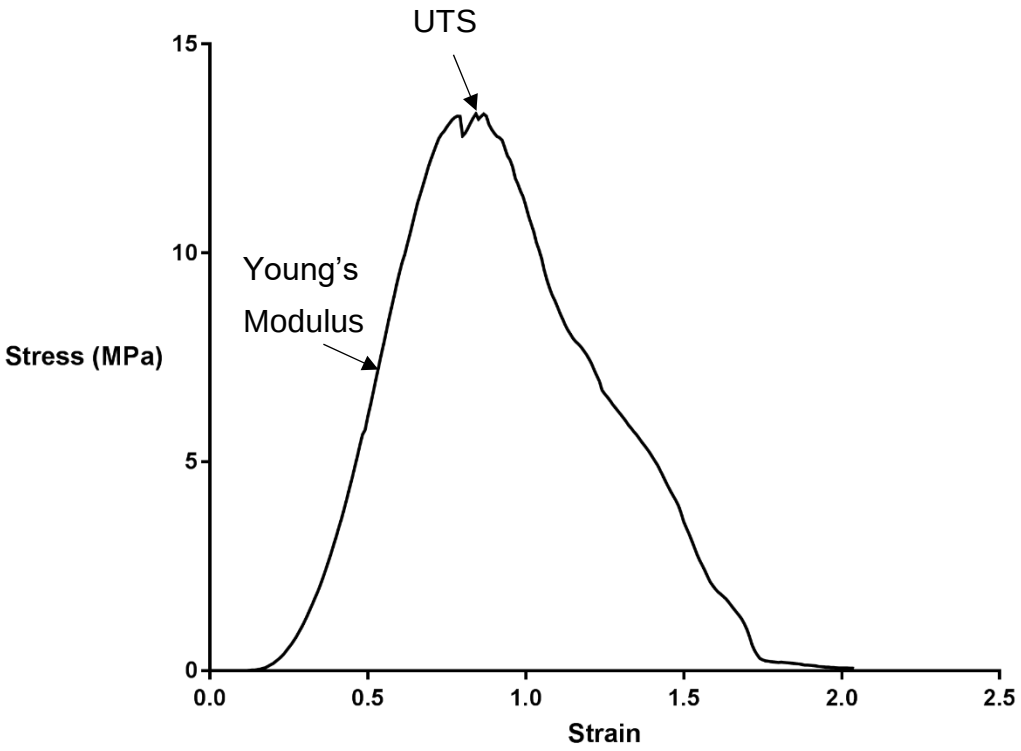

Figure 6-1 Stress-strain curve for a sample of native peripheral nerve

Stress-strain curve produced from combining load-extension data with the measured cross-sectional area and a known gauge length. Labels indicate the peak value for stress (UTS) and the region of linear extension from which the Young's modulus is defined.

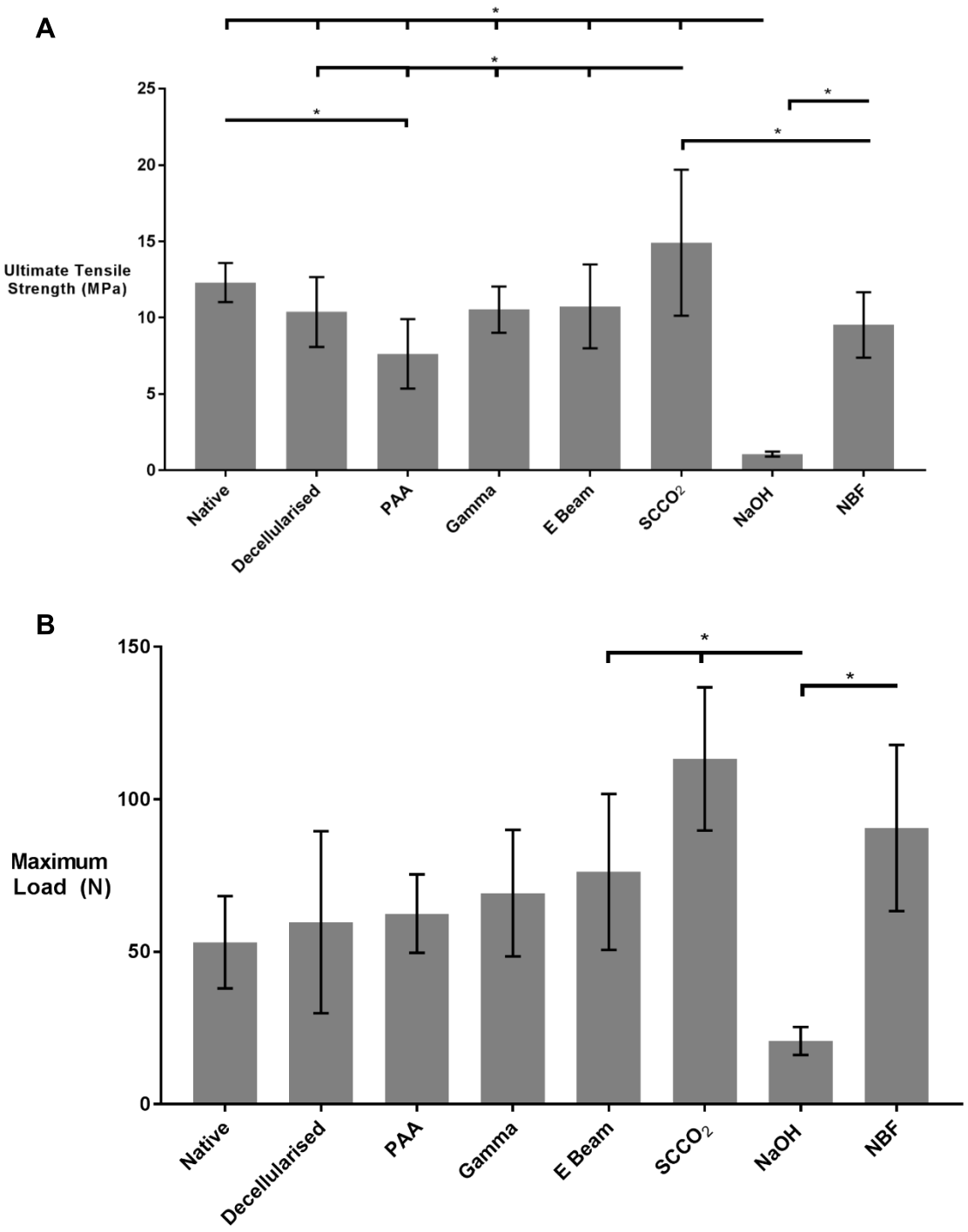

Figure 6-2 UTS and Maximum Load of native, decellularised and sterilised peripheral nerves

(A) UTS and (B) Maximum Load of peripheral nerves from all treatment groups. Data shown as mean +/- 95 % confidence interval, n = 6. Statistical analysis was by (A) one-way ANOVA or (B) Kruskall-Wallis. * denotes groups which are significantly different ($p<0.05$).

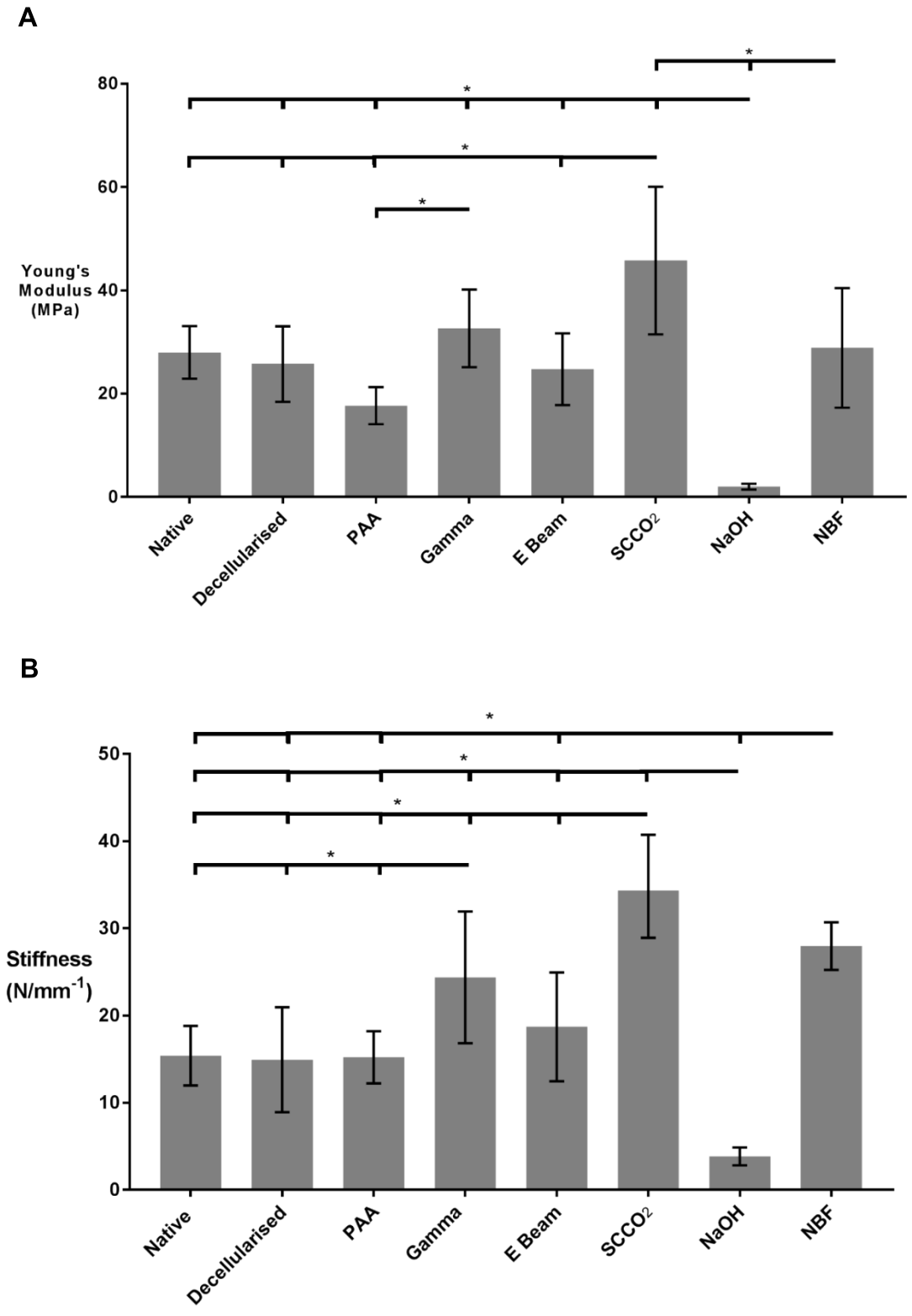

Figure 6-3 Young's Modulus and Stiffness of native, decellularised and sterilised peripheral nerves

(A) Young's Modulus and (B) Stiffness of peripheral nerves from all treatment groups. Data shown as mean +/- 95 % confidence interval, n = 6. Statistical analysis was by (A) Kruskal-Wallis or (B) one-way ANOVA. * denotes groups which are significantly different ($p<0.05$).

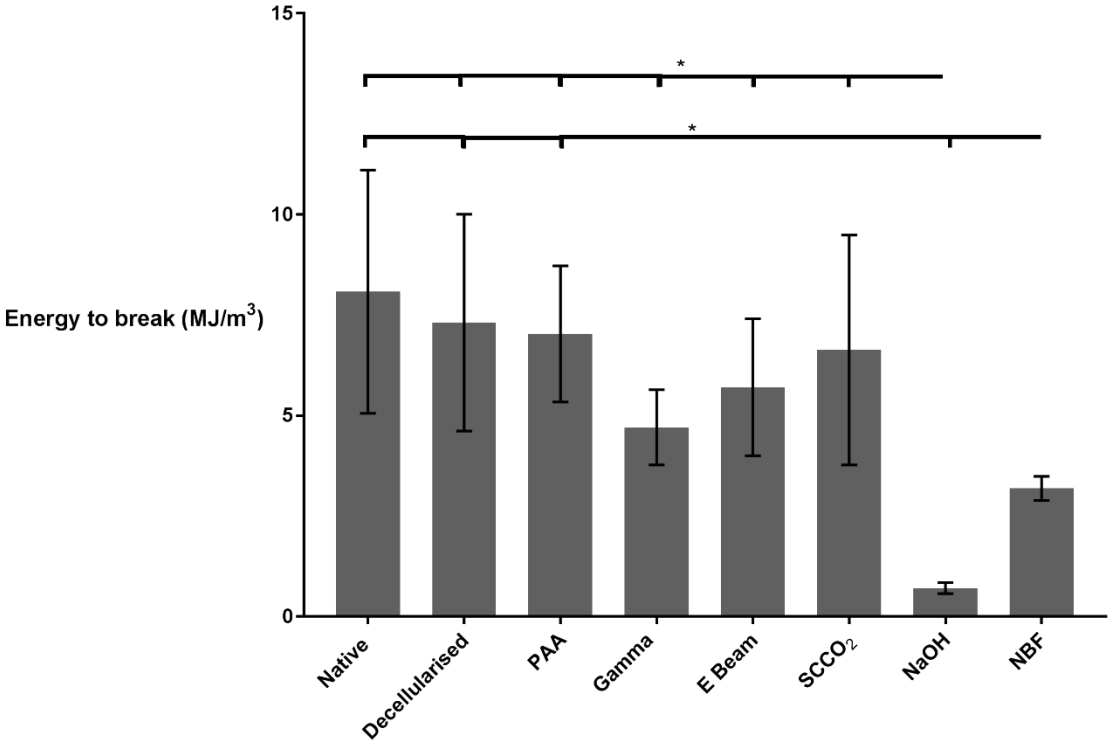

Figure 6-4 Energy to break values for native, decellularised and sterilised peripheral nerves

(A) Young's Modulus and (B) Stiffness of peripheral nerves from all treatment groups. Data shown as mean +/- 95 % confidence interval, n = 6. Statistical analysis was by one-way ANOVA. * denotes groups which are significantly different ($p<0.05$).

6.4.2 Uniaxial tensile testing of desiccated nerves

Samples of desiccated decellularised nerves were rehydrated and subjected to uniaxial tensile testing to determine the effects of desiccation on the material properties of decellularised nerves. As desiccation represents a potential preparation method for a sterilisation method (ethylene oxide treatment) rather than a sterilisation method in it's own right, the desiccated decellularised nerves were analysed separately to the groups of sterilised nerves. Extra groups of native and decellularised nerves were also tested and included in the analysis.

The UTS of desiccated decellularised nerves, at 16.28 (+/- 6.49) MPa, was significantly higher than native nerves but not untreated decellularised nerves at 11.35 (+/- 2.03) MPa and 9.84 (+/- 2.79) MPa respectively (Figure 6-5 A).

The Young's Modulus of desiccated decellularised nerves, at 48.11 (+/- 26.7) MPa, was significantly higher than both native and untreated decellularised nerves at 29.97 (+/- 5.46) MPa and 23.09 (+/- 6.45) MPa respectively (Figure 6-6 A).

The values for maximum load at failure, stiffness, and energy to break for desiccated decellularised nerves were not significantly different from either native or decellularised nerves (Figure 6-5 B, Figure 6-6 B, and Figure 6-7).

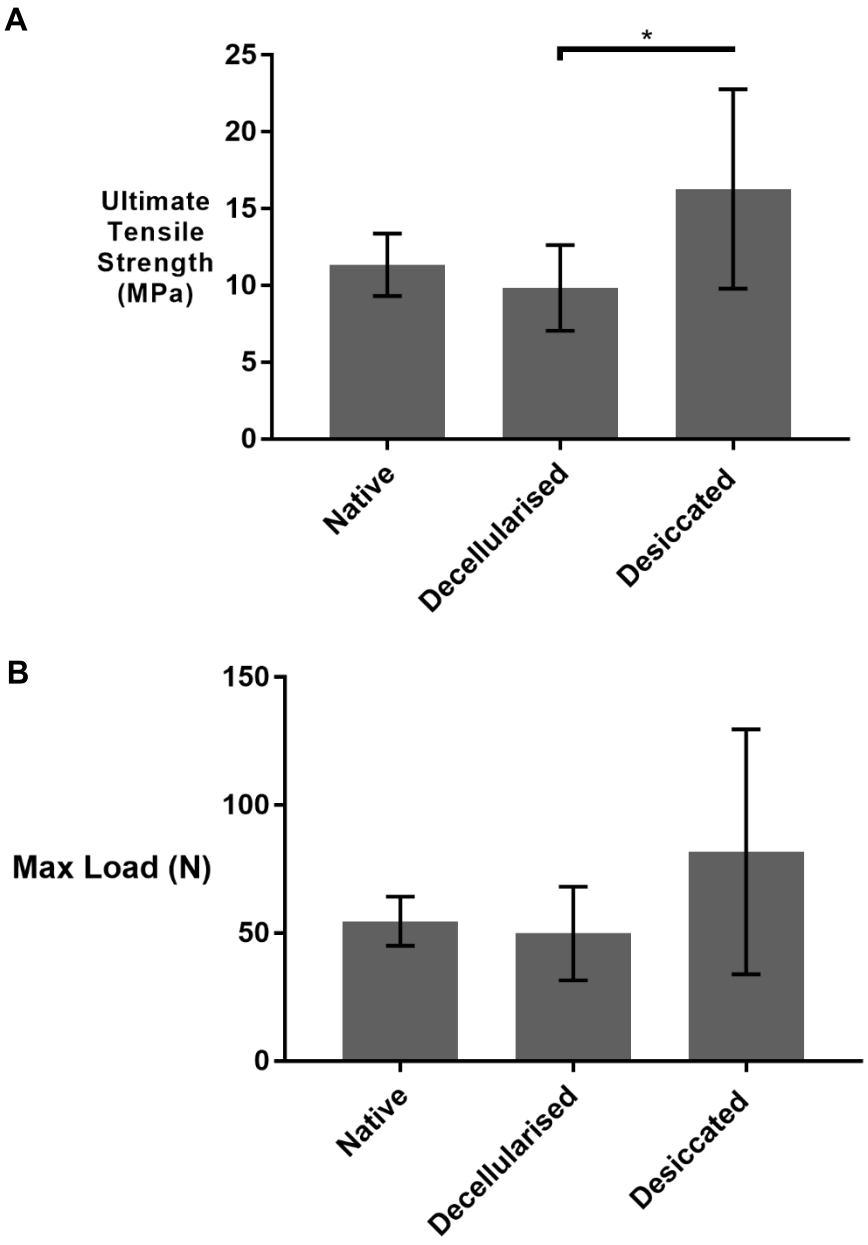

Figure 6-5 UTS and Maximum Load of native, decellularised and desiccated peripheral nerves

(A) UTS and (B) Max Load of native, decellularised and desiccated peripheral nerves. Data shown as mean +/- 95 % confidence interval, n = 6. Statistical analysis was by one-way ANOVA. * denotes groups which are significantly different ($p<0.05$).

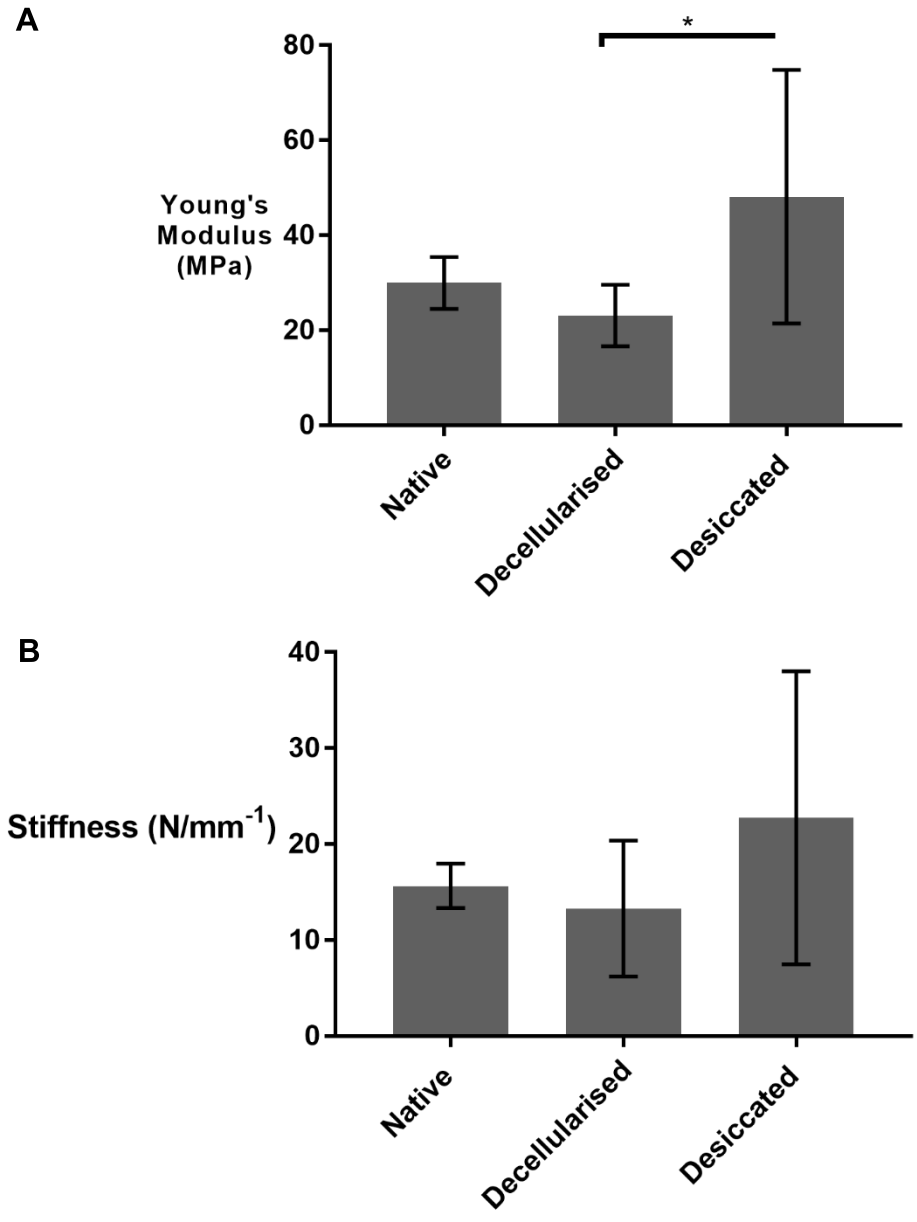

Figure 6-6 Young's Modulus and Stiffness of native, decellularised and desiccated peripheral nerves

(A) Young's Modulus and (B) Stiffness of native, decellularised and desiccated peripheral nerves. Data shown as mean +/- 95 % confidence interval, n = 6. Statistical analysis was by one-way ANOVA. * denotes groups which are significantly different ($p<0.05$).

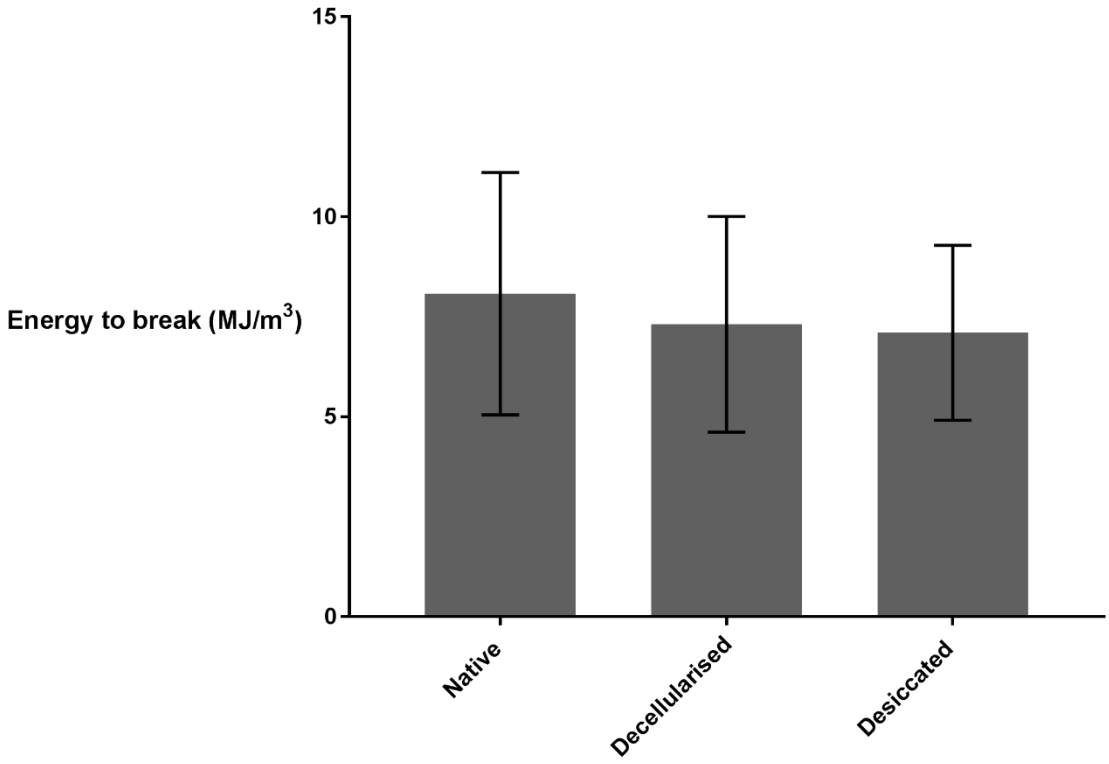

Figure 6-7 Energy to break values for native, decellularised and desiccated peripheral nerves

Energy to break values for native, decellularised and desiccated peripheral nerves. Data shown as mean +/- 95 % confidence interval, n = 6. Statistical analysis was by one-way ANOVA. * denotes groups which are significantly different ($p<0.05$).

6.4.3 DSC analysis of native, decellularised and sterilised nerves

The denaturation temperatures of samples for each group were quantified by measuring heat flow (W/g) in a differential scanning calorimeter (Figure 6-8). Mean denaturation temperatures in nerves from each of the treatment groups were found to be significantly different to most or all of the other groups (Figure 6-9). The denaturation temperatures of untreated decellularised nerves at 65 (+/- 0.65) and PAA-treated nerves at 64.29 (+/- 0.26) °C were not significantly different from that of native nerves at 65 (+/- 0.4) °C. The denaturation temperatures of PAA-treated and $SCCO_2$-treated nerves were not significantly different from each other, at 64.29 (+/- 0.26) °C and 64.2 (+/- 0.35) °C respectively. The denaturation temperatures of gamma irradiated and E Beam-treated nerves were approximately 5 – 6 °C lower than the other groups but were not significantly different from each other, at 58.98 (+/- 0.22) °C and 58.53 (+/- 0.23) °C respectively. The NaOH-treated control had a denaturation temperature of 44.96 (+/- 1.29) °C, approximately 20 °C lower than untreated decellularised nerve. The NBF-treated control had a denaturation temperature of 88.46 (+/- 0.17) °C, approximately 23 °C higher than untreated decellularised nerve.

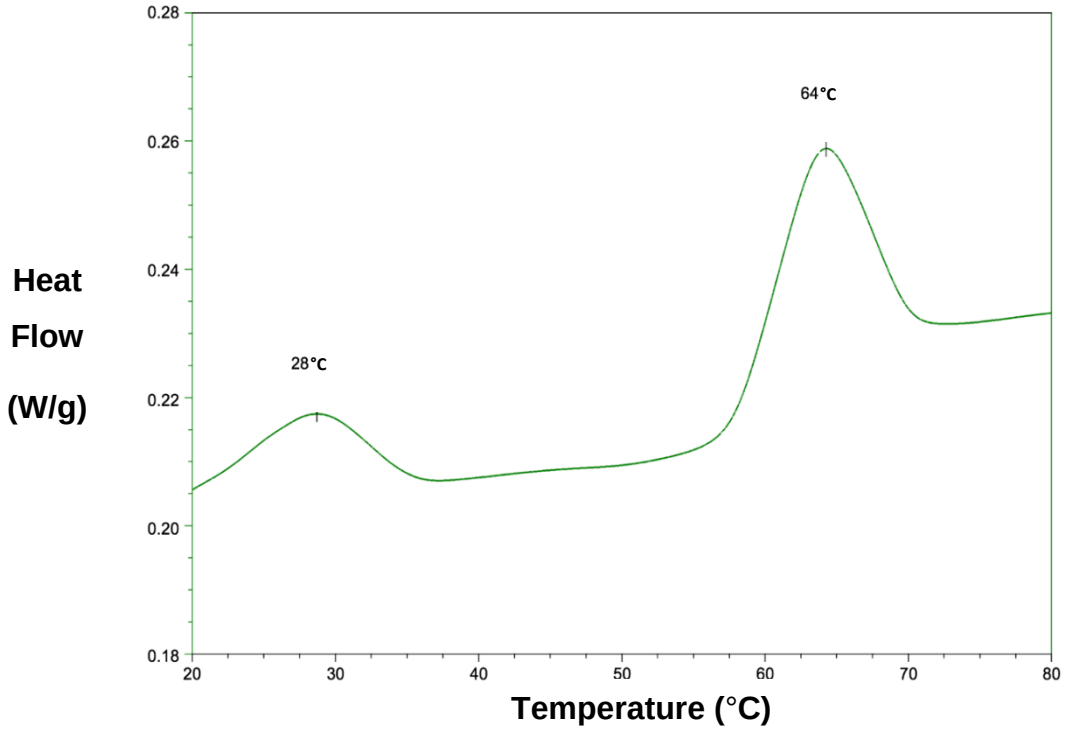

Figure 6-8 Example of thermogram from native porcine peripheral nerve

Data output from Q2000 differential scanning calorimeter, showing heat flow through a sample of native porcine peripheral nerve. Two peaks in heat flow are seen, with denaturation temperature taken as the point of greatest heat flow at 64 °C.

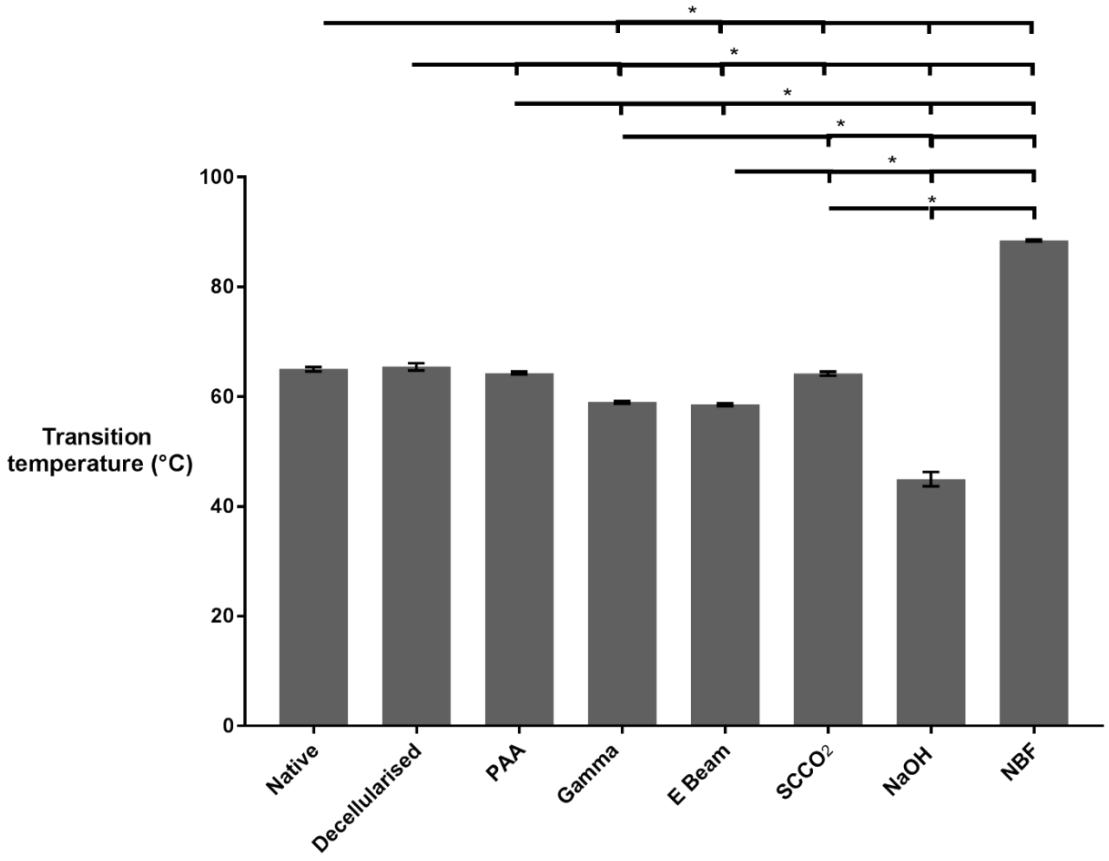

Figure 6-9 Denaturation temperatures of native, decellularised and sterilised porcine peripheral nerves

Denaturation temperatures of peripheral nerves from all treatment groups. Data shown as mean +/- 95 % confidence interval, n = 6. Statistical analysis was by one-way ANOVA. * denotes groups which are significantly different ($p<0.05$).

6.4.4 Determination of collagenase susceptibility in native, decellularised and sterilised nerves

The susceptibility of nerves to digestion by collagenase A did not significantly change following either decellularisation or treatment of the decellularised nerves with gamma radiation or E Beam (Figure 6-10). Decellularised nerves treated with PAA were significantly more susceptible to digestion, with the collagen digested as proportion of overall tissue mass at 269.7 (+/- 41.7) $\mu g.mg^{-1}$ compared to 180.7 (+/- 21.25) $\mu g.mg^{-1}$ and 190.7 (+/- 17.85) $\mu g.mg^{-1}$ for native nerves and untreated decellularised nerves respectively. Significantly more collagen was digested in decellularised nerves treated with $SCCO_2$ compared to native nerves, but not untreated decellularised nerves, at 248.5 (+/- 34.75) $\mu g.mg^{-1}$. Collagenase susceptibility in gamma irradiated, PAA-treated and $SCCO_2$-treated nerves was not significantly different from the NaOH-treated positive control.

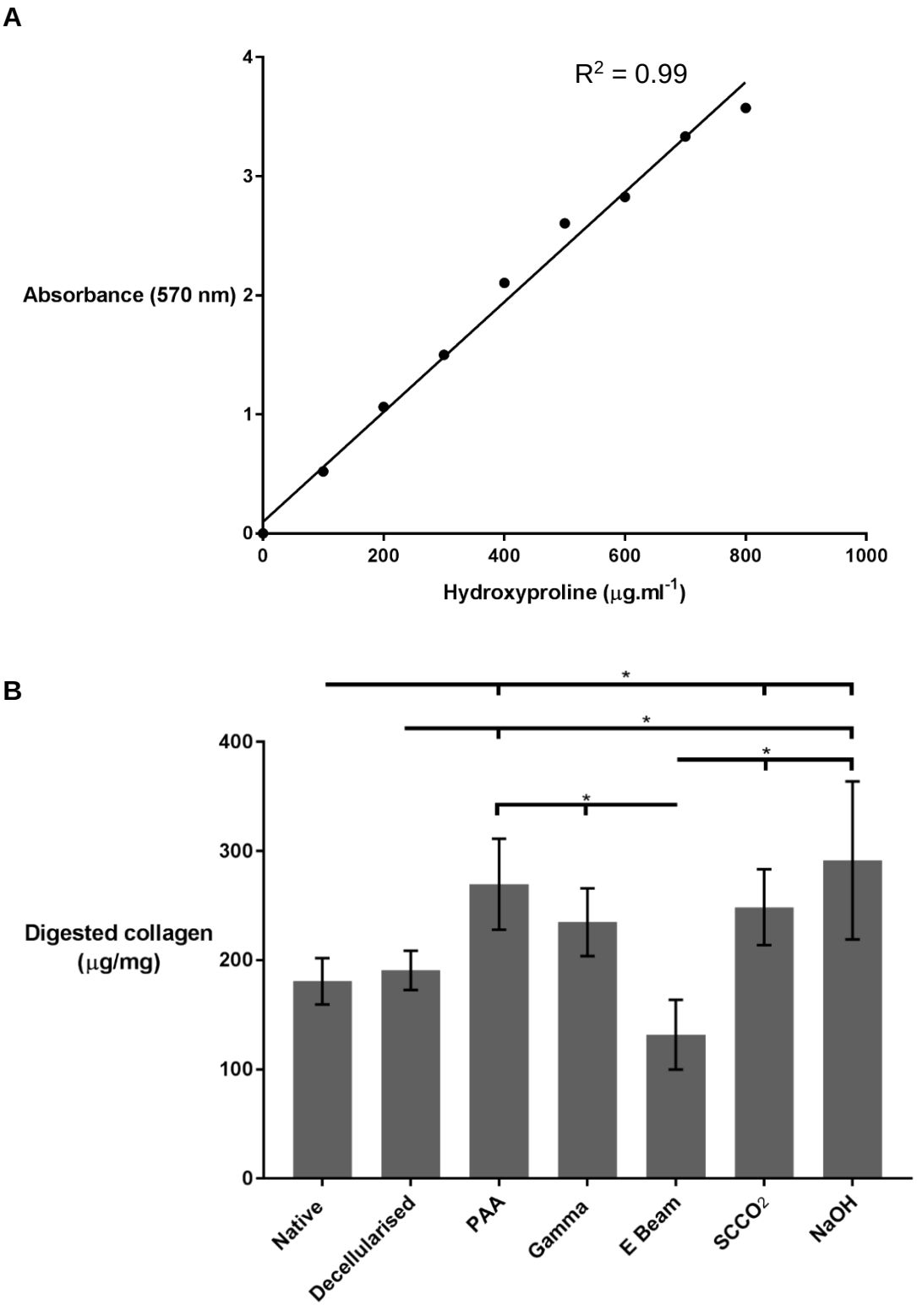

Figure 6-10 Collagenase susceptibility of native, decellularised and sterilised porcine peripheral nerves

(A) Standard curve for interpolation of digest samples and (B) the mass of collagen digested by collagenase A from peripheral nerves in all treatment groups. Data shown as mean +/- 95 % confidence interval, n = 6. Statistical analysis was by one-way ANOVA. * denotes groups which are significantly different ($p<0.05$).

6.5 Discussion

The sterilisation treatment methods used in the present study induced changes to the material properties of the decellularised nerves. These changes were particularly evident in terms of collagen molecular and structural integrity, but less pronounced at the level of whole tissue biomechanics.

The UTS of decellularised nerves were altered following treatment with PAA. A possible explanation for this may have been the slightly increased levels of structural disruption which were observed histologically (see Chapter 5). However, the structure of peripheral nerve ECM is heterogenous, with a large degree of variation between different regions. The layered lamellar structure of the perineurium, composed of aligned and highly organised collagen fibrils, surrounds each fascicle and is thought to be the primary contributor to the tensile mechanical properties of peripheral nerve [74]. Structural disruption in decellularised nerves treated with PAA was limited to the epineurium and endoneurium. The epineurium is composed of loosely organised adipose tissue and collagenous ECM, and is primarily thought to modulate compressive stress and enable movement of the nerve within the connective tissue sheath (excursion) [43]. The endoneurium, composed of a fine honeycomb structure of collagens and basement membrane components including fibronectin and laminin, provides guidance and attachment sites for Schwann cells and neurons.

As the structural disruption observed following PAA treatment was limited to the epineruium and endoneurium, it is unlikely to have contributed to the reduced tensile strength. Instead, the increased spacing/looseness in the epineurium may have led to an overall increase in cross sectional area, thereby altering the material properties of the nerve as a whole without altering the mechanical properties of the perineurium surrounding each fascicle. Evidence for this is provided by the fact that while PAA-treated nerves had a reduced UTS (which is dependent on cross-sectional area) compared to native nerves, there was no difference in the maximum load at failure. Considering the retention of overall load-bearing capacity, the distribution of the structural disruption and the uneven contribution of the different ECM structures to the mechanical properties

of peripheral nerves, it is unlikely that the reduction in UTS would affect the efficacy of the decellularised tissue *in vivo*.

Treatment with $SCCO_2$ caused increases in all mechanical parameters compared to untreated decellularised nerves. Previous studies into the effect of $SCCO_2$ treatment on the biomechanical properties of decellularised tissue grafts have yielded mixed results. $SCCO_2$ treatment did not appear to affect strength or Young's modulus in studies of decellularised human and rabbit cortical bone; however, as bone is a mineralised hard tissue these effects may not be directly comparable to peripheral nerve [371, 372]. However, $SCCO_2$ treatment caused an approximate increase of 135 % in the Young's modulus of decellularised rat lung matrices and an approximate 15 % increase in the Young's modulus of a synthetic collagen scaffold crosslinked with EDC [214, 243]. The mechanism underlying these changes and those observed in the present study is currently unknown. Balestrini *et al* suggested that the high pressure in the $SCCO_2$ reaction chamber could have mediated the formation of crosslinks between and/or within collagen molecules in the decellularised lung ECM [243].

Dehydration of the decellularised nerves would be a necessary step prior to sterilisation with ethylene oxide, enabling diffusion of the ethylene oxide into the tissue, reducing the potential for the formation the toxic breakdown products ethylene glycol and ethylene chlorohydrin, and enabling the removal of the ethylene oxide (and any associated breakdown products) from the tissue through an aeration process [194]. Due to the structural damage to the endoneurium observed when decellularised nerves subject to lyophilisation (section 5.4.1), desiccation was considered as an alternative method of dehydration. However, desiccation increased the Young's modulus of the decellularised nerves. Histological analysis indicated that the decellularised nerves were not fully rehydrated after desiccation. Increases in Young's modulus as a result of dehydration have been demonstrated both on a whole tissue and a molecular scale, through uniaxial mechanical testing of tissues including human skin and bovine cornea, and measurement of individual collagen fibrils using atomic force microscopy [54, 373, 374]. Inter and intramolecular hydrogen bond-mediated "water bridges" form between pairs of amino acids, including hydroxyproline and glycine, during the synthesis and folding of the individual collagen molecules and higher order structures [375].

The results of a computational simulation study evaluating the molecular dynamics of collagen-like peptides before and after dehydration indicated that the removal of water molecules (and therefore the water bridges) significantly increased hydrogen bonding between pairs of amino acids as well as the structural rigidity of the molecules [376]. The study also found that the increase in rigidity mediated by the hydrogen bonds was unlikely to be reversed by the reintroduction of water molecules (i.e. the water molecules would be unable to disrupt the hydrogen bonds). This implies that while water molecules may be able to re-infiltrate inter and intramolecular spaces of dehydrated collagen molecules, the increase in stiffness mediated by the formation of hydrogen bonds in place of water bridges may not be reversible. Experimental data supporting this hypothesis have been gathered using Raman spectroscopy analysis of collagen I and DSC analysis of cross-linked and partially dehydrated rat tail tendon [171, 377]. The formation of the intramolecular hydrogen bonds and increased structural “tightness” mediated by dehydration within the individual alpha helices has been further evidenced by measurement of the intermolecular overlap, or D-period, within collagen fibrils [378]. An atomic force microscopy study of scleral collagen I indicated that the D-period decreased from 64 nm in hydrated collagen to 21 nm in dehydrated collagen, as well as a decrease in lateral spacing between tropocollagen units [379]. Similarly, a study of collagen I in decellularised bovine dermis using synchotron-based small angle X-ray scattering revealed a significant decrease in fibril width and intermolecular spacing following dehydration. These mechanisms may partially explain the findings of the 2013 study by Meyer et al, which demonstrated that collagenous porcine tissues (especially adipose tissue) do not fully rehydrate after dehydration [347]. The increase in Young’s modulus seen here may therefore be an irreversible consequence of dehydration.

Whilst an increase in UTS or maximum load at failure is unlikely to be of concern in a peripheral nerve graft, changes to the Young’s Modulus and stiffness may have a negative effect on axonal function [8]. The elastic properties of peripheral nerve ECM modulate the tensile stress experienced by axons carried within the endoneurium. This function is particularly important in regions of nerves travelling close to articulating joints; for example, levels of strain in the ulnar and median nerves of the human arm can change by up to

approximately 35 % during elbow and wrist joint flexion and extension. Axons interact with (and bind to) basement membrane ECM components in the endoneurium through integrins, such as the $\alpha 7\beta 1$ receptor for laminin and the $\alpha 5\beta 1$ receptor for fibronectin [380]. Changes in strain to the nerve ECM are therefore directly transduced to the axons contained within the endoneurium [381].

Given that the perineurium primarily determines the mechanical properties of peripheral nerve, the increase in stiffness but not Young's modulus seen in gamma irradiated nerves is likely to be due to changes (e.g. increased intermolecular crosslinking) being localised to the perineurium. In the nerve as a whole the epineurium, a heterogeneous structure composed of of adipose and collagenous tissue which is a comparatively minor contributor to tensile mechanical strength, makes up the majority of the cross sectional area of peripheral nerve [104]. It is likely that if individual fascicles (made up of a perineurial sheath surrounding the endoneurium) were dissected away from the epineurium in the gamma irradiated nerves and subject to uniaxial tensile testing, the Young's Modulus would be altered in addition to the stiffness.

An increase in the Young's Modulus (and/or stiffness) of the decellularised nerve graft, such as that seen following $SCCO_2$ treatment, desiccation and gamma radiation, could lead to axonal bodies experiencing increased tensile stress in the regions immediately proximal and distal to the graft-tissue interface. Graft material with an increased Young's Modulus would not deform to the same extent as native tissue under a given load; therefore, the surrounding nerve tissue would be required to deform further during the peak strain levels induced by joint flexion to compensate. Elevated local levels of strain would increase the probability of tensile stress exceeding normal physiological levels. The severity of this effect would likely be dictated by the size and location of the defect. The greater the proportion (in terms of length) of a given nerve replaced with an inherently stiffer graft material, the greater the change in peak strain levels within the distal and proximal tissue.

High levels of tensile stress in axons can lead to increased local expression of transmembrane voltage-gated sodium channels, which mediate the conduction of action potentials along the length of the axon through localised membrane

depolarisation [382]. The effects of increased ion channel expression are compounded by changes in distribution; normally restricted to specific sites, most commonly the Nodes of Ranvier between myelinated regions, excessive tensile stress induces sodium channel insertion over wider regions of the axonal cell membrane, thereby potentially impeding the conduction speed of action potentials.

Multiple *in vivo* studies have shown that blood flow in the network of vessels local to the peripheral nerve, the vasa nervorum, can be impeded by excessive levels of tensile strain. A tensile strain of 16 % in the sciatic nerve of a New Zealand white rabbit resulted in a 49 % reduction in blood flow [383]. A strain of 8 % to a rat sciatic nerve was found to induce a 50 % reduction in blood flow, increasing to an 80 % reduction under strain levels of 15 % [384].

Excessive tensile stress can also negatively impact upon Schwann cells, inducing either cell death or a decrease in the expression of myelin-associated adhesion molecules and regulatory genes including neuregulin 1, neural cell adhesion molecule, Krox20 and Sox10, and therefore resulting in localised (segmental) demyelination of axons [385, 386].

The speed of signal transduction in peripheral nerve axons is dependent on the concept of saltatory conduction, where membrane depolarisation propagates between the Nodes of Ranvier (length 1 – 2 μm) which separate the longer regions of membrane insulated with myelin (length 766 – 1739 μm) [387]. Decreased blood flow within the nerve, loss of the insulating myelin coating the axon and increased sodium channel expression over wider areas of the axonal membrane would likely slow and/or impede the conduction of action potentials, as membrane depolarisation no longer propagates between relatively small and well-spaced regions [388]. *In vivo* studies have demonstrated this effect. Driscoll *et al* demonstrated that a tensile strain of 16 % to the sciatic nerve of New Zealand white rabbits induced a 34 % decrease in nerve conduction velocity [383]. Given the documented negative impact of increased strain on nerve function, and the fact that a stiffer graft material is likely to result in locally elevated strain, it is therefore desirable for a terminally sterilised graft material to retain elastic properties similar to native nerves.

Changes to the denaturation temperature of collagen in the decellularised nerves appeared to be directly linked to the type of sterilisation method used. Decellularisation and sterilisation can affect inter and intramolecular structure and interactions of collagen in the ECM. Higher order structure and organisation of collagen molecules, including α-helices and the fibrillar organisation of tropocollagen units in collagen type I, and β-sheets in collagen type IV, is determined by a range of covalent and non-covalent bonds between amino acid side chains including hydrogen bonds, pyridinoline crosslinks, ionic bonds and dipole-dipole interactions [389].

Decellularisation appeared to have no detectable effect on denaturation temperature, inferring that treatment with decellularisation reagents such as SDS induced minimal disruption to the structural integrity of collagen in the nerves. Sterilised decellularised nerves could be separated into two separate groups based on type of sterilisation method, defined by statistically similar changes in denaturation temperature; the ionising radiations (gamma radiation and E Beam) and methods utilising oxidising agents (PAA and $SCCO_2$).

Treatment with both gamma radiation (25 kGy) and E Beam (34 kGy) appeared to cause an approximate 6 °C drop in the denaturation temperature, indicative of some level of denaturation within collagen structures in the decellularised nerves. Similar results have been seen in decellularised porcine superflexor tendons. Tendons treated with 0.1 % (v/v) PAA, gamma radiation (30 kGy) and E Beam (34 kGy) were found to have denaturation temperatures of 66.2 °C, 58.3 °C and 58.2 °C respectively [336]. As in the present study, the tissue was in a hydrated (wet) state during irradiation.

It is accepted that ionising radiation can induce both chain scission (direct interaction) and crosslinking (indirect interaction) in collagen molecules [172, 390]. While crosslinking is thought to be the predominant mechanism in the presence of water molecule-generated free radicals, chain scission still occurs. The process of native crosslink formation is induced enzymatically by lysyl oxidase during collagen maturation [391]. Due to the specificity of native crosslinks to the amino acids lysine and hydroxylysine, the occurrence and contribution to structural stability of such crosslinks is governed by the distribution of these amino acids within the primary structure. Radiation-induced

crosslinks, formed due to interactions with the hydroxyl radicals produced by radiolysis of water molecules, are likely to be more randomly distributed as no specific enzyme action is required to mediate their formation [1].

Chain scission is thought to be primarily an intramolecular process, disrupting covalent peptide bonds within the primary collagen structure [228]. Hydroxyl radicals are also thought to disrupt hydrogen bonds, further accounting for the reduction in denaturation temperature observed in this study. It has been postulated that the formation of additional crosslinks during irradiation primarily affects higher levels of structure, such as between individual tropocollagen units [152]. Chain scission could therefore cause the α helix structure of collagen (including types I and III) to be destabilised and mean that less thermal energy is required to initiate denaturation and uncoiling, without compromising tensile mechanical properties which are primarily mediated through higher order structures determined by intermolecular interactions.

The findings presented here corroborate previous studies indicating that superior preservation of collagen molecular integrity is achieved when collagenous tissues are irradiated in a wet state, inducing synergistic chain scission and crosslinking, rather a dry state favouring the predomination of chain scission through direct interaction of radiation with collagen molecules [392]. A previous study examined the effects of lyophilisation prior to gamma irradiation (28.6 kGy) on decellularised human dermis. After rehydration and DSC analysis, the induced decrease in denaturation temperature was measured as approximately 20 °C [393]. This was accompanied by a deterioration in tensile mechanical properties, a decrease in histoarchitectural integrity, and a 75 % decrease in overall tissue mass, all of which correlate with widespread fragmentation of collagen structure through chain scission [6]. In contrast, a study of decellularised porcine superflexor tendons found that treatment with gamma radiation (30 kGy) and E Beam (34 kGy) induced only a 6 °C decrease in denaturation temperature, and minimal alterations to histoarchitecture and mechanical properties [336]. Porcine toe extensor tendons which were gamma irradiated (25 kGy) in a frozen hydrated state retained native-like tensile mechanical properties, whereas the UTS and Young’s modulus of tendons irradiated (25 kGY) after lyophilisation decreased by approximately 80 % and 50 % respectively [228]. While relatively limited data

exist towards the likely clinical efficacy of irradiated decellularised grafts, the efficacy and safety of allograft tissues sterilised with gamma radiation in a hydrated state has been demonstrated clinically in both soft and hard tissues (including amniotic membrane and bone) [394, 395].

The denaturation temperature of decellularised nerves treated with 0.1 % PAA was not significantly different from that of $SCCO_2$. This finding provides further evidence to suggest that a common mechanism of oxidative damage is causing alterations to ECM components in decellularised nerves treated with both methods. The NovaKill™ additive solution used during $SCCO_2$ contains the oxidising agents PAA and H_2O_2. A study of decellularised porcine aortic valves found that sterilisation with either PAA solution or $SCCO_2$ with the NovaKill™ additive solution both induced 4 °C increase in denaturation temperature from native tissue. Although $SCCO_2$ treatment appeared to cause a slight reduction in the denaturation temperature of decellularised nerves, the reduction was less than 1 °C. The small reduction in denaturation temperature induced by PAA treatment was not significantly significant. Therefore, despite the potential changes to ECM component surface chemistry observed in sections 5.4.3, 5.4.4 and 5.4.5, both methods appear to have minimal effect on structurally integral inter or intramolecular collagen bonding.

A smaller peak in heat flow was observed in all samples between a temperature range of approximately 25 – 35 °C. While it is possible that a partially denatured protein structure could produce such a peak, a more likely explanation is melting of adipose tissue within the peripheral nerve. A quantitative biochemical assay, detailed in section 4.4.10, showed that fat makes up approximately 50 % of peripheral nerve dry mass. Previous studies into the thermal properties of adipose tissue yielded a similar peak in heat flow within this temperature range. DSC analysis revealed a peak heat flow of approximately 28 °C for bovine adipose tissue [396]. A DSC study of porcine adipose tissue from different anatomical locations revealed differences in the temperature of peak heat flow [397]. Peak heat flow was 31.1 °C in subcutaneous adipose tissue, 32.6 °C in intermuscular adipose tissue and 32.9 °C in kidney leaf adipose tissue. In contrast, the measured denaturation temperature for native porcine skin, which like peripheral nerve has an ECM primarily composed of collagen I, is 66.8 °C [398]. In all of the samples (except

NaOH and NBF controls) measured here the greatest peak in heat flow was observed between 55 - 66 °C, indicating that the primary causative factor was uncoiling of the collagen I α helix.

Changes to the susceptibility of ECM-based grafts to digestion with collagenase enzymes can give further indication of molecular level changes to structure and bonding. A study of different decellularised porcine dermis grafts revealed the effects of different processing techniques on collagenase susceptibility [399]. Permacol®, composed of decellularised porcine dermis crosslinked with hexamethylene diisocyanate, had a higher collagenase resistance than the non-crosslinked Strattice®. The authors of the study hypothesised that both crosslinking and physical “spacing” within the matrix could influence the extent of matrix digestion by collagenase over a given timeframe. In the present study, treatment with the ionising radiations gamma radiation and E Beam enabled retention of “native-like” collagenase susceptibility, whereas PAA and $SCCO_2$-treated decellularised nerves were both more susceptible to collagenase digestion. Despite the likely scission of peptide bonds within the primary structure of collagen in irradiated samples, which was implied by the decrease in denaturation temperature, increased intermolecular crosslinking appears to have a protective effect with regard to digestion by collagenase enzyme. In contrast, the oxidative modifications (including possible partial solubilisation) to ECM components which are likely to have occurred during treatment with PAA and the NovaKill™ $SCCO_2$ additive solution may have increased access of the collagenase enzyme to specific binding sites and thereby increased susceptibility to digestion [242]. The collagenase used in this assay, Collagenase A, specifically cleaves the peptide bond between glycine and amino acid “X” in the primary sequence proline-X-glycine-proline, which is common in collagens but occurs infrequently in other proteins [400]. Increased looseness was seen histologically in the epineurium of decellularised nerves treated with PAA, and to a lesser extent samples treated with the standard $SCCO_2$ process. It is possible that such histoarchitectural changes may also have increased collagenase digestion, enabling the enzyme to access to a greater proportion of the ECM.

Susceptibility to collagenase digestion is likely to influence tissue remodelling and retention of histoarchitectural structure *in vivo.* Little difference was

observed in regeneration (including parameters such as cell infiltration and fibrous encapsulation) of a porcine abdominal wall defect over 12 months when Permacol® was compared to Strattice®, despite the difference in collagenase susceptibility [401]. The main differentiating factor was the rate of degradation and deposition of ECM components, which appeared to be twofold higher in the non-crosslinked Strattice® compared to the crosslinked Permacol®. This was especially notable in the early stages, one month post-implantation. The implications of these findings for function *in vivo* are unclear. It has been postulated that retention of the ECM histoarchitecture is favourable for the promotion of neuroregeneration by peripheral nerve graft, providing physical and chemotrophic guidance to infiltrating Schwann cells and regenerating axons [18, 58]. A higher susceptibility to collagenase digestion implies that greater remodelling of the matrix may take place post-implantation.

The optimal level of tissue remodelling depends on the tissue type. Faster remodelling, facilitated by a graft material with a greater susceptibility to enzymes such as collagenase, which may be favourable in some tissue types such as dermis [401]. The network of endoneurial tubules provided by autografts, the current gold standard therapy for the repair of large defects, is thought to be a key factor in their clinical efficacy [402]. Based on the measured growth rate of human peripheral nerve axons, a maximum of 1 mm/day, optimal guidance of regeneration across a defect of 30 mm would require a high level of endoneurial structural maintenance for at least 30 days post-implantation [403]. Therefore, in peripheral nerve regeneration the native-like resistance to collagenase digestion (mediating a slower ECM remodelling process) of decellularised nerves sterilised with gamma radiation or E Beam is likely to be preferable during the initial period of regeneration.

Each sterilisation method appeared to affect at least one measured physical parameter of the decellularised nerves. Treatment with SCCO2 under standard conditions, or methods requiring dehydration of the tissue (e.g. ethylene oxide), induced multiple alterations and so may not be appropriate for use with decellularised porcine peripheral nerves. E Beam treatment appeared to mediate the best overall preservation of material properties and molecular collagen integrity.

7 Cytotoxicity and immunoreactivity of sterilised nerves

7.1 Introduction

The biocompatibility of a biomaterial (such as a decellularised tissue graft) can be evaluated at different levels, from the relatively simple measure of cytotoxicity through to the local and systemic response of the host immune system. Given that terminal sterilisation processes may induce alterations to the structural, biochemical and physical properties of decellularised tissues, the potential of such grafts to induce an adverse cellular response should be assessed prior to clinical use [37, 132]. For a number of reasons, *in vitro* assays are preferred for the initial assessment of the biological response to biomaterials before conducting *in vivo* implantation studies.

During the initial development of a biomaterial, it is common practice to assess the toxicity to mammalian cells using recognised cytocompatibility assays [404]. While this this can be carried out *in vivo, in vitro* methods are more appropriate when considering an initial screening process. Although not truly representative of the *in vivo* response, the use of *in vitro* methods allows a high degree of control over experimental parameters and the simple outcome measures enable sensitive detection of any cytotoxic effects resulting from a biomaterial. Multiple cell types are used to ensure cytocompatibility across different tissue types. Conducting an initial cytotoxicity screen *in vitro* has the further advantage of reducing the need for animal experimentation in a given study, lessening suffering in accordance with the principles of the 3R's (Replacement, Reduction and Refinement) [405].

ISO standard 10993-5 (2009) defines two distinct *in vitro* assays for assessing cytotoxicity compared with positive and negative controls [406]. The direct interaction of cells with a biomaterial is tested through the contact cytotoxicity assay. A sample of a given biomaterial is placed onto a cell monolayer; the growth and morphology of cells at the interface between the biomaterial and tissue culture plastic is observed. The extract cytotoxicity assay enables the evaluation of any soluble matter which may be released from the biomaterial following implantation. A sample of the biomaterial is incubated in a solvent (often cell culture media); aliquots are added to pre-seeded wells, which are

then incubated and observed for evidence of changes. Evidence of cytotoxicity during this initial screening process indicates that the biomaterial is likely to induce local and/or systemic toxicity *in vivo*.

After establishing the basic cytocompatibility of a biomaterial, further aspects of biocompatibility should be considered prior to implantation in an *in vivo* system. The immunoreactivity of a biomaterial should be characterised, in terms of both the level and nature of the induced host immune response [407]. At the most basic level, the response of the innate and adaptive immune system impacts upon the potential integration or rejection of a biomaterial following implantation [36]. However, this does not fully describe the complexity of the host response, which is massively variable in terms of distribution within the body, contributory pathways and effect. Host immune cells can influence the graft integration process through debris clearance and wound repair following surgical implantation, stimulation of site-specific cells and immune cells towards a phenotypic change, secretion of chemoattractants and secretion of matrix metalloproteases to aid cell ingrowth and tissue remodelling.

The host response to an ECM-derived biomaterial, such as a decellularised tissue graft, is complicated by the inherent variability in composition versus a comparatively uniform and inert material (such as a metal or ceramic hip replacement). The most important modulators of adverse host immune response in decellularised tissue grafts are residual cellular component debris including nucleic acids, cytosolic components and phospholipid membrane fragments; these are collectively referred to as damage-associated molecular patterns (DAMPs) [132, 133]. Untreated cellular tissue (e.g. murine heart allografts) and decellularised grafts (e.g. decellularised porcine lungs implanted into rhesus macaques) have been observed to elicit an adaptive T cell-driven response but also an innate immune response; however, the magnitude of any response is likely to be much reduced due to the inherently lower concentration of cellular components present in decellularised tissues [37, 408-410]. The immune response to decellularised tissues may therefore be more favourable to graft integration and eventual functional restoration compared with an untreated (cellular) allo/xenograft [36, 37, 132]. The magnitude and exact nature of the immune response to a decellularised tissue graft is likely to vary in response to a range of factors. Tissues may retain relatively high levels of DNA and cellular

debris after a given decellularisation process has been applied; for example, a 2015 study examined the effects of this on the macrophage response to decellularised porcine-SIS *in vivo* [132]. The porcine-SIS was decellularised through treatment with PAA solution for either 0 (PBS wash only), 1 or 2 hours, which resulted in correspondent differences in the retention of intact nuclei and DNA fragments; histological analysis indicated that scaffolds treated with PBS only (i.e. not decellularised) or the 1 hour PAA protocol elicited a much greater innate inflammatory response compared with scaffolds treated with the 2 hour PAA protocol (which achieved the greatest relative reduction in DNA content), which showed the greatest level of ECM remodelling and integration to the surrounding tissue. Furthermore, some tissue types may have higher levels of resident immune cells and/or greater potential for the infiltration of circulating immune cells compared with others (e.g. immune access to the CNS is much more restricted than to other tissues such as dermis) [411, 412].

In both arms of the immune system, the nature of the response to an implanted tissue graft is driven by the polarisation of key mediating cells. In the adaptive immune system, CD4+ T helper cells are the initial effector cells [134]. T helper cells can adopt either a pro-inflammatory (Th1; characterised by the secretion of pro-inflammatory cytokines including IL-2, IFN-γ, TNFα and TNFβ,) phenotype or anti-inflammatory (Th2; characterised by the secretion of anti-inflammatory cytokines such as IL-4, 5, 6 and 10) phenotype, in response to stimulation from antigen-presenting cells such as macrophages and dendritic cells [413, 414] Decellularised tissue grafts appear to induce a predominantly Th2-mediated response, as demonstrated following subcutaneous implantation of decellularised porcine SIS into mice [415, 416] [417]. Both IL-4 and IFN-γ were present in the graft after 7 days; however, IFN-γ expression was 100-fold lower than in animals implanted with a non-decellularised control tissue. Gross histological analysis of explanted decellularised SIS grafts revealed an initial inflammatory response characterised by the infiltration of monocytes, followed by extensive remodelling and integration of the ECM after 28 days *in situ*. In contrast, the non-decellularised control tissue consistently stimulated pro-inflammatory processes for the duration of the study, including monocyte activation and giant cell formation, T cell infiltration, structural degeneration of the graft and the formation of a fibrotic capsule surrounding the graft. This

encapsulation and fibrosis is characteristic of chronic rejection. A similar response was seen when the decellularised SIS was implanted in humans, with no evidence of rejection or significant adverse events [418].

The innate immune system is dominant in the acute response following implantation and strongly influences the nature of the chronic response, stimulating pathways favouring either ECM remodelling and integration or fibrosis and encapsulation [36]. Macrophages are the primary mediators of the innate response to tissue grafts. Similarly to CD4+ T cells, macrophages undergo activation and phenotypic polarisation in response to external stimuli; these stimuli vary in nature but in the case of tissue grafts they are generally interaction with DAMPs [133]. Pro/anti-inflammatory cytokines secreted by local cells (and already activated macrophages) can amplify the activation and polarisation of macrophages. Macrophages polarise towards two phenotypes: M1, characterised by the secretion of pro-inflammatory cytokines such as IL-1β, IL-6, IL-12 and TNFα, and M2, characterised by the secretion of the anti-inflammatory cytokines IL-10 and TGF-β [419]. Recent evidence suggests that changes in macrophage phenotype can be more accurately characterised as a spectrum rather than two distinct categories, with the amount and type of cytokines secreted being particularly variable in the classical M2 category [419]. Regardless of the classification system used, high levels of M1 type cytokines are associated with a pro-inflammatory microenvironment and increased likelihood of tissue graft rejection, especially upon stimulation of a CD4+ cells towards a Th1 phenotype and the induction of an associated chronic immune response [132].

Beyond modulating the phenotype and distribution of cells, macrophages can also aid the integration of a graft through phagocytosis of wound-associated debris and the production of MMPs (including MMP1, 2, 7, 10 and 12) which enable the process of ECM remodelling to begin [420]. Conversely, chronic exposure to a pro-inflammatory microenvironment can cause macrophages to merge and form multi-nuclear “giant cells”, which are key mediators of the fibrotic capsule formation during graft rejection [421].

An increasing body of literature supports the assertion that a strong macrophage response, briefly M1-dominated followed by predominantly M2

macrophages, is necessary for optimal remodelling and integration of decellularised tissue [37]. Elimination of macrophages in animal models, in an attempt to prevent an “adverse” M1 type response, results in inferior graft integration; this has been demonstrated though the study of implanted skeletal muscle, skin, and myocardium regeneration patterns in monocyte-depleted/deficient murine models [422-424].

Changes to the properties of decellularised tissue grafts induced as a result of specific production processes can modulate the magnitude and nature of the host immune response induced following implantation. Insufficient elimination of some decellularisation reagents, such as SDS, can lead to an adverse host response [425]. In a study evaluating immunostimulatory potential, excised rat abdominal wall segments were decellularised using 0.25 % (v/v) SDS solution. One group of wall segments were subject to a wash step with 0.5 mM $CaCl_2$, resulting in the elimination of 98.4 % (w/w) of the residual SDS from the tissue. The decellularisation process for the second group of wall segments did not include this step, resulting in only 81.4 % (w/w) of the residual SDS being removed. The *in vitro* human macrophage response and *in vivo* performance of the scaffolds was then assessed. *In vitro,* secretion of TNFα by macrophages was significantly increased in the high-SDS group compared to a non-stimulated control, and expression of the pro-inflammatory marker chemokine receptor type 7 (CCR7) was significantly increased compared to the low-SDS group. PCR analysis of gene expression levels indicated that macrophages cultured with the low-SDS group (but not the high-SDS group) were polarised towards an M2-type expression profile. Implantation of grafts from the high-SDS group in a rat muscle defect model resulted in significantly higher expression of TNFα and IL-1β compared to grafts from the low-SDS group. Gross histological analysis of explanted grafts from the low-SDS group revealed evidence of ECM remodelling, integration with the surrounding tissue and full infiltration of site-appropriate myocytes. In comparison explanted grafts from the high-SDS group had a much reduced level of cell infiltration. Numerous giant multinuclear cells were observed surrounding the graft, together with the fibrotic capsule which is typically indicative of graft rejection. The response was further characterised by antibody labelling for the phenotypic cell surface markers, specifically CCR7 (M1) and CD206 (M2). The ratio M1:M2 markers was significantly greater in the

high-SDS grafts, indicating a pro-inflammatory microenvironment induced as a result of increased local SDS concentrations.

The immunomodulatory effects of different sterilisation methods for decellularised tissue grafts are not well characterised [37]. However, it is likely that sterilisation-associated effects such as crosslinking and chain scission of ECM components, the deposition of toxic residues and alterations to immunostimulatory antigens would affect how immune cells interact with the tissue. As the dynamics of macrophage phenotypic changes are the most important factor in determining the acute response to an implanted tissue (and heavily modulate the chronic response), they should be the initial focus of research.

The development of an *in vitro* screening process could provide vital insight into macrophage phenotypic changes when seeded onto decellularised nerves sterilised with different methods; in addition, such data may also have wider applicability across other decellularised tissues.

7.2 Aims and Objectives

Aim

The aim of this study was to assess the cytocompatibility and immunoreactivity of the sterilised decellularised nerves in a controlled *in vitro* environment.

Objectives

i. To determine the cytotoxicity of the sterilised nerves through contact culture with two distinct cell types.
ii. To optimise a cell viability assay, alamarBlue®, for use with RAW 264.7 cells.
iii. To determine the efficacy of LPS in solution as a pro-inflammatory control.
iv. To establish the sensitivity of enzyme-linked immunosorbent assays (ELISAs) for the detection of cytokines secreted by RAW 264.7 cells.
v. To optimise a methodology for seeding RAW 264.7 cells onto segments of sterilised nerve.
vi. To determine the effect of sterilisation on the viability and levels of cytokine secretion of RAW 264.7 cells seeded onto nerve segments over 48 hours in culture.

7.3 Materials and Methods

7.3.1 Contact cytotoxicity assay of sterilised decellularised nerves

Sterilised decellularised nerves were subject to contact cytotoxicity testing, as described in section 2.12.

7.3.2 Culture of RAW 264.7 cells and optimisation of alamarBlue® assay

RAW 264.7 cells are a murine macrophage cell line commonly used in preliminary *in vitro* assays to evaluate the immunostimulatory capacity of a given biomaterial.

7.3.2.1 RAW 264.7 cell culture medium

RAW 264.7 cells were cultured in Roswell Park Memorial Institute (RPMI) medium containing 10 % (v/v) FBS, 100 $U.ml^{-1}$ penicillin-streptomycin and 2 mM L-glutamine (supplemented medium hereafter referred to as culture medium).

7.3.2.2 Resurrection and culture of RAW 264.7 cells from cryostorage

Vials containing RAW 264.7 cells were removed from cryostorage in liquid nitrogen. The vials were thawed rapidly in a water bath at 37 °C and the cell pellets were transferred to individual sterile universal tubes in a class II environment. Culture medium (10 ml) was added drop wise to each universal, before centrifugation at 150 x g for ten minutes. The supernatant was discarded and the cells re-suspended in 5 ml of culture medium and seeded into a T75 flask. The cells were incubated for 24 hours at 37 °C in an atmosphere of 5 % (v/v) CO_2 in air. The culture medium was replaced 24 hours after revival, then every 48 - 72 hours. Cell growth was observed by light microscopy.

7.3.2.3 Passaging of RAW 264.7 cells

RAW 264.7 cells were passaged upon reaching a confluency of approximately 80 %. The medium was aspirated from the culture flask and the cell layer washed twice in PBS (without magnesium or calcium). Fresh culture media (10 ml) was added and the cells were carefully dislodged using a cell scraper. The total volume present in the flask was then transferred to a universal tube and centrifuged at 150 x g for ten minutes. The supernatant was discarded, and the cells suspended in 1 ml of medium.

Cell suspension and Trypan Blue (20 µl each) were mixed, and 10 µl was added to a haemocytometer. The number of viable cells per grid was then determined, and the total number of cells.ml^{-1} was calculated using the equation detailed below.

$$Number\ of\ viable\ cells.ml^{-1} = \frac{number\ of\ viable\ cells}{number\ of chambers}\ x\ 10^4\ x\ Dilution\ factor$$

The cell suspension was then diluted as appropriate (to give a starting confluency of approximately 10 - 20 %), seeded to a T75 or T175 flask and incubated at 37 °C in an atmosphere of 5 % (v/v) CO_2 in air.

7.3.2.4 Optimisation of alamarBlue® assay for cell viability

Viability and proliferation of RAW 264.7 cells was measured using the alamarBlue® assay. The functional reagent in alamarBlue® is 7-hydroxy-10-oxidophenoxazin-10-ium-3-one (resazurin) [426, 427]. Resazurin is able to diffuse though phospholipid membranes, allowing monitoring of live cell viability *in vitro*. AlamarBlue® acts an intermediate electron acceptor; upon accepting electrons, the oxidised form (resazurin) is reduced to resofurin. Within the cell this process is predominantly mediated by mitochondrial enzymes such as nicotimamide adenine dinucleotide phosphate (NADPH) and the cytochromes, but to a lesser extent also by cytoplasmic enzymes such as dihydrolipoamine dehydrogenase. Upon reduction the colour of the reagent changes from blue to pink. Reduction also causes the reagent to become fluorescent.

Determining the relative percentage reduction of alamarBlue® in wells containing cells compared to a medium and alamarBlue®-only negative control enables quantification of cell viability and proliferation. Reduction of alamarBlue can be determined fluorescently or colorimetrically.

The alamarBlue® assay was carried out in six well plates. AlamarBlue® regent was added to culture medium (2 ml/well) in a sterile universal to give a working concentration of 10 % (v/v). The medium was then added to the test and control wells, and incubated in conditions of darkness at 37 °C in an atmosphere of 5 % (v/v) CO_2 in air. The length of the incubation period was optimised according to the approximate expected cell number (see below). Aliquots of medium were

then transferred in triplicate to a fresh 96 well plate and the absorbance of individual wells at 570 and 600 nm was measured using a spectrophotometer. The percentage reduction of the alamarBlue® reagent was calculated using the equation detailed below (Equation 7-1).

$$Percentage\ reduction = \frac{(E_{oxi}600\ x\ A_{570}) - (E_{oxi}570\ x\ A_{600})}{(E_{red}570\ x\ C_{600}) - (E_{red}600\ x\ C_{570})}\ x\ 100$$

$$E = molar\ extinction\ coefficient$$

$$E_{oxi}570 = \ E\ of\ oxidised\ alamarBlue®\ at\ 570\ nm = 80586$$

$$E_{oxi}600 = E\ of\ oxidised\ alamarBlue®\ \ at\ 600\ nm = 117216$$

$$A_{570} = absorbance\ of\ test\ wells\ at\ 570\ nm$$

$$A_{600} = \ absorbance\ of\ test\ wells\ at\ 600\ nm$$

$$E_{red}570 = E\ of\ reduced\ alamarBlue®\ at\ 570\ nm = 155677$$

$$E_{red}600 = E\ of\ reduced\ alamarBlue®\ at\ 600\ nm = 14652$$

$$C_{570} = absorbance\ of\ negative\ control\ wells\ at\ 570\ nm$$

$$C_{600} = absorbance\ of\ negative\ control\ wells\ at\ 600\ nm$$

Equation 7-1 Equation used to calculate percentage reduction of alamarBlue® reagent

To enable determination of approximate seeding efficiency and cell proliferation, a standard curve of RAW 264.7 cell number against the percentage reduction of alamarBlue® was required. Data in the literature predominantly refers to the use of the alamarBlue® assay in 96 well plates. Therefore, the length of incubation time in alamarBlue® was optimised according to cell number in individual wells of a six well plate containing 2 ml of culture medium. Serial dilutions of RAW 264.7 cell number were prepared to give a range of 0.0153 x 10^6 – 1 x 10^6 cells/well. Cell suspension at each dilution was added in triplicate to the wells of six well plates. Separate groups were incubated for times of 3, 12

and 18 hours. The data was used to prepare standard curves of cell number against percentage reduction of the alamarBlue® reagent.

7.3.3 Determination of lipopolysaccharide efficacy as pro-inflammatory control

The bacterial endotoxin lipopolysaccharide (LPS) was used as a positive control agent to stimulate a pro-inflammatory response in RAW 264.7 cells. An experiment was devised to determine the effect of LPS stimulation on cell proliferation and cytokine secretion. Two separate medium solutions were prepared. For the test (positive control) groups, 200 $mg.ml^{-1}$ LPS stock solution was diluted 1:1000 in culture medium to give a working concentration of 200 $ng.ml^{-1}$. The negative control consisted of culture medium without the addition of LPS.

RAW 264.7 cells were passaged, counted and diluted in either in test or negative control culture medium. Cells from each group were seeded to two six well plates at a density of 2.5×10^5 cells/well and 1.25×10^5 cells/well respectively. The plates were incubated at 37 °C in an atmosphere of 5 % (v/v) CO_2 in air for 24 hours. After 24 hours, the culture media was removed and transferred to individual sterile 2 ml eppendorfs corresponding to each well. The eppendorfs were centrifuged at 10000 x g for 10 minutes at 4 °C. The supernatants were transferred to fresh 2 ml eppendorfs and stored at -80 °C prior to quantification of IL-10 and TNFα by ELISA. The effects of LPS stimulation on cell viability and proliferation were determined through the alamarBlue® assay (Section 7.3.2.4).

7.3.4 Enzyme-linked immunosorbent assay (ELISA) quantification of TNFα, IL-10, IL-1β and IL-6

The concentrations of the cytokines IL-10, TNFα, IL-1β and IL-6 in medium supernatants were quantified by ELISA.

7.3.4.1 Solutions

Supplied kit solutions

The ELISAs were carried out with READY-SET-GO kits from Invitrogen, according to the manufacturer’s instructions. Reagents were supplied as

concentrated stock solutions, which were diluted prior to use. Stock solutions of capture antibody were diluted in PBS. Stock solutions of detection antibody and avidin-horseradish peroxidase (avidin-HRP) were diluted in ELISASPOT diluent. Lyophilised cytokine standard were rehydrated and diluted in distilled water. Test samples were diluted as necessary in distilled water. Tetramethylbenzidine (TMB) solution was supplied at working concentration.

Wash Buffer

TWEEN™-20 (1 ml) was added to 2 L of PBS to give a working concentration of 0.05 % (v/v).

Stop solution

1 M Sulphuric acid (H_2SO_4) was used as a stop solution in the ELISA assays.

7.3.4.2 Assay Method

The same method was used for ELISA quantification of each cytokine in medium supernatants. Excess solution was removed between steps by blotting. All wash steps were carried out by the addition and aspiration of 300 µl/well of wash buffer.

Capture antibody solution (100 µl/well) was added to the assay plates (96 well MaxiSorp™ plates), before being sealed with parafilm and incubated overnight at 4 °C to ensure coating of the wells. The solution was aspirated and the wells were washed three times. Wells were blocked with 200 µl/well of ELISASPOT diluent for one hour at room temperature. The ELISASPOT diluent was aspirated and the wells were washed once in wash buffer. Standards (3.9 – 4000 $pg.ml^{-1}$) and samples were added to the plates in duplicate 100 µl/well aliquots. ELISASPOT diluent was included as a negative control. The plates were incubated for two hours at room temperature. The contents of each well was aspirated and the wells were washed three times. Detection antibody solution (100 µl/well) was added and the plates were incubated for one hour at room temperature. The detection antibody solution was aspirated and the wells were washed three times. Avidin-HRP solution (100 µl/well) was added and the plates were incubated for one hour at room temperature. The avidin-HRP solution was aspirated and the wells were washed six times. TMB solution (100 µl/well) was added and the plates were incubated for 15 minutes at room

temperature. Stop Solution (50 µl/well) was added, and the absorbance was read at 450 nm and 570 nm. Values read at 570 nm were subtracted from those at 450 nm, and a standard curve of cytokine concentration against adjusted absorbance was plotted to enable interpolation of unknown values.

7.3.5 Optimisation of methodology for seeding RAW 264.7 cells to segments of decellularised nerve

A method was developed for seeding RAW 264.7 cells onto decellularised nerve segments, to enable quantification of changes in proliferation and cytokine secretion according to the specific sterilisation method. The seeding process was optimised with non-sterilised decellularised nerve segments, produced under aseptic conditions.

7.3.5.1 Seeding methodology

Stainless steel seeding rings, with a chamber dimensions of approximately 10 x 5 x 5 mm, were placed in individual wells of six well plates. Five ml of sterile water was added to the space between individual wells to humidify the local atmosphere within the plate and further limit media loss during seeding.

Segments of decellularised nerve were resized using sterile dissection tools to give a uniform size of 5 x 10 mm, and transferred to individual seeding rings (Figure 7-2). The tissue segments and seeding chambers were washed with PBS (without magnesium or calcium).

RAW 264.7 cells were passaged, counted and diluted in fresh medium to achieve a cell suspension of the required seeding density. Aliquots (200 µl) of cell suspension were transferred to each seeding ring, and incubated for a given time period.

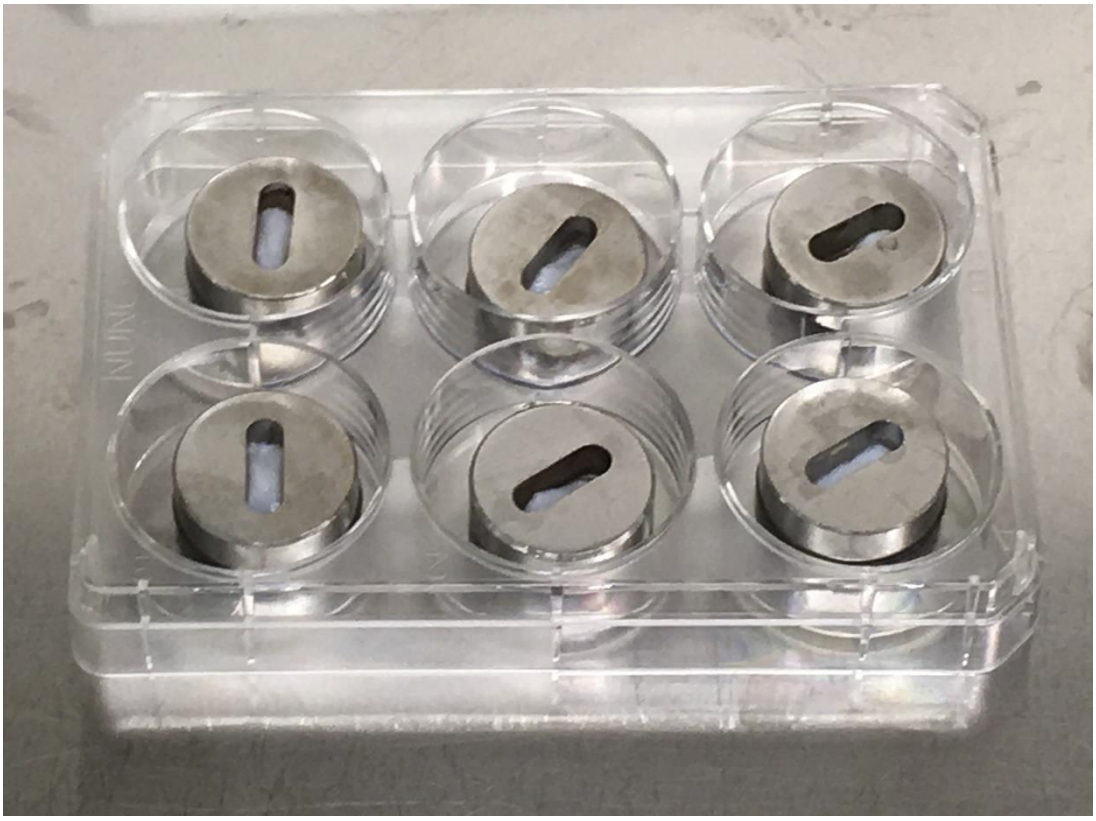

Figure 7-2 Seeding setup used with nerve segments

Pre-sized segments of decellularised nerve, sited within the wells of individual seeding rings prior to the addition of RAW 264.7 cell suspension.

The length of the incubation period and the seeding density were optimised to ensure maximum seeding efficiency and subsequent cell viability. The appropriate incubation time in alamarBlue® for RAW 264.7 cells seeded to decellularised nerve segments was determined following quantification of seeding efficiency and subsequent calculation of the cell number on each seeded segment. A linear regression was generated for each curve and the fit quantified through calculation of R-square.

7.3.5.2 Optimisation of media retention and seeding protocol

The use of agarose for the sealing of seeding rings within wells was identified as a method for the prevention of media loss and tissue dehydration. Agarose powder was added to distilled water (4 g in 100 ml) and heated in the microwave until dissolved to give a 4 % (w/v) solution. The solution was then autoclaved to ensure sterility.

Two sets of seeding rings (n = 12 per group) were placed in individual wells of separate six well plates. The edges of the wells in two plates were filled with approximately 2 ml/well of 4 % (w/v) agarose, which was then left to cool for approximately 30 minutes. Seeding rings within the other plate were left without agar sealing. Two groups each of decellularised nerve segments (n = 6 per group) were seeded with 1 x 10^6 RAW 264.7 cells per well. Individual plates were incubated for three hours at 37 °C in an atmosphere of 5 % (v/v) CO_2 in air. Tissue segments (n = 6) from each group were then transferred to individual wells of fresh six well plates, and the alamarBlue® assay (7.3.2.4) was used to determine the approximate seeding efficiency. The remaining tissue segments from each group (n = 6) were fixed, processed and sectioned as previously described (2.11). The sections were stained with H & E and analysed by light microscopy to determine differences in cell attachment patterns.

7.3.6 Determining the effect of sterilisation on RAW 264.7 cell viability and cytokine secretion

The immunostimulatory capacity of decellularised nerves treated with different sterilisation methods were analysed by seeding with RAW 264.7 cells.

7.3.6.1 Sample preparation

Seeding rings were placed in individual wells of six well plates (5 plates per group) and the edges sealed with 4 % (w/v) agarose as described above. Groups of decellularised nerve segments, sterilised with PAA, gamma radiation, E Beam or $SCCO_2$ as previously described (section 2.10.3; n = 30 per treatment group) were resized in preparation for seeding. A further group of non-sterilised decellularised nerves (n = 30) were included, to be incubated with culture media containing 200 $ng.ml^{-1}$ LPS as a positive control. There was considered to be a lack of a suitable true negative control; collagen gels do not offer a representative comparison to ECM tissue grafts due to differences in processing and source materials, whilst non-sterilised decellularised nerves present an unacceptable risk of introducing contaminating organisms (e.g. bacteria) to the culture media, which would both compromise cell viability assay results and potentially lead to changes in cytokine secretion. For these reasons, no negative control was included in the study. The segments were transferred to individual seeding rings.

7.3.6.2 Seeding, culture, data collection and analysis

For each group, RAW 264.7 cells were passaged, counted and diluted in culture media to give a density of 5 x 10^6 cells/ml. Aliquots of cell suspension (200 µl) were transferred to each seeding ring, and the plates were incubated for three hours at 37 °C in an atmosphere of 5 % (v/v) CO_2 in air. The tissue segments were then transferred to individual wells of new six well plates, and 2 ml of fresh culture media was added to each well. Each plate (n = 6 segments in each) was incubated for different time periods, with the end points defined as 0, 6, 12, 24 and 48 hours. Additional six well plates containing culture media-only (no tissue or cells) were included as a negative control for each timepoint.

When each endpoint was reached, the media was removed from each well and supernatant obtained and stored as previously described (7.3.3). Fresh culture media (2 ml) containing 10 % (v/v) alamarBlue® was added to each well and the plates were incubated for a further 12 hours.

Cell viability (and therefore approximate relative cell number) was determined by the alamarBlue® assay as previously described (7.3.2.4). The concentrations of IL-10, TNFα, IL-1β and IL-6 in medium supernatants were quantified by ELISA (7.3.4) and normalised to cell number by reference to the alamarBlue® estimated cell population (to give a value in pg.ml^{-1} per 1 x 10^6 cells).

7.3.7 Statistical analysis

Differences between means in the timecourse experiments were determined using a two-way ANOVA. The location of significant differences was determined by Tukey's Honestly Significant Difference test. The level of significance for the difference between two means was defined as p = 0.05. Data was displayed as +/- 95 % confidence limits.

7.4 Results

7.4.1 Contact cytotoxicity assay of sterilised nerves

The biocompatibility of decellularised nerves after different sterilisation treatments was assessed by contact culture studies with two distinct cell lines, BHK epithelial cells (Figure 7-3) and L929 fibroblasts (Figure 7-4). As previously described in section 2.12.4, cyanoacrylate contact adhesive was used as a positive control and a commercially available surgical closure strip (Steri-Strip) as a negative control.

No evidence of cytotoxicity was observed in either cell line when cultured with nerves from each treatment group. Cells of both lines were observed to grow up to and in contact with the samples, maintaining a consistent morphology.

The rounded appearance characteristic of the dead cells cultured in wells with the cyanoacrylate positive control was not observed in cells cultured with decellularised nerves from any of the treatment groups.

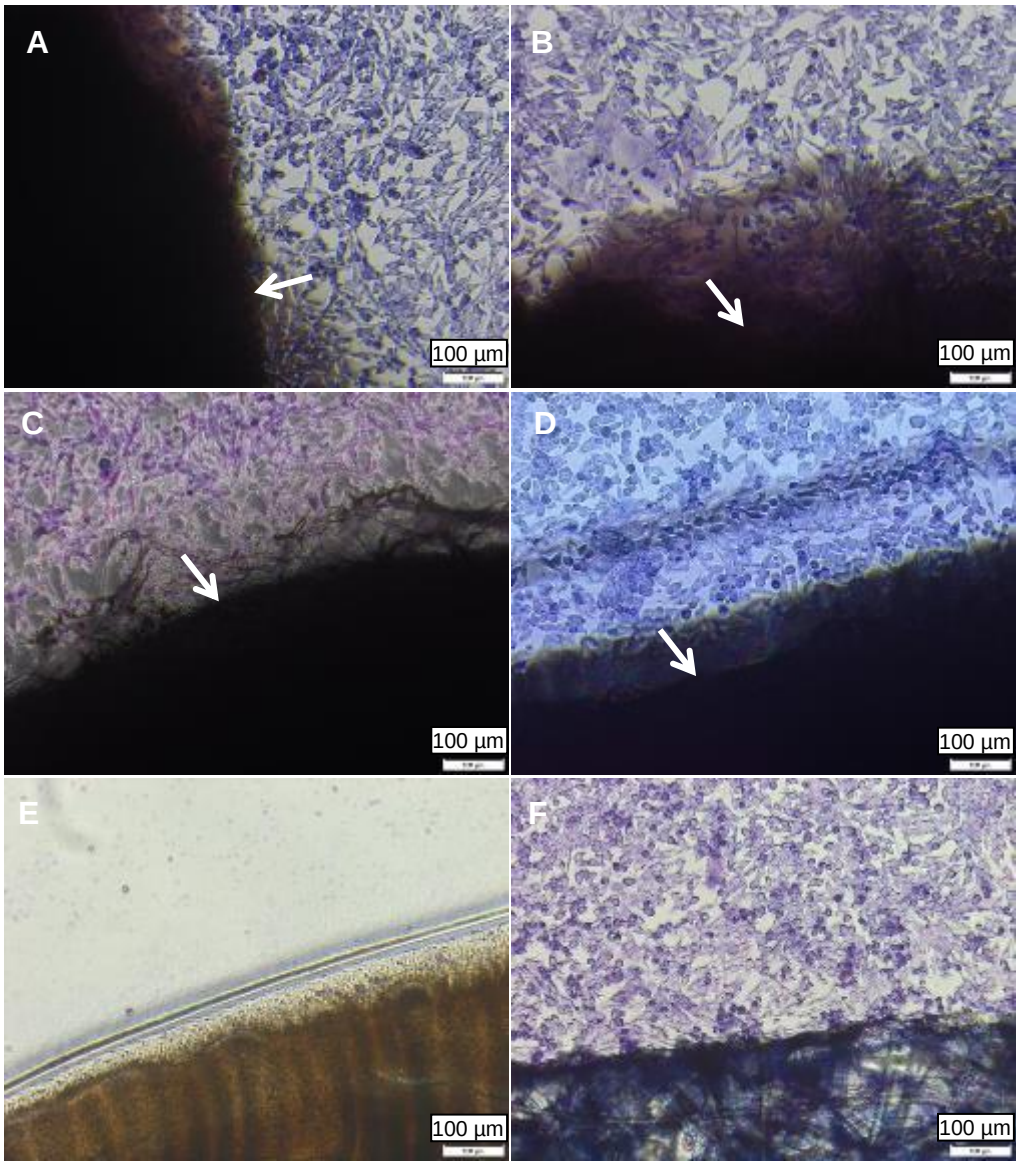

Figure 7-3 Representative images of Giemsa-stained BHK cells cultured for 48 hours with decellularised nerves

Images show BHK cells cultured with decellularised nerve treated with (A) PAA, (B) gamma radiation, (C) E Beam, (D) $SCCO_2$, (E) cyanoacrylate positive control and (F) Steri-Strip negative control. Tissue segments are indicated by arrows. Images were acquired under Brightfield illumination using a x10 objective. Scale bars = 100 µm.

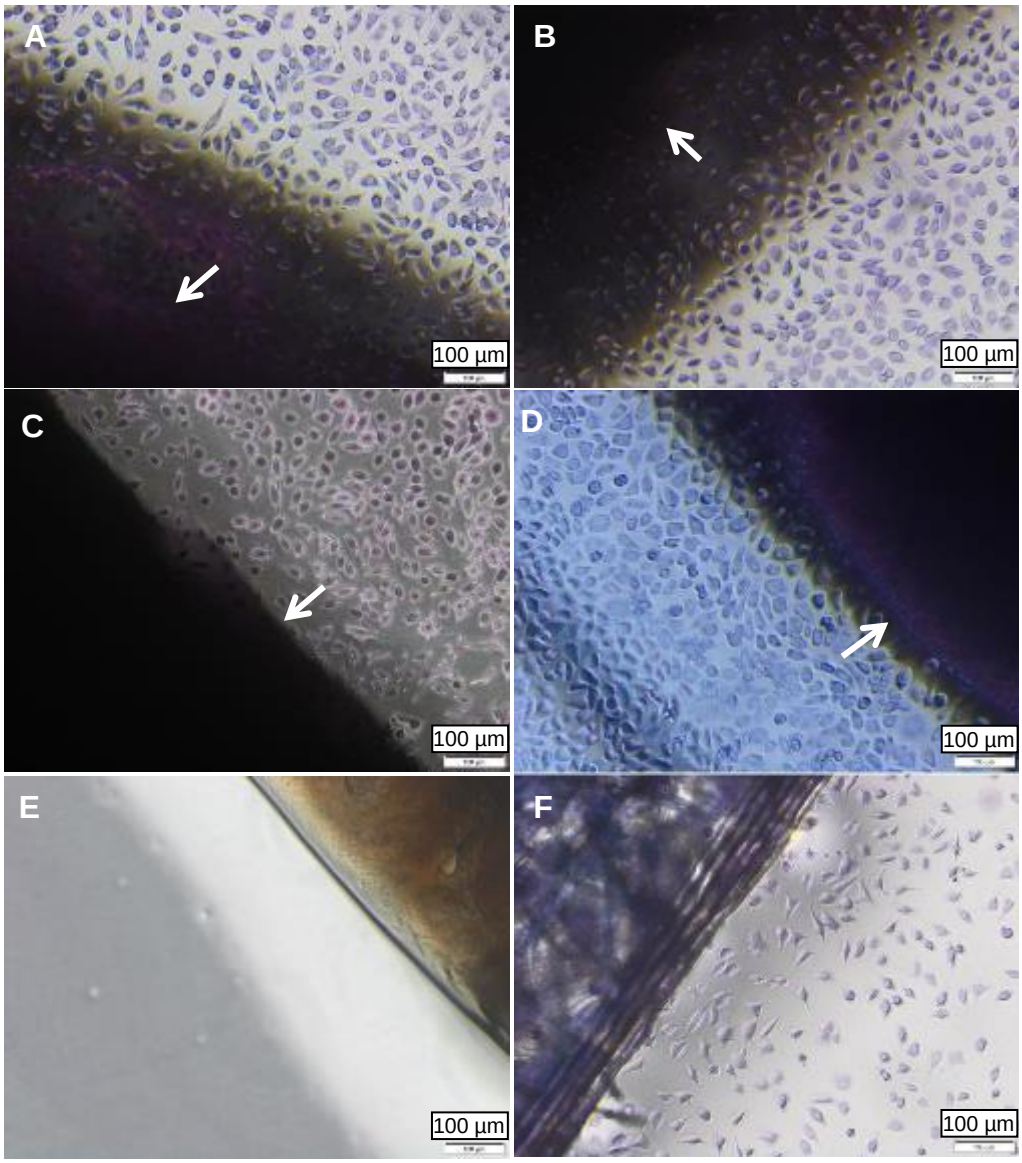

Figure 7-4 Representative images of Giemsa-stained L929 cells cultured for 48 hours with decellularised nerves

Images show L929 cells cultured with decellularised nerve treated with (A) PAA, (B) gamma radiation, (C) E Beam, (D) $SCCO_2$, (E) cyanoacrylate positive control and (F) Steri-Strip negative control. Tissue segments are indicated by arrows. Images were acquired under Brightfield illumination using a x10 objective. Scale bars = 100 µm.

7.4.2 Optimisation of alamarBlue® assay for use with Raw 264.7 cells

Serially-diluted populations of RAW 264.7 cells were incubated in alamarBlue® for three different time periods. The range of the linear relationship between percentage alamarBlue® reduction and cell number was assessed.

A linear relationship between percentage alamarBlue® reduction and cell number was apparent for cell numbers of up to 0.5×10^6, 0.125×10^6 and 0.06125×10^6 after incubation periods of 3, 12 and 18 hours respectively, evidenced by the fit of linear regression between 0 and 0.125×10^6 cells (Figure 7-5). Plateauing was observed above the linear range within each group, caused by a decreased relative gain in the percentage reduction of alamarBlue® compared to the increase in cell number.

Since low seeding efficiencies were expected in the later experiments with decellularised nerves, it was considered particularly important to identify the most suitable incubation period for populations up to 0.125×10^6 cells.

An incubation time of up to 12 hours was found to produce the best fit for the interpolation of cell numbers up to 0.125×10^6 cells, with an R-square value of 0.998 compared to 0.983 and 0.949 for incubation periods of three and 18 hours respectively.

A

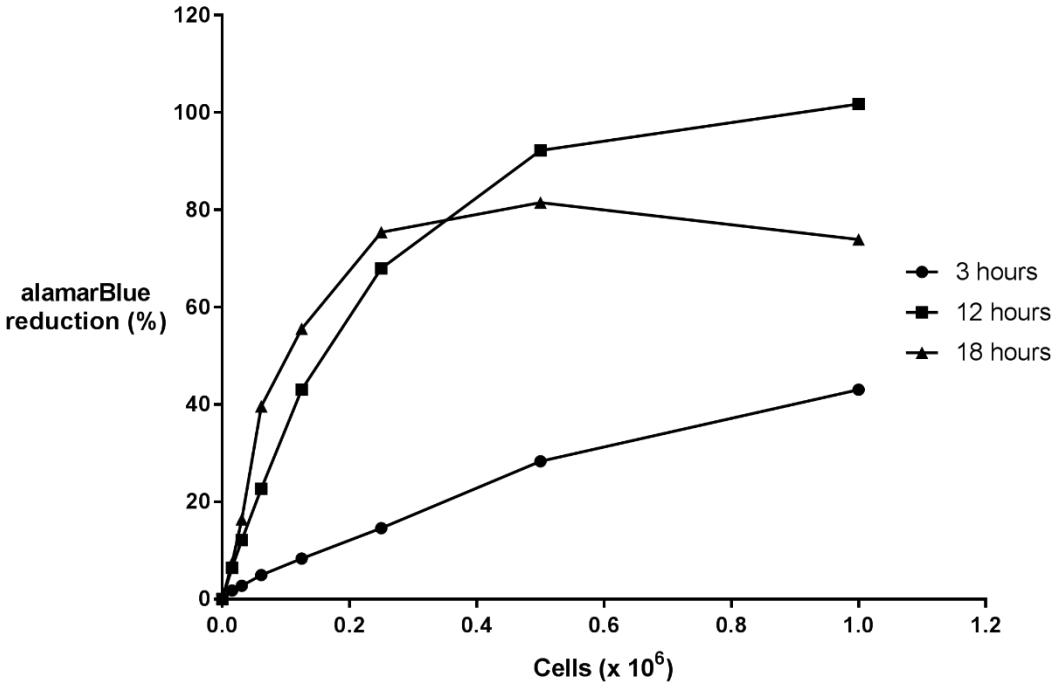
120
100
80
60
40
20
0
alamarBlue reduction (%)
0.0
0.2
0.4
0.6
0.8
1.0
1.2
Cells (x 10^6)
3 hours
12 hours
18 hours

B

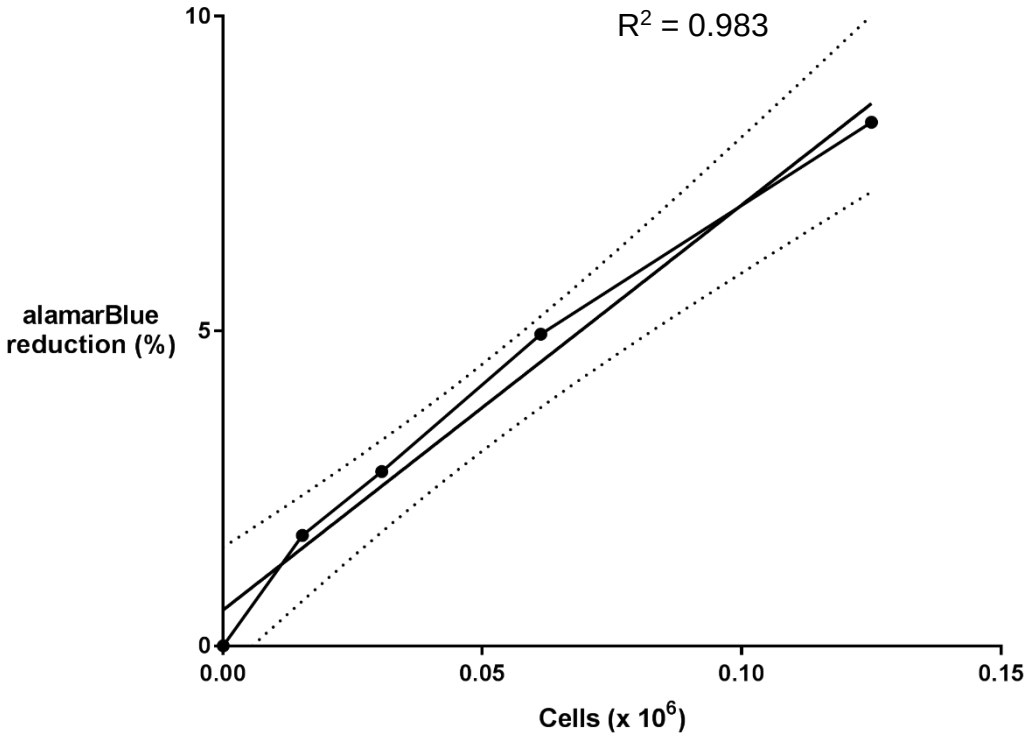
R^2 = 0.983
10
5
0
alamarBlue reduction (%)
0.00
0.05
0.10
0.15
Cells (x 10^6)

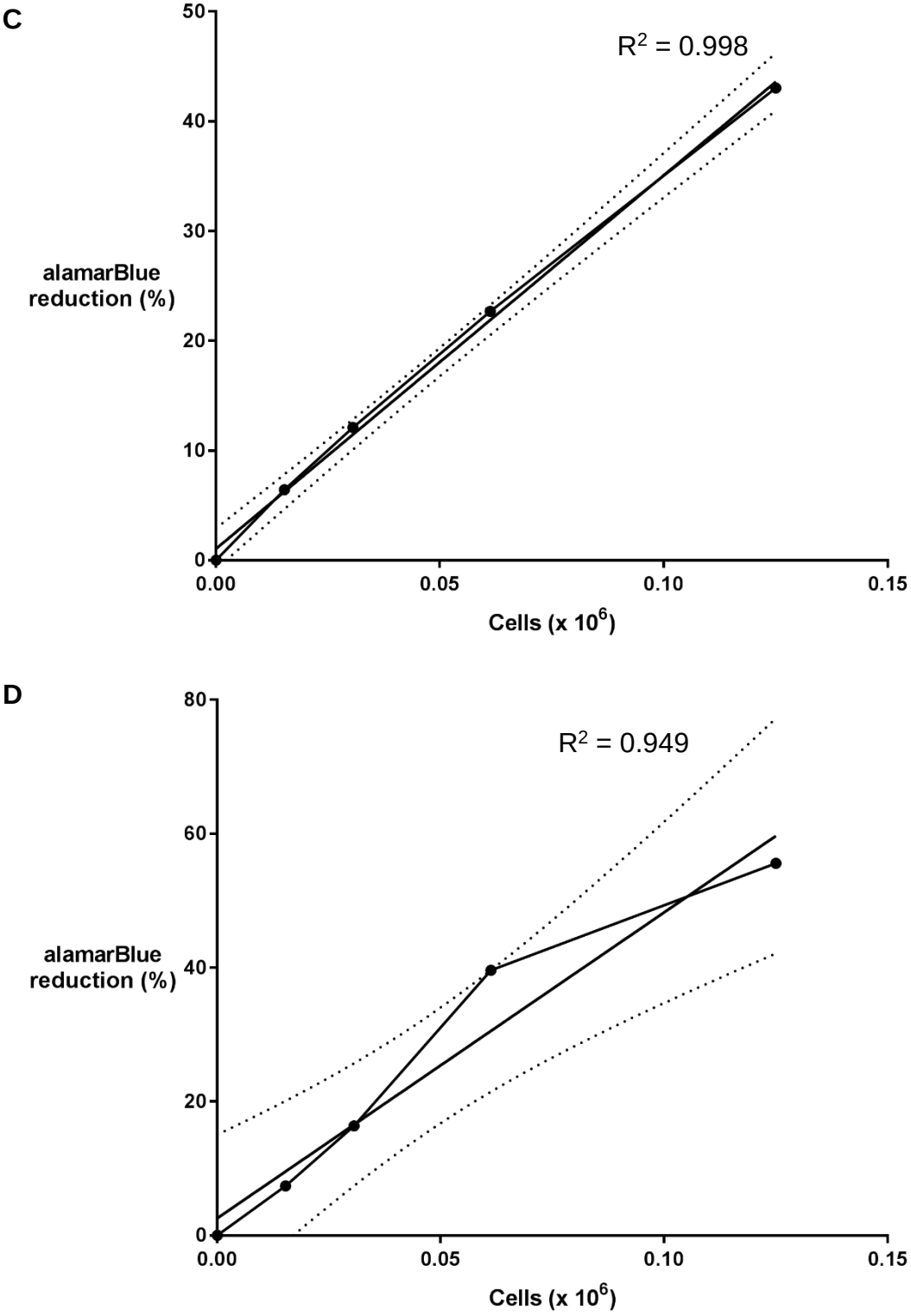

Figure 7-5 The effect of varying incubation time on the percentage alamarBlue® reduction according to cell number

Changes in percentage alamarBlue® reduction across serially diluted cell populations from (A) 0 – 1 x 10^6 cells incubated over 3, 12 and 18 hours, and 0 – 0.125 x 10^6 cells over incubation periods of (B) 3 hours, (C) 12 hours and (D) 18 hours. The R-square value for each curve is displayed.

7.4.3 Efficacy of LPS as stimulator of pro-inflammatory response

Two groups of RAW 264.7 cells were seeded to individual wells of a six well plate at 0.25 x 10^6 and 0.125 x 10^6 cells/well respectively. The effects of a 24 hour incubation in media containing 200 $ng.ml^{-1}$ LPS on cell proliferation were determined by interpolation of cell number from measured values for percentage alamarBlue® reduction. The effect of LPS on TNFα secretion was determined by ELISA quantification.

Significantly fewer RAW 264.7 cells ($p < 0.05$) were detected after 24 hours culture in the presence of LPS compared to the negative control (Figure 7-6). In wells seeded with 0.25 x 10^6 cells, LPS stimulation caused a decrease in cell population to 0.225 (+/- 0.019) x 10^6 compared to an increase of 0.268 (+/- 0.009) x 10^6 in the negative control. In wells seeded with 0.125 x 10^6 cells, LPS stimulation again caused a decrease ($p < 0.05$) in cell population to 0.099 (+/- 0.039) x 10^6 compared to an increase of 0.137 (+/- 0.007) x 10^6 in the negative control.

TNFα secretion (relative to cell number) was significantly increased in both LPS-stimulated populations compared to the negative control. In wells seeded with 0.25 x 10^6 cells, LPS stimulation induced a significant increase ($p < 0.05$) in TNFα secretion, at 3184 (+/- 544.5) $pg.ml^{-1}$ per 10^6 cells compared to 22.97 (+/- 11.79) $pg.ml^{-1}$ per 10^6 cells in the negative control. In wells seeded with 0.125 x 10^6 cells high levels of TNFa secretion were detected following LPS stimulation, at 4067 (+/- 1597) $pg.ml^{-1}$ per 10^6 cells, whereas very low levels were seen in the negative control (below the limit of accurate determination).

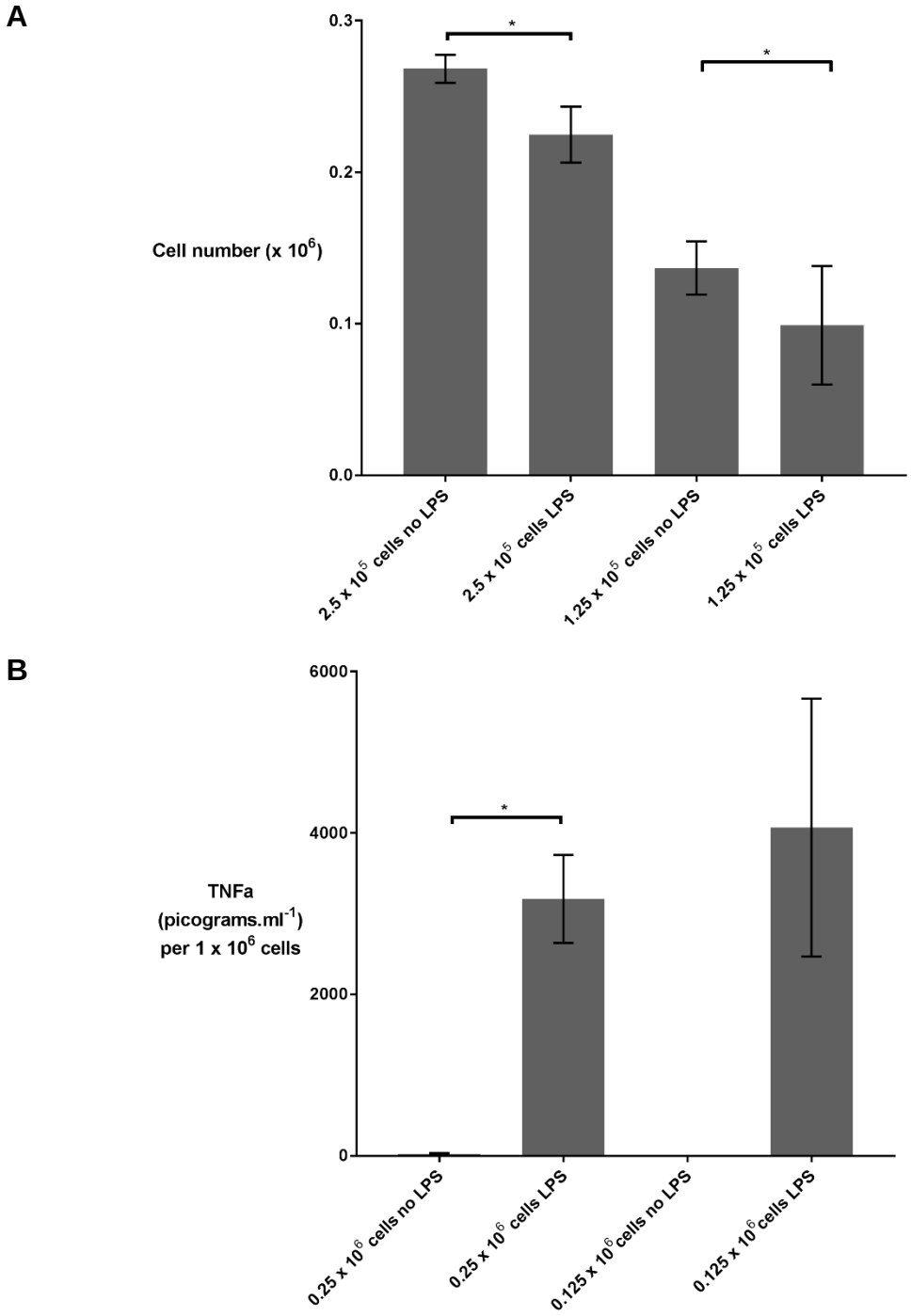

Figure 7-6 Effect of LPS on cell proliferation and TNFα secretion at two different cell seeding densities

The effects of 24 hours culture in medium containing 200 ng.ml^{-1} LPS on (A) RAW 264.7 cell number, interpolated from measured values of percentage alamarBlue® reduction, and (B) TNFα normalised to RAW 264.7 cell number. Data shown as mean +/- 95 % confidence interval, n = 6. Statistical analysis was by students t-test. * denotes groups which are significantly different ($p<0.05$).

7.4.4 Optimisation of methodology for seeding RAW 264.7 cells to segments of peripheral nerve

The efficiency of seeding RAW 264.7 cells onto decellularised nerves with and without sealing of seeding rings with 4 % (w/v) agarose was determined by interpolation of cell number from measured values of percentage alamarBlue® reduction. Tissue segments seeded in agarose-sealed rings appearing to have a higher surface cell density when histological sections were examined (Figure 7-7). The alamarBlue® measured cell populations were 0.150 (+/- 0.086) x 10^6 and 0.054 (+/- 0.046) x 10^6 ($p<0.05$) for decellularised nerve segments seeded in agarose-sealed or non-sealed rings respectively (Figure 7-8). The approximate seeding efficiencies, from an initial population of 1 x 10^6 cells, were therefore 15 % (+/- 8.6) % and 5.4 (+/- 4.6) % for agarose-sealed and non-sealed rings respectively.

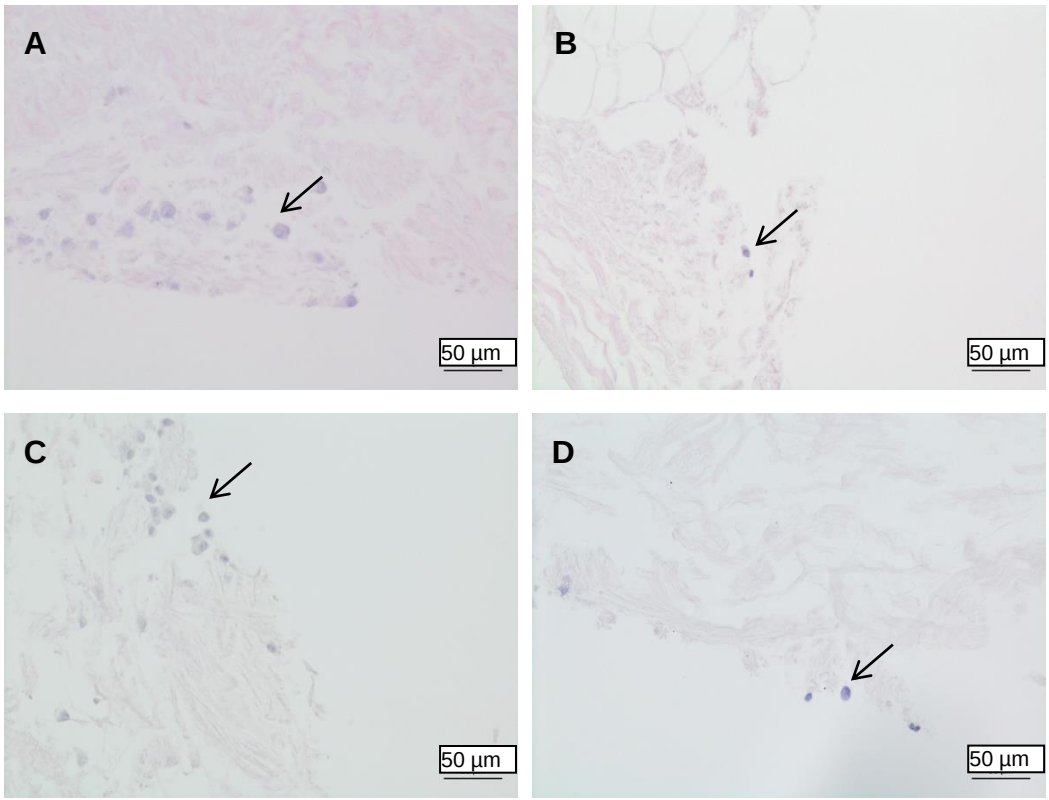

Figure 7-7 Representative images of sections stained with H & E

Images show decellularised nerves seeded with 1 x 10^6 RAW 264.7 cells in rings either (A and C) sealed with 4 % (w/v) agarose or (B and D) not sealed. Arrows indicate position of cells. Cell density appears to be greater on tissue segments from agarose-sealed rings. Images were acquired under Brightfield illumination using a x10 objective, scale bars = 50 µm.

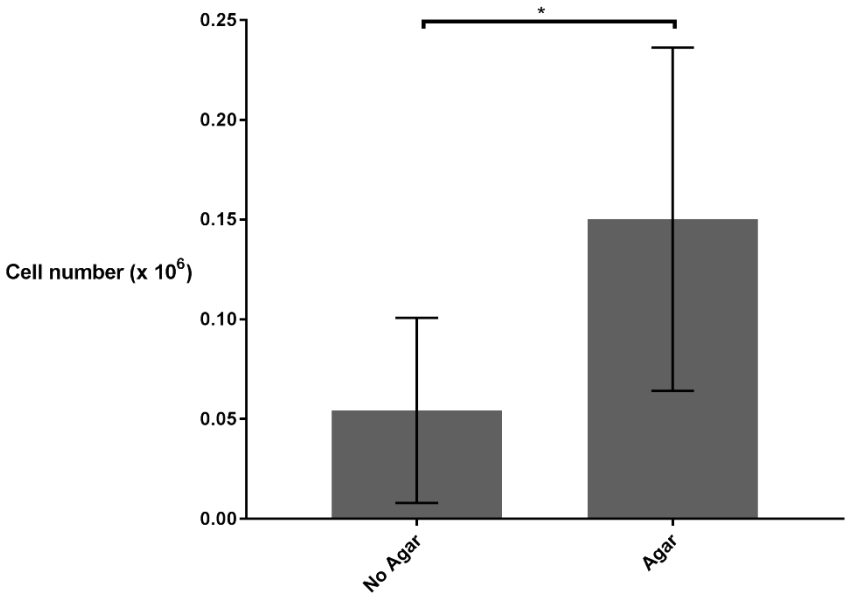

Figure 7-8 Seeding efficiencies with and without agar sealing of seeding rings

Number of cells on decellularised nerve segments seeded with 1 x 10^6 RAW 264.7 cells in 200 µl of medium in stainless steel seeding rings, either sealed with 4 % (v/v) agar or left unsealed. Cell number was interpolated from measured values of percentage alamarBlue® reduction. Data shown as mean +/- 95 % confidence interval, n = 6. Statistical analysis was by students T-test. * denotes groups which are significantly different ($p<0.05$).

7.4.5 Viability and cytokine expression in RAW 264.7 cells seeded onto segments of sterilised nerve

RAW 264.7 cells were seeded onto segments of decellularised nerve sterilised with PAA, gamma radiation, E Beam or $SCCO_2$. Non-sterilised decellularised nerves seeded with RAW 264.7 cells and incubated in medium containing 200 $ng.ml^{-1}$ LPS were used as a positive control. The effects on cell proliferation were determined by interpolation of cell number from measured values for percentage alamarBlue® reduction. The effects of sterilisation on the secretion of TNFα, IL-10, IL-1β and IL-6 were determined by ELISA quantification.

7.4.5.1 Changes in cell population

The number of cells on the seeded nerve segments appeared to increase between 0 – 24 hours on seeded PAA, gamma and $SCCO_2$-treated nerves, before plateauing or decreasing slightly between 24 – 48 hours (Figure 7-9 Changes in cell population on sterilised nerve segments over 48 hours in culture. Initial cell populations on E Beam-treated nerves and those stimulated with LPS were much lower than the other groups, at 0.04 – 0.05 x 10^6 cells compared to 0.08 – 0.15 x 10^6 cells. This difference was statistically significant ($p < 0.05$) and persisted throughout the course of the experiment. Cell populations in the E Beam and LPS treatment groups remained relatively static for the initial 24 hour period, before rising towards 48 hours.

7.4.5.2 Cytokine expression patterns

The specific sterilisation treatment applied to decellularised nerve segments prior to seeding appeared to have some influence on the pattern of TNFα, IL-1β, IL-6 and IL-10 secretion by RAW 264.7 cells (Figure 7-10 – 7-13). However, due to the wide variability within each group no statistical significance was detected by two-way ANOVA analysis. The exception was the LPS positive control, in which levels of secreted TNFα were higher ($p < 0.05$) than in all other groups at all timepoints from 6 hours onwards.

Despite the lack of statistical significance, some broad trends could be observed within the data. Both gamma irradiated and E Beam-treated nerves appeared to induce a spike in TNFα secretion at the 12 hour timepoint which was not observed in wells containing nerves treated with PAA or $SCCO_2$. All

sterilisation methods appeared to induce an increase in TNFα secretion up until the endpoint of the experiment at 48 hours.

E Beam appeared to induce higher expression levels of all cytokine at some or all of the timepoints, relative to all of the other sterilisation groups, with significant differences observed in IL-1β expression at the 24 hour timepoint ($p < 0.05$). However, the margin of difference was relatively small and, due to the wide intra-group variability, no other significant differences were identified.

In contrast to the steady increase in TNFα secretion over time from cells cultured on sterilised nerves was very different from that of cells cultured in the presence of LPS. TNFα secretion increased steeply to the 6 hour timepoint in response to LPS treatment, peaked at 24 hours and then decreased by approximately 50 % by the final 48 hour timepoint. LPS stimulation caused a steady rise in the secretion of IL-1β and IL-6 throughout the measured timepoints, with higher expression levels relative to the sterilisation treatment groups ($p<0.05$). An initial spike in IL-10 secretion ($p<0.05$) was seen after 6 hours of LPS stimulation, relative to the sterilisation treatment groups. No differences in IL-10 secretion were seen at later timepoints.

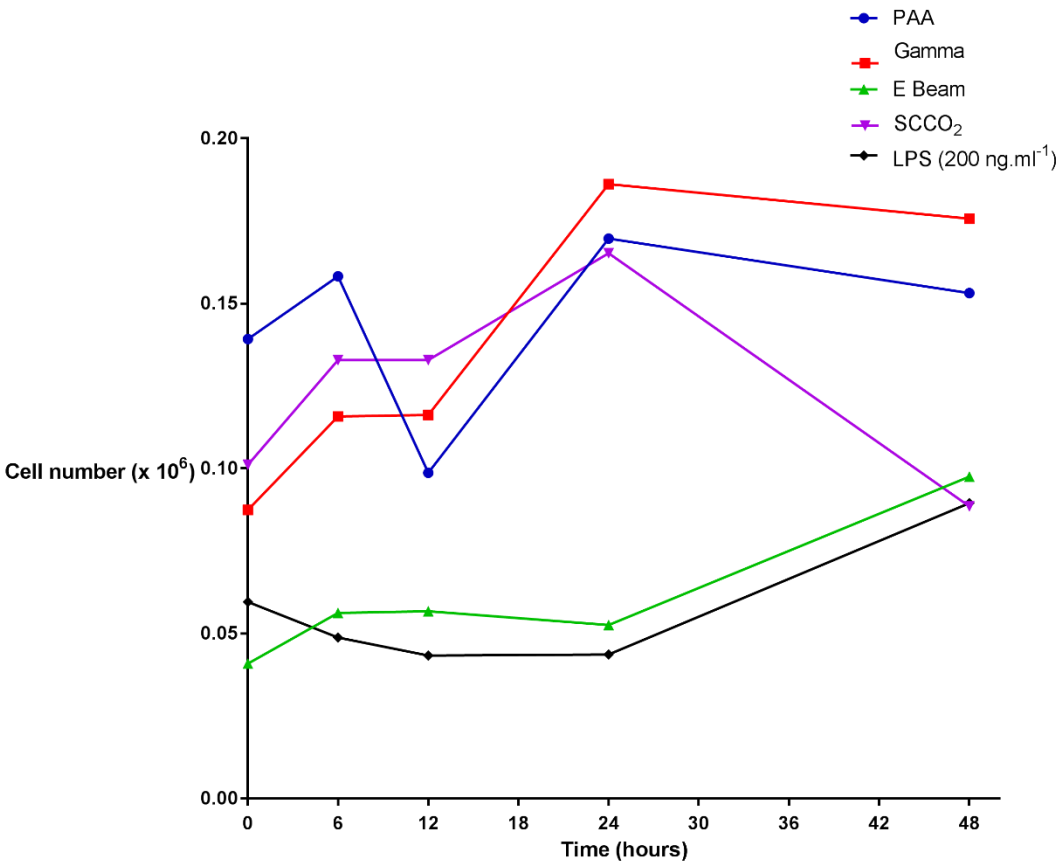

Figure 7-9 Changes in cell population on sterilised nerve segments over 48 hours in culture

Change in RAW 264.7 cell number over 48 hours after seeding onto decellularised nerve sterilised with PAA, gamma radiation, E Beam or $SCCO_2$. RAW 264.7 cells seeded onto segments of unsterilised decellularised nerve and cultured in media containing 200 $ng.ml^{-1}$ LPS were included as a positive control. At each timepoint, cell number was interpolated from measured values of percentage alamarBlue® reduction. Data shown as means, n = 6 for each timepoint. Statistical analysis was by two-way ANOVA ($p<0.05$).

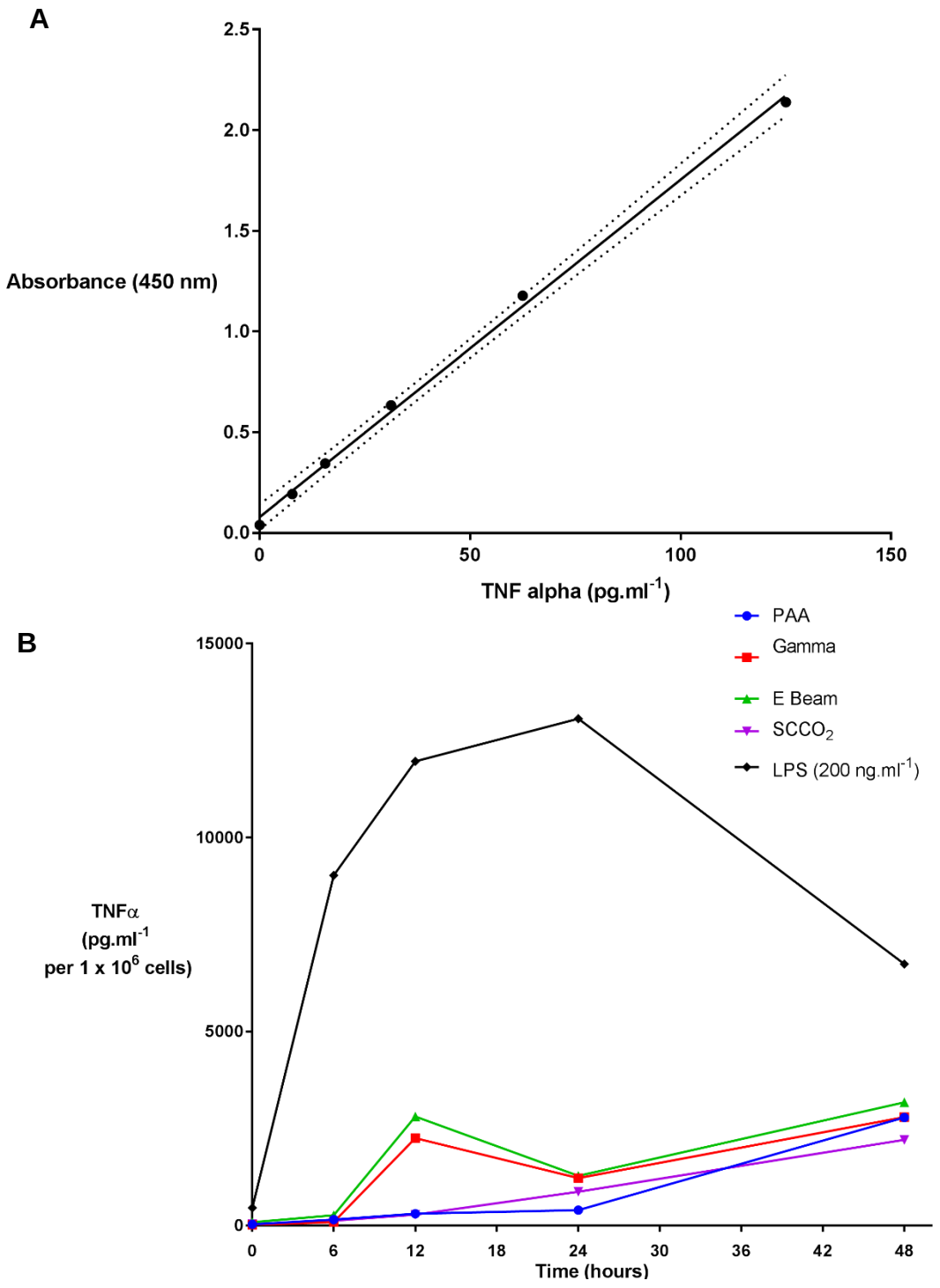

Figure 7-10 Changes in TNFα concentration over 48 hours in culture

(A) Standard curve of TNFα concentration against absorbance at 450 nm and (B) changes in TNFα secretion by RAW 264.7 cells seeded onto decellularised nerve sterilised with PAA, gamma radiation, E Beam or $SCCO_2$. Cytokine levels were measured 0, 6, 12, 24 and 48 hours, and normalised to cell number. RAW 264.7 cells seeded onto segments of unsterilised decellularised nerve and cultured in medium containing 200 $ng.ml^{-1}$ LPS were included as a positive control. Data shown as means, n = 6 for each timepoint. Statistical analysis was by two-way ANOVA ($p<0.05$).

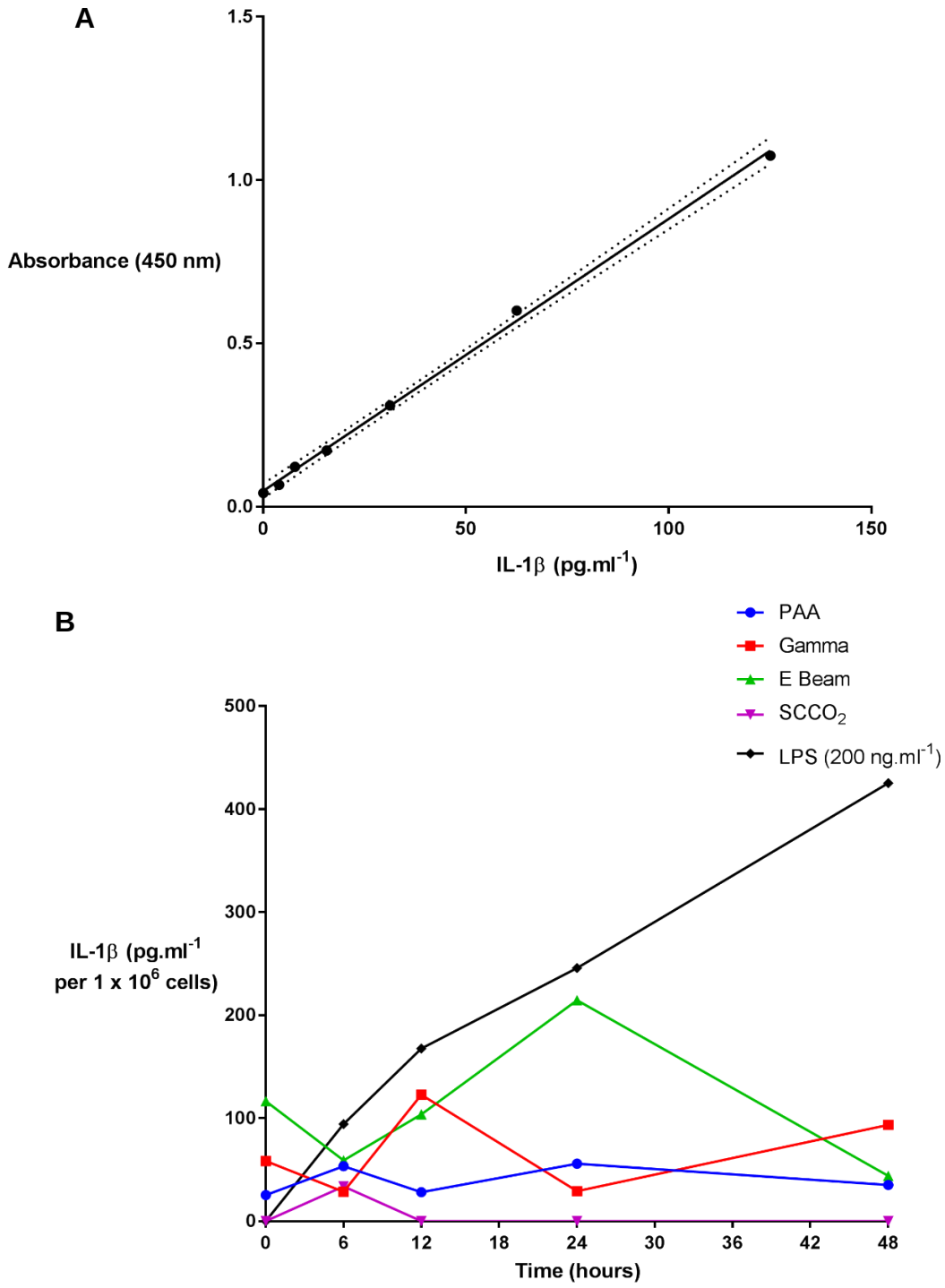

Figure 7-11 Changes in IL-1β concentration over 48 hours in culture

(A) Standard curve of IL-1β concentration against absorbance at 450 nm and (B) changes in IL-1β secretion by RAW 264.7 cells seeded onto decellularised nerve sterilised with PAA, gamma radiation, E Beam or $SCCO_2$. Cytokine levels were measured at timepoints of 0, 6, 12, 24 and 48 hours, and normalised to cell number. RAW 264.7 cells seeded onto segments of unsterilised decellularised nerve and cultured in medium containing 200 $ng.ml^{-1}$ LPS were included as a positive control. Data shown as means, n = 6 for each timepoint. Statistical analysis was by two-way ANOVA ($p<0.05$).

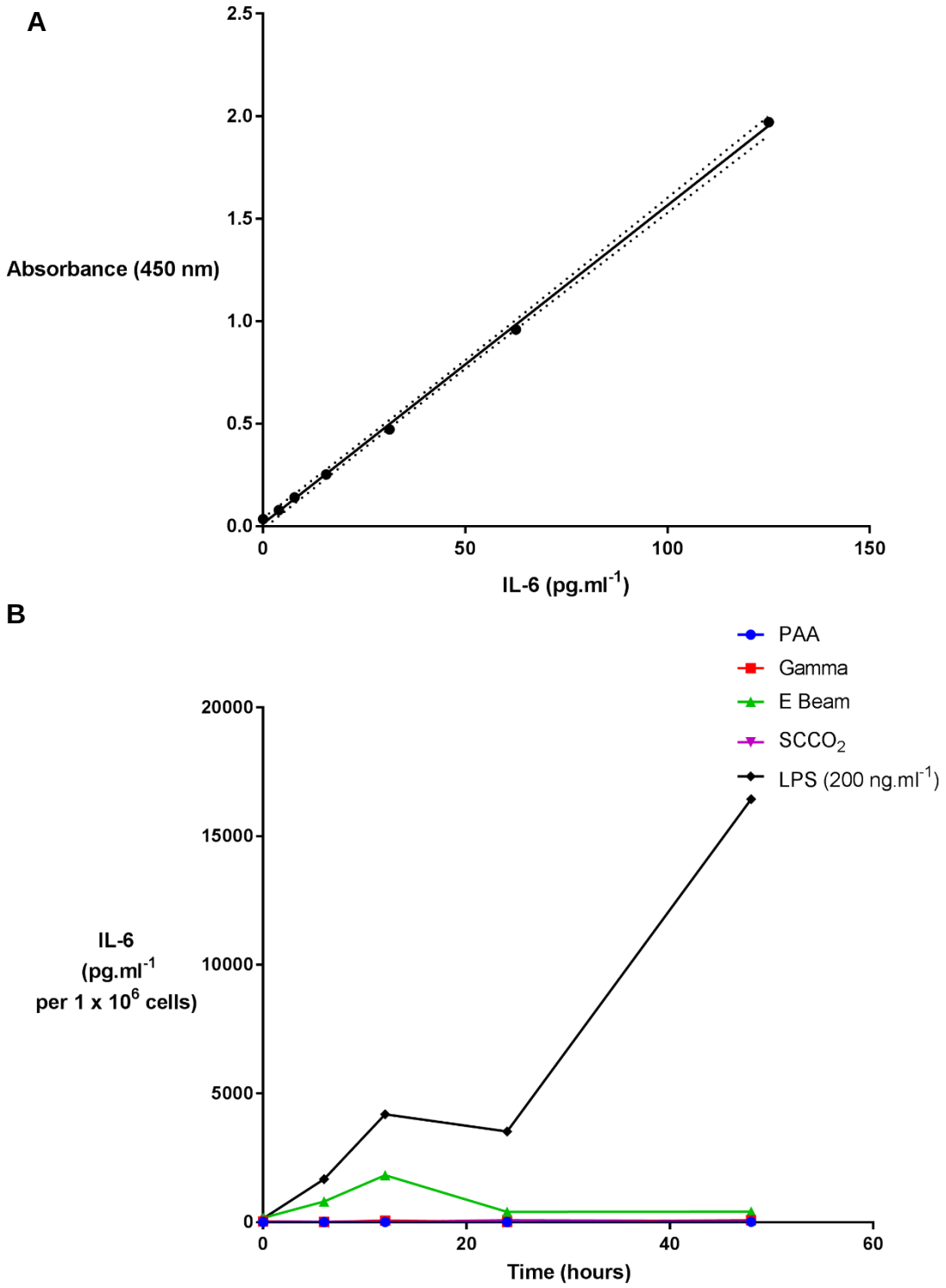

Figure 7-12 Changes in IL-6 concentration over 48 hours in culture

(A) Standard curve of IL-6 concentration against absorbance at 450 nm and (B) changes in IL-6 secretion by RAW 264.7 cells seeded onto decellularised nerve sterilised with PAA, gamma radiation, E Beam or $SCCO_2$. Cytokine levels were measured at timepoints of 0, 6, 12, 24 and 48 hours, and normalised to cell number. RAW 264.7 cells seeded onto segments of unsterilised decellularised nerve and cultured in medium containing 200 $ng.ml^{-1}$ LPS were included as a positive control. Data shown as means, n = 6 for each timepoint. Statistical analysis was by two-way ANOVA ($p<0.05$).

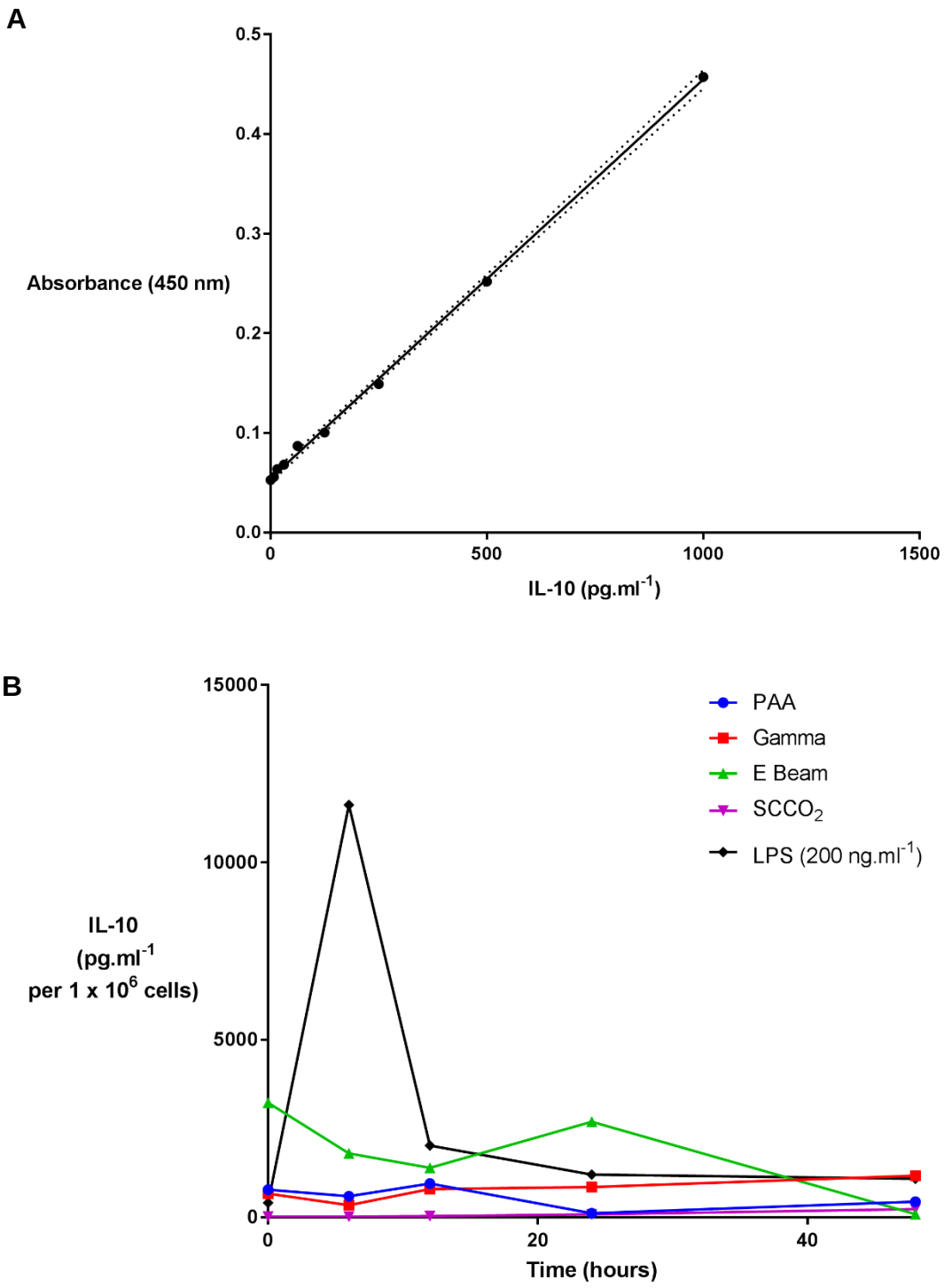

Figure 7-13 Changes in IL-10 concentration over 48 hours in culture

(A) Standard curve of IL-10 concentration against absorbance at 450 nm and (B) changes in IL-10 secretion by RAW 264.7 cells seeded onto decellularised nerve sterilised with PAA, gamma radiation, E Beam or $SCCO_2$. Cytokine levels were measured at timepoints of 0, 6, 12, 24 and 48 hours, and normalised to cell number. RAW 264.7 cells seeded onto segments of unsterilised decellularised nerve and cultured in medium containing 200 $ng.ml^{-1}$ LPS were included as a positive control. Data shown as means, n = 6 for each timepoint. Statistical analysis was by two-way ANOVA ($p<0.05$).

7.5 Discussion

Sterilisation did not appear to negatively affect the cytocompatibility of decellularised nerves. No evidence of a strong pro-inflammatory response (in comparison to that elicited by incubation in media containing LPS) was seen when a murine macrophage cell line was seeded onto segments of sterilised nerve.

Decellularised nerves treated with either PAA, gamma radiation, E Beam or $SCCO_2$ did not appear to negatively impact the growth or morphology of L929 fibroblasts and BHK epithelial cells. These two distinct cell types were selected in line with the protocol used being based on that stipulated in ISO standard 10993-5 (2009); variants on this type of cytotoxicity testing are often applied to medical devices as a basic first test of biocompatibility [299, 301, 326, 406]. These findings correlate with those of previous studies investigating sterilised allogeneic or xenogeneic tissue grafts. Cytocompatibility was retained when porcine superflexor tendons were decellularised using a variant of the patented Leeds protocol and sterilised with PAA, gamma radiation or E Beam [336]. *In vitro* culture studies did not reveal evidence of cytotoxicity in powdered allogeneic bone or allogeneic amniotic membrane sterilised with $SCCO_2$ [428, 429]. Furthermore, $SCCO_2$ sterilisation did not prevent a decellularised lung matrix from supporting seeded populations of A549 human epithelial-like cells and rat microvascular lung endothelial cells *in vitro* [243]. The observed cytocompatibility can be considered a positive prognostic indicator for the ability of the sterilised nerves to support a viable cell population post-implantation [406].

The likely innate immune response to the sterilised nerves was characterised *in vitro* through seeding of the murine macrophage cell line RAW 264.7 onto sterilised nerve segments and quantification of subsequent cytokine secretion. The experiment was designed as an *in vitro* screen, with the aim of identifying if treatment of the decellularised nerves with any of the sterilisation methods caused the induction of a strong pro-inflammatory response (i.e. seeded cells polarised towards an M1-like phenotype, as would be stimulated by exposure to a potent stimulant such as LPS).

A sustained M1 phenotypic response, characterised by the secretion of pro-inflammatory cytokines including TNFα, IL-1β, IL-6 and IL-12, is associated with an inferior prognosis for graft integration due to impaired cell infiltration, reduced ECM remodelling and the formation of a fibrotic tissue capsule surrounding the implanted graft [134]. Stimulation of RAW 264.7 cells with the Gram negative bacterial cell membrane component LPS appeared to induce such a phenotypic response, with the secretion of high levels of TNFα, peaking at 24 hours, and gradually increasing levels of IL-1β and IL-6 over the full experimental duration of 48 hours.

Nerve segments from the sterilisation treatment groups did not appear to induce high levels of pro-inflammatory cytokine secretion, compared with those seen when seeded nerve segements were incubated incubated with media containing LPS. There was some difference in response according to the type of method used, with an initial rise in TNFα secretion apparent from cells cultured on tissue segments treated with ionising radiations (gamma radiation and E Beam) but not segments treated with sterilisation methods utilising oxidising agents (PAA, $SCCO_2$ with PAA and H_2O_2). However, this trend was not statistically significant and levels of TNFα secretion in all groups appeared to converge at later timepoints. Therefore, the findings presented here do not provide evidence that sterilisation with ionising radiation increases the probability of a sustained pro-inflammatory response (and therefore inferior integration) post-implantation. However, the results presented here should be considered with the caveat that they do not fully preclude the potential induction of some degree of pro-inflammatory response upon implantation *in vivo*, and similarly do not prove that such a response would not be clinically significant and have consequent implications for successful graft integration (and therefore eventual functional restoration). This is due to the relative potency of LPS as a stimulator of the pro-inflammatory response in cellular components of the innate immune system (or cell lines derived from such components, e.g. the macrophage-like RAW 264.7 cell line used in the present study) [430]. LPS was chosen as a positive control in this study due to its proven ability to stimulate a pro-inflammatory response, and due to the relative lack of an appropriate alternative: for example, synthetic alternatives (such as collagen-based biogels) were considered unlikely to definitively elicit a pro-inflammatory response [431].

Limited evidence is available in the literature regarding the interaction of macrophages with sterilised (either decellularised or unprocessed) tissue grafts *in vitro* and the potential implications for the *in vivo* host response. When radiation sterilisation of tissue grafts is carried out under hydrated conditions, as in the present study, hydroxyl radicals are generated [1]. These radicals may interact with ECM components and induce the formation of novel inter and intra-molecular crosslinks [1, 368]. A 2010 study assessed the effects of crosslinked decellularised porcine dermal grafts on the secretion of the pro-inflammatory cytokines IL-1β, IL-6 and IL-8 by human peripheral blood monocytes [432]. Two chemically-crosslinked grafts, Permacol™ (decellualirsed porcine dermis sterilised with gamma radiation) and CollaMend™ (decellularised porcine dermis sterilised with ethylene oxide), induced several fold greater levels of cytokine secretion compared to both the non-crosslinked Strattice™ (decellularised porcine dermis sterilised with low-dose E Beam) and cells stimulated with an LPS positive control at a concentration of 100 $ng.ml^{-1}$. The crosslinking of the grafts, which was mediated through treatment with 1-ethyl-3-(3-dimethylaminopropyl) carbodiimide hydrochloride (EDC) and hexamethylene di-isocyanate (HMDI) for CollaMend™ and Permacol™ respectively (rather than terminal sterilisation processes used), was carried out to improve the mechanical properties of the grafts and ensure the retention of ECM structure following implantation [433]. A similar pro-inflammatory macrophage response to crosslinked decellularised grafts has been observed *in vivo.* A carbodiimide-crosslinked decellularised porcine SIS graft (CuffPatch™) induced a M1-style macrophage response following implantation into a rat, characterised by a heavy infiltration of macrophages positive for the M1-associated surface markers CD80+ and CCR7+, chronic inflammation up to the final 16 week timepoint and limited evidence of ECM remodelling or integration with the surrounding tissue [421]. In contrast, the analogous non-crosslinked Restore™ graft appeared to induce infiltrating macrophages to polarise towards a CD163-positive M2 phenotype with evidence of cell infiltration, ECM remodelling and graft integration. There is a possiblity that residual chemical crosslinking agents and/or cellular debris may have been present in the grafts, and if so may have influenced cellular interactions with the tissue. Notwithstanding this potential study limitation, ECM-crosslinking mediated through chemical agents appeared

to induce polarisation of macrophages towards a pro-inflammatory M1 phenotype; it is conceivable that radiation-mediated ECM crosslinking could induce a similar response.

In the present study, TNFα secretion after 48 hours appeared consistently elevated across all groups compared to the initial values (measurements taken at 0 hour timepoint). Despite the differences in the profile and magnitude of TNFα secretion between the test groups and the LPS positive control, and the fact that the rise in TNFα secretion at 48 hours was a pattern seen in all sterilisation treatment groups, this may nonetheless have indicated some degree of polarisation towards an M1 phenotype, with the reduced magnitude of cytokine secretion compared with LPS being due to differences in the relative potency of the stimuli. A similar pattern was seen for the cytokines IL-1β and (to a lesser extent) IL-6, with the exception of E Beam-treated nerve which induced a significant rise in IL-1β secretion peaking at the 24 hour timepoint. However, considering that the observed increases were relatively transient compared to the LPS control, it may be that the available evidence is indicative of a lower likelihood of severe chronic adverse macrophage response *in vivo* (at least in the context of the magnitude of response which would be expected upon exposure of the same cell type to pathogenic material, e.g. LPS). However, limited inference can be drawn from these data towards the wider immune response.

Emerging evidence from attempts to modulate the polarisation of macrophages in tissue engineering applications suggests that the initial secretion of pro-inflammatory cytokines and polarisation of the macrophage population towards an M1 phenotype may play a beneficial role following implantation of a graft material, enabling further recruitment of macrophages from circulation, debris clearance through phagocytosis and stimulating angiogenesis [434]. A transient increase in the secretion of cytokines such as TNFα following graft implantation could therefore favour the induction of such processes. A later transition of the macrophage population towards a predominantly M2 phenotype enables optimal ECM remodelling and integration of the graft.

In addition to the possible induction of a strong and sustained pro-inflammatory response leading to graft rejection, the role of macrophages should also be

considered in the context of tissue-specific injury response processes. In peripheral nerve, the resident population of macrophages adopt some phenotypic characteristics of the M1 classification in the period immediately following injury, acting synergistically with Schwann cells to mediate the clearance of cell debris by phagocytosis in a process which is stimulated by factors including TNFα, IL-1β and IL-6 [32, 435]. Signalling from Schwann cells and resident macrophage stimulates the recruitment and activation of macrophages from circulation to the site of injury [436]. This occurs around two – seven days after injury, and is mediated through the secretion of a range of factors including chemokines such as monocyte chemoattractant protein-1 and cytokines such as TNFα, IL-1β and IL-6. TNFα secreted by macrophages stimulates the maintenance of a dedifferentiated phenotype in Schwann cells, in addition to inhibiting their proliferation, during the initial phases of Wallerian degeneration [437].

As Wallerian degeneration progresses from the myelin clearance phase towards axonal regeneration, signalling from Schwann cells induces the macrophage population to adopt a primarily M2 phenotype (mediated through an as yet unidentified ligand, though gene knockout studies suggest the expression of the responsible ligand(s) may be associated with a pathway requiring the c-Jun transcription factor component) [438]. Macrophages are thought to have a key regulatory role in the ongoing process of neuroregeneration, though the extent of, and mechanisms responsible for, this modulatory capacity have not been fully elucidated [439]. Macrophage-secreted cytokines such as TNFα upregulate Schwann cell production of enzymes such as matrix metalloprotease-1 (MMP-1) mediating ECM remodelling and, together with the later secretion of ECM components including laminin and fibronectin sub-units, the formation of novel endoneurial basement membrane [106]. Macrophages are also thought to stimulate axonal growth through the release of neurotrophic factors including IL-6, IGF-1 and PDGF [111, 439].

The recruitment and activation of a large macrophage population from the circulation following peripheral nerve injury, and the growing body of evidence attributing cytokine signalling from these cells to the regulation of debris clearance and neuroregeneration, means that any changes in cytokine secretion patterns as a result of interaction with an implanted scaffold have the

potential to modulate the regenerative process. The initial rise in TNFα and IL-1β implied in some groups within the present study is relatively transient compared to the sustained secretion of such cytokines by the Schwann cells and macrophages which would already be present in the injury site prior to implantation. Furthermore, a small and transient increase in the secretion of cytokines such as TNFα, IL-1β or IL-6 into such a microenvironment would be unlikely to impede neuroregeneration given the implicated roles of these cytokines in the modulation of Schwann cell phenotype, macrophage recruitment, phagocytosis of debris, ECM remodelling and axonal outgrowth.

RAW 264.7 cells were chosen for use in this study due to their well-characterised properties as an adherent macrophage cell line with consistent phenotypic responses (demonstrated up to 50 passages) and rapid growth capabilities [440]. RAW 264.7 cells have been used for the *in vitro* assessment of a diverse range of biomaterials; examples include magnesium-doped titanium implant surfaces for orthopaedic applications, polyethylene glycol-based hydrogels and polydimethylsiloxane implants encapsulated in a collagen and hyaluronic acid film [441-443]. A further aspect of the rationale for conducting an *in vitro* screen of macrophage response using a cell line was to eliminate potentially unnecessary use of animals in accordance with the principles of the 3R's. Flow cytometric characterisation has revealed the composition of the murine peritoneal cell population to be approximately 50 – 60 % B cells, 30 % macrophages and 5 – 10 % T cells, with an expected total yield of 5 – 10 million cells [444]. Given that a total of 150 x 10^6 cells were required for the main experiment (in addition to those required for optimisation), the acquisition of the required primary murine macrophages via peritoneal lavage would have required the sacrifice of approximately 50 – 100 mice (10 – 20 per group).

The initial seeded cell population on the nerve segments varied widely, both between groups and between individual samples within groups. An experimental limitation which may have contributed to the variance in initial cell population is the requirement for individual groups to be seeded on separate days. The time required to passage and count cell populations from several T175 flasks, seed 30 individual samples of decellularised nerve, transfer the samples to the final culture plates and conduct the 0 hour data collection was a limiting factor preventing simultaneous seeding. The cells in each group were

therefore sourced from separate populations (i.e. passaged on separate days, cultured in separate flasks with different batches of media etc). The inconsistent efficiency of the seeding methodology used in the present study, together with differences in the size and surface topography of the tissue segments, may also have contributed to the inter and intra-group variability in seeded cell population. Some inter-group inconsistency in terms of initial macrophage population has been seen in RAW 264.7 cells seeded onto a range of polymeric fibres and in primary murine peritoneal macrophages seeded onto alkyl-aminated polymeric hydrogels [445, 446].

A further explanation for the variation in initial cell population may be the relative availability of ECM motifs. Decellularised nerves sterilised with PAA, gamma radiation and $SCCO_2$ were found to have an greater susceptibility to collagenase compared to E Beam-treated nerves. If a higher susceptibility to collagenase digestion is reflective of an ECM structure with a more specific enzymatic cleavage sites exposed, it is likely that a greater proportion of cell attachment motifs would also be exposed. This would account for the greater seeding efficiency seen, especially in PAA and $SCCO_2$-treated nerves. A similar pattern was seen in a study of two different decellularised human dermal matrices, FlexHD® Pliable and BellaDerm® [426]. The susceptibility of BellaDerm® to digestion with collagenase was approximately 25 % lower than that of FlexHD® Pliable. This corresponded to increased levels of cell attachment on FlexHD® Pliable compared to BellaDerm® after seeding with human dermal fibroblasts, especially in in the initial 48 hour period, and a more even pattern of cell attachment across both the dermal and epidermal faces of the graft. This finding may have implications for cell attachment and infiltration into the decellularised nerves in the present study, with the caveat that the *in vitro* cell surface seeding with a macrophage cell line is not representative of cell infiltration in an *in vivo* environment post-implantation. The growth and attachment of key cell types into the decellularised nerves, such as Schwann cells and neurons is likely to be influenced by other factors such as the retention of endoneurial tubule structure and key basement membrane components (e.g. fibronectin, laminin).

The biocompatibility and immunoreactivity of the decellularised nerves did not appear to have been negatively impacted by any of the sterilisation methods,

within the context and inherent limitations of the experimental designs utilised. Ultimately, *in vivo* implantation of the sterilised decellularised nerves within an animal model (e.g. rat sciatic defect model) would be required to more definitively define the likely host immune response; such an experiment would enable a fuller characterisation of the complex integrated immune response to which the sterilised nerves would be exposed, and as such would enable fuller consideration of the likely effects of tissue integration and the resulting implications for the support of site-specific cell growth and eventual functional restoration. Based on these results, greater emphasis during this initital study should be placed upon other factors, such as retention of basement membrane components and mechanical properties, when considering the optimal sterilisation method for use with the decellularised nerves.

8 Effects of long-term storage on the properties of decellularised nerves sterilised with PAA, gamma radiation or E Beam

8.1 Introduction

The required shelf life of a decellularised tissue graft (i.e. from the end of the decellularisation process to implantation) is unpredictable. The ability to maintain stability of the functional properties of a graft, including structure and composition of the ECM, biocompatibility and mechanical properties, over a long-term period of storage is therefore advantageous. The ability to store decellularised tissue grafts in ambient conditions (i.e. without the requirement for highly-controlled storage conditions such as refrigeration or cryopreservation) is also desirable, reducing costs associated with transportation and storage and decreasing the risk of graft degradation in the event that such conditions are not achieved.

There is limited evidence in the literature regarding the effects of storage on the properties of decellularised tissue grafts. Physical and chemical treatments mediating the decellularisation of tissues are known to disrupt ECM structure, both in terms of the whole tissue histoarchitecture and at the level of inter- and intramolecular bonds and interactions [17, 309, 447, 448]. It is conceivable that such alterations may decrease the stability of the ECM and therefore increase the likelihood of further degradation over time whilst in storage. A 2012 study demonstrated negative changes to the histoarchitecture, a reduction in collagen fibril integrity, an approximate 50 % increase in susceptibility to collagenase digestion and an approximate 50 % reduction in the Young's Modulus and tensile strength of decellularised human tracheas after 12 months of storage [449].

A further factor which may influence the preservation of decellularised tissue grafts over a long-term storage period is sterilisation. The elimination of microorganisms is essential to reduce the risk of infection post-implantation, and prevents ECM degradation by bacterial collagenase enzymes [450]. However, aside from a few focussed studies (e.g. examining the effects of storage on the viscoelastic properties of decellularised tendons sterilised with

PAA, gamma radiation or E Beam), there are very limited data regarding the effects of storage on sterilised decellularised tissues [451]. Treatment with ionising radiation or oxidising agents may induce changes to the structure of ECM components at a molecular level, through mechanisms such as cross-linking, chain scission and oxidative damage [1, 242]. For example mass spectrometric analysis of decellularised murine lungs treated with PAA demonstrated a higher proportion of solubilised ECM components compared with non-sterilised decellularised tissue; this was likely due to partial denaturation as a result of oxidative damage [242]. Such alterations could make ECM components more susceptible to further degradation over time, with potential implications for graft integration and the ability to support functional restoration.

Assessment of the effects of long-term storage on sterilised decellularised peripheral nerves is crucial due to the potential induction of efficacy-altering changes with increasing age of the tissue. Good retention of key functional properties during the storage period would be advantageous when considering use in the clinical environment.

8.2 Aims and Objectives

Aim

The aim of this chapter was to determine the effects of 12 months storage at room temperature on the biological and biomechanical properties and biochemical composition of decellularised nerves sterilised with PAA, gamma radiation or E Beam.

Objectives

i. To treat decellularised peripheral nerves with PAA solution, gamma radiation, E Beam and store for 12 months.
ii. To determine effect of storage on the biocompatibility of the aged sterilised nerves.
iii. To determine the effects of storage on sterilised peripheral nerve ECM structure through staining of histological sections with H & E and Sirius Red & Miller's.
iv. To determine the effects of storage on the distribution of collagen type IV, laminin and fibronectin within the ECM of sterilised nerves through antibody labelling.
v. To determine the effects of storage on the mechanical properties of sterilised nerves through uniaxial tensile testing.
vi. To determine the effects of storage on the biochemical composition of sterilised nerves, through quantification of collagen and denatured collagen.

8.3 Materials and Methods

All results were compared to the previously acquired dataset for freshly produced sterilised nerves (meaning that data acquisition experiments were conducted separately for the 0 month and 12 month storage groups).

8.3.1 Sterilisation and storage of decellularised nerves

Three groups of porcine peripheral nerves (n = 30) were dissected and decellularised as described in sections 2.9 and 2.10. One group each was sterilised by treatment with 0.1 % (v/v) PAA, gamma radiation and E Beam, as described in section 2.10.3.

The sterilised nerves were stored in bijous containing 5 ml PBS, further sealed with parafilm, at room temperature (15 – 25 °C) for a period of 12 months. Long-term storage of decellularised nerves treated with $SCCO_2$ was not possible during the study period due to time constraints.

8.3.2 Contact cytotoxicity

The cytotoxicity of the aged nerves (n = 6 per group) was assessed by contact culture with two distinct cell lines, as described in section 2.12.

8.3.3 Histological analysis

Processing and sectioning of tissue was carried out as described in section 2.11. Staining of sections (n = 3 per group) with H & E and Sirius Red was carried out as described in section 2.11.

8.3.4 Antibody labelling for collagen IV, laminin and fibronectin

Processing and sectioning of tissue was carried out as described in section 2.11. Labelling of sections with specific antibodies for collagen IV, laminin and fibronectin (n = 3 per group) was carried out as described in section 2.11.8.

8.3.5 Uniaxial tensile testing

Samples of aged sterilised nerve (n = 6 per group) were subject to uniaxial tensile testing, as described in section 2.13.

8.3.6 Quantification of collagen and denatured collagen content

The amount of collagen (n = 6 per group) and denatured collagen (n = 6 per group) in the sterilised nerves was quantified as described in sections 2.14.4 and 2.14.5.

8.4 Results

8.4.1 Contact cytotoxicity testing of aged sterilised nerves

The biocompatibility of the sterilised nerves after 12 months was assessed by contact culture studies with two distinct cell lines, L929 and BHK (Figure 8-1 and). As previously described in section 2.12.4, cyanoacrylate contact adhesive was used as a positive control and a commercially available surgical closure strip (Steri-Strip) as a negative control.

No evidence of cytotoxicity was observed in either cell line when cultured with sterilised nerves stored for 12 months. Both cell lines were observed to grow up to and in contact with the samples, maintaining a consistent morphology.

The rounded appearance characteristic of the dead cells cultured in wells with the cyanoacrylate positive control was not observed in cells cultured with nerves from any of the treatment groups (data not shown).

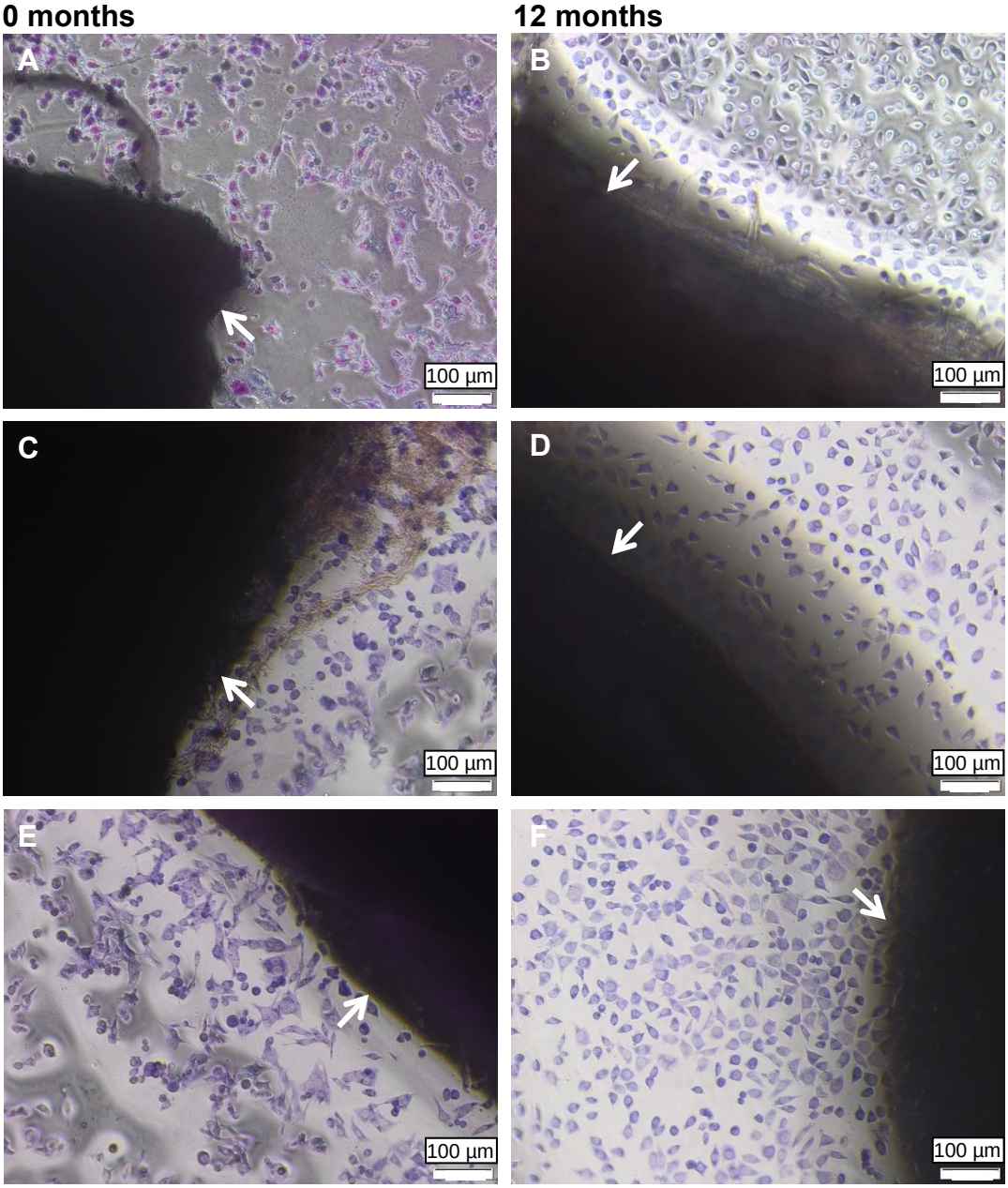

Figure 8-1 Representative images of Giemsa-stained L929 cells cultured for 48 hours with decellularised nerves

L929 cells cultured with: decellularised nerves treated with PAA and stored for (A) 0 months and (B) 12 months, treated with gamma radiation stored for (C) 0 months and (D) 12 months, and treated with E Beam stored for (E) 0 months and (F) 12 months. Cells were fixed with NBF and stained with Giemsa following 48 h in culture. Position of tissue segments indicated by arrows. Images were acquired under Köhler illumination using a x10 objective, scale bars = 100 µm.

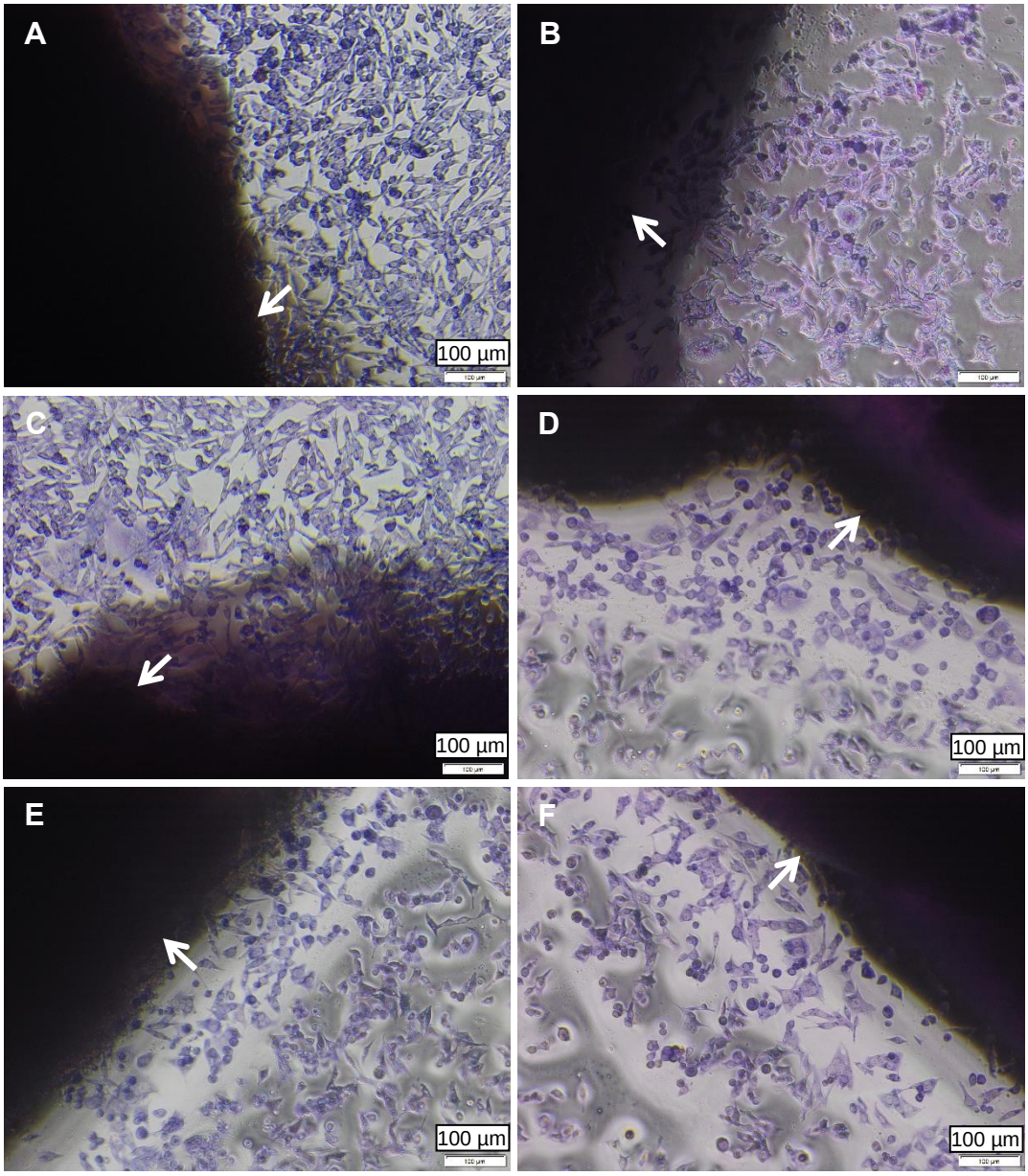

Figure 8-2 Representative images of Giemsa-stained BHK cells cultured for 48 hours with decellularised nerves

BHK cells cultured with: decellularised nerves treated with PAA and stored for (A) 0 months and (B) 12 months, treated with gamma radiation stored for (C) 0 months and (D) 12 months, and treated with E Beam stored for (E) 0 months and (F) 12 months. Cells were fixed with NBF and stained with Giemsa following 48 h in culture. Position of tissue segments indicated by arrows. Images were acquired under Köhler illumination using a x10 objective, scale bars = 100 µm.

8.4.2 Histological analysis of changes to ECM structure

H & E staining was used to enable assessment of the effects of the 12 month storage period on the histoarchitecture of the sterilised nerves (Figure 8-3). No differences were apparent between samples stored for 0 and 12 months, with structural disruption only seen in the epineurium and endoneurium of PAA-treated nerves. The extent and/or severity of this disruption did not appear to have increased during the storage period. All major ECM structures (endoneurium, perineurium and epineurium) appeared well conserved following 12 months storage of nerves treated with gamma radiation or E Beam. The eosin staining intensity appeared to be different between the two timepoints, possibly due to the stains being carried independently for each (and therefore being processed using different batches of reagent).

Sirius Red was used to define the distribution and structure of collagen in the stored sterilised nerves (Figure 8-4). Some changes to the collagen structures were observed in the epineurium of PAA-treated nerves after 12 months storage, with the fibrils appearing less closely associated and organised. No obvious differences were observed between nerves treated with gamma radiation or E Beam when stored for 0 or 12 months.

Increased spacing was observed between the perineurium and endoneurium in Figure 8-3 F. This is likely representative of an artefact introduced during sectioning.

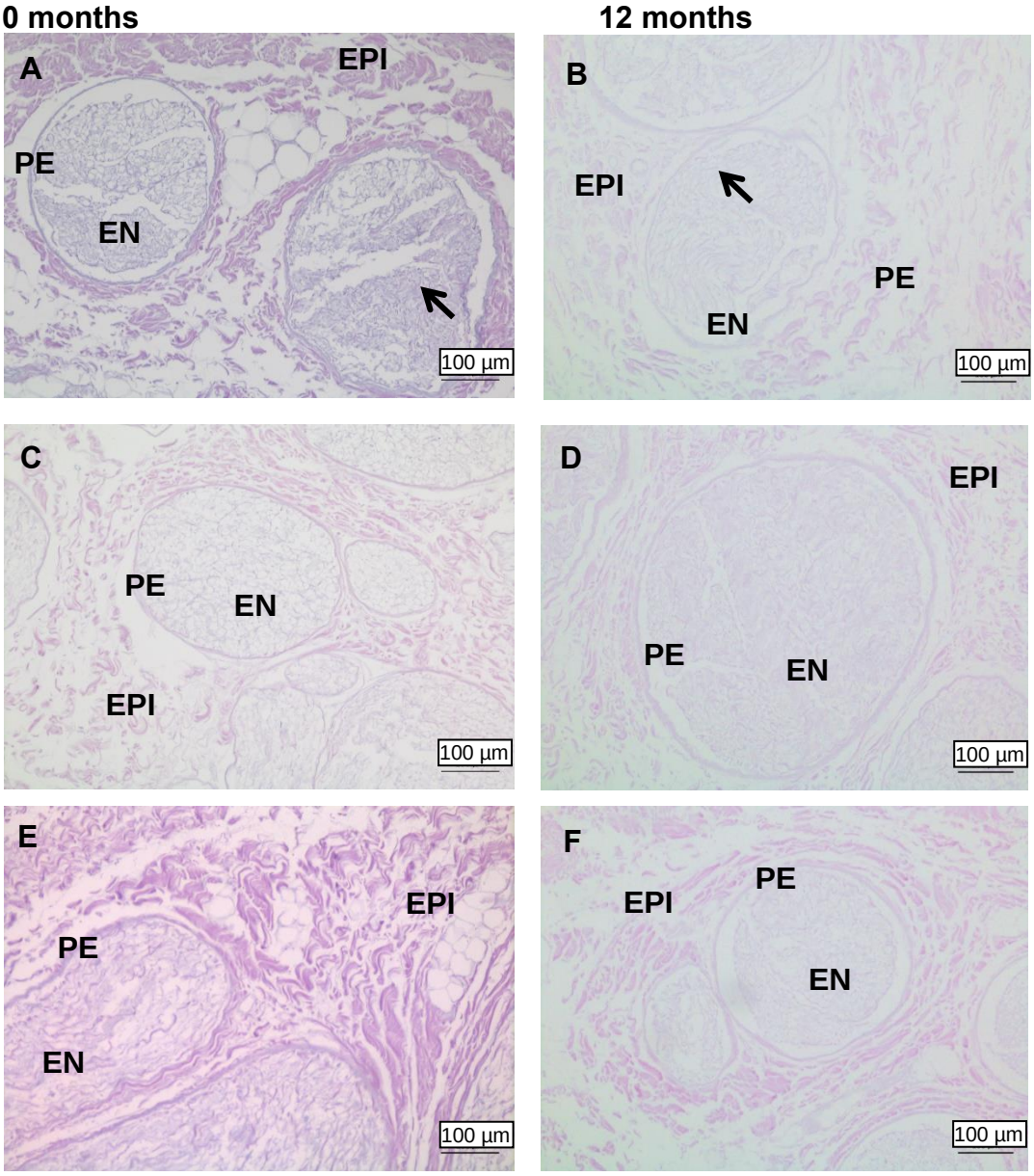

Figure 8-3 Representative images of sections stained with H & E

Decellularised nerves treated with PAA and stored for (A) 0 months and (B) 12 months, treated with gamma radiation and stored for (C) 0 months and (D) 12 months, and treated with E Beam and stored for (E) 0 months and (F) 12 months. There was some evidence of disruption to stored decellularised nerves treated PAA, predominantly located in the epineurium (EPI; indicated by arrows). The perineurium (PE) and endoneurium (EN) are also indicated. Images were acquired under Köhler illumination using a x10 objective, scale bars = 100 µm.

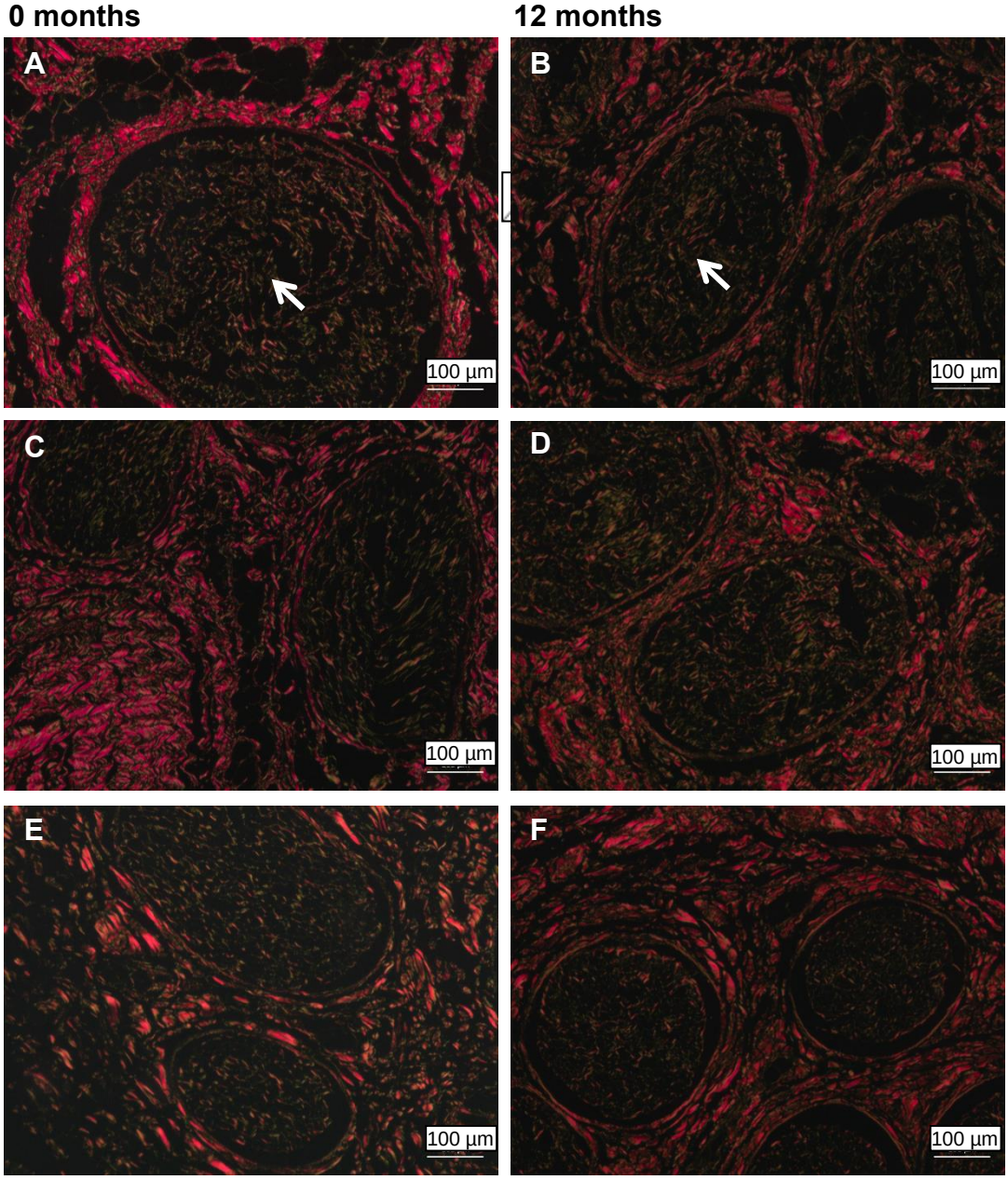

Figure 8-4 Representative images of sections stained with Sirius Red/Miller's Elastin

Decellularised nerves treated with PAA and stored for (A) 0 months and (B) 12 months, treated with gamma radiation and stored for (C) 0 months and (D) 12 months, and treated with E Beam and stored for (E) 0 months and (F) 12 months. Sections were viewed under polarised light conditions. Some evidence of structural changes was evident, particularly to the endoneurium (indicated by arrows). Images were acquired under Polarised light conditions and using a x10 objective, scale bars = 100 µm.

8.4.3 Antibody labelling for collagen IV, laminin and fibronectin

Sections of sterilised nerve from different groups were labelled with specific antibodies to demonstrate the effects of a 12 month storage period on the distribution of collagen IV, laminin and fibronectin.

There was no difference in the distribution of labelling for collagen IV in nerves sterilised with gamma radiation and E Beam after 12 months of storage (
Figure 8-5). However, there was a slight reduction in the intensity of labelling. No positive labelling for collagen IV was seen in decellularised nerves treated with PAA after either 0 or 12 months of storage..

No change to either the distribution or intensity of labelling for laminin was observed in the perineurium and endoneurium of nerves treated with gamma radiation and E Beam after 12 months of storage (Figure 8-6). However, while the distribution of labelling in PAA-treated samples appeared to be unchanged, a slight reduction in intensity was evident after 12 months of storage.

Labelling for fibronectin was almost completely absent in PAA-treated samples after 12 months of storage, and appeared to be reduced in intensity in E Beam-treated samples (Figure 8-7).

Increased spacing was observed between the perineurium and endoneurium in some images, including Figure 8-5 F, Figure 8-6 E, Figure 8-6 F, and Figure 8-7 E. This is likely representative of artefacts introduced during sectioning.

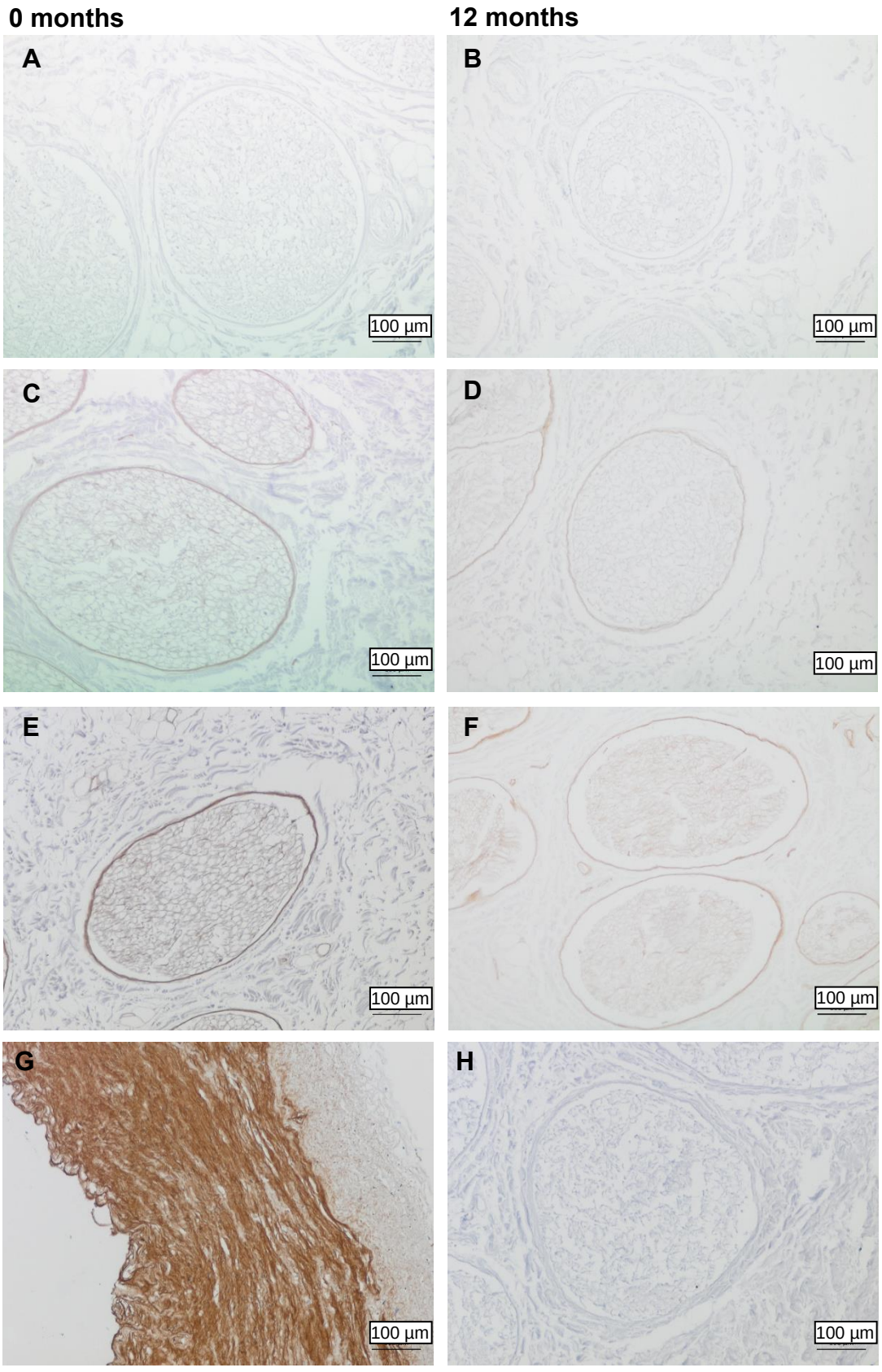
0 months
12 months
A
B
C
D
E
F
G
H
100 µm

Figure 8-5 Representative images of sections labelled with monoclonal antibodies against collagen IV (previous page)

Decellularised nerves treated with PAA and stored for (A) 0 months and (B) 12 months, treated with gamma radiation and stored for (C) 0 months and (D) 12 months, and treated with E Beam and stored for (E) 0 months and (F) 12 months. A porcine artery positive control (G) and an isotype control (H) were included. Images were acquired under Köhler illumination using a x10 objective, scale bars = 100 µm.

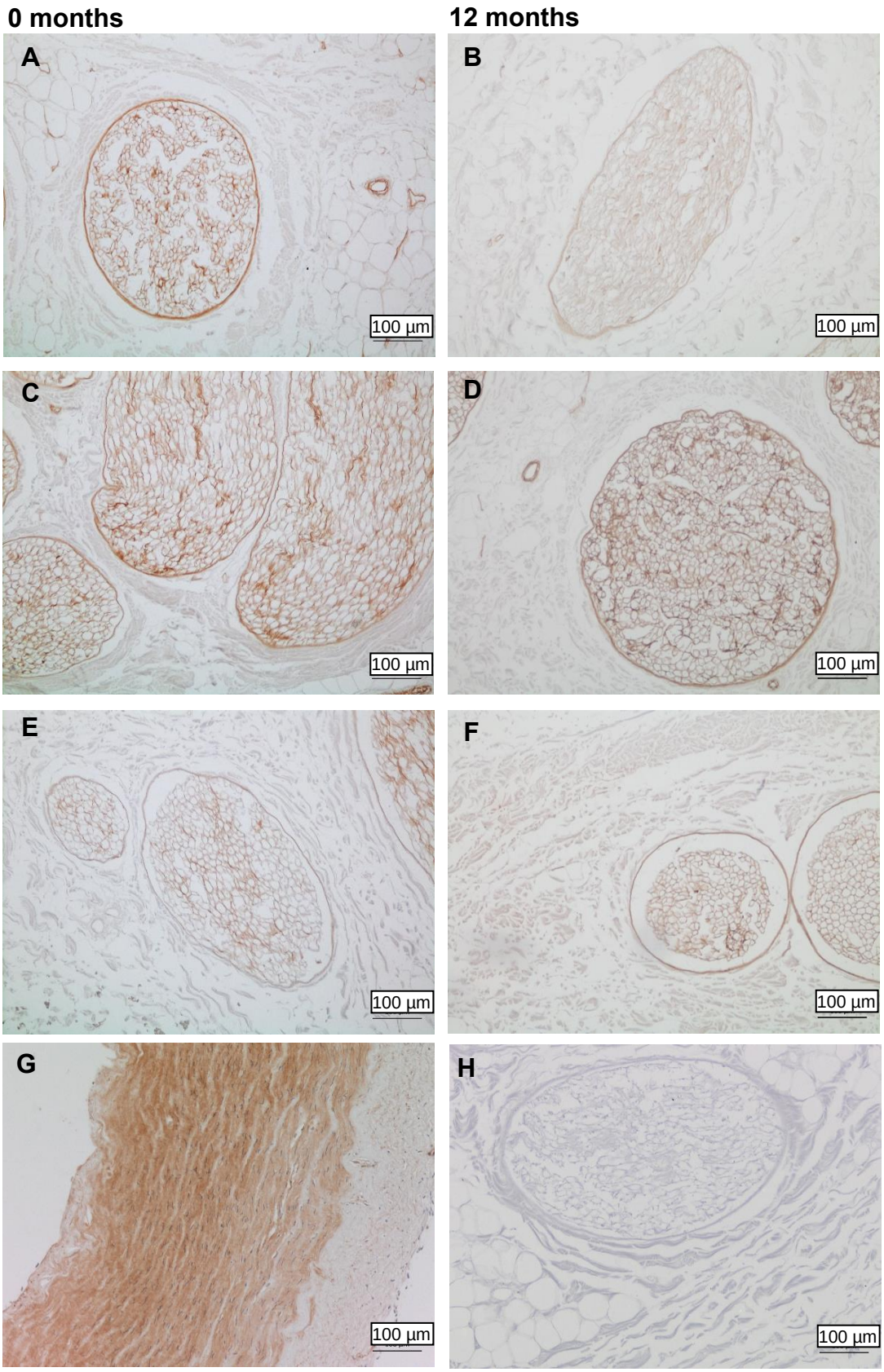
0 months
12 months
A
B
C
D
E
F
G
H
100 µm

Figure 8-6 Representative images of sections labelled with monoclonal antibodies against laminin

Decellularised nerves treated with PAA and stored for (A) 0 months and (B) 12 months, treated with gamma radiation and stored for (C) 0 months and (D) 12 months, and treated with E Beam and stored for (E) 0 months and (F) 12 months, immunohistochemically labelled for the presence of laminin. A porcine artery positive control (G) and an isotype control (H) were included. Images were acquired under Köhler illumination using a x10 objective, scale bars = 100 µm.

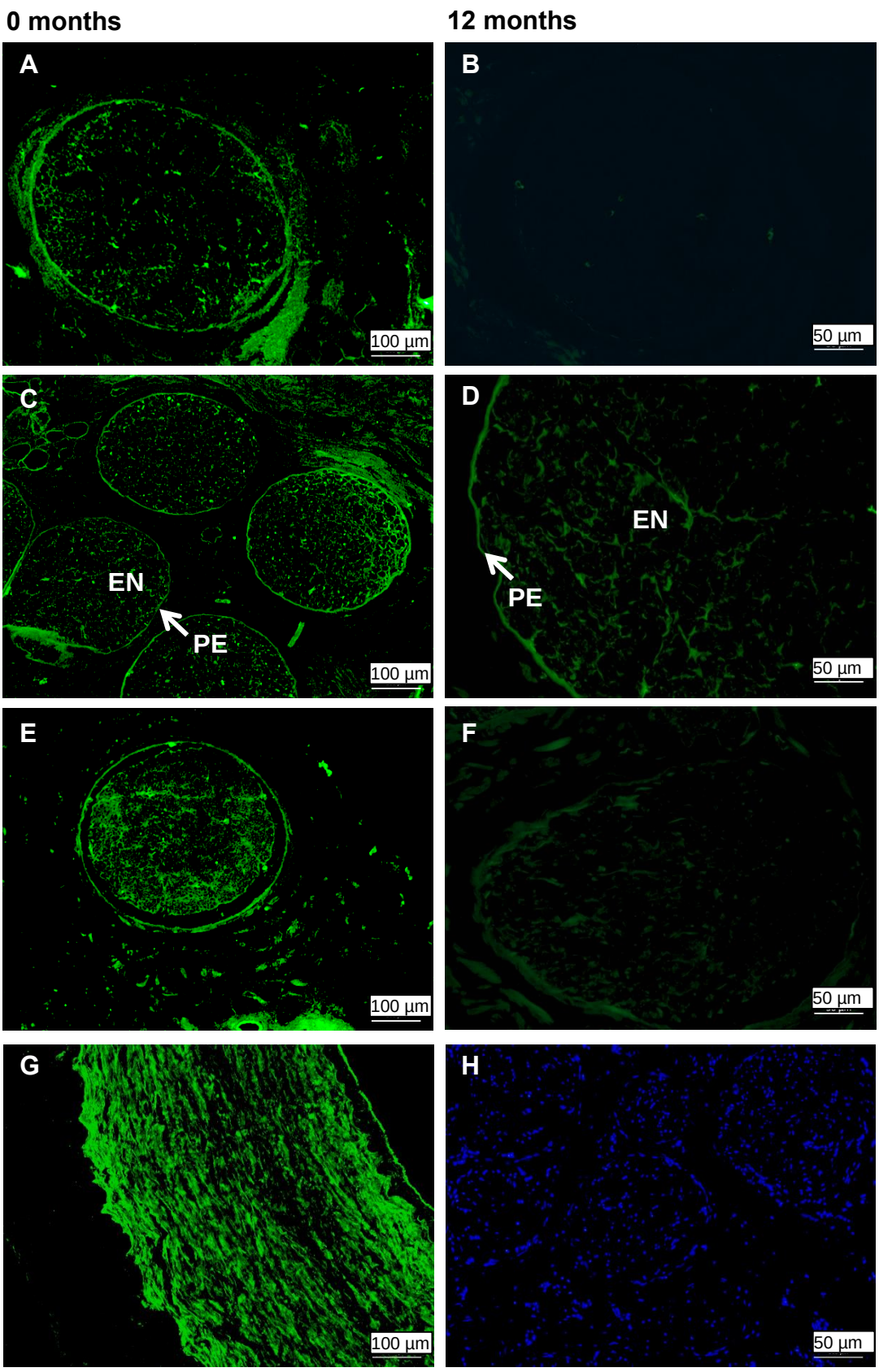
0 months
12 months
A
B
100 µm
50 µm
C
D
EN
PE
EN
PE
100 µm
50 µm
E
F
100 µm
50 µm
G
H
100 µm
50 µm

Figure 8-7 Representative images of sections labelled with a monoclonal antibody against fibronectin and counterstained with DAPI

Decellularised nerves treated with PAA and stored for (A) 0 months and (B) 12 months, treated with gamma radiation and stored for (C) 0 months and (D) 12 months, and treated with E Beam and stored for (E) 0 months and (F) 12 months, immunofluorescently labelled for the presence of fibronectin. A porcine artery positive control (G) and an isotype control (H) were included. The endoneurium (EN) and perineurium (PE, arrow) are labelled on the first image for reference. Images were acquired at a wavelength of 488 nm using a x10 objective, scale bars = 100 µm.

8.4.4 Uniaxial tensile testing

Samples of aged sterilised nerve were subject to uniaxial tensile testing to determine the effects of 12 months of storage on the material properties.

The UTS, maximum load at failure, Young's Modulus, stiffness, and energy to break values for sterilised nerves were not significantly different after 12 months of storage (Figure 8-8, Figure 8-9, and Figure 8-10).

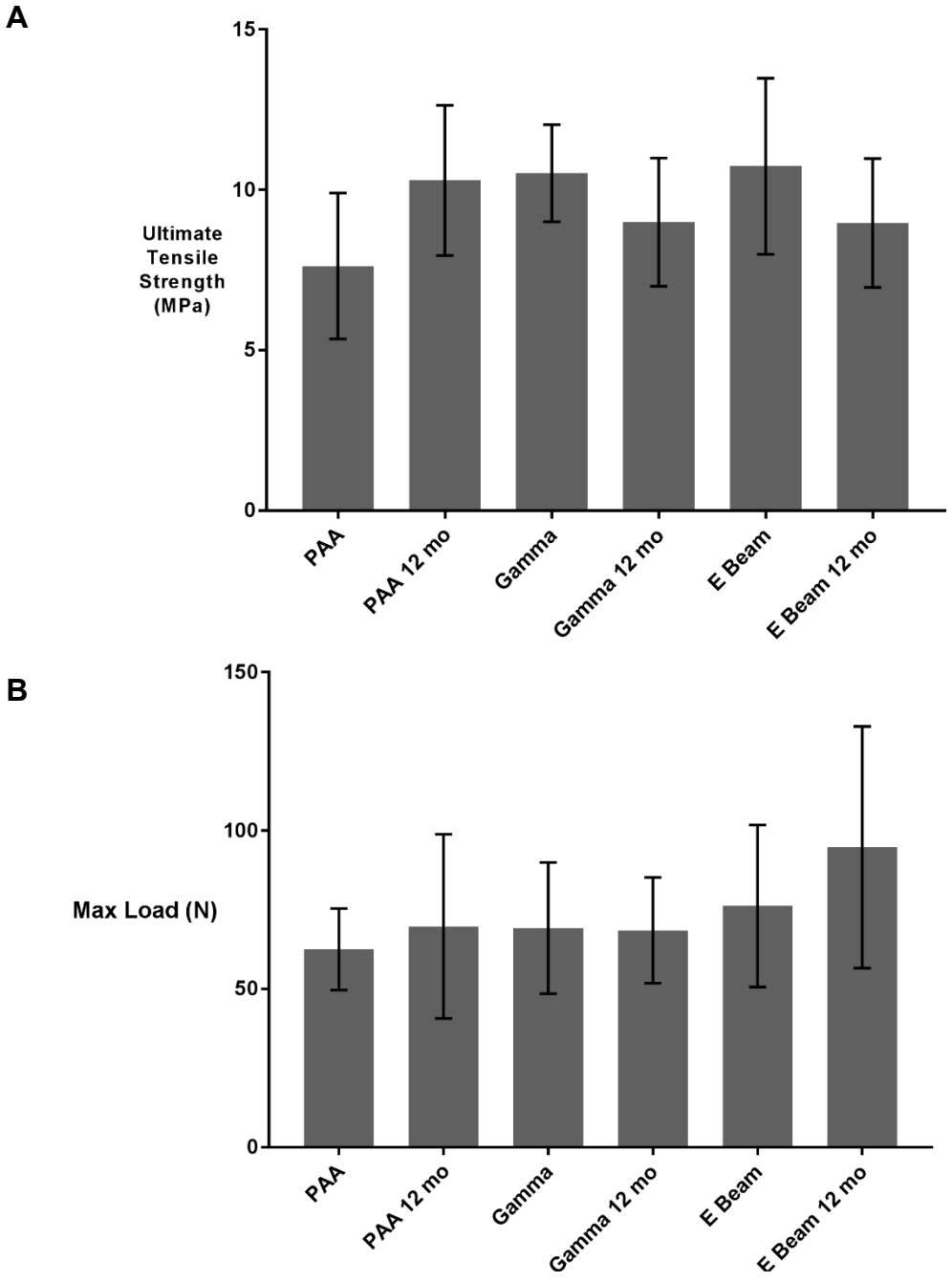

Figure 8-8 UTS and maximum load at failure of aged sterilised peripheral nerves

(A) UTS and (B) maximum load at failure of peripheral nerves treated with PAA, gamma radiation and E Beam and stored for 0 or 12 months. Data shown as mean +/- 95 % confidence interval, n = 6. Statistical analysis was by two-way ANOVA.

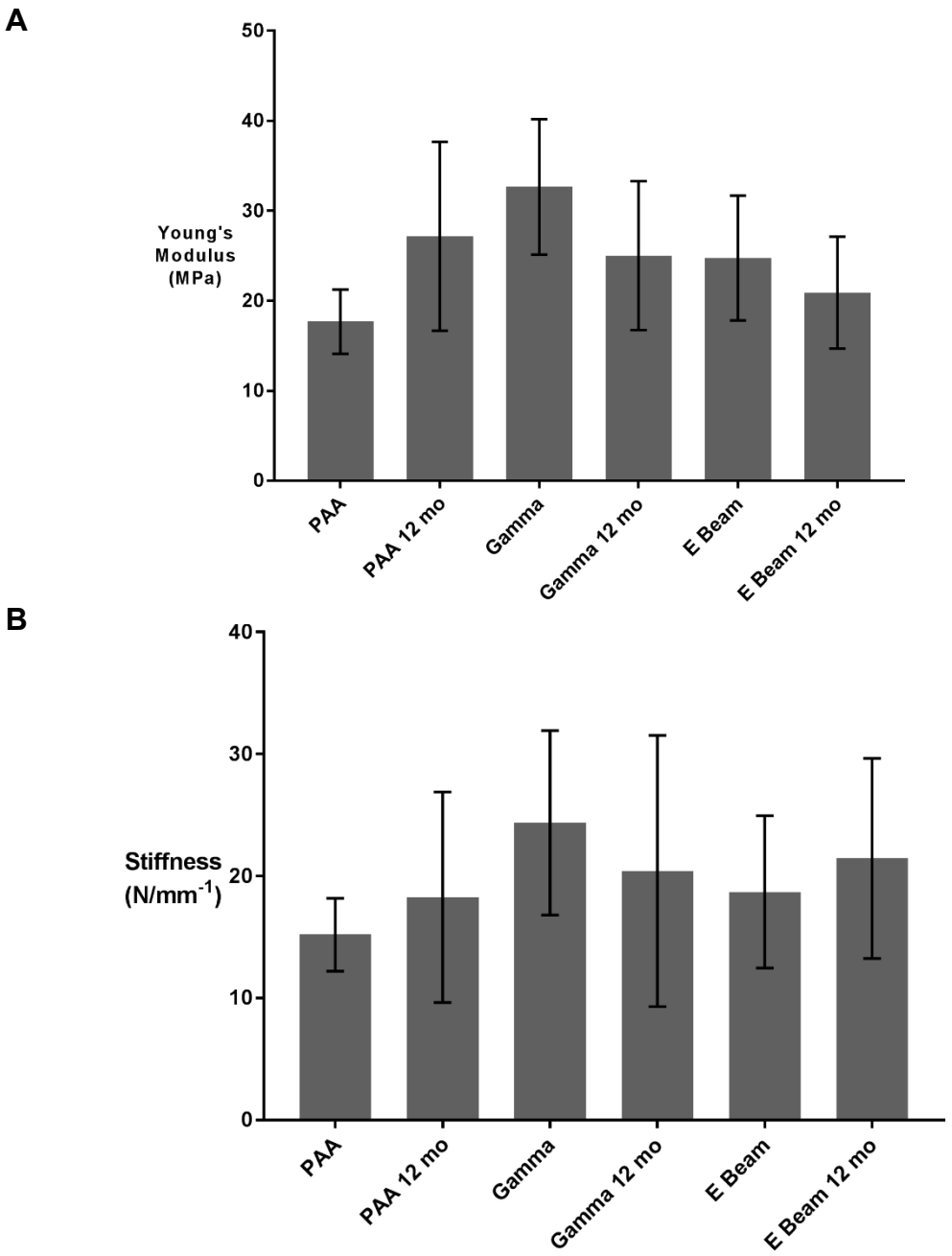

Figure 8-9 Young's Modulus and Stiffness of aged sterilised peripheral nerves.

(A) Young's Modulus and (B) Stiffness of peripheral nerves treated with PAA, gamma radiation and E Beam and stored for 0 or 12 months. Data shown as mean +/- 95 % confidence interval, n = 6. Statistical analysis was by two-way ANOVA.

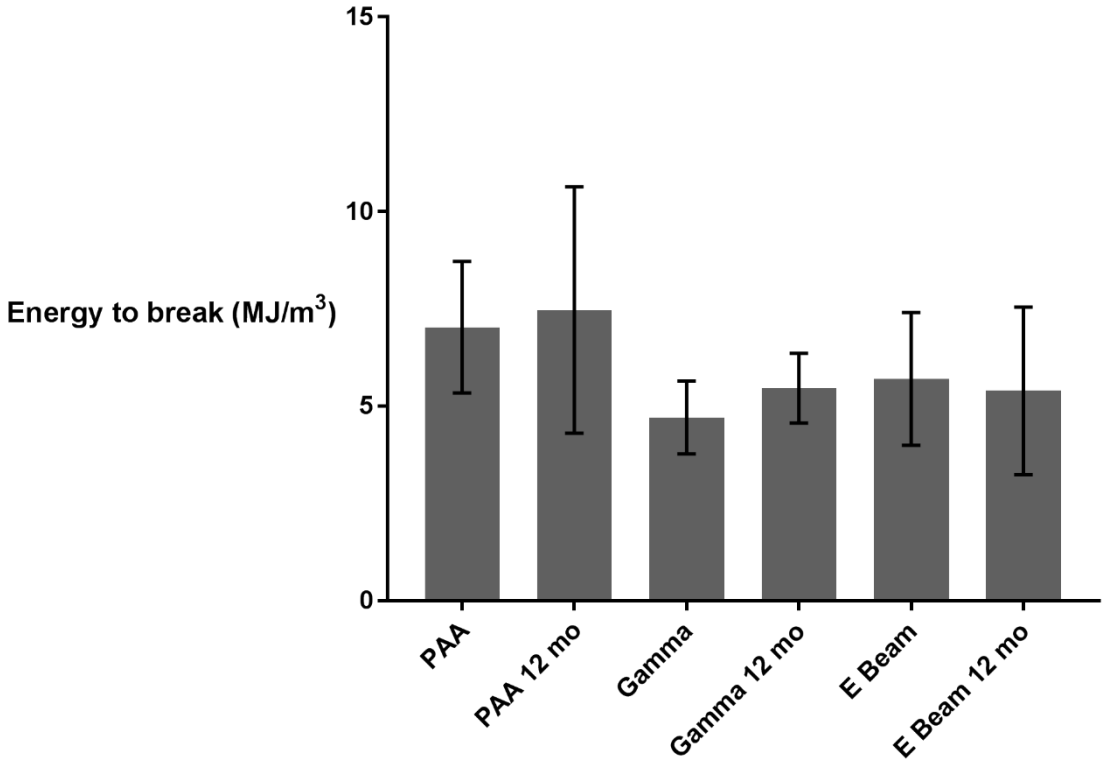

Figure 8-10 Energy to break values for aged sterilised peripheral nerves

Energy to break values for peripheral nerves treated with PAA, gamma radiation and E Beam and stored for 0 or 12 months. Data shown as mean +/- 95 % confidence interval, n = 6. Statistical analysis was by two-way ANOVA.

8.4.5 Quantification of collagen and denatured collagen content

No significant differences were found in the collagen content or denatured collagen content of sterilised nerves after 12 months of storage (Figure 8-11).

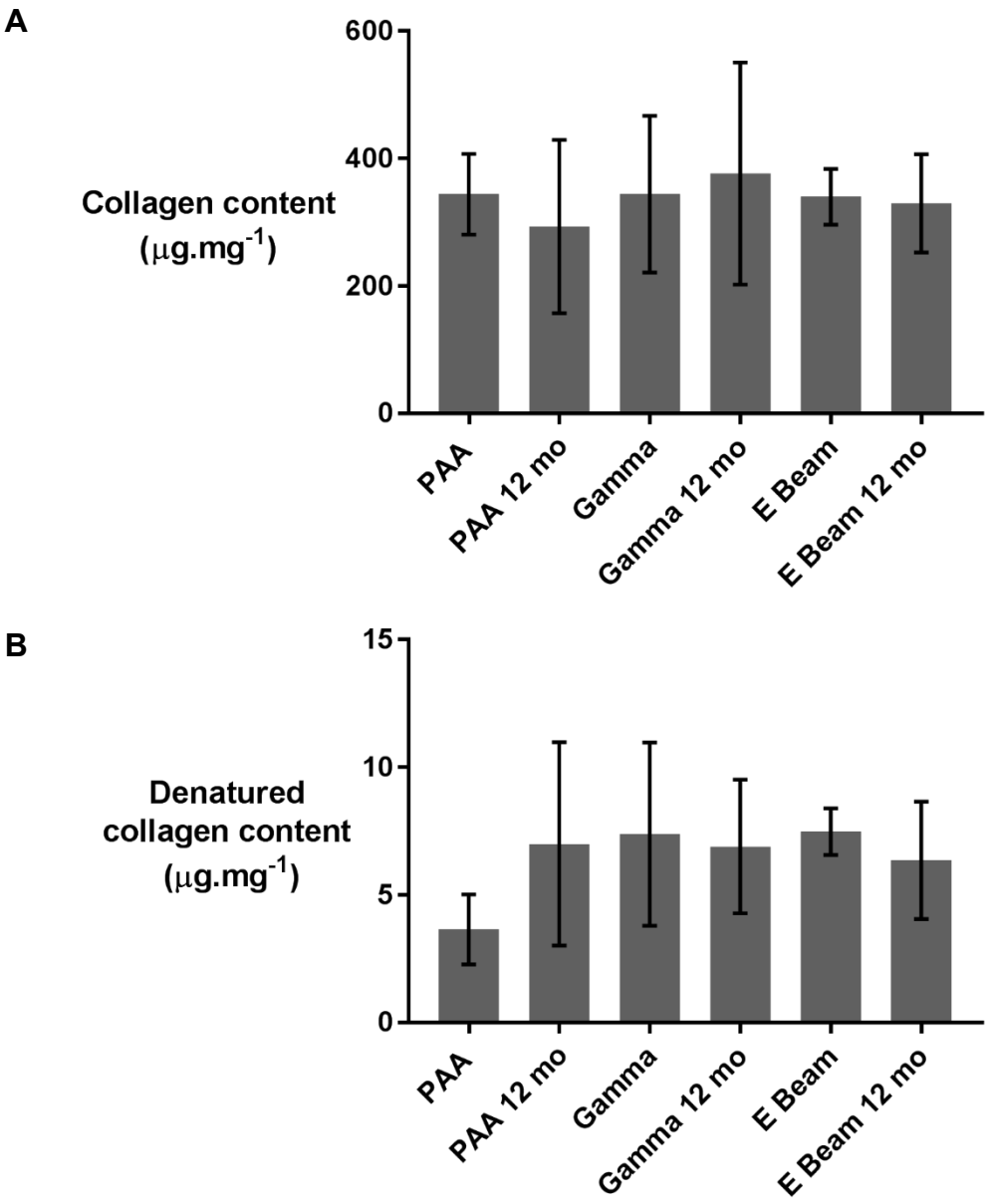

Figure 8-11 Collagen and denatured collagen content of aged sterilised porcine peripheral nerves

(A) Collagen content and (B) denatured collagen content of peripheral nerves treated with PAA, gamma radiation and E Beam and stored for 0 or 12 months. Data shown as mean +/- 95 % confidence interval, n = 6. Statistical analysis was by two-way ANOVA.

8.5 Discussion

The biocompatibility, structure, and mechanical properties of the decellularised nerves treated with PAA, gamma radiation and E Beam appeared to be well retained after 12 months of storage at room temperature.

Previous studies into the effects of long-term storage on decellularised tissues (including human trachea, murine lung and rabbit oesophagi) have employed antibiotic and antimycotic compounds, in combination with controlled temperature environments (maintained at 4 °C or cryopreserved in protectant medium and stored in liquid nitrogen), to ensure preservation [242, 449, 452]. Terminal sterilisation may negate the requirement for such storage conditions (although such conditions have been employed as a further protective measure e.g. for decellularised human dermis and frozen cellular human bone allografts sterilised with gamma radiation); the data from the present study demonstrate retention of functional properties in sterilised nerves stored in an unmodified PBS solution and at room temperature [453, 454].

In the present study graft deterioration was limited to some disorder in the collagenous structures of the epineurium and possible alterations to the distribution of basement membrane components, particularly in PAA-treated samples. It is possible that treatment of decellularised nerves with gamma radiation or E Beam may mediate inter and intra-molecular crosslinking of collagens in the ECM, providing ultrastructural stability and preventing degradation; however, due to the inherent difficulties in storing non-sterilised tissue for long periods of time, no negative control comparator group was available against which to evaluate this possibility [228, 336].

In contrast, oxidative degradation and/or solubilisation of ECM components may have contributed to the changes seen in PAA-treated samples [242]. Bonenfant et al (2013) observed an increase in solubilised ECM components, including laminin, fibronectin and collagen IV, in decellularised murine lungs treated with PAA compared to freshly decellularised samples. The reduction in labelling intensity for laminin and fibronectin observed here may be the result of a similar process. It is possible that in the initial period following PAA-mediated oxidative degradation of the basement membrane, laminin and fibronectin remained localised to the perineurium and endoneurium. This would account for the

positive labelling seen in the samples which were fixed and processed immediately after PAA treatment.

There are two possible explanations for the different results seen in PAA-treated samples after 12 months storage. If the oxidative damage has primarily resulted in solubilisation of laminin and fibronectin, the affected proteins may have gradually diffused away from the basement membrane regions and therefore caused a weaker signal to be detected upon labelling. Alternatively, destabilisation of the inter- and intra-molecular bonds of laminin and fibronectin sub-units may have led to conformational alterations and/or changes to surface chemistry, altering the target epitope of the specific antibodies used in the study and reducing the level of antibody binding. As the interaction of Schwann cells and neurons with these proteins is thought to facilitate processes including cell attachment, migration and myelination, removal or alteration of laminin and fibronectin from the endoneurial basement membrane may slow or inhibit the process of reinnervation and restoration of function post-implantation.

The slight increase in disorder within the collagen structures of PAA-treated nerves after 12 months of storage was not accompanied by a corresponding reduction in the mechanical properties. This finding differs from the observations of several previous studies. The UTS and Young's Modulus of decellularised rabbit oesophagi were reduced by approximately 60 % and 50 % respectively after storage for 6 months at 4 °C in the presence of antibiotics and antimycotics. A proportionally smaller reduction in Young's Modulus (approximately 30 %) was seen in decellularised oesphagi which were cryopreserved in protectant medium and stored in liquid nitrogen. Histological staining revealed much greater deterioration of collagen structures within the decellularised oesophagi stored at 4 °C compared to cryopreserved oesophagi. Similar changes to collagen structures and corresponding degradation of mechanical properties was seen in decellularised human tracheas stored for 12 months at 4 °C in the presence of antibiotic and antimycotic compounds [449]. In both cases, the changes were considered to be sufficiently extensive that implantation of the decellularised material after the given storage period could not be recommended. A possible reason underlying such differences compared with the present study may be the different decellularisation protocols used; the oesophagi and the tracheas were decellularised through cycles of treatment

with 4 % (v/v) sodium deoxycholate and DNase-I. The oesophagi and tracheas were treated for a total of three and 25 cycles, respectively. This may have led to greater degradation of collagen structures relative to the decellularised nerves, therefore resulting in a correspondingly greater impacts on mechanical properties. Unlike the tracheas, the decellularised oesophagi were not subject to sterility testing before or after the storage period; therefore, degradation of the ECM by secreted bacterial enymes (e.g. collagenases) cannot be discounted as a possible mechanism of scaffold degradation.

The changes to collagen structures seen in the present study were primarily limited to the epineurium. However, given that the perineurium surrounding each fascicle is thought to be the primary contributing structure to the tensile strength of peripheral nerves, it is unlikely that the observed changes would significantly alter the mechanical forces experienced by infiltrating cells *in vivo*.

Studies examining the effect of long-term storage on the properties of terminally sterilised decellularised tissue grafts are limited. A 2016 study investigated the effects of a 12 months storage on decellularised procine superflexor tendons sterilised with either PAA, gamma radiation or E Beam [451]. Similarly to the findings of the present study, no significant alterations were detected to biocompatibility, histological structure, mechanical properties and biochemical composition after the storage period.

Notwithstanding the apparent slight changes to the endoneurial and perineurial basement membranes and the organisation of collagen in the epineurium of PAA-treated nerves, storage for 12 months and without extensive control of environmental conditions did not appear to negatively impact upon key functional properties.

9 Discussion

9.1 General Discussion

There is a need for a novel graft material to promote and support functional regeneration across peripheral nerve defects; this is underlined by the inherent limitations of the current clinical options. NGCs may facilitate neuroregeneration over smaller defects, but efficacy appears to be limited in defects greater than a critical value of length (approximately 3 cm) [7]. Furthermore, while autografting is the current gold standard method, autograft repair of larger defects necessitates the harvest of increasing quantities of material from designated donor sites (e.g. the sural nerve), resulting in greater levels of donor site morbidity being incurred [50].

A previously developed decellularisation process for porcine peripheral nerves may provide a promising alternative graft material for peripheral nerve repair. Tissue grafts derived from xenogeneic sources present many of the advantages of unprocessed autografts, providing a scaffold material with a native-like ECM structure, cell attachment motifs / chemotrophic cues and biomechanical properties [17, 134]. Whilst allogeneic tissues present the same advantages, porcine tissue (as a xenogeneic material sourced from relatively young animals) provides the additional advantage of ensuring a consistent supply of high quality tissue without the inherent inter-donor variability associated with the human donor tissue [58]. The use of non-autograft material to repair peripheral nerve defects also removes the need to harvest graft material from the patient (thereby preventing the associated donor-site morbidity). Decellularised porcine peripheral nerves have been demonstrated to support site-specific cell growth during preliminary *in vivo* and *in* vitro studies [18, 139].

In order to reduce the risk of an FBRI following implantation, medical devices must be terminally sterilised using a method which meets the conditions for bioburden reduction stipulated in BS-EN 556-1 [334]. Therefore, the identification a suitable terminal sterilisation method is required for decellularised tissues (e.g. decellularised nerves) to be safely employed in the clinical environment. A range of sterilisation processes, including heat-mediated methods (e.g. steam), chemical methods (e.g. ethylene oxide, PAA, H_2O_2) and

ionising radiations (e.g. gamma radiation, E Beam), have been developed for use with medical devices. However, the relative sensitivity of tissue components (e.g. proteins such as collagen) to factors such as excessive heat, oxidative damage and ionising radiations results in an increased risk of incurring damage from such methods compared to devices comprising metals and/or polymers [141].

Therefore, the overarching aim of the present study was to identify a sterilisation method (or methods) suitable for use with a previously developed decellularised porcine peripheral nerve graft. Towards this aim, a hypothesis was generated stating that “a terminal sterilisation process, novel or established, can be used to treat decellularised porcine peripheral nerves without compromising biological and/or physical properties”. The identification of such a method would represent an important step in the translation of the decellularised nerves towards an “off-the-shelf” clinical product with preserved functional properties, minimal risk of graft-related infection post-implantation and the capacity to withstand long-term storage (ideally without the requirement for highly-controlled environmental conditions).

Prior to evaluating the effects of candidate sterilisation methods, the previously described decellularisation process was optimised in an attempt to reduce the length of time required for processing the nerves whilst maintaining the preservation of ECM histioarchitecture achieved with the original process [18].

The principle reason for carrying out decellularisation of potentially highly-immunogenic xenogeneic (and allogeneic) tissues is to reduce the potential for the induction of an adverse host response following implantation, enabling such materials to be considered for use in clinical procedures [37]. Therefore, ensuring a consistent reduction in the quantities of potentially immunogenic materials (e.g. cells and nucleic acids) while preserving key functional properties of the peripheral nerve tissue remained the primary consideration during the optimisation process [132]. The peripheral nerve decellularisation process was shortened through the elimination of a proportion of the hypotonic buffer and PBS wash steps (implying a reduction in the cost and resources required for graft production). Further optimisation resulted in a reduction of the agitation speed applied to the nerves, from 240 rpm to 120 rpm, in order to

minimise the structural damage to the ECM induced by mechanical forces during decellularisation. Structural damage to nerves processed at 240 rpm was most evident in the endoneurium; as in autografts, the structure of the endoneurium is thought to be particularly important for the guidance and protection of regenerating axons following implantation into a defect site [7, 135, 137]. Evaluation of the nerves decellularised using the final process indicated a high level of retention of ECM structures compared with native tissue. The basement membrane components laminin, fibronectin and collagen IV, also appeared to be retained; furthermore, the biochemical composition and biomechanical properties were not significantly different to unprocessed porcine nerve samples, indicating the preservation of a native-like ECM scaffold. Based on these results, this decellularisation process was then utilised throughout the remainder of the study.

For all prospective medical devices, including xenogeneic tissue grafts such as the decellularised porcine peripheral nerves described in this thesis, the identification of a suitable terminal sterilisation process is required prior to consideration for clinical use [334]. The scope of the present study was to evaluate the effects of sterilisation methods on the biological and physical properties of the decellularised nerves, rather than validating sterilisation efficacy (i.e. bioburden reduction). Sterilisation methods have been shown to degrade ECM components and structure through mechanisms such as cross-linking, chain scission, oxidation and heat-mediated damage [335]. The properties of the ECM which are most affected differ according to the mechanism of action of the given sterilisation method, any associated processes required (e.g. lyophiisation) and the specific tissue properties. For example, some hard tissues such as bone (which may undergo lyophilisation without degradation of structural or mechanical properties) have been lyophilised and sterilised with ethylene oxide without negatively impacting clinical efficacy [187]. However, soft tissues such as arteries and dermis have been shown to be susceptible to lyophilisation-induced structural disruption, and therefore the use of ionising radiation (under wet-state conditions) or oxidising agents in solution may be more applicable [1, 338, 455]. For example, decellularised human dermis products sterilised with either gamma radiation (kGy) or 0.1% PAA in solution are currently in clinical use [454, 456, 457]. The

choice of a sterilisation method for a graft should therefore be guided by assessment of the specific tissue in question; in particular, evaluation of which biological and/or physical properties are considered most important to retain may be crucial for ultimate function of the graft.

As with dermis, peripheral nerve is a soft tissue. Peripheral nerve tissue is likely to be susceptible to physical alterations to the histioarchitecture due to the complex and delicate nature of the ECM structures which comprise the majority of the tissue (particularly the endoneurium) [18, 58]. Several tissue properties were identified as potentially crucial for the optimal function of decellularised nerves *in vivo.* These included the structure and basement membrane composition of the endoneurium, which provides chemotrophic and physical guidance to infiltrating Schwann cells and neurons, the structure of the perineurium (an important determinant of peripheral nerve mechanical properties) and the retention of a native-like Young's Modulus to ensure regenerating neurons residing within the graft are not subject to excessive tensile mechanical forces [8, 73].

Currently, two decellularised nerve grafts (both derived from human tissue) have undergone clinical testing (a human decellularised nerve graft evaluated in a multicentre study China) or are licensed for clinical use (Avance® nerve graft, licensed in the USA) [71, 458, 459]. Both are sterilised with gamma radiation at a dose level of 25 kGy; however, it is unclear why this method was selected, and limited data are available regarding the effects of the sterilisation process in isolation on the properties of the decellularised nerve tissue. Gamma sterilisation has been commonly used historically for the sterilisation of both unprocessed allografts and decellularised allo/xenografts; examples include decellularised human dermis, allogeneic bone grafts, and allogeneic amniotic membrane [395, 456, 460-462]. However, the potential negative effects of processing with gamma radiation are also well documented; as one example, gamma irradiation (12 kGy) was demonstrated to induce disruption to the fine ECM structure, and a reduction in the ultimate tensile strength, of a decellularised human dermal graft [6]. Whilst the specific conditions used (e.g. dose level, whether the tissue is dehydrated prior to irradiation) are increasingly recognised as important determinants of the effects of gamma irradiation on tissue, the screening of a range of sterilisation methods (functioning through

differing mechanisms, and therefore presenting differing advantages and disadvantages) was considered to be the best approach for the identification of an optimal method for the decellularised porcine peripheral nerves in the present study [335, 451].

PAA solution, gamma radiation, E Beam and $SCCO_2$ (with an additive solution comprising 1.5 – 18.5 % [v/v] PAA) and 4.5 – 6 % [v/v] H_2O_2) were initially selected as candidate sterilisation methods due to their proven efficacy in terms of bioburden reduction, demonstrated either through the existence of a relevant standard (e.g. ISO 11137 for ionising radiations), or via prior data indicating that a sterility level equivalent to that stipulated in BS EN 556-1 can be achieved through the application of a given method [216, 463-465]. In addition, there is an established evidence base for the use of PAA (e.g. decelllarised human dermis), gamma radiation (e.g. allogeneic amniotic membrane, decellularised human dermis, decellularised porcine superflexor tendon), and E Beam (e.g. decellularised porcine superflexor tendon, human flexor digitorum superficialis tendon) indicating possible compatibility with soft tissue grafts [231, 335, 336, 395, 454, 456, 466]. While the application of $SCCO_2$ for tissue graft sterilisation is relatively recent compared to the more established methods of PAA, gamma and E Beam, previous studies have demonstrated effective reduction of bacterial endospore and viral populations can be achieved when $SCCO_2$ is used in conjunction with an oxidising agent (which also enables bioburden reduction to be achieved under more moderate environmental conditions in terms of temperature and pressure) [3, 216, 467]. The ability to carry out processing under moderate environmental conditions is especially advantageous when considering a sterilisation method for use with medical devices composed of biological materials (e.g. collagens) rather than polymers or metals, which may be comparatively more sensitive to extremes of temperature and pressure [170]. Retention of tissue ECM structure, mechanical properties and biocompatibility have been observed when decellularised rat lungs and porcine heart valves were treated using $SCCO_2$ in conjunction with a low volume of additive solution containing PAA and H_2O_2; these promising results provided evidence justifying the inclusion of $SCCO_2$ processing in the present study [19, 243].

Ethylene oxide was considered for inclusion as a candidate sterilisation method due to its efficacy (in terms of bioburden reduction) and previous history of use in tissue banking, particularly with bone allografts [187]. However, prior dehydration of ECM-based grafts is required for the safe and effective use of ethylene oxide. Dehydration enables sufficient diffusion of the reagent throughout the graft and also ensures effective post-processing elimination (through aeration) of the toxic breakdown products ethylene glycol and ethylene chlorohydrin [468]. Despite attempts to reduce the formation of large ice crystals during the process, lyophilisation appeared to induce widespread structural disruption to the endoneurial tubules of the decellularised nerves. Desiccation at ambient temperature, through the use of silica beads in a sealed glass chamber, enabled preservation of decellularised nerve ECM structure. However, the internal structure of the nerves did not appear to fully rehydrate even after a seven day incubation period in PBS, and furthermore uniaxial tensile testing revealed an increased Young's Modulus. Such mechanical changes may have negative implications for neuronal growth and signal transduction, as tissue with an increased Young's Modulus would not deform to the same extent as native tissue under a given load; therefore, the surrounding nerve tissue would be required to deform further at peak strain levels to compensate. Elevated local levels of strain would increase the probability of tensile stress experienced by the neurons resident within the nerve exceeding normal physiological levels; this could lead to increased local expression and wider distribution of transmembrane voltage-gated sodium channels, potentially impeding the conduction speed of action potentials [382]. Furthermore, if the observed increase in tissue stiffness is mirrored at a microscale-level, this would have negative implications for the promotion of neuronal growth. For example, an *in vitro* study of chick dorsal root ganglia cultured with collagen gels of increasing stiffness suggested that there is an inverse relationship between substrate stiffness and the growth of extending axons [366]. The relatively high fat content of the epineurium, and the hydrophobicity of the constituent lipid molecules, were considered the most likely mechanism limiting the diffusion of water molecules into the proteinaceous ECM structures of the perineurium and endoneurium. Meyer *et al* demonstrated that porcine adipose tissue had a lower rehydration capacity than muscle, cartilage, skin, tendon or

lung, only achieving 80 % (w/w) of its original mass after 60 minutes of rehydration [347]. Due to the failure to identify a non-destructive dehydration process, and the documented negative impacts of toxic residues on tissue graft integration (relative to the other methods considered in this study; see section 1.8.4), ethylene oxide was considered to be unsuitable for use with the decellularised nerves [188, 191].

In the present study, the effects of individual sterilisation methods on the properties of decellularised nerve ECM appeared to be strongly related to whether the method utilised ionising radiation (e.g. gamma radiation, E Beam) or oxidising agents (PAA in solution, PAA / H_2O_2 additive solution for $SCCO_2$ treatment). Qualitative assessment through histological examination and antibody labelling revealed only limited changes to the ECM of decellularised nerves treated with ionising radiation, whereas treatment with oxidising agents resulted in some disruption to ECM structures (primarily to the endoneurium but also in the epineurium) and an observed decrease in the localisation and intensity of antibody labelling for key basement membrane components.

The distinction between the effects of radiation-based methods and those utilising oxidising agents was further apparent when the physical properties of the sterilised nerves were evaluated. Treatment with both PAA and $SCCO_2$ caused an increase in the susceptibility of decellularised nerves to digestion with collagenase, whilst gamma radiation and E Beam reduced the transition temperature of collagen within the nerves. Changes in susceptibility to collagenase digestion could have implications for the degree (and rate) of ECM remodelling post-implantation, and therefore could potentially affect the retention of ECM structure *in vivo.* One example of such a difference was demonstrated through a comparison study of non-crosslinked deceullarised porcine dermis (Strattice®) compared with a crosslinked alternative (Permacol®), both of which were implanted into porcine abdominal wall defects; notwithstanding the small sample sizes used (n=8 per group), proportionally more ECM remodelling and neovascularisation was observed after one month in defects repaired with the non-crosslinked Strattice®, which was previously demonstrated as being significantly more susceptible to collagenase digestion [401]. These results suggest that, within the context of the specific defect/graft combination investigated, a greater susceptibility to collagenase digestion may

aid graft integration to the surrounding tissue; however, it should be noted that a reduction in collagenase susceptibility mediated through chemical crosslinking may be a greater relative impediment to tissue graft integration than retention of a level of collagenase susceptibility which is not significantly different to that of native/non-sterilised decellularised tissue, as was seen with decellularised nerves sterilised with either gamma radiation or E Beam in the present study. Furthermore, the degree to which peripheral nerve ECM is remodelled during neuroregeneration, and therefore the implications for the support and promotion of processes such as Schwann cell attachment and migration, axonal regrowth and (ultimately) distal target reinnervation, is unclear. It has been postulated that retention of the ECM histoarchitecture is favourable for the promotion of neuroregeneration by peripheral nerve grafts, providing physical and chemotrophic guidance to infiltrating Schwann cells and regenerating axons [18, 58]. Based on this hypothesis, modifications to graft materials potentially enabling ECM remodelling to occur at an increased rate could result in a more rapid loss of the distinct ECM structures within regions such as the endoneurium; therefore, such alterations may not be favourable to the support of axonal regrowth in peripheral nerve defects. Furthermore, when considering the measured growth rate of human axons (approximately 1 mm/day) regenerating neurons would require the guiding endoneurial tubule structures to be maintained for at least 30 days, which would favour the retention of a native-like resistance to enzymatic digestion (and therefore the rate of ECM remodelling to occur in parallel with the growth of the extending axons) [403].

PAA treatment reduced the UTS of the decellularised nerves, whilst $SCCO_2$ treatment caused an increase in UTS and Young's Modulus. A reduction in UTS could lead to physical failure of the graft if subject to high tensile forces *in situ*, potentially increasing the chance of re-injury; however, the levels of stress required for this to occur would likely be high enough as to induce injury in axons irrespective of such changes to the mechanical properties of a graft material. However, an increased Young's Modulus could (especially if such changes were mirrored at the microscale ECM level) have negative implications for the support of neuronal growth, as well as potentially mediating localised disruption of signal transduction to propagating action potentials [366, 382].

Such alterations to tissue mechanical properties are therefore likely to have a negative impact upon the function of a decellularised peripheral nerve graft.

Possible mechanisms underlying the differential effects to ECM-based grafts of ionising radiations and oxidative agents have previously been described. Irradiation of collagenous tissues (e.g. human bone, decellularised human dermis, porcine tendon) have been observed to cause changes to structural and mechanical properties [6, 220, 336, 390, 451]. Such changes are thought to be indicative of scission of the collagen polypeptide backbone and/or the formation of novel inter-molecular crosslinks, the occurrence of which has been demonstrated with purified and irradiated collagen *in vitro* [1, 172, 228, 230, 390]. When tissues are irradiated in a wet state (i.e. in the presence of water molecules), as in the present study, crosslinking is favoured due to interactions of amino acid side chains with free radicals formed through radiolysis of water molecules [1]. However, a reduction in measured transition temperature was observed in nerves treated with either gamma radiation or E Beam; this may be indicative of disruption of intramolecular hydrogen bonds caused by hydroxyl radicals formed during irradiation [1, 228]. While the reduced transition temperature seen in decellularised nerves treated with gamma radiation or E Beam in the present study suggests some chain scission has taken place, the maintained/reduced collagenase susceptibility and retention of ECM structure and mechanical properties in irradiated nerves may be indicative of the formation of novel inter-molecular crosslinks. This proposed scenario is reinforced by the observed results of previous studies: structural damage and compromised material properties have been documented following dry-state irradiation of allograft human bone and decellularised human dermis, while (similarly to the findings of the present study), wet-state irradiation of decellularised porcine superflexor tendon did not appear to induce negative effects to these properties [179, 336, 393]. Therefore, the observed changes to transition temperature are unlikely to imply reductions to the gross parameters of the decellularised nerves (such as ECM structure or tensile mechanical properties); indeed, the stiffness of the decellularised nerves was found to increase following gamma radiation, and the histioarchitecture appeared to be well preserved [172]. Whilst the specific implications of such molecular-scale changes for the biological properties of the decellularised nerves are not clear, it

should be noted that allogeneic tissue grafts irradiated under similar conditions (and therefore likely to have undergone similar molecular scale alterations to collagen bonding patterns; e.g. amniotic membrane and bone) have been demonstrated to be efficacious in clinical practice, with no notable safety concerns [394, 395].

Previous studies have demonstrated evidence of oxidative damage to ECM components in decellularised tissue grafts sterilised with PAA. Fourier transform infrared spectroscopy (FTIR) revealed an increase in –OH groups and C=O groups and a decrease in C-H groups in decellularised porcine temporomandibular discs sterilised with 0.2 % (v/v) PAA in 4 % (v/v) ethanol solution, compared to native samples or those sterilised with gamma radiation (13 kGy) [179]. This was accompanied by an approximate 30 % increase in surface free energy and a reduction in the contact angle of distilled water from 65 ° to 40 ° (indicative of increased hydrophilicity); furthermore, samples treated with the PAA/ethanol solution supported a greater population of seeded human umbilical cord Warton's jelly matrix cells compared with gamma irradiated or ethylene oxide-treated samples. Mass spectrometric analysis of decellularised murine lung samples revealed an increase in residual basement membrane sub-units (e.g. laminin sub-units alpha-5 and beta-1, collagen IV alpha-1, 2 and 3) after sterilisation with 0.2 % (v/v) PAA in 4 % (v/v) ethanol solution, indicative of increased solubilisation of these molecules (and hence increased likelihood of detection through the mass spectrometry protocol employed in the study) [242]. It is possible that similar mechanisms are responsible for the structural and chemical alterations seen in decellularised nerve ECM after treatment of the decellularised nerves with either 0.1 % (v/v) PAA solution or $SCCO_2$ (with the NovaKill™ additive solution).

A further decrease in the signal intensity of antibody labelling for laminin, fibronectin and collagen IV was seen in the perineurium and endoneurium of PAA-treated nerves after 12 months storage at room temperature compared with those fixed immediately after production (0 months), which was considered as likely to be indicative of further degradation to these components (e.g. changes to the surface chemistry and/or localisation/solubilisation). Such changes were not observed in the endoneurium/perineurium of either gamma irradiated or E Beam-treated nerves stored under the same conditions. ECM

degradation has previously been observed in decellularised rat lungs sterilised with 0.1 % (v/v) PAA solution, with further degradation apparent after a 6 month storage period [243]. As with the non-aged PAA-treated samples, the mechanisms underlying such changes have not been fully elucidated, but could include oxidative degradation, solubilisation of the ECM components, and/or destabilisation of the inter-/intramolecular bonds of laminin and fibronectin sub-units, either in isolation or combination [179, 242].

It is possible that the observed changes to antibody labelling detailed above, and the proposed mechanisms underlying such changes, could have implications for the ability of the decelluarised nerves to support of neuroregeneration. Both laminin and fibronectin function as chemoattractants for Schwann cells and facilitate the direct binding of regenerating axons to the ECM; this is underlined by the fact that the expression of both molecules is upregulated in Schwann cells following injury [361]. The $\alpha 2$, $\alpha 4$ and $\gamma 1$ laminin sub-chains (contained within the isoforms laminin 2 and laminin 8) and the “V region” of fibronectin have been implicated as particularly crucial for mediating the aforementioned cell-matrix interactions [42, 61]. The reduction in intensity of specific antibody labelling for fibronectin, and the loss of localisation for laminin labelling, observed in decellularised nerves treated with $SCCO_2$ (plus the NovaKill™ additive solution) implies a greater level of basement membrane degradation compared with that seen in nerves treated with 0.1 % (v/v) PAA solution. If, through the possible mechanisms detailed above, treatment with one/both of these sterilisation methods has caused changes to the localisation, surface chemistry and/or conformation of key binding sites within laminins and/or fibronectin in the basement membrane, it follows that neuroregenerative processes thought to be dependent on these molecules, such as Schwann cell growth and migration, ECM remodelling, and axon attachment, may be impeded. In addition the proposed mechanisms underlying the apparent changes to these components could lead to fragments of solubilised laminin/fibronectin molecules (or associated fragments) to be recognised as DAMPs; this could induce the activation of the innate immune system and thereby potentially compromise graft integration into the surrounding tissue [132, 133]. However, it is possible that the specific target epitopes of the antibodies used to label fibronectin and laminin have been altered by oxidative

reactions but key cell attachment motifs for Schwann cells and axons have not; in this scenario, the ability of the decellularised nerves to effectively promote neuroregeneration may not have been compromised by treatment with PAA or $SCCO_2$.

There is some evidence that, beyond its primary function as a scaffold to support other basement membrane components, collagen IV also facilitates cell-matrix interactions [321]. Axons (through α1β1 integrin) and Schwann cells (through integrins α1β1 and α2β1 and G-protein coupled receptor GPR126) sourced from rats have both been demonstrated to interact with collagen IV *in vitro* [362-364]. Downstream signalling from GPR126, mediated though cAMP, induces rat Schwann cells to differentiate and adopt pro-myelinating characteristics, whereas altering the conformation of GPR126 through a genetic knockout animal model prevented the expression of myelin basic protein [365]. If a similar pathway exists in human Schwann cells, it is plausible that alterations to collagen IV which prevent antibody binding (such as those seen in nerves treated with oxidising agents in the present study) may also disrupt cell-matrix interactions such as that mediated by GPR126.

Data acquired within this study indicated that whilst decellularised nerves sterilised with gamma radiation and E Beam retained localised labelling for collagen IV, laminin and fibronectin, the most complete preservation of these basement membrane components was achieved when $SCCO_2$ sterilisation was carried out under submerged conditions (rather than the standard process, in which the tissue is only submerged in PBS post-processing). With the exception of a study evaluating the effects of $SCCO_2$ sterilisation on decellularised rat lungs, which demonstrated retention of laminin after processing, there is limited evidence in the literature regarding the effects of $SCCO_2$ treatment on basement membrane components [243]. When considered in isolation, the results suggest that ECM-based scaffolds treated with $SCCO_2$ under submerged conditions may provide a superior substrate for the growth and migration of infiltrating cells compared to scaffolds sterilised with gamma radiation or E Beam. However, due to the relative novelty of the submerged process and practical limitations in terms of the production of decellularised nerves, a smaller group of samples was allocated to this treatment group. This restricted the feasible extent of characterisation to histological examination of

ECM structure and antibody labelling for selected basement membrane components. $SCCO_2$ processing under standard conditions had a negative effect on the mechanical properties of the decellularised nerves, mirroring alterations seen previously in $SCCO_2$-processed decellularised rat lungs and porcine heart valves [19, 243]. The preliminary data presented suggests that sterilisation with $SCCO_2$ under submerged conditions should be considered with other tissue grafts for which preservation of basement membrane structure and composition would be considered a positive functional prognostic indicator. Examples could include the endothelial basement membrane in vascular tissues and the epithelial basement membrane in gastrointestinal submucosa and dermis.

Histological examination indicated that treatment with PAA and $SCCO_2$ resulted in some disruption to the tubular structures of the endoneurium, which could negatively impact upon directional guidance and physical support to individual regenerating neurons [18, 138]. The importance of retaining an undamaged endoneurium for the support of neuroregenerative processes was highlighted by a comparative *in vivo* study of a synthetic guidance conduit composed of collagen type I (NeuraGen®) and a decellularised nerve graft produced using the patented AxoGen, Inc process and sterilised by gamma radiation; both grafts were implanted into a rat sciatic defect model [138]. The decellularised nerves were shown to retain endoneurial tubule structure and basement membrane laminin localisation, whereas the conduit did not incorporate laminin and provided no topographical guidance structures. The conduit and decellularised nerve were implanted into a rat sciatic nerve defect and left *in situ* for 22 weeks. While both scaffolds were inferior to the use of an isograft, decellularised nerves supported the growth of approximately 20-fold more axons into peripheral nerve tissue distal to the site of injury, indicating superior guidance and promotion of axonal growth compared to the conduit. A separate study showed that implantation of a previous iteration of the decellularised porcine nerves used in the present study, sterilised with 0.1 % (v/v) PAA solution, enabled the growth of axons across a rat sciatic defect over 11 weeks; however, an autograft control supported an average regrowth length of 14 mm compared to only 8.5 mm in the decellularised graft [139]. In light of these findings, retention of the physical structure and basement membrane

composition of the endoneurium was considered a key prognostic indicator for the function of sterilised nerves in the present study. The superior preservation of endoneurial structure and composition mediated by treatment of decellularised nerves with E Beam or gamma radiation may therefore enable greater reinnervation of target effectors post-implantation and, ultimately, restoration of function.

None of the sterilisation methods adversely affected the biocompatibility of the decellularised nerves during *in vitro* contact assays, or caused the induction of detectable sustained pro-inflammatory response when seeded with a murine macrophage cell line. Despite this evidence supporting the cytocompatibility and relatively low immunoreactivity of the sterilised nerves, the lack of an *in vitro* and/or *in vivo* experiment investigating the ability of the decellularised nerves to support the growth of site-specific cells (e.g. neurons and Schwann cells) represents a limitation of this thesis. It is not clear how the observed changes to the basement membrane, endoneurial structure and mechanical properties may influence the interaction of cells with the ECM. In peripheral nerve, laminin and fibronectin provide cell attachment motifs which mediate the infiltration and growth of Schwann cells and neurons, while the β-sheet structures of collagen IV act as a supporting scaffold and are provide key cell attachment motifs [380]. As the use of oxidising agents appeared to degrade the target epitopes of the antibodies specific for these ECM components in the present study, it is possible that the attachment of cells could be altered or disrupted in a similar manner.

However, previous *in vitro* studies evaluating cell attachment in other tissue types sterilised with PAA or $SCCO_2$ suggest that cell attachment may not be affected by the process of sterilisation. Decellularised porcine temporomandibular discs sterilised with 0.2 % (v/v) PAA in 4 % (v/v) ethanol were shown by independent studies to support greater levels of cell attachment compared with gamma irradiated (13 kGy) samples [179]. The authors postulated that the high observed levels of cell adhesion in PAA-treated samples compared with gamma irradiated (dry state) was due to oxidative changes resulting in the addition of hydroxyl groups and carboxyl groups to the amino acids within the tissue. These were linked to a study by Keselowsky et al, which examined the relative affinity of specific integrins for specifc chemical

groups and the implications for cell binding; hydroxyl groups and carboxylic acid groups were found to facilitate the highest levels of integrin adhesion (for $\alpha_5\beta_1$ and $\alpha_V\beta_3$ integrins, respectively). Hydroxyl groups, followed by carboxylic acid groups, also mediated the highest level of adhesion from seeded M3CTC-E1 cells [469]. Matuska et al further speculated upon the importance of the relative location of oxidative damage to ECM components; FTIR analysis revealed that this was predominantly in aliphatic side chains. The authors suggested that, considering the non-aliphatic composition of the common cell attachment motif RGD (arginine-glycine-aspartic acid), such changes would be less likely to negatively impact cellular interaction with the ECM.

It is possible that the mechanisms detailed above may at least partially underlie the similar patterns of cell attachment observed in the present study, when sterilised nerves were seeded with the RAW 264.7 murine macrophage cell line. PAA and $SCCO_2$-treated nerves appeared to support greater initial attachment of macrophages compared to E Beam-treated samples. However, as this only represented surface attachment of a non-specific cell type, only very limited inference can be made towards the attachment of neurons or Schwann cells to the endoneurial basement membrane. Histological evidence in a study of decellularised murine lung matrices appeared to show that PAA-treated tissue supported a greater viable population of C10 epithelial cells compared to gamma irradiated tissue, whilst the opposite was true for mesenchymal stem cells [242]. This appears to be indicative of differences in the functional susceptibility of cell attachment motifs to radiation-induced or oxidative damage mechanisms. Alterations to patterns of attachment and support as a result of treatment with a given sterilisation method may therefore be specific to individual cell types, and the likely response of site-specific cells (e.g. Schwann cells, neurons) to the basement membrane of nerves treated with different sterilisation methods remains unknown.

The safety and efficacy of two decellularised human nerve grafts, developed by He *et al* and AxoGen, Inc (Avance® nerve graft) respectively, has been tested in small scale clinical studies, and have either recently completed or are currently undergoing larger multicentre trials . Both grafts are terminally sterilised with gamma radiation (25 kGy) [137, 310, 458, 459]. The results of initial trials indicated that both grafts were safe and did not elicit an adverse host

immune response. Initial clinical trials evaluating efficacy revealed that (at least partial) functional restoration was achieved in 65.3 % (defect length 1 – 5 cm, 72 repair procedures) and 87.3 % (defect length 0.5 – 3 cm, 132 repair procedures) for the grafts developed by He *et al* and AxoGen, Inc respectively. These initial data suggest that sterilisation with ionising radiation does not impair functional properties of decellularised nerves; however, data from larger scale trials comparing the clinical applicability of decellularised nerves to the current direct suturing (coaptation) or autografting procedures would enable more definitive conclusions to be drawn. These *in vivo* results are encouraging, as the findings of the present study appeared to be in line with the previous *in vitro* results observed for the human nerve grafts developed by He *et al* and Axogen, Inc; treatment of the decellularised porcine nerves with ionising radiation appeared to enable good preservation of functional properties considered important to the provision of a pro-neuroregenerative environment (e.g. ECM structure and composition, particularly in the endoneurium) compared with other tested sterilisation methods (0.1% PAA in solution and $SCCo_2$ treatment under standard conditions). However, in the present study gamma radiation induced some slight differences in terms of mechanical properties (significantly increased stiffness) and the intensity of basement membrane component labelling compared with non-sterilised decellularised nerves, suggesting that, if utilising ionising radiation, sterilisation with E Beam rather than gamma radiation may result in a superior graft material.

9.2 Future work

The present study demonstrated alterations to decellularised nerve ECM across a range of parameters as a result of sterilisation. Observed results indicative of alterations to the properties of ECM components included decreased intensity of labelling for basement membrane components, and increase or decrease (depending on the specific sterilisation method) in collagenase susceptibility, collagen denaturation temperature and mechanical properties. Elucidating the precise nature of these changes and the underlying mechanisms responsible may enable prediction of the likely implications for graft efficacy.

Confirmation of oxidative damage to/solubilisation of ECM components following treatment with PAA or $SCCO_2$ could be achieved through analysis of sterilised nerve samples with mass spectrometry and FTIR, as previously described by Bonenfant *et al* and Matuska et al respectively [179, 242]. FTIR would enable significant changes in the abundance of –OH, C-H and C=O groups, associated with oxidation of the ECM components, to be quantified. Mass spectrometric identification of residual ECM proteins was attempted within thus study, in order to understand if the observed changes in antibody labelling intensity for basement membrane components corresponded to changes in the abundance of the proteins in the matrix. However, despite the use of a cryomill to increase the speed of processing and the repeated optimisation of a tryptic digest protocol for use with peripheral nerve samples (based on that provided by Bonenfant et al) the detected protein fragments always represented an incomplete fraction of the known ECM constituents. For example, despite representing approximately 90 % of ECM mass in peripheral nerve tryptic digest fragments from collagen type I were only identified in 30 % of samples processed according to the final protocol. A possible reason for the apparent incomplete digestion and/or lack of recovery of fragments may be the high fat content of peripheral nerve, at approximately 50 % of the dry mass. The use of a defatting protocol may therefore increase the efficiency of ECM protein digestion, and allow the detection of a more complete spectra and enable the quantification of relative changes to the abundance of specific protein sub-units (e.g. the alpha chains of collagen IV) compared to native or non-sterilised decellularised nerves. However, defatting protocols for tissue utilise solvents such as acetone or ethanol [17, 470]. These compounds are known to mediate crosslinking and precipitation of collagens and are likely to induce alterations to other ECM components. Alterations to the ECM incurred by defatting with solvents could therefore alter the protein fragment spectra obtained after tryptic digest and prevent the determination of changes mediated solely by the sterilisation methods.

Treatment of decellularised tissue with ionising radiation under hydrated conditions favours the formation of novel crosslinks within and between collagen molecules over chain scission [276]. Increased crosslinking could be responsible for the raised stiffness and decreased collagenase susceptibility

seen in gamma irradiated and E Beam treated nerves respectively. Quantification of crosslinks within decellularised nerve ECM and characterisation of the higher order structure of the collagen would provide further evidence supporting these theories. Quantification of crosslinks could be achieved through an assay using ninhydrin, which enables the proportion of free amino groups per given mass of tissue to be determined by the measurement of absorbance at 570 nm [471]. This assay has previously been used to determine the degree of crosslinking in decellularised porcine articular cartilage and decellularised porcine myocardium [472, 473]. In the articular cartilage study, which compared the use of different synthetic crosslinking compounds (e.g. glutaraldehyde, genipin, epigallocatechin gallate [EGCG]) to stabilise ECM structure, it was found that the approximate 33 % lower level of crosslinking in EGCG-treated samples compared to other groups corresponded with an approximate 33 % greater mass of tissue lost during collagenase susceptibility testing. Quantification of crosslinking in the the sterilised nerves could reveal similar patterns and provide additional evidence supporting the reason for the superior retention of mechanical properties and resistance to collagenase digestion of decellularised nerves treated with E Beam. The overlap and spacing between two aligned tropocollagen molecules in a fibril, known as a D-period, is 67 nm in length in the native collagen type I [378]. Crosslinking of collagen in human corneas with glutaraldehyde resulted in a shortening of the D-period length to 61 nm, with both the length of the overlap and the gap between tropocollagen molecules decreasing. It is possible that crosslinking mediated by ionising radiation could induce a similar effect, and therefore measurement of the D-period could provide further evidence of this effect. The D-period of collagen type I in native, decellularised and sterilised nerves could be visualised using either transmission electron microscopy or atomic force microscopy, and the D-period length deduced from the images.

A further aspect of peripheral nerve biomechanics which is relevant in the context of tissue regeneration (and therefore should be considered when evaluating the potential utility of a potential graft material such as decellularised nerves) is viscoelasticity. Peripheral nerve is recognised as a viscoelastic tissue [474-476], and while the effects of alterations to the viscoelastic properties on cellular function have not yet been fully characterised, it is likely that significant

deviation from native-like properties in this regard could have an effect on the function of key peripheral nerve effector cells (e.g. the viscosity of peripheral nerve tissue from diabetic individuals is reduced; this has been identified as a factor which may contribute to diabetic-associated neuropathic pathologies) [477]. The viscoelastic properties of the sterilised decellularised peripheral nerves should therefore be characterised; this could be achieved through dynamic mechanical analysis (DMA) [478]. DMA involves the application of stress (or strain) to a sample in an oscillating sinusoidal pattern; the corresponding strain (stress) is measured, and the resulting data can be used to calculate several parameters with relevance to tissue function. These include the storage modulus and the loss modulus, which are representative of the relative contributions of the elastic solid phase (stored/recoverable strain energy) and viscous fluid phase (energy dissipating during the sinusoidal application of stress/strain, primarily as heat) contributions to the dynamic modulus. The dynamic modulus is also known as the complex modulus, and describes as the ratio of stress to strain under the oscillatory [or “vibratory”] conditions). Previous studies conducted into the viscoelastic properties of another soft tissue, tendon, have postulated that observed differences to dynamic mechanical properties are primarily conferred by the crimp pattern of, and crosslinking associated with, the collagen fibres in the tissue [479-481]. As noted previously, collagen crosslinking may be altered by the sterilisation processes used in the present study (and collagen crimp patterns can be altered by changes to intramolecular crosslinking), and this process in turn may underlie some of the observed alterations to mechanical properties. Significant variation was observed in the tensile mechanical data obtained during the present study. Therefore, in addition to investigating sterilisation-induced changes to collagen structure through crosslink quantification and D-period measurement, it is possible that subjecting the sterilised decellularised nerves to DMA analysis could yield more definitive data regarding the changes to mechanical properties of the sterilised deceullarised nerves.

It may be possible to mitigate the negative effects of treatment with ionising radiations through altering the regime of dose application. The same overall dose can be achieved through the application of a series of smaller doses, in a process known as dose fractionation [482]. For example, gamma radiation in

the present study was applied in a single dose of 25 kGY; this could be applied instead in ten individual doses of 2.5 kGy. The use of dose fractionation mediates the same level of sterility assurance but has been demonstrated to reduce adverse effects to the mechanical properties of a human bone-tendon-bone allograft sterilised with 34 kGy E Beam [483]. The application of a fractionated dose regimen may reduce the magnitude of alterations to the physical properties of decellularised nerves seen following treatment of decellularised nerves with gamma radiation. However, consideration of a tailored (non-standard 25 kGy dose) regimen such as fractionation as a treatment methodology would require sole use of a gamma irradiator/electron accelerator, which may incur increases in processing costs.

While the epineurium is not thought to be a major contributor to the tensile mechanical properties of peripheral nerves, the heterogeneous mixture of collagenous and adipose tissue is thought to modulate the impact of compressive forces on the axonal cell bodies and Schwann cells located within the fascicles. Excessive compression over both acute (e.g. blunt trauma) or chronic (e.g. Saturday night palsy, carpal tunnel syndrome) timescales can impair signal conduction function and, although normally only considered a Grade I injury on the Seddon and Sunderland classification scale, may induce full Wallerian regeneration in severe instances [48]. In the present study, the physical properties of the nerves were only tested though the application of tensile strain on a longitudinal axis. The compressive properties, particularly the compressive modulus and stiffness, should be evaluated to determine the extent of any degradation of such properties, which could lead to an increase in compressive forces experienced by axons growing within the nerves and a corresponding reduction in functional restoration.

A promising retention of basement membrane labelling intensity and histioarchitectural structure was seen in decellularised nerves treated with $SCCO_2$ under submerged conditions, implying a reduced level of oxidative damage to ECM components. The effects of this $SCCO_2$ treatment under these conditions on the mechanical and physical properties, biocompatibility and biochemical composition of the decellularised nerves should be fully characterised. If improved preservation (in comparison to treatment with $SCCO_2$ under standard conditions) of such parameters is observed, and the treated

nerves can be stored for 12 months without undergoing adverse alterations, treatment with $SCCO_2$ under submerged conditions may be considered together with E-Beam as a candidate method for the sterilisation of decellularised nerves.

In order to be considered for clinical trials in humans, the safety and efficacy of the sterilised nerves should first be demonstrated in both *in vitro* and *in vivo* model systems [484]. An *in vitro* screen designed to interrogate the possible host immune response to the sterilised nerves has been described in this thesis. A similar *in vitro* screening process, involving seeding with Schwann cells and neurons, would be an appropriate first step when investigating the potential for the sterilised nerve segments to support neuroregeneration. Conducting such an experiment prior to *in vivo* implantation studies would enable quantification of differences in metabolic activity, axonal extension, the expression of cell surface markers (e.g. Schwann cell markers enabling differentiation of myelinating or non-myelinating phenotypes, such as myelin basic protein) and the composition of the protein secretome (particularly relative levels of neuroregeneration-associated cytokines [such as NGF, LIF, BDNF and FGF] and ECM components [including fibronectin, laminin and collagens]), via quantitative mass spectrometry, and qualitative histological analysis to identify the degree of ECM remodelling, within a controlled environment [48, 111, 485, 486].

Considering the potentially low *in vitro* growth rate of regenerating axonal stumps, a future *in vitro* study would ideally incorporate co-culture of Schwann cells and neurons for a period of 28 days or longer to elucidate the likely ability of the sterilise nerves to support and promote neuroregeneration [487]. The choice of appropriate cells for the seeding process would be crucial for the validity of such an experiment. The use of rat dorsal root ganglia cells (DRGs) as a source of primary peripheral neurons would be preferable to currently available neuronal cell lines, such as PC12 and NG108-15, which are derived from CNS sources [60, 485]. If rat DRGs were used as a source of neurons, the Schwann cells used in the experiment should also be sourced from a rat to ensure compatibility of paracrine signalling molecules. Rat Schwann cells could be obtained from a primary source or via a cell line [488]. Primary cells derived from explanted tissue would be preferable to cell lines in terms of phenotypic

characteristics; however, complications could be induced due to batch-to-batch variation of cell characteristics and the difficulty of isolating a sufficiently homogeneous population (with minimal fibroblastic contamination). Immortalised cell lines, such as RN22, S16 or RT4-D6P2T, may provide a more consistent response and have been shown to retain key phenotypic characteristics [488].

Following *in vitro* screening, the sterilisation treatment groups which appear to support the survival and growth of Schwann cells and neurons would be considered for *in vivo* testing in a surgically-created defect. This would enable the concurrent investigation of Schwann cell and neuronal growth and the host immune response (including the innate and adaptive immune system). Implantation into a rat model, typically in a sciatic nerve defect, is a common first step used to assess the efficacy of peripheral nerve repair devices [489]. The implanted nerve segment would be retained in the defect site for at least three months. Control groups of animals should be included, with the defect either repaired via an autograft procedure, to represent current clinical practice, or not repaired at all (or repaired with a simple NGC providing no physical or chemotrophic cues) [340, 490-492]. Appropriate quantitative outcome measures would include axonal extension, analysis of the relative numbers of different cell types (e.g. Schwann cells, macrophages, perineurial cells etc), tests of muscular function and conduction speed, and analysis of the mechanical properties of excised grafts [137, 383, 485, 489]. Qualitative measures could include the antibody labelling for cell surface markers to determine phenotype (e.g. Schwann cell markers enabling differentiation of myelinating or non-myelinating phenotypes, such as myelin basic protein), histological anlaysis to determine the degree of remodelling within the decellularised nerves (particularly at the interface between the decellularised graft and the native nerve, antibody labelling to analyse the deposition of specific ECM components of interest (e.g. laminin, fibronectin and collagen IV), and histological/antibody labelling-mediated analsysis of the extent and nature of the host immune response to the graft (e.g. is the phenotype of the macrophage population present predominantly M1 or M2, is there evidence of fibrosis and encapsulation).

Any sterilisation treatment groups which displayed favourable results in a small animal model should then be tested in a large animal model; historically, such models have not been employed frequently in the testing of peripheral nerve repair methods and, as such, an optimal large animal model has not been identified [489]. The principal reasons underlying this are thought to be based on the relatively high costs associated with conducting long-term studies in large animals compared to a similar study in a rat or mouse, as well as the inherent increased complexity of surgical procedures and functional tests. As the decellularised nerves are derived from porcine tissue, it may be more representative to use an ovine model rather than porcine model (as a same species graft does not mirror the intended cross-species application) [493-495]. An ovine median nerve model has previously been used to assess the efficacy of Corglaes Wrap (similar in design to an NGC, but sized and sealed during the surgical procedure [494]. The outcome measures used would be the same as in the small animal model, and a control groups would be included in which the defects are either not repaired or repaired via autografting. The defect size should be sufficient to demonstrate the efficacy of the decellularised peripheral nerves over larger defects (i.e. those greater than approximately 3 cm in length), given that applications within defects of a larger size may be a crucial niche in which decellularised nerves present advantages (in terms of providing directional physical and chemotrophic cues) for the promotion of neuroregeneration compared with synthetic NGCs.

9.3 Conclusions

Decellularised porcine peripheral nerves represent a potential nerve graft material, which may enable promotion of regeneration in a similar manner to an autograft whilst eliminating the need for a second site of surgery and providing a much greater volume and size range (diameter, length) of available tissue for the repair of larger defects [496]. The main aim of this study was to identify a terminal sterilisation method which would be suitable for use with decellularised porcine peripheral nerves; such a method would minimally impact upon the ECM structure, biochemical composition, biomechanical properties and biocompatibility of the decellularised nerves. Treatment with 0.1 % (v/v) PAA solution was not considered to be suitable for the sterilisation of decellularised

nerves due to the observed alterations to the ECM structure and basement membrane components of the decellularised nerves (specifically disruption to the structure of the endoneurium and reductions in the intensity of antibody labelling for basement membrane components, particularly collagen IV). Furthermore, the severity of basement membrane component alteration in the PAA-treated nerves appeared to have increased after 12 months of storage, and treatment with PAA solution presents an additional problem due to the fact that, as it requires an aseptic transfer procedure post-processing, it does not represent a truly terminal sterilisation method. As $SCCO_2$ treatment under standard conditions appeared to induce similar negative effects to the histioarchitecture whilst additionally causing significant alterations to tensile mechanical properties, it was also not considered to be a suitable method of sterilisation. Subjecting the decellularised nerves to $SCCO_2$ processing under submerged conditions appeared to protect against the occurence of such effects; high levels of structural preservation were observed histologically, and antibody labelling for the basement membrane components collagen IV, laminin and fibronectin retained intensity and remained highly localised to the endoneurium and perineurium.

Treatment with gamma radiation and E Beam appeared to mediate retention of the ECM structure of the decellularised nerves, and changes to the localisation and intensity of labelling for basement membrane components were minimal compared with those observed following treatment with PAA solution or $SCCO_2$ under standard conditions. However, treatment with gamma radiation appeared to cause an increase in the stiffness of the nerves.

Contact culture experiments did not yield evidence of cytotoxicity following any of the sterilisation methods; furthermore, the sterilised nerves did not induce any significant changes in the secretion of pro-inflammatory cytokines by a murine macrophage cell line.

In summary, whilst the results obtained during this study indicate E Beam to be the most promising sterilisation method for decellularised nerves with respect to the current dataset, preliminary results indicated that $SCCO_2$ processing under submerged conditions may have the potential to enable retention of a superior substrate for neuronal cell growth.

10 References

1. Aquino, K.A.d.S., *Sterilization by Gamma Irradiation,*, in *Gamma Radiation* F. Adrovic, Editor. 2012, IntechOpen: https://www.intechopen.com/books/gamma-radiation/sterilization-by-gamma-irradiation.
2. Grinsell, D. and C.P. Keating, *Peripheral Nerve Reconstruction after Injury: A Review of Clinical and Experimental Therapies.* BioMed Research International, 2014. **2014**: p. 13.
3. White, A., D. Burns, and T.W. Christensen, *Effective terminal sterilization using supercritical carbon dioxide.* Journal of Biotechnology, 2006. **123**(4): p. 504-515.
4. Peltonen, S., M. Alanne, and J. Peltonen, *Barriers of the peripheral nerve.* Tissue Barriers, 2013. **1**(3): p. e24956.
5. Beirowski, B., et al., *The progressive nature of Wallerian degeneration in wild-type and slow Wallerian degeneration (Wld(S)) nerves.* BMC Neuroscience, 2005. **6**: p. 6-6.
6. Gouk, S.-S., et al., *Alterations of human acellular tissue matrix by gamma irradiation: Histology, biomechanical property, stability, in vitro cell repopulation, and remodeling.* Journal of Biomedical Materials Research Part B: Applied Biomaterials, 2008. **84B**(1): p. 205-217.
7. Moore, A.M., et al., *Limitations of conduits in peripheral nerve repairs.* Hand (N Y), 2009. **4**(2): p. 180-6.
8. Topp, K.S. and B.S. Boyd, *Structure and biomechanics of peripheral nerves: nerve responses to physical stresses and implications for physical therapist practice.* Phys Ther, 2006. **86**(1): p. 92-109.
9. Setlow, P., *Spores of Bacillus subtilis: their resistance to and killing by radiation, heat and chemicals.* J Appl Microbiol, 2006. **101**(3): p. 514-25.
10. Ray, W.Z. and S.E. Mackinnon, *Management of nerve gaps: Autografts, allografts, nerve transfers, and end-to-side neurorrhaphy.* Experimental neurology, 2010. **223**(1): p. 77-85.
11. Ciaramitaro, P., et al., *Traumatic peripheral nerve injuries: epidemiological findings, neuropathic pain and quality of life in 158 patients.* Journal of the Peripheral Nervous System, 2010. **15**(2): p. 120-127.
12. Burke, F.D., et al., *Providing care for hand disorders a re-appraisal of need.* The Journal of Hand Surgery: British & European Volume, 2004. **29**(6): p. 575-579.
13. Wuthrich, P., *[Epidemiology and socioeconomic significance of hand injuries].* Z Unfallchir Versicherungsmed Berufskr, 1986. **79**(1): p. 5-14.
14. Rosberg, H.-E., K.S. Carlsson, and L.B. Dahlin, *Prospective study of patients with injuries to the hand and forearm: Costs, function, and general health.* Scandinavian Journal of Plastic and Reconstructive Surgery and Hand Surgery, 2005. **39**(6): p. 360-369.
15. Nouraei, M.H., et al., *Median and ulnar nerve injuries; what causes different repair outcomes?* Advanced biomedical research, 2015. **4**: p. 215-215.

16. Chhabra, A., et al., *Peripheral nerve injury grading simplified on MR neurography: As referenced to Seddon and Sunderland classifications.* The Indian Journal of Radiology & Imaging, 2014. **24**(3): p. 217-224.
17. Crapo, P.M., T.W. Gilbert, and S.F. Badylak, *An overview of tissue and whole organ decellularization processes.* Biomaterials, 2011. **32**(12): p. 3233-43.
18. Zilic, L., S.-P. Wilshaw, and J.W. Haycock, *Decellularisation and histological characterisation of porcine peripheral nerves.* Biotechnology and Bioengineering, 2016. **113**(9): p. 2041-2053.
19. Hennessy, R.S., et al., *Supercritical Carbon Dioxide–Based Sterilization of Decellularized Heart Valves.* JACC: Basic to Translational Science, 2017. **2**(1): p. 71-84.
20. Møller, A., *Anatomy and Physiology of Peripheral Nerves*, in *Intraoperative Neurophysiological Monitoring*. 2011, Springer New York. p. 261-267.
21. Birch, R., *The Peripheral Nervous System: Anatomy and Function*, in *Peripheral Nerve Injuries: A Clinical Guide*. 2013, Springer London: London. p. 1-67.
22. Commons, W. *Nervous System Diagram*. 2006; Available from: https://commons.wikimedia.org/wiki/File:Nervous_system_diagram.png.
23. Lodish, H.B., A; Zipursky, SL;, *Molecular Cell Biology*. 2000, W. H. Freeman: New York.
24. Krames, E.H.P., P; Rezia, AR., *Neuromodulation: Comprehensive Textbook of Principles, Technologies, and Therapies*. 2nd ed. Vol. 1. Elsevier.
25. Ackerman, S.D. and K.R. Monk, *The scales and tales of myelination: using zebrafish and mouse to study myelinating glia.* Brain Research.
26. Kidd, G.O., N; Trapp, BD., *Chapter 5. Biology of Schwann cells*, in *Peripheral Nerve Disorders*, G.K.C. Said, Editor. 2013, Elsevier.
27. Simpson, A.H., et al., *Effect of Limb Lengthening on Internodal Length and Conduction Velocity of Peripheral Nerve.* The Journal of Neuroscience, 2013. **33**(10): p. 4536-4539.
28. Lewis, G.M. and S. Kucenas, *Perineurial glia are essential for motor axon regrowth following nerve injury.* J Neurosci, 2014. **34**(38): p. 12762-77.
29. Pina-Oviedo, S. and C. Ortiz-Hidalgo, *The normal and neoplastic perineurium: a review.* Adv Anat Pathol, 2008. **15**(3): p. 147-64.
30. Richard, L., et al., *Endoneurial fibroblast-like cells.* J Neuropathol Exp Neurol, 2012. **71**(11): p. 938-47.
31. Muller, M., et al., *On the longevity of resident endoneurial macrophages in the peripheral nervous system: a study of physiological macrophage turnover in bone marrow chimeric mice.* J Peripher Nerv Syst, 2010. **15**(4): p. 357-65.
32. Fregnan, F., et al., *Role of inflammatory cytokines in peripheral nerve injury.* Neural Regeneration Research, 2012. **7**(29): p. 2259-2266.
33. Rosenberg, A., et al., *In vivo nerve-macrophage interactions following peripheral nerve injury.* The Journal of Neuroscience, 2012. **32**(11): p. 3898-3909.
34. Sakalidou, M., et al., *Interleukin-10 and regeneration in an end-to-side nerve repair model of the rat.* J Peripher Nerv Syst, 2011. **16**(4): p. 334-40.

35. Atkins, S., et al., *Interleukin-10 reduces scarring and enhances regeneration at a site of sciatic nerve repair.* J Peripher Nerv Syst, 2007. **12**(4): p. 269-76.
36. Badylak, S.F. and T.W. Gilbert, *Immune Response to Biologic Scaffold Materials.* Seminars in immunology, 2008. **20**(2): p. 109-116.
37. Keane, T.J. and S.F. Badylak, *The host response to allogeneic and xenogeneic biological scaffold materials.* J Tissue Eng Regen Med, 2015. **9**(5): p. 504-11.
38. Stolinski, C., *Structure and composition of the outer connective tissue sheaths of peripheral nerve.* J Anat, 1995. **186 (Pt 1)**: p. 123-30.
39. Verheijen, M.H.G., et al., *Local regulation of fat metabolism in peripheral nerves.* Genes & Development, 2003. **17**(19): p. 2450-2464.
40. Ishibe, K., et al., *Morphological study of the vasa nervorum in the peripheral branch of human facial nerve.* Okajimas Folia Anat Jpn, 2011. **88**(3): p. 111-9.
41. Thomas, P.K., *The connective tissue of peripheral nerve: An electron microscope study.* Journal of Anatomy, 1963. **97**(Pt 1): p. 35-44.4.
42. Gardiner, N.J., *Integrins and the extracellular matrix: Key mediators of development and regeneration of the sensory nervous system.* Developmental Neurobiology, 2011. **71**(11): p. 1054-1072.
43. Bilston, L.E., *Neural Tissue Biomechanics*. 2011: Springer.
44. Weerasuriya, A. and A.P. Mizisin, *The Blood-Nerve Barrier: Structure and Functional Significance*, in *The Blood-Brain and Other Neural Barriers: Reviews and Protocols*, S. Nag, Editor. 2011, Humana Press: Totowa, NJ. p. 149-173.
45. Ushiki, T. and C. Ide, *Three-dimensional architecture of the endoneurium with special reference to the collagen fibril arrangement in relation to nerve fibers.* Arch Histol Jpn, 1986. **49**(5): p. 553-63.
46. Zhang, G.K., DL., *Neural Engineering: From Advanced Biomaterials to 3D Fabrication Techniques*. 2016: Springer Nature.
47. Geuna, S.P., I; Tos, P; Battison, B., *Tissue Engineering of the Peripheral Nerve: Stem cells and Regeration Promoting Factors*. 2013, London: Elsevier.
48. Menorca, R.M.G., T.S. Fussell, and J.C. Elfar, *Peripheral Nerve Trauma: Mechanisms of Injury and Recovery.* Hand clinics, 2013. **29**(3): p. 317-330.
49. Masand, S.N., et al., *Neural cell type-specific responses to glycomimetic functionalized collagen.* Biomaterials, 2012. **33**(3): p. 790-7.
50. Gao, X., et al., *The role of peripheral nerve ECM components in the tissue engineering nerve construction.* Rev Neurosci, 2013. **24**(4): p. 443-53.
51. Koopmans, G., B. Hasse, and N. Sinis, *Chapter 19: The role of collagen in peripheral nerve repair.* Int Rev Neurobiol, 2009. **87**: p. 363-79.
52. Kadler, K.E., et al., *Collagens at a glance.* Journal of Cell Science, 2007. **120**(12): p. 1955-1958.
53. Yang, L., et al., *Mechanical properties of single electrospun collagen type I fibers.* Biomaterials, 2008. **29**(8): p. 955-62.
54. Wenger, M.P.E., et al., *Mechanical Properties of Collagen Fibrils.* Biophysical Journal, 2007. **93**(4): p. 1255-1263.

55. Abreu-Velez, A.M. and M.S. Howard, *Collagen IV in Normal Skin and in Pathological Processes.* North American journal of medical sciences, 2012. **4**(1): p. 1-8.
56. Aumailley, M. and R. Timpl, *Attachment of cells to basement membrane collagen type IV.* J Cell Biol, 1986. **103**(4): p. 1569-75.
57. Tassler, P.L., A.L. Dellon, and C. Canoun, *Identification of elastic fibres in the peripheral nerve.* J Hand Surg Br, 1994. **19**(1): p. 48-54.
58. Zilic, L., et al., *An anatomical study of porcine peripheral nerve and its potential use in nerve tissue engineering.* Journal of Anatomy, 2015. **227**(3): p. 302-314.
59. Nishiuchi, R., et al., *Ligand-binding specificities of laminin-binding integrins: a comprehensive survey of laminin-integrin interactions using recombinant alpha3beta1, alpha6beta1, alpha7beta1 and alpha6beta4 integrins.* Matrix Biol, 2006. **25**(3): p. 189-97.
60. Armstrong, S.J., et al., *ECM molecules mediate both Schwann cell proliferation and activation to enhance neurite outgrowth.* Tissue Eng, 2007. **13**(12): p. 2863-70.
61. Wallquist, W., et al., *Impeded interaction between Schwann cells and axons in the absence of laminin alpha4.* J Neurosci, 2005. **25**(14): p. 3692-700.
62. Mosahebi, A., M. Wiberg, and G. Terenghi, *Addition of fibronectin to alginate matrix improves peripheral nerve regeneration in tissue-engineered conduits.* Tissue Eng, 2003. **9**(2): p. 209-18.
63. Gandhi, N.S. and R.L. Mancera, *The Structure of Glycosaminoglycans and their Interactions with Proteins.* Chemical Biology & Drug Design, 2008. **72**(6): p. 455-482.
64. Zhang, F., Z. Zhang, and R.J. Linhardt, *Chapter 3 - Glycosaminoglycans*, in *Handbook of Glycomics*, R.D. Cummings and J.M. Pierce, Editors. 2010, Academic Press: San Diego. p. 59-80.
65. Freddo, L., W.H. Sherman, and N. Latov, *Glycosaminoglycan antigens in peripheral nerve: Studies with antibodies from a patient with neuropathy and monoclonal gammopathy.* Journal of Neuroimmunology, 1986. **12**(1): p. 57-64.
66. Braunewell, K.H.e.a., *Functional Involvement of Sciatic Nerve-derived Versican- and Decorin-like Molecules and other Chondroitin Sulphate Proteoglycans in ECM-mediated Cell Adhesion and Neurite Outgrowth.* Euro. J. Neurosci, 1995. **7**: p. 805-814.
67. Braunewell, K.H.e.a., *Up-regulation of a Chondroitin Sulphate Eptiope during Regeneration of Mouse Sciatic Nerve: Evidence that the Immunoreactive Molecules are Related to the Chondroitin Sulphate Proteoglycans Decorin and Versican.* Euro. J. Neurosci, 1995. **7**: p. 792-804.
68. Zuo, J., Y.J. Hernandez, and D. Muir, *Chondroitin sulfate proteoglycan with neurite-inhibiting activity is up-regulated following peripheral nerve injury.* J Neurobiol, 1998. **34**(1): p. 41-54.
69. Zuo, J., et al., *Regeneration of Axons after Nerve Transection Repair Is Enhanced by Degradation of Chondroitin Sulfate Proteoglycan.* Experimental neurology, 2002. **176**(1): p. 221-228.
70. Wang, J.T., Z.A. Medress, and B.A. Barres, *Axon degeneration: Molecular mechanisms of a self-destruction pathway.* The Journal of Cell Biology, 2012. **196**(1): p. 7-18.

71. Muir, D., *Materials And Methods To Promote Repair Of Nerve Tissue*. 2004.
72. Snow, D.M., N. Mullins, and D.L. Hynds, *Nervous system–derived chondroitin sulfate proteoglycans regulate growth cone morphology and inhibit neurite outgrowth: A light, epifluorescence, and electron microscopy study.* Microscopy Research and Technique, 2001. **54**(5): p. 273-286.
73. Topp, K.S. and B.S. Boyd, *Peripheral Nerve: From the Microscopic Functional Unit of the Axon to the Biomechanically Loaded Macroscopic Structure.* Journal of Hand Therapy, 2012. **25**(2): p. 142-152.
74. Borschel, G.H., et al., *Mechanical properties of acellular peripheral nerve.* J Surg Res, 2003. **114**(2): p. 133-9.
75. Lowry, A., et al., *Immunohistochemical methods for semiquantitative analysis of collagen content in human peripheral nerve.* J Anat, 1997. **191 (Pt 3)**: p. 367-74.
76. Wright, T.W., et al., *Excursion and strain of the median nerve.* J Bone Joint Surg Am, 1996. **78**(12): p. 1897-903.
77. Phillips, J.B., Smit, X., Zoysa, N. D., Afoke, A. and Brown, R. A. , *Peripheral nerves in the rat exhibit localized heterogeneity of tensile properties during limb movement.* The Journal of Physiology, 2004. **557**: p. 879–887.
78. Martin, R.B., et al., *Mechanical Properties of Ligament and Tendon*, in *Skeletal Tissue Mechanics*. 2015, Springer New York: New York, NY. p. 175-225.
79. Trumbull, A., G. Subramanian, and E. Yildirim-Ayan, *Mechanoresponsive musculoskeletal tissue differentiation of adipose-derived stem cells.* Biomedical engineering online, 2016. **15**: p. 43-43.
80. Gaur, P., et al., *Characterisation of human diaphragm at high strain rate loading.* Journal of the Mechanical Behavior of Biomedical Materials, 2016. **60**: p. 603-616.
81. Bianchi, F., et al., *Probing multi-scale mechanics of peripheral nerve collagen and myelin by X-ray diffraction.* Journal of the Mechanical Behavior of Biomedical Materials, 2018. **87**: p. 205-212.
82. Mason, S. and J.B. Phillips, *An ultrastructural and biochemical analysis of collagen in rat peripheral nerves: the relationship between fibril diameter and mechanical properties.* Journal of the Peripheral Nervous System, 2011. **16**(3): p. 261-269.
83. Bianchi, F., et al., *Probing multi-scale mechanical damage in connective tissues using X-ray diffraction.* Acta Biomaterialia, 2016. **45**: p. 321-327.
84. Karunaratne, A., S. Li, and A.M.J. Bull, *Nano-scale mechanisms explain the stiffening and strengthening of ligament tissue with increasing strain rate.* Scientific Reports, 2018. **8**(1): p. 3707.
85. Griffin, M., et al., *Biomechanical Characterization of Human Soft Tissues Using Indentation and Tensile Testing.* Journal of visualized experiments : JoVE, 2016(118): p. 54872.
86. Siviour, C.R., *High strain rate characterization of polymers.* 2017. **1793**(1): p. 060029.
87. Kwan, M.K., et al., *Strain, stress and stretch of peripheral nerve. Rabbit experiments in vitro and in vivo.* Acta Orthop Scand, 1992. **63**(3): p. 267-72.

88. Szikszay, T., T. Hall, and H. von Piekartz, *In vivo effects of limb movement on nerve stretch, strain, and tension: A systematic review.* J Back Musculoskelet Rehabil, 2017. **30**(6): p. 1171-1186.
89. Remache, D., et al., *The effects of cyclic tensile and stress-relaxation tests on porcine skin.* Journal of the Mechanical Behavior of Biomedical Materials, 2018. **77**: p. 242-249.
90. Nicola Maffulli, P.R., Wayne B. Leadbetter, *Tendon Injuries: Basic Science and Clinical Medicine*. 2005: Springer.
91. Iida, H., Schmeichel, A. M., Wang, Y., Schmelzer, J. D. and Low, P. A., *Schwann cell is a target in ischemia–reperfusion injury to peripheral nerve.* Muscle Nerve, 2004. **30**(761–766).
92. Abe, I., et al., *Internodes can nearly double in length with gradual elongation of the adult rat sciatic nerve.* Journal of Orthopaedic Research, 2004. **22**(3): p. 571-577.
93. OGATA, K. and M. NAITO, *Blood Flow of Peripheral Nerve Effects of Dissection, Stretching and Compression.* Journal of Hand Surgery (British and European Volume), 1986. **11**(1): p. 10-14.
94. Mohanna, P.N., et al., *A composite poly-hydroxybutyrate–glial growth factor conduit for long nerve gap repairs.* Journal of Anatomy, 2003. **203**(6): p. 553-565.
95. *Repair, protection and regeneration of peripheral nerve injury.* Neural Regeneration Research, 2015. **10**(11): p. 1777-1798.
96. Chen, S.-l., et al., *Repair, protection and regeneration of peripheral nerve injury.* 2015. **10**(11): p. 1777-1798.
97. Castillo-Galván, M.L., et al., *Study of peripheral nerve injury in trauma patients.* Gaceta Médica de México, 2014. **150**: p. 519-23.
98. Bekelis, K., S. Missios, and R.J. Spinner, *Falls and peripheral nerve injuries: an age-dependent relationship.* Journal of Neurosurgery, 2015. **123**(5): p. 1223-1229.
99. Wojtkiewicz, D.M., et al., *Social impact of peripheral nerve injuries.* Hand (N Y), 2015. **10**(2): p. 161-167.
100. Novak, C.B., et al., *Biomedical and psychosocial factors associated with disability after peripheral nerve injury.* J Bone Joint Surg Am, 2011. **93**(10): p. 929-36.
101. Noble, J., et al., *Analysis of upper and lower extremity peripheral nerve injuries in a population of patients with multiple injuries.* J Trauma, 1998. **45**(1): p. 116-22.
102. Spinner, R.J., M.B. Poliakoff, and R.L. Tiel, *The origin of "Saturday night palsy"?* Neurosurgery, 2002. **51**(3): p. 737-41; discussion 741.
103. Campbell, W.W., *Evaluation and management of peripheral nerve injury.* Clinical Neurophysiology, 2008. **119**(9): p. 1951-1965.
104. Sunderland, S., *Nerves and nerve injuries. By Sydney Sunderland, C.M.G., M.D., B.S., D.Sc., F.R.A.C.S.(Hon.), F.R.A.C.P., F.A.A. (Melbourne). 10 × 7 in. Pp. 116 + xvi, with 197 illustrations. 1968. Edinburgh: E. & S. Livingstone Ltd. £ 12 10s.* BJS, 1969. **56**(5): p. 401-401.
105. Tsao, B., et al., *Daroff: Bradley's Neurology in Clinical Practice. 2012.* p. 984-1001.
106. Gaudet, A.D., P.G. Popovich, and M.S. Ramer, *Wallerian degeneration: gaining perspective on inflammatory events after peripheral nerve injury.* J Neuroinflammation, 2011. **8**: p. 110.

107. Stirling, D.P. and P.K. Stys, *Mechanisms of axonal injury: internodal nanocomplexes and calcium deregulation.* Trends Mol Med, 2010. **16**(4): p. 160-70.
108. Jung, J., et al., *Actin polymerization is essential for myelin sheath fragmentation during Wallerian degeneration.* The Journal of neuroscience : the official journal of the Society for Neuroscience, 2011. **31**(6): p. 2009-2015.
109. Thumm, M. and M. Simons, *Myelinophagy: Schwann cells dine in.* J Cell Biol, 2015. **210**(1): p. 9-10.
110. Jessen, K.R. and R. Mirsky, *The repair Schwann cell and its function in regenerating nerves.* The Journal of Physiology, 2016. **594**(13): p. 3521-3531.
111. Naidu, M., *The Role Of Cells, Neurotrophins, Extracellular Matrix And Cell Surface Molecules In Peripheral Nerve Regeneration.* The Malaysian Journal of Medical Sciences : MJMS, 2009. **16**(2): p. 10-14.
112. Shim, S. and G.L. Ming, *Roles of channels and receptors in the growth cone during PNS axonal regeneration.* Exp Neurol, 2010. **223**.
113. Brenner, M.J., et al., *Role of timing in assessment of nerve regeneration.* Microsurgery, 2008. **28**(4): p. 265-272.
114. Kehoe, S., X.F. Zhang, and D. Boyd, *FDA approved guidance conduits and wraps for peripheral nerve injury: A review of materials and efficacy.* Injury, 2012. **43**(5): p. 553-572.
115. M.F, G., et al., *Peripheral Nerve Injury: Principles for Repair and Regeneration.* The Open Orthopaedics Journal, 2014. **8**: p. 199-203.
116. Isaacs, J. and T. Browne, *Overcoming short gaps in peripheral nerve repair: conduits and human acellular nerve allograft.* Hand (N Y), 2014. **9**(2): p. 131-137.
117. Pfister, B.J., et al., *Biomedical engineering strategies for peripheral nerve repair: surgical applications, state of the art, and future challenges.* Critical Reviews™ in Biomedical Engineering, 2011. **39**(2).
118. Dahlin, L.B., *Techniques of peripheral nerve repair.* Scand J Surg, 2008. **97**(4): p. 310-6.
119. Gerth, D.J., J. Tashiro, and S.R. Thaller, *Clinical outcomes for Conduits and Scaffolds in peripheral nerve repair.* World Journal of Clinical Cases : WJCC, 2015. **3**(2): p. 141-147.
120. Terzis, J., B. Faibisoff, and B. Williams, *The nerve gap: suture under tension vs. graft.* Plast Reconstr Surg, 1975. **56**(2): p. 166-70.
121. Slutsky, D.J., *A practical approach to nerve grafting in the upper extremity.* Atlas Hand Clin, 2005. **10**: p. 73-92.
122. Citak, M., et al., *Anatomy of the sural nerve in a computer-assisted model: implications for surgical minimal-invasive Achilles tendon repair.* 2007. **41**(7): p. 456-458.
123. Rayegani, S.M., *Basic Principles of Peripheral Nerve Disorders*. 2012: InTech.
124. Lackington, W.A., A.J. Ryan, and F.J. O'Brien, *Advances in Nerve Guidance Conduit-Based Therapeutics for Peripheral Nerve Repair.* ACS Biomaterials Science & Engineering, 2017. **3**(7): p. 1221-1235.
125. Meek, M.F. and J.H. Coert, *US Food and Drug Administration /Conformit Europe- approved absorbable nerve conduits for clinical repair of peripheral and cranial nerves.* Ann Plast Surg, 2008. **60**(4): p. 466-72.

126. Shah, M.B., W. Chang, and X. Yu, *Evaluating nerve guidance conduits for peripheral nerve injuries: a novel normalization method.* Neural Regeneration Research, 2014. **9**(22): p. 1959-1960.
127. Lohmeyer, J.A., et al., *The Clinical Use of Artificial Nerve Conduits for Digital Nerve Repair: A Prospective Cohort Study and Literature Review.* J reconstr Microsurg, 2009. **25**(01): p. 055-061.
128. Hudson, T.W., G.R. Evans, and C.E. Schmidt, *Engineering strategies for peripheral nerve repair.* Orthop Clin North Am, 2000. **31**(3): p. 485-98.
129. Zeyland, J., et al., *Transgenic pigs designed to express human α-galactosidase to avoid humoral xenograft rejection.* Journal of Applied Genetics, 2013. **54**(3): p. 293-303.
130. Chen, S.-G., Y.-S. Tzeng, and C.-H. Wang, *Treatment of severe burn with DermACELL(®), an acellular dermal matrix.* International Journal of Burns and Trauma, 2012. **2**(2): p. 105-109.
131. Nagata, S., R. Hanayama, and K. Kawane, *Autoimmunity and the clearance of dead cells.* Cell, 2010. **140**(5): p. 619-30.
132. Keane, T.J., et al., *Consequences of ineffective decellularization of biologic scaffolds on the host response.* Biomaterials, 2012. **33**(6): p. 1771-81.
133. Julier, Z., et al., *Promoting tissue regeneration by modulating the immune system.* Acta biomaterialia, 2017. **53**: p. 13-28.
134. Badylak, S.F., *Decellularized Allogeneic and Xenogeneic Tissue as a Bioscaffold for Regenerative Medicine: Factors that Influence the Host Response.* Annals of Biomedical Engineering, 2014. **42**(7): p. 1517-1527.
135. Liu, D., et al., *Tubulation repair mitigates misdirection of regenerating motor axons across a sciatic nerve gap in rats.* Scientific Reports, 2018. **8**(1): p. 3443.
136. Liu, K., et al., *Neuronal intrinsic mechanisms of axon regeneration.* Annu Rev Neurosci, 2011. **34**.
137. Moore, A.M., et al., *Acellular Nerve Allografts in Peripheral Nerve Regeneration: A Comparative Study.* Muscle Nerve, 2011. **44**(2): p. 221-234.
138. Whitlock, E.L., et al., *Processed allografts and type I collagen conduits for repair of peripheral nerve gaps.* Muscle Nerve, 2009. **39**(6): p. 787-99.
139. Zilic, L., *Development of Acellular Porcine Peripheral Nerves*, in *Department of Materials Science and Engineering*. 2016, University of Sheffield.
140. von Eiff, C.J., B; Kohnen, W; Becker, K;, *Infections Associated with Medical Devicaes: Pathogenesis, Management and Prophylaxis.* Drugs, 2005. **65**(2): p. 179-214.
141. Lerouge, S.S., A;, *Sterilisation of Biomaterials and Medical Devices*. 2012: Elsevier.
142. Greenwald, M.A., M.J. Kuehnert, and J.A. Fishman, *Infectious Disease Transmission during Organ and Tissue Transplantation.* Emerging Infectious Diseases, 2012. **18**(8): p. e1-e1.
143. McGuire, D.A. and S.D. Hendricks, *Allograft tissue in ACL reconstruction.* Sports Med Arthrosc, 2009. **17**(4): p. 224-33.
144. Guggenbichler, J.P., et al., *Incidence and clinical implication of nosocomial infections associated with implantable biomaterials –*

catheters, ventilator-associated pneumonia, urinary tract infections. GMS Krankenhaushygiene interdisziplinär, 2011. **6**(1): p. Doc18.
145. Parenteau-Bareil, R., R. Gauvin, and F. Berthod, *Collagen-Based Biomaterials for Tissue Engineering Applications.* Materials, 2010. **3**(3): p. 1863.
146. Lambert, B.J., T.A. Mendelson, and M.D. Craven, *Radiation and Ethylene Oxide Terminal Sterilization Experiences with Drug Eluting Stent Products.* AAPS PharmSciTech, 2011. **12**(4): p. 1116-1126.
147. ISO, *ISO 14937: Sterilization of health care products-general requirements for characterization of a sterilizing agent and the development, validation and routine control of a sterilization process for medical devices.* 2009, ISO.
148. Moore, M.A., *Inactivation of enveloped and non-enveloped viruses on seeded human tissues by gamma irradiation.* Cell and Tissue Banking, 2012. **13**(3): p. 401-407.
149. Mazzola, P.G., T.C.V. Penna, and A.M. da S Martins, *Determination of decimal reduction time (D value) of chemical agents used in hospitals for disinfection purposes.* BMC Infectious Diseases, 2003. **3**: p. 24-24.
150. Kowalski, J.B. and A. Tallentire, *Substantiation of 25 kGy as a sterilization dose: a rational approach to establishing verification dose.* Radiation Physics and Chemistry, 1999. **54**(1): p. 55-64.
151. Commision, E.P., *European Pharmacopoeia - 8th Edition*. Vol. 8.6-8.8. 2015: Council of Europe European Directorate for the Quality of Medicines (EDQM).
152. Nather, A.Y., N; Hilmy, N;, *Radiation in Tissue Banking*. 2007: World Scientific Publishing.
153. Scheffers, D.-J. and M.G. Pinho, *Bacterial Cell Wall Synthesis: New Insights from Localization Studies.* Microbiology and Molecular Biology Reviews, 2005. **69**(4): p. 585-607.
154. Silhavy, T.J., D. Kahne, and S. Walker, *The Bacterial Cell Envelope.* Cold Spring Harbor Perspectives in Biology, 2010. **2**(5): p. a000414.
155. Galdiero, S., et al., *Microbe-Host Interactions: Structure and Role of Gram-Negative Bacterial Porins.* Current Protein & Peptide Science, 2012. **13**(8): p. 843-854.
156. Mack, D., et al., *Biofilm formation in medical device-related infection.* Int J Artif Organs, 2006. **29**(4): p. 343-59.
157. Bhattacharya, S., et al., *Surgical Site Infection by Methicillin Resistant Staphylococcus aureus– on Decline?* Journal of Clinical and Diagnostic Research : JCDR, 2016. **10**(9): p. DC32-DC36.
158. Friedline, A.W., et al., *Sterilization Resistance of Bacterial Spores Explained with Water Chemistry.* J Phys Chem B, 2015. **119**(44): p. 14033-44.
159. Leggett, M.J., et al., *Bacterial spore structures and their protective role in biocide resistance.* Journal of Applied Microbiology, 2012. **113**(3): p. 485-498.
160. Moeller, R., et al., *Resistance of Bacillus subtilis spore DNA to lethal ionizing radiation damage relies primarily on spore core components and DNA repair, with minor effects of oxygen radical detoxification.* Appl Environ Microbiol, 2014. **80**(1): p. 104-9.
161. Moeller, R., et al., *Roles of the Major, Small, Acid-Soluble Spore Proteins and Spore-Specific and Universal DNA Repair Mechanisms in*

Resistance of Bacillus subtilis Spores to Ionizing Radiation from X Rays and High-Energy Charged-Particle Bombardment. Journal of Bacteriology, 2008. **190**(3): p. 1134-1140.
162. Deijkers, R.L.M., et al., *CONTAMINATION OF BONE ALLOGRAFTS.* ANALYSIS OF INCIDENCE AND PREDISPOSING FACTORS, 1997. **79-B**(1): p. 161-166.
163. Denner, J., *How Active Are Porcine Endogenous Retroviruses (PERVs)?* Viruses, 2016. **8**(8): p. 215.
164. Karcher, H.L., *HIV transmitted by bone graft.* BMJ : British Medical Journal, 1997. **314**(7090): p. 1300-1300.
165. Cole, G., *Basic Biology of Fungi.* 4th ed. 1996, Galveston: University of Texas Medical Branch.
166. Wang, S., et al., *Infections and human tissue transplants: review of FDA MedWatch reports 2001-2004.* Cell Tissue Bank, 2007. **8**(3): p. 211-9.
167. Soto, C., *Prion Hypothesis: The end of the Controversy?* Trends in biochemical sciences, 2011. **36**(3): p. 151-158.
168. Gibbs, C.J., Jr., et al., *Creutzfeldt-Jakob disease (spongiform encephalopathy): transmission to the chimpanzee.* Science, 1968. **161**(3839): p. 388-9.
169. Masters, C.L., D.C. Gajdusek, and C.J. Gibbs, Jr., *Creutzfeldt-Jakob disease virus isolations from the Gerstmann-Straussler syndrome with an analysis of the various forms of amyloid plaque deposition in the virus-induced spongiform encephalopathies.* Brain, 1981. **104**(3): p. 559-88.
170. Dai, Z., et al., *Sterilization techniques for biodegradable scaffolds in tissue engineering applications.* Journal of Tissue Engineering, 2016. **7**: p. 2041731416648810.
171. Miles, C.A., et al., *The Increase in Denaturation Temperature Following Cross-linking of Collagen is Caused by Dehydration of the Fibres.* Journal of Molecular Biology, 2005. **346**(2): p. 551-556.
172. Cheung, D.T., et al., *The effect of gamma-irradiation on collagen molecules, isolated alpha-chains, and crosslinked native fibers.* J Biomed Mater Res, 1990. **24**(5): p. 581-9.
173. Hodde, J., et al., *Effects of sterilization on an extracellular matrix scaffold: part I. Composition and matrix architecture.* J Mater Sci Mater Med, 2007. **18**(4): p. 537-43.
174. Huang, Q., et al., *Use of peracetic acid to sterilize human donor skin for production of acellular dermal matrices for clinical use.* Wound Repair and Regeneration, 2004. **12**(3): p. 276-287.
175. Scheffler, S.U., et al., *Remodeling of ACL Allografts is Inhibited by Peracetic Acid Sterilization.* Clinical Orthopaedics and Related Research, 2008. **466**(8): p. 1810-1818.
176. Rauh, J., et al., *Comparative Biomechanical and Microstructural Analysis of Native versus Peracetic Acid-Ethanol Treated Cancellous Bone Graft.* BioMed Research International, 2014. **2014**: p. 11.
177. Sode, F., *Simultaneous determination of peracetic acid and acetic acid by titration with NaOH.* Analytical Methods, 2014. **6**(7): p. 2406-2409.
178. Rutala, W.A.W., D. J;, *Guideline for Disinfection and Sterilization in Healthcare Facilities*. 2008, Healthcare Infection Control Practices Advisory Committee; Centres for Disease Control and Prevention.
179. Matuska, A.M. and P.S. McFetridge, *The effect of terminal sterilization on structural and biophysical properties of a decellularized collagen-based*

scaffold; implications for stem cell adhesion. Journal of Biomedical Materials Research Part B: Applied Biomaterials, 2015. **103**(2): p. 397-406.
180. Finnegan, M., et al., *Mode of action of hydrogen peroxide and other oxidizing agents: differences between liquid and gas forms.* J Antimicrob Chemother, 2010. **65**(10): p. 2108-15.
181. Baldry, M.G., *The bactericidal, fungicidal and sporicidal properties of hydrogen peroxide and peracetic acid.* J Appl Bacteriol, 1983. **54**(3): p. 417-23.
182. Mendes, G.C., T.R. Brandao, and C.L. Silva, *Ethylene oxide sterilization of medical devices: a review.* Am J Infect Control, 2007. **35**(9): p. 574-81.
183. Freytes, D.O., R.M. Stoner, and S.F. Badylak, *Uniaxial and biaxial properties of terminally sterilized porcine urinary bladder matrix scaffolds.* J Biomed Mater Res B Appl Biomater, 2008. **84**(2): p. 408-14.
184. Kearney, J.N., R. Bojar, and K.T. Holland, *Ethylene oxide sterilisation of allogenic bone implants.* Clinical Materials, 1993. **12**(3): p. 129-135.
185. Kearney, J.N., et al., *Evaluation of ethylene oxide sterilization of tissue implants.* J Hosp Infect, 1989. **13**(1): p. 71-80.
186. Moore, T.M., E. Gendler, and E. Gendler, *Viruses adsorbed on musculoskeletal allografts are inactivated by terminal ethylene oxide disinfection.* J Orthop Res, 2004. **22**(6): p. 1358-61.
187. Prolo, D.J.O., S.K; Borer, M.J., *Efficacy and Safety of Ethylene Oxide Sterilization of Allogeneic Bone for Human Transplantation : A Forty-Year Experience.* Cureus, 2015.
188. Kudryk, V.L., et al., *Toxic effect of ethylene-oxide-sterilized freeze-dried bone allograft on human gingival fibroblasts.* Journal of Biomedical Materials Research, 1992. **26**(11): p. 1477-1488.
189. ISO, *ISO 10993-7:2008 Biological evaluation of medical devices Part 7: Ethylene oxide sterilization residuals*

2008, International Organisation for Standardization.
190. Board, T.N., et al., *Impaction allografting in revision total hip replacement.* Journal of Bone & Joint Surgery, British Volume, 2006. **88-B**(7): p. 852-857.
191. Jackson, D.W., G.E. Windler, and T.M. Simon, *Intraarticular reaction associated with the use of freeze-dried, ethylene oxide-sterilized bone-patella tendon-bone allografts in the reconstruction of the anterior cruciate ligament.* Am J Sports Med, 1990. **18**(1): p. 1-10; discussion 10-1.
192. Stayner, L., et al., *Exposure-Response Analysis of Cancer Mortality in a Cohort of Workers Exposed to Ethylene Oxide.* American Journal of Epidemiology, 1993. **138**(10): p. 787-798.
193. Kakiuchi, M., et al., *Preparation of bank bone using defatting, freeze-drying and sterilisation with ethylene oxide gas. Part 1. Experimental evaluation of its efficacy and safety.* Int Orthop, 1996. **20**(3): p. 142-6.
194. Silindir, M. and A. Ozer, *Sterilization methods and the comparison of E-Beam sterilization with gamma radiation sterilization.* FABAD J Pharm Sci, 2009. **34**(34): p. 43-53.
195. Srun, S.W., et al., *Medical device SALs and surgical site infections: a mathematical model.* Biomedical Instrumentation & Technology, 2012. **46**(3): p. 230-237.

196. Joshi, C.P., et al., *Practical and clinical considerations in Cobalt-60 tomotherapy.* J Med Phys, 2009. **34**(3): p. 137-40.
197. Samsell, B.J. and M.A. Moore, *Use of controlled low dose gamma irradiation to sterilize allograft tendons for ACL reconstruction: biomechanical and clinical perspective.* Cell and Tissue Banking, 2012. **13**(2): p. 217-223.
198. ISO, *Sterilization of health care products-Radiation*. 2011, International Organization for Standardization.
199. Silverman, J., *Radiation processing: The industrial applications of radiation chemistry.* Journal of Chemical Education, 1981. **58**(2): p. 168.
200. Gupta, R., *Biomarkers in Toxicology*. 1st ed, ed. Gupta. 2014: Elsevier.
201. Trampuz, A., et al., *Effect of gamma irradiation on viability and DNA of Staphylococcus epidermidis and Escherichia coli.* J Med Microbiol, 2006. **55**(Pt 9): p. 1271-5.
202. Harewood, P., S. Rippey, and M. Montesalvo, *Effect of gamma irradiation on shelf life and bacterial and viral loads in hard-shelled clams (Mercenaria mercenaria).* Appl Environ Microbiol, 1994. **60**(7): p. 2666-70.
203. Dertinger, H.J., H. , *Molecular Radiation Biology: The action of ionising radiation on Elementary Biological Objects*. Vol. 2. 1970, Berlin: Springer.
204. Pruss, A., et al., *Effect of gamma irradiation on human cortical bone transplants contaminated with enveloped and non-enveloped viruses.* Biologicals, 2002. **30**(2): p. 125-33.
205. Fideler, B.M., et al., *Effects of gamma irradiation on the human immunodeficiency virus. A study in frozen human bone-patellar ligament-bone grafts obtained from infected cadavera.* J Bone Joint Surg Am, 1994. **76**(7): p. 1032-5.
206. Hernigou, P., et al., *Influence of Irradiation on the Risk of Transmission of HIV in Bone Grafts Obtained from Appropriately Screened Donors and Followed by Radiation Sterilization.* Cell Tissue Bank, 2000. **1**(4): p. 279-89.
207. Mucka, V., et al., *Influence of various scavengers of *OH radicals on the radiation sensitivity of yeast and bacteria.* Int J Radiat Biol, 2013. **89**(12): p. 1045-52.
208. Zimek, Z. and I. Kaluska, *Economical aspects of radiation sterilization with electron beam.* Radiation technology for conservation of the environment, 1998: p. 457.
209. Hoburg, A., et al., *High-dose electron beam sterilization of soft-tissue grafts maintains significantly improved biomechanical properties compared to standard gamma treatment.* Cell and Tissue Banking, 2015. **16**(2): p. 219-226.
210. Seto, A., C.J. Gatt, Jr., and M.G. Dunn, *Radioprotection of tendon tissue via crosslinking and free radical scavenging.* Clinical orthopaedics and related research, 2008. **466**(8): p. 1788-1795.
211. ISO, *Practice for dosimetry in an electron beam facility for radiation processing at energies between 300 keV and 25 MeV*. 2005, International Organization for Standardization.
212. Benson, R.S., *Use of radiation in biomaterials science.* Nuclear Instruments and Methods in Physics Research Section B: Beam Interactions with Materials and Atoms, 2002. **191**(1–4): p. 752-757.

213. Schmidt, T., et al., *Inactivation Effect of Standard and Fractionated Electron Beam Irradiation on Enveloped and Non-Enveloped Viruses in a Tendon Transplant Model.* Transfusion Medicine and Hemotherapy, 2012. **39**(1): p. 29-35.
214. Bernhardt, A., et al., *Improved Sterilization of Sensitive Biomaterials with Supercritical Carbon Dioxide at Low Temperature.* PLoS ONE, 2015. **10**(6): p. e0129205.
215. Hemmer, J.D., et al., *Sterilization of bacterial spores by using supercritical carbon dioxide and hydrogen peroxide.* J Biomed Mater Res B Appl Biomater, 2007. **80**(2): p. 511-8.
216. Qiu, Q.Q., et al., *Inactivation of bacterial spores and viruses in biological material using supercritical carbon dioxide with sterilant.* J Biomed Mater Res B Appl Biomater, 2009. **91**(2): p. 572-8.
217. Linley, E., et al., *Use of hydrogen peroxide as a biocide: new consideration of its mechanisms of biocidal action.* Journal of Antimicrobial Chemotherapy, 2012. **67**(7): p. 1589-1596.
218. McDonnell, G., *The Use of Hydrogen Peroxide for Disinfection and Sterilization Applications*, in *PATAI'S Chemistry of Functional Groups*. 2014.
219. Näther, N., et al., *Detection of Hydrogen Peroxide (H(2)O(2)) at Exposed Temperatures for Industrial Processes.* Sensors (Basel, Switzerland), 2006. **6**(4): p. 308-317.
220. Akkus, O., R.M. Belaney, and P. Das, *Free radical scavenging alleviates the biomechanical impairment of gamma radiation sterilized bone tissue.* J Orthop Res, 2005. **23**(4): p. 838-45.
221. Dickerson, D.A., et al., *In vitro and in vivo evaluation of orthopedic interface repair using a tissue scaffold with a continuous hard tissue-soft tissue transition.* Journal of Orthopaedic Surgery and Research, 2013. **8**: p. 18-18.
222. Leow-Dyke, S.F.R., P; Kearney, JN;, *Evaluation of copper and hydrogen peroxide treatments on the biology, biomechanics and cytotoxicity of decellularised dermal allografts* Tissue Engineering Part C: Methods, 2015. **Online Ahead of Print**.
223. Cao, H. and Y. Wang, *Quantification of oxidative single-base and intrastrand cross-link lesions in unmethylated and CpG-methylated DNA induced by Fenton-type reagents.* Nucleic Acids Research, 2007. **35**(14): p. 4833-4844.
224. Badylak, S.F., D.O. Freytes, and T.W. Gilbert, *Extracellular matrix as a biological scaffold material: structure and function.* Acta biomaterialia, 2009. **5**(1): p. 1-13.
225. Grant, R.A., R.W. Cox, and C.M. Kent, *The effects of gamma irradiation on the structure and reactivity of native and cross-linked collagen fibres.* Journal of Anatomy, 1973. **115**(Pt 1): p. 29-43.
226. Helder, M.R.K., et al., *Low-Dose Gamma Irradiation of Decellularized Heart Valves Results in Tissue Injury in Vitro and in Vivo.* The Annals of thoracic surgery, 2016. **101**(2): p. 667-674.
227. Johnson, C.M., et al., *The feasibility of gamma radiation sterilization for decellularized tracheal grafts.* Laryngoscope, 2017. **127**(8): p. E258-E264.

228. Smith, C.W. and J.N. Kearney, *The effects of irradiation and hydration upon the mechanical properties of tendon.* Journal of Materials Science: Materials in Medicine, 1996. **7**(11): p. 645-650.
229. Somers, P., et al., *Gamma radiation alters the ultrastructure in tissue-engineered heart valve scaffolds.* Tissue Eng Part A, 2009. **15**(11): p. 3597-604.
230. Dziedzic-Goclawska, A., et al., *Irradiation as a safety procedure in tissue banking.* Cell Tissue Bank, 2005. **6**(3): p. 201-19.
231. Wei, W., et al., *Fractionation of 50kGy electron beam irradiation: Effects on biomechanics of human flexor digitorum superficialis tendons treated with ascorbate.* Journal of Biomechanics, 2013. **46**(4): p. 658-661.
232. Asquith, J.C., *The effect of dose fractionation on gamma-radiation induced mutations in mammalian cells.* Mutat Res, 1977. **43**(1): p. 91-100.
233. Kajbafzadeh, A.M., et al., *Determining the optimal decellularization and sterilization protocol for preparing a tissue scaffold of a human-sized liver tissue.* Tissue Eng Part C Methods, 2013. **19**(8): p. 642-51.
234. Schmidt, T., et al., *Sterilization with electron beam irradiation influences the biomechanical properties and the early remodeling of tendon allografts for reconstruction of the anterior cruciate ligament (ACL).* Cell and Tissue Banking, 2012. **13**(3): p. 387-400.
235. Hodde, J., A. Janis, and M. Hiles, *Effects of sterilization on an extracellular matrix scaffold: part II. Bioactivity and matrix interaction.* Journal of Materials Science: Materials in Medicine, 2007. **18**(4): p. 545-550.
236. Woon, C.Y., et al., *Optimization of human tendon tissue engineering: peracetic acid oxidation for enhanced reseeding of acellularized intrasynovial tendon.* Plast Reconstr Surg, 2011. **127**(3): p. 1107-17.
237. Huang, Q., et al., *Production of a sterilised decellularised tendon allograft for clinical use.* Cell and Tissue Banking, 2013. **14**(4): p. 645-654.
238. Aldridge, A., et al., *Development and characterisation of a large diameter decellularised vascular allograft.* Cell Tissue Bank, 2017.
239. Granados, M., et al., *Development and Characterization of a Porcine Mitral Valve Scaffold for Tissue Engineering.* J Cardiovasc Transl Res, 2017.
240. Luo, J., et al., *Development and Characterization of Acellular Porcine Pulmonary Valve Scaffolds for Tissue Engineering.* Tissue Engineering. Part A, 2014. **20**(21-22): p. 2963-2974.
241. Bolland, F., et al., *Development and characterisation of a full-thickness acellular porcine bladder matrix for tissue engineering.* Biomaterials, 2007. **28**(6): p. 1061-1070.
242. Bonenfant, N.R., et al., *The Effects of Storage and Sterilization on De-Cellularized and Re-Cellularized Whole Lung.* Biomaterials, 2013. **34**(13): p. 3231-3245.
243. Balestrini, J.L., et al., *Sterilization of Lung Matrices by Supercritical Carbon Dioxide.* Tissue Eng Part C Methods, 2016. **22**(3): p. 260-9.
244. Arizono, T., et al., *Ethylene oxide sterilization of bone grafts. Residual gas concentration and fibroblast toxicity.* Acta Orthop Scand, 1994. **65**(6): p. 640-2.
245. Lomas, R.J., et al., *An evaluation of the capacity of differently prepared demineralised bone matrices (DBM) and toxic residuals of ethylene oxide*

(EtOx) to provoke an inflammatory response in vitro. Biomaterials, 2001. **22**(9): p. 913-921.
246. Lutsenko, S., *Human copper homeostasis: a network of interconnected pathways.* Current opinion in chemical biology, 2010. **14**(2): p. 211-217.
247. Semisch, A., et al., *Cytotoxicity and genotoxicity of nano - and microparticulate copper oxide: role of solubility and intracellular bioavailability.* Part Fibre Toxicol, 2014. **11**: p. 10.
248. Das, S.K. and K. Ray, *Wilson's disease: an update.* Nat Clin Pract Neurol, 2006. **2**(9): p. 482-93.
249. Taly, A.B., et al., *Wilson disease: description of 282 patients evaluated over 3 decades.* Medicine (Baltimore), 2007. **86**(2): p. 112-21.
250. Edwards, C.A. and W.D. O'Brien, Jr., *Modified assay for determination of hydroxyproline in a tissue hydrolyzate.* Clin Chim Acta, 1980. **104**(2): p. 161-7.
251. Goll, D.E., R.W. Bray, and W.G. Hoekstra, *Age-Associated Changes in Muscle Composition. The Isolation and Properties of a Collagenous Residue from Bovine Musclea.* Journal of Food Science, 1963. **28**(5): p. 503-509.
252. Cross, H.R., Z.L. Carpenter, and G.C. Smith, *EFFECTS OF INTRAMUSCULAR COLLAGEN AND ELASTIN ON BOVINE MUSCLE TENDERNESS.* Journal of Food Science, 1973. **38**(6): p. 998-1003.
253. Farndale, R.W., C.A. Sayers, and A.J. Barrett, *A direct spectrophotometric microassay for sulfated glycosaminoglycans in cartilage cultures.* Connect Tissue Res, 1982. **9**(4): p. 247-8.
254. Stern, I. and B. Shapiro, *A Rapid and Simple Method for the Determination of Esterified Fatty Acids and for Total Fatty Acids in Blood.* Journal of Clinical Pathology, 1953. **6**(2): p. 158-160.
255. Kawecki, M., et al., *A review of decellurization methods caused by an urgent need for quality control of cell-free extracellular matrix' scaffolds and their role in regenerative medicine.* J Biomed Mater Res B Appl Biomater, 2017.
256. Ning, L.-J., et al., *The utilization of decellularized tendon slices to provide an inductive microenvironment for the proliferation and tenogenic differentiation of stem cells.* Biomaterials, 2015. **52**: p. 539-550.
257. Flynn, L.E., *The use of decellularized adipose tissue to provide an inductive microenvironment for the adipogenic differentiation of human adipose-derived stem cells.* Biomaterials, 2010. **31**(17): p. 4715-4724.
258. Zheng, M.H., et al., *Porcine small intestine submucosa (SIS) is not an acellular collagenous matrix and contains porcine DNA: possible implications in human implantation.* J Biomed Mater Res B Appl Biomater, 2005. **73**(1): p. 61-7.
259. Booth, C., et al., *Tissue engineering of cardiac valve prostheses I: development and histological characterization of an acellular porcine scaffold.* J Heart Valve Dis, 2002. **11**(4): p. 457-62.
260. Gilbert, T.W., J. Freund, and S.F. Badylak, *Quantification of DNA in Biologic Scaffold Materials.* The Journal of surgical research, 2009. **152**(1): p. 135-139.
261. Wong, M.L., et al., *Stepwise solubilization-based antigen removal for xenogeneic scaffold generation in tissue engineering.* Acta Biomater, 2013. **9**(5): p. 6492-501.

262. Park, S., et al., *Removal of Alpha-Gal Epitopes from Porcine Aortic Valve and Pericardium using Recombinant Human Alpha Galactosidase A.* Journal of Korean Medical Science, 2009. **24**(6): p. 1126-1131.
263. Jorge-Herrero, E., et al., *Inhibition of the calcification of porcine valve tissue by selective lipid removal.* Biomaterials, 1994. **15**(10): p. 815-20.
264. Ahyayauch, H., et al., *Detergent Effects on Membranes at Subsolubilizing Concentrations: Transmembrane Lipid Motion, Bilayer Permeabilization, and Vesicle Lysis/Reassembly Are Independent Phenomena.* Langmuir, 2010. **26**(10): p. 7307-7313.
265. White, L.J., et al., *The impact of detergents on the tissue decellularization process: A ToF-SIMS study.* Acta Biomater, 2017. **50**: p. 207-219.
266. Ferng, A.S.C., A.M; Marsh, K.M; Qu, N; Medina, A.O; Bajaj, N; Palomares, D; Iwanski, J; Tran, P.l; Lotun, K; Johnson, K; Khalpey, Z., *Acellular porcine heart matrices: whole organ decellularization with 3D-bioscaffold & vascular preservation.* Jounral of Clinical and Translational Research, 2017. **3**(2).
267. Oliveira, A.C., et al., *Evaluation of Small Intestine Grafts Decellularization Methods for Corneal Tissue Engineering.* PLoS ONE, 2013. **8**(6): p. e66538.
268. Seddon, A.M., P. Curnow, and P.J. Booth, *Membrane proteins, lipids and detergents: not just a soap opera.* Biochimica et Biophysica Acta (BBA) - Biomembranes, 2004. **1666**(1–2): p. 105-117.
269. Faulk, D.M., et al., *The Effect of Detergents on the Basement Membrane Complex of a Biologic Scaffold Material.* Acta biomaterialia, 2014. **10**(1): p. 10.1016/j.actbio.2013.09.006.
270. Bhuyan, A.K., *On the mechanism of SDS-induced protein denaturation.* Biopolymers, 2010. **93**(2): p. 186-99.
271. Lee, A., et al., *Denaturation of Proteins by SDS and by Tetra-alkylammonium Dodecyl Sulfates.* Langmuir : the ACS journal of surfaces and colloids, 2011. **27**(18): p. 11560-11574.
272. Roosens, A., et al., *Impact of Detergent-Based Decellularization Methods on Porcine Tissues for Heart Valve Engineering.* Annals of Biomedical Engineering, 2016. **44**(9): p. 2827-2839.
273. Dahl, S.L.M., et al., *Decellularized Native and Engineered Arterial Scaffolds for Transplantation.* Cell Transplantation, 2003. **12**(6): p. 659-666.
274. Grauss, R.W., et al., *Decellularization of rat aortic valve allografts reduces leaflet destruction and extracellular matrix remodeling.* The Journal of Thoracic and Cardiovascular Surgery, 2003. **126**(6): p. 2003-2010.
275. Nara, S., et al., *Preservation of biomacromolecular composition and ultrastructure of a decellularized cornea using a perfusion bioreactor.* RSC Advances, 2016. **6**(3): p. 2225-2240.
276. Ducheyne, P., *Comprehensive Biomaterials*. Vol. 1. 2011: Elsevier.
277. Petersen, T.H., et al., *Tissue-engineered lungs for in vivo implantation.* Science, 2010. **329**(5991): p. 538-41.
278. O'Neill, J.D., et al., *Decellularization of human and porcine lung tissues for pulmonary tissue engineering.* Ann Thorac Surg, 2013. **96**(3): p. 1046-55; discussion 1055-6.

279. Cebotari, S., et al., *Detergent decellularization of heart valves for tissue engineering: toxicological effects of residual detergents on human endothelial cells.* Artif Organs, 2010. **34**(3): p. 206-10.
280. Cox, B. and A. Emili, *Tissue subcellular fractionation and protein extraction for use in mass-spectrometry-based proteomics.* Nat Protoc, 2006. **1**(4): p. 1872-8.
281. Syed, O., et al., *Evaluation of decellularization protocols for production of tubular small intestine submucosa scaffolds for use in oesophageal tissue engineering.* Acta biomaterialia, 2014. **10**(12): p. 5043-5054.
282. Rosario, D.J., et al., *Decellularization and sterilization of porcine urinary bladder matrix for tissue engineering in the lower urinary tract.* Regenerative Medicine, 2008. **3**(2): p. 145-156.
283. Faulk, D.M., J.D. Wildemann, and S.F. Badylak, *Decellularization and Cell Seeding of Whole Liver Biologic Scaffolds Composed of Extracellular Matrix.* Journal of Clinical and Experimental Hepatology, 2015. **5**(1): p. 69-80.
284. Yamniuk, A.P. and H.J. Vogel, *Calcium- and magnesium-dependent interactions between calcium- and integrin-binding protein and the integrin αIIb cytoplasmic domain.* Protein Science : A Publication of the Protein Society, 2005. **14**(6): p. 1429-1437.
285. Deeken, C.R., et al., *Method of preparing a decellularized porcine tendon using tributyl phosphate.* Journal of Biomedical Materials Research Part B: Applied Biomaterials, 2011. **96B**(2): p. 199-206.
286. Gratzer, P.F., *Methods for Tissue Decellularisation*, USPTO, Editor. 2016, Decell Technologies Inc, Gratzer Paul Frank: USA.
287. Fehily, D.B., S.A; Kearney, J.N; Wolfinbarger, L., *Tissue and Cell Processing: An Essential Guide*. 2012: John Wiley & Sons, Ltd.
288. Healy, K.H., D.W; Grainger, D.W; Kirkpatrick, J., *Comprehensive Biomaterials II*. 2017: Elsevier.
289. Bronzino, J.D.P., D.R; , *Tissue Engineering and Artificial Organs*. 2006: CRC Press: Taylor and Francis
290. Zou, Y. and Y. Zhang, *Mechanical evaluation of decellularized porcine thoracic aorta.* The Journal of surgical research, 2012. **175**(2): p. 359-368.
291. Kasimir, M.T., et al., *Comparison of different decellularization procedures of porcine heart valves.* Int J Artif Organs, 2003. **26**(5): p. 421-7.
292. Rana, D., et al., *Development of decellularized scaffolds for stem cell-driven tissue engineering.* J Tissue Eng Regen Med, 2015.
293. Rahman, S., et al., *Optimising the decellularization of human elastic cartilage with trypsin for future use in ear reconstruction.* Scientific Reports, 2018. **8**(1): p. 3097.
294. Poornejad, N., et al., *Freezing/Thawing without Cryoprotectant Damages Native but not Decellularized Porcine Renal Tissue.* Organogenesis, 2015. **11**(1): p. 30-45.
295. Liu, Q.W., H., *Tissue Regeneration: Where Nano-structure Meets Biology*, in *Frontiers in Nanobiomedical Research: Volume 2*, Q.W. Liu, H., Editor. 2014, World Scientific
296. Venkatasubramanian, R.T., et al., *Effects of freezing and cryopreservation on the mechanical properties of arteries.* Ann Biomed Eng, 2006. **34**(5): p. 823-32.

297. Montoya, C.V. and P.S. McFetridge, *Preparation of Ex Vivo–Based Biomaterials Using Convective Flow Decellularization.* Tissue Eng Part C Methods, 2009. **15**(2): p. 191-200.
298. Ingham, E.B., C; Fisher, J., *Decellularisation of Matrices*, U.S.P.a.T. Office, Editor. 2004, Ingham, E; Booth, C; Fisher, J.
299. Hogg, P., et al., *Development of a decellularised dermis.* Cell Tissue Bank, 2013. **14**(3): p. 465-74.
300. Wilshaw, S.P., et al., *Production of an acellular amniotic membrane matrix for use in tissue engineering.* Tissue Eng, 2006. **12**(8): p. 2117-29.
301. Wilcox, H.E., et al., *Biocompatibility and recellularization potential of an acellular porcine heart valve matrix.* J Heart Valve Dis, 2005. **14**(2): p. 228-36; discussion 236-7.
302. Stapleton, T.W., et al., *Development and characterization of an acellular porcine medial meniscus for use in tissue engineering.* Tissue Eng Part A, 2008. **14**(4): p. 505-18.
303. Jones, G.L.L., A; Berry, H; Fisher, J; Ingham, E., *Decellularisation of Super Flexor Tendon.* European Cells and Materials, 2011. **22**(Supplement 33): p. 13.
304. Fermor, H.L., et al., *Development and characterisation of a decellularised bovine osteochondral biomaterial for cartilage repair.* Journal of Materials Science: Materials in Medicine, 2015. **26**(5): p. 1-11.
305. Schulze-Tanzil, G., et al., *Decellularized Tendon Extracellular Matrix—A Valuable Approach for Tendon Reconstruction?* Cells, 2012. **1**(4): p. 1010-1028.
306. Akhyari, P., et al., *The quest for an optimized protocol for whole-heart decellularization: a comparison of three popular and a novel decellularization technique and their diverse effects on crucial extracellular matrix qualities.* Tissue Eng Part C Methods, 2011. **17**(9): p. 915-26.
307. Ren, H., et al., *Evaluation of two decellularization methods in the development of a whole-organ decellularized rat liver scaffold.* Liver Int, 2013. **33**(3): p. 448-58.
308. Petersen, T.H., et al., *Matrix composition and mechanics of decellularized lung scaffolds.* Cells Tissues Organs, 2012. **195**(3): p. 222-31.
309. Xu, H., et al., *Comparison of Decellularization Protocols for Preparing a Decellularized Porcine Annulus Fibrosus Scaffold.* PLoS ONE, 2014. **9**(1): p. e86723.
310. Inc, A., *Avance: Process Matters*. 2013.
311. Liao, J., E.M. Joyce, and M.S. Sacks, *EFFECTS OF DECELLULARIZATION ON THE MECHANICAL AND STRUCTURAL PROPERTIES OF THE PORCINE AORTIC VALVE LEAFLET.* Biomaterials, 2008. **29**(8): p. 1065-1074.
312. Wilson, S.L., et al., *Keeping an Eye on Decellularized Corneas: A Review of Methods, Characterization and Applications.* Journal of Functional Biomaterials, 2013. **4**(3): p. 114-161.
313. Gustafson, K.J., et al., *Human distal sciatic nerve fascicular anatomy: implications for ankle control using nerve-cuff electrodes.* J Rehabil Res Dev, 2012. **49**(2): p. 309-21.
314. Perlas, A., et al., *Ultrasound-guided popliteal block through a common paraneural sheath versus conventional injection: a prospective,*

randomized, double-blind study. Reg Anesth Pain Med, 2013. **38**(3): p. 218-25.
315. Groth, C.G., *The potential advantages of transplanting organs from pig to man: A transplant Surgeon's view.* Indian Journal of Urology : IJU : Journal of the Urological Society of India, 2007. **23**(3): p. 305-309.
316. Sundaram, S., et al., *Tissue-Engineered Vascular Grafts Created From Human Induced Pluripotent Stem Cells.* Stem Cells Translational Medicine, 2014. **3**(12): p. 1535-1543.
317. Xu, H., et al., *A porcine-derived acellular dermal scaffold that supports soft tissue regeneration: removal of terminal galactose-alpha-(1,3)-galactose and retention of matrix structure.* Tissue Eng Part A, 2009. **15**(7): p. 1807-19.
318. Jønsson, K.L., et al., *IFI16 is required for DNA sensing in human macrophages by promoting production and function of cGAMP.* Nature Communications, 2017. **8**: p. 14391.
319. Paludan, S.R. and A.G. Bowie, *Immune sensing of DNA.* Immunity, 2013. **38**(5): p. 870-880.
320. Fercana, G., et al., *Platform Technologies for Decellularization, Tunic-Specific Cell Seeding, and In Vitro Conditioning of Extended Length, Small Diameter Vascular Grafts.* Tissue Eng Part C Methods, 2014. **20**(12): p. 1016-1027.
321. A., C.M., et al., *Regulation of Schwann cell function by the extracellular matrix.* Glia, 2008. **56**(14): p. 1498-1507.
322. Azhim, A., et al., *The use of sonication treatment to decellularize aortic tissues for preparation of bioscaffolds.* J Biomater Appl, 2014. **29**(1): p. 130-41.
323. Koch, H., et al., *Tissue Engineering of Ureteral Grafts: Preparation of Biocompatible Crosslinked Ureteral Scaffolds of Porcine Origin.* Frontiers in Bioengineering and Biotechnology, 2015. **3**(89).
324. Luo, L., et al., *Decellularization of porcine articular cartilage explants and their subsequent repopulation with human chondroprogenitor cells.* J Mech Behav Biomed Mater, 2015. **55**: p. 21-31.
325. White, L.J., et al., *The impact of detergents on the tissue decellularization process: a ToF-SIMS study.* Acta biomaterialia, 2017. **50**: p. 207-219.
326. Helliwell, J.A., et al., *Development and characterisation of a low-concentration sodium dodecyl sulphate decellularised porcine dermis.* Journal of Tissue Engineering, 2017. **8**: p. 2041731417724011.
327. Tayyebeh, V., et al., *Decellularization of human donor aortic and pulmonary valved conduits using low concentration sodium dodecyl sulfate.* J Tissue Eng Regen Med, 2018. **12**(2): p. e841-e853.
328. Hill, R.E. and P.E. Williams, *A quantitative analysis of perineurial cell basement membrane collagen IV, laminin and fibronectin in diabetic and non-diabetic human sural nerve.* Journal of Anatomy, 2002. **201**(2): p. 185-192.
329. Jones, G., et al., *Decellularization and Characterization of Porcine Superflexor Tendon: A Potential Anterior Cruciate Ligament Replacement.* Tissue Engineering. Part A, 2017. **23**(3-4): p. 124-134.
330. Vavken, P., S. Joshi, and M.M. Murray, *TRITON-X Is Most Effective among Three Decellularization Agents for ACL Tissue Engineering.*

Journal of orthopaedic research : official publication of the Orthopaedic Research Society, 2009. **27**(12): p. 1612-1618.
331. Maravilla, K.R. and B.C. Bowen, *Imaging of the peripheral nervous system: evaluation of peripheral neuropathy and plexopathy.* AJNR Am J Neuroradiol, 1998. **19**(6): p. 1011-23.
332. Boezaart, A.P., *The anatomical foundations of regional anaethesia and acute pain medicine: Microanatomy; Sonoanatomy; Funtional Anatomy*. 2016: Bentham Science Publishers.
333. von Woedtke, T. and A. Kramer, *The limits of sterility assurance.* GMS Krankenhaushygiene interdisziplinär, 2008. **3**(3): p. Doc19.
334. BSI, *BS EN 556-1: Sterilization of medical devices. Requirements for medical devices to be designated "STERILE". Requirements for terminally sterilized medical devices*. 2001, BSI: British Standards Institution. p. 12.
335. Singh, R., D. Singh, and A. Singh, *Radiation sterilization of tissue allografts: A review.* World Journal of Radiology, 2016. **8**(4): p. 355-369.
336. Edwards, J.H., et al., *The effects of irradiation on the biological and biomechanical properties of an acellular porcine superflexor tendon graft for cruciate ligament repair.* Journal of biomedical materials research. Part B, Applied biomaterials, 2017. **105**(8): p. 2477-2486.
337. Milton-Barker, J., *Development of Methods for Assessment of the Effects of Sterilisation on Acellular Vascular Grafts*. 2015, University of Leeds.
338. Sheridan, W.S., G.P. Duffy, and B.P. Murphy, *Optimum Parameters for Freeze-Drying Decellularized Arterial Scaffolds.* Tissue Eng Part C Methods, 2013. **19**(12): p. 981-990.
339. Polak, R. and R.N. Pitombo, *Care during freeze-drying of bovine pericardium tissue to be used as a biomaterial: a comparative study.* Cryobiology, 2011. **63**(2): p. 61-6.
340. Graham, J., et al., *A chondroitinase-treated, decellularized nerve allograft compares favorably to the cellular isograft in rat peripheral nerve repair*. Vol. 2. 2009. 19-29.
341. Nguyen, H., D.A.F. Morgan, and M.R. Forwood, *Sterilization of allograft bone: effects of gamma irradiation on allograft biology and biomechanics.* Cell and Tissue Banking, 2007. **8**(2): p. 93-105.
342. Bechtold, J.E., et al., *The effects of freeze-drying and ethylene oxide sterilization on the mechanical properties of human patellar tendon.* Am J Sports Med, 1994. **22**(4): p. 562-6.
343. Laurell, L., et al., *Treatment of intrabony defects by different surgical procedures. A literature review.* J Periodontol, 1998. **69**(3): p. 303-13.
344. Wilshaw, S.-R., P; Berry, H; Kearney, JN; Homer-Vanniasinkam, S; Fisher, J and Ingham, E., *Development and Characterization of Acellular Allogeneic Arterial Matrices.* Tissue Engineering Part A, 2012. **18**(5-6): p. 471-483.
345. Nail, S.L., et al., *Fundamentals of freeze-drying.* Pharm Biotechnol, 2002. **14**: p. 281-360.
346. Rey, L., *Freeze-Drying/Lyophilization of Pharmaceutical and Biological Products*. 2010: CRC Press.
347. Meyer, J.P., K.E. McAvoy, and J. Jiang, *Rehydration Capacities and Rates for Various Porcine Tissues after Dehydration.* PLoS ONE, 2013. **8**(9): p. e72573.

348. Williams, M.J., et al., *Differences in the Microstructure and Biomechanical Properties of the Recurrent Laryngeal Nerve as a Function of Age and Location.* Journal of Biomechanical Engineering, 2014. **136**(8): p. 0810081-0810089.
349. K., H.S., et al., *Misdirection of regenerating axons and functional recovery following sciatic nerve injury in rats.* Journal of Comparative Neurology, 2011. **519**(1): p. 21-33.
350. Napoli, I., et al., *A Central Role for the ERK-Signaling Pathway in Controlling Schwann Cell Plasticity and Peripheral Nerve Regeneration In Vivo.* Neuron, 2012. **73**(4): p. 729-742.
351. Hoffman-Kim, D., J.A. Mitchel, and R.V. Bellamkonda, *Topography, Cell Response, and Nerve Regeneration.* Annual review of biomedical engineering, 2010. **12**: p. 203-231.
352. de Ruiter, G.C., et al., *Accuracy of motor axon regeneration across autograft, single-lumen, and multichannel poly(lactic-co-glycolic acid) nerve tubes.* Neurosurgery, 2008. **63**(1): p. 144-155.
353. Yurchenco, P.D., *Basement Membranes: Cell Scaffoldings and Signaling Platforms.* Cold Spring Harbor Perspectives in Biology, 2011. **3**(2): p. a004911.
354. Shacter, E., *Protein oxidative damage.* Methods Enzymol, 2000. **319**: p. 428-36.
355. Rahman, M., *Handbook of Food Preservation*. Second ed. 2007: CRC Press.
356. Jones, C.W., *Applications of Hydrogen Peroxide and Derivatives*. 1999: The Royal Society of Chemistry.
357. Khoshnoodi, J., V. Pedchenko, and B. Hudson, *Mammalian Collagen IV.* Microscopy Research and Technique, 2008. **71**(5): p. 357-370.
358. Kitis, M., *Disinfection of wastewater with peracetic acid: a review.* Environment International, 2004. **30**(1): p. 47-55.
359. Alexander, P., M. Fox, and R.F. Hudson, *The reaction of oxidizing agents with wool. 5. The oxidation products of the disulphide bond and the formation of a sulphonamide in the peptide chain.* Biochemical Journal, 1951. **49**(2): p. 129-138.
360. Van de Pol, G.J., et al., *Supercritical Carbon Dioxide–Sterilized Bone Allograft in the Treatment of Tunnel Defects in 2-Stage Revision Anterior Cruciate Ligament Reconstruction: A Histologic Evaluation.* Arthroscopy: The Journal of Arthroscopic & Related Surgery, 2018. **34**(3): p. 706-713.
361. Wallquist, W., et al., *Laminin chains in rat and human peripheral nerve: Distribution and regulation during development and after axonal injury.* The Journal of Comparative Neurology, 2002. **454**(3): p. 284-293.
362. Paavola, K.J., et al., *Type IV collagen is an activating ligand for the adhesion G protein-coupled receptor GPR126.* Science signaling, 2014. **7**(338): p. ra76-ra76.
363. Lein, P.J., et al., *The NC1 domain of type IV collagen promotes axonal growth in sympathetic neurons through interaction with the alpha 1 beta 1 integrin.* J Cell Biol, 1991. **113**(2): p. 417-28.
364. Chernousov, M.A., R.C. Stahl, and D.J. Carey, *Schwann cell type V collagen inhibits axonal outgrowth and promotes Schwann cell migration via distinct adhesive activities of the collagen and noncollagen domains.* J Neurosci, 2001. **21**(16): p. 6125-35.

365. Bacallao, K. and P.V. Monje, *Requirement of cAMP Signaling for Schwann Cell Differentiation Restricts the Onset of Myelination.* PLoS ONE, 2015. **10**(2): p. e0116948.
366. Willits, R.K. and S.L. Skornia, *Effect of collagen gel stiffness on neurite extension.* J Biomater Sci Polym Ed, 2004. **15**(12): p. 1521-31.
367. Breda, A.V., N.F; Norberto de Souza, O; Garrat, R.C., *Protein Structure, Modelling and Applications*, in *Bioinformatics in Tropical Disease Research: A Practical and Case-Study Approach* D.A. Gruber A, Huynh C, et al., Editor. 2006, National Center for Biotechnology Information.
368. Saito, M. and K. Marumo, *Collagen cross-links as a determinant of bone quality: a possible explanation for bone fragility in aging, osteoporosis, and diabetes mellitus.* Osteoporos Int, 2010. **21**(2): p. 195-214.
369. Samouillan, V., et al., *The Use of Thermal Techniques for the Characterization and Selection of Natural Biomaterials.* Journal of Functional Biomaterials, 2011. **2**(3): p. 230-248.
370. Sun, W.Q., et al., *Process-induced extracellular matrix alterations affect the mechanisms of soft tissue repair and regeneration.* Journal of Tissue Engineering, 2013. **4**: p. 2041731413505305.
371. Russell, N., et al., *The effect of sterilization on the dynamic mechanical properties of paired rabbit cortical bone.* J Biomech, 2013. **46**(10): p. 1670-5.
372. Nichols, A.B., D.Cp; Christopher, R., *Studies on the Sterilization of Human Bone and Tendon Musculoskeletal Allograft Tissue Using Supercritical Carbon Dioxide.* J. Orthopaedics, 2009. **6**(9).
373. Liang, X. and S.A. Boppart, *Biomechanical Properties of In Vivo Human Skin From Dynamic Optical Coherence Elastography.* IEEE transactions on bio-medical engineering, 2010. **57**(4): p. 953-959.
374. C., J.A., et al., *Piezoelectric and mechanical properties in bovine cornea.* Journal of Biomedical Materials Research Part A, 2003. **66A**(2): p. 260-265.
375. Rabotyagova, O.S., P. Cebe, and D.L. Kaplan, *Collagen Structural Hierarchy and Susceptibility to Degradation by Ultraviolet Radiation.* Materials science & engineering. C, Materials for biological applications, 2008. **28**(8): p. 1420-1429.
376. Mogilner, I.G., G. Ruderman, and J.R. Grigera, *Collagen stability, hydration and native state.* Journal of Molecular Graphics and Modelling, 2002. **21**(3): p. 209-213.
377. Leikin, S., et al., *Raman spectral evidence for hydration forces between collagen triple helices.* Proceedings of the National Academy of Sciences of the United States of America, 1997. **94**(21): p. 11312-11317.
378. Jastrzebska, M., et al., *New insight into the shortening of the collagen fibril D-period in human cornea.* Journal of Biomolecular Structure and Dynamics, 2017. **35**(3): p. 551-563.
379. Wells, H.C., et al., *Collagen Fibril Intermolecular Spacing Changes with 2-Propanol: A Mechanism for Tissue Stiffness.* ACS Biomaterials Science & Engineering, 2017. **3**(10): p. 2524-2532.
380. Cheah, M. and M.R. Andrews, *Integrin Activation: Implications for Axon Regeneration.* Cells, 2018. **7**(3): p. 20.
381. Kerstein, P.C.N.I., R.H; GOmez, T.M., *Neuronal Mechanics and Transport*, D.S.M. Suter, K.E., Editor. 2016, Frontiers Media SA: Frontiers in Cellular Neuroscience.

382. Caterina, A., et al., *Ionic channels and neuropathic pain: Phisiopatology and applications.* Journal of Cellular Physiology, 2008. **215**(1): p. 8-14.
383. Driscoll, P.J., M.A. Glasby, and G.M. Lawson, *An in vivo study of peripheral nerves in continuity: biomechanical and physiological responses to elongation.* J Orthop Res, 2002. **20**(2): p. 370-5.
384. Clark, W.L., et al., *Nerve tension and blood flow in a rat model of immediate and delayed repairs.* The Journal of Hand Surgery, 1992. **17**(4): p. 677-687.
385. Kolt, G.S.S.-M., L., *Physical Therapies in Sport and Exercise*. 2007: Elsevier.
386. L., Z., et al., *Cyclic mechanical stress modulates neurotrophic and myelinating gene expression of Schwann cells.* Cell Proliferation, 2015. **48**(1): p. 59-66.
387. Friede, R.L., *The Significance of Internode Length for Saltatory Conduction: Looking Back at the Age of 90.* Journal of Neuropathology & Experimental Neurology, 2017. **76**(4): p. 258-259.
388. Dilley, A. and G.M. Bove, *Resolution of Inflammation-Induced Axonal Mechanical Sensitivity and Conduction Slowing in C-Fiber Nociceptors.* The Journal of Pain, 2008. **9**(2): p. 185-192.
389. Shoulders, M.D. and R.T. Raines, *COLLAGEN STRUCTURE AND STABILITY.* Annual review of biochemistry, 2009. **78**: p. 929-958.
390. Hamer, A.J., I. Stockley, and R.A. Elson, *Changes in allograft bone irradiated at different temperatures.* J Bone Joint Surg Br, 1999. **81**(2): p. 342-4.
391. Eekhoff, J.D., F. Fang, and S.P. Lake, *Multiscale mechanical effects of native collagen cross-linking in tendon.* Connect Tissue Res, 2018: p. 1-13.
392. Bailey, A.J. and W.J. Tromans, *Effects of Ionizing Radiation on the Ultrastructure of Collagen Fibrils.* Radiation Research, 1964. **23**(1): p. 145-155.
393. Sun, W.Q. and P. Leung, *Calorimetric study of extracellular tissue matrix degradation and instability after gamma irradiation.* Acta biomaterialia, 2008. **4**(4): p. 817-826.
394. Mehendale, S., et al., *Use of irradiated bone graft for impaction grafting in acetabular revision surgery: a review of fifty consecutive cases.* Hip Int, 2009. **19**(2): p. 114-9.
395. Singh, R., et al., *Radiation processed amniotic membranes in the treatment of non-healing ulcers of different etiologies.* Cell Tissue Bank, 2004. **5**(2): p. 129-34.
396. Noriyuki, K., et al., *Evaluation of the thermal property of bovine intramuscular adipose tissue using differential scanning calorimetry.* Animal Science Journal, 2017. **88**(10): p. 1615-1622.
397. Sasaki, K., et al., *Differential scanning calorimetry of porcine adipose tissues.* Meat Science, 2006. **72**(4): p. 789-792.
398. Rodrigues, F.T., V.C.A. Martins, and A.M.G. Plepis, *Porcine skin as a source of biodegradable matrices: alkaline treatment and glutaraldehyde crosslinking.* Polímeros, 2010. **20**: p. 92-97.
399. Helling, A.L., et al., *In Vitro Enzymatic Degradation of Tissue Grafts and Collagen Biomaterials by Matrix Metalloproteinases: Improving the Collagenase Assay.* ACS Biomaterials Science & Engineering, 2017. **3**(9): p. 1922-1932.

400. Harper, E. and A.H. Kang, *Studies on the specificity of bacterial collagenase.* Biochemical and Biophysical Research Communications, 1970. **41**(2): p. 482-487.
401. Cavallo, J.A., et al., *Remodeling characteristics and biomechanical properties of a crosslinked versus a non-crosslinked porcine dermis scaffolds in a porcine model of ventral hernia repair.* Hernia : the journal of hernias and abdominal wall surgery, 2015. **19**(2): p. 207-218.
402. Johnson, P.J., et al., *Tissue engineered constructs for peripheral nerve surgery.* European surgery : ACA : Acta chirurgica Austriaca, 2013. **45**(3): p. 10.1007/s10353-013-0205-0.
403. Gordon, T., *Electrical Stimulation to Enhance Axon Regeneration After Peripheral Nerve Injuries in Animal Models and Humans.* Neurotherapeutics, 2016. **13**(2): p. 295-310.
404. Li, W., J. Zhou, and Y. Xu, *Study of the in vitro cytotoxicity testing of medical devices.* Biomedical Reports, 2015. **3**(5): p. 617-620.
405. Törnqvist, E., et al., *Strategic Focus on 3R Principles Reveals Major Reductions in the Use of Animals in Pharmaceutical Toxicity Testing.* PLoS ONE, 2014. **9**(7): p. e101638.
406. ISO, *ISO 10993-5: Biological evaluation of medical devices--Part 5: Tests for in vitro cytotoxicity*. 2009, International Organisation for Standardization. p. 34.
407. Morais, J.M., F. Papadimitrakopoulos, and D.J. Burgess, *Biomaterials/Tissue Interactions: Possible Solutions to Overcome Foreign Body Response.* The AAPS Journal, 2010. **12**(2): p. 188-196.
408. Stahl, E.C., et al., *Evaluation of the host immune response to decellularized lung scaffolds derived from α-Gal knockout pigs in a non-human primate model.* Biomaterials, 2018. **187**: p. 93-104.
409. He, H., J.R. Stone, and D.L. Perkins, *Analysis of differential immune responses induced by innate and adaptive immunity following transplantation.* Immunology, 2003. **109**(2): p. 185-196.
410. Allman, A.J., et al., *Xenogeneic extracellular matrix grafts elicit a TH2-restricted immune response.* Transplantation, 2001. **71**(11): p. 1631-40.
411. Louveau, A., T.H. Harris, and J. Kipnis, *Revisiting the Mechanisms of CNS Immune Privilege.* Trends in immunology, 2015. **36**(10): p. 569-577.
412. Clark, R.A., *Skin-resident T cells: the ups and downs of on site immunity.* The Journal of investigative dermatology, 2010. **130**(2): p. 362-370.
413. Ingulli, E., *Mechanism of cellular rejection in transplantation.* Pediatric Nephrology (Berlin, Germany), 2010. **25**(1): p. 61-74.
414. Illigens, B.M., et al., *Dual effects of the alloresponse by Th1 and Th2 cells on acute and chronic rejection of allotransplants.* European journal of immunology, 2009. **39**(11): p. 3000-3009.
415. Muraille, E., O. Leo, and M. Moser, *Th1/Th2 Paradigm Extended: Macrophage Polarization as an Unappreciated Pathogen-Driven Escape Mechanism?* Frontiers in Immunology, 2014. **5**: p. 603.
416. Niederkorn, J.Y., et al., *Allergic Conjunctivitis Exacerbates Corneal Allograft Rejection by Activating Th1 and Th2 Alloimmune Responses.* The Journal of Immunology, 2010. **184**(11): p. 6076-6083.
417. Allman, A.J., et al., *XENOGENEIC EXTRACELLULAR MATRIX GRAFTS ELICIT A TH2-RESTRICTED IMMUNE RESPONSE1.* Transplantation, 2001. **71**(11): p. 1631-1640.

418. Ansaloni, L., et al., *Immune response to small intestinal submucosa (surgisis) implant in humans: preliminary observations.* J Invest Surg, 2007. **20**(4): p. 237-41.
419. Martinez, F.O. and S. Gordon, *The M1 and M2 paradigm of macrophage activation: time for reassessment.* F1000Prime Reports, 2014. **6**: p. 13.
420. Minutti, C.M., et al., *Tissue-specific contribution of macrophages to wound healing.* Seminars in Cell & Developmental Biology, 2017. **61**: p. 3-11.
421. Badylak, S.F., et al., *Macrophage phenotype as a determinant of biologic scaffold remodeling.* Tissue Eng Part A, 2008. **14**(11): p. 1835-42.
422. Arnold, L., et al., *Inflammatory monocytes recruited after skeletal muscle injury switch into antiinflammatory macrophages to support myogenesis.* J Exp Med, 2007. **204**(5): p. 1057-69.
423. Mahdavian Delavary, B., et al., *Macrophages in skin injury and repair.* Immunobiology, 2011. **216**(7): p. 753-62.
424. Nahrendorf, M., et al., *The healing myocardium sequentially mobilizes two monocyte subsets with divergent and complementary functions.* J Exp Med, 2007. **204**(12): p. 3037-3047.
425. E., F.E., et al., *Residual sodium dodecyl sulfate in decellularized muscle matrices leads to fibroblast activation in vitro and foreign body response in vivo.* J Tissue Eng Regen Med, 2018. **12**(3): p. e1704-e1715.
426. Rampersad, S.N., *Multiple Applications of Alamar Blue as an Indicator of Metabolic Function and Cellular Health in Cell Viability Bioassays.* Sensors (Basel, Switzerland), 2012. **12**(9): p. 12347-12360.
427. Zachari, M.A., et al., *Evaluation of The Alamarblue Assay for Adherent Cell Irradiation Experiments.* Dose-Response, 2014. **12**(2): p. 246-258.
428. Chang, L., et al., *Biocompatibility of human bone allograft powder processed by supercritical CO2.* Formosan Journal of Musculoskeletal Disorders, 2011. **2**(2): p. 55-61.
429. Wehmeyer, J.L., S. Natesan, and R.J. Christy, *Development of a Sterile Amniotic Membrane Tissue Graft Using Supercritical Carbon Dioxide.* Tissue Eng Part C Methods, 2015. **21**(7): p. 649-59.
430. Tucureanu, M.M., et al., *Lipopolysaccharide-induced inflammation in monocytes/macrophages is blocked by liposomal delivery of G(i)-protein inhibitor.* International journal of nanomedicine, 2017. **13**: p. 63-76.
431. Martin, I., et al., *Fasciola hepatica fatty acid binding protein inhibits TLR4 activation and suppresses the inflammatory cytokines induced by lipopolysaccharide in vitro and in vivo.* J Immunol, 2015. **194**(8): p. 3924-36.
432. Orenstein, S.B., et al., *Activation of human mononuclear cells by porcine biologic meshes in vitro.* Hernia, 2010. **14**(4): p. 401-407.
433. de Castro Brás, L.E., S. Shurey, and P.D. Sibbons, *Evaluation of crosslinked and non-crosslinked biologic prostheses for abdominal hernia repair.* Hernia, 2012. **16**(1): p. 77-89.
434. Alvarez, M.M., et al., *Delivery strategies to control inflammatory response: Modulating M1-M2 polarization in tissue engineering applications.* Journal of controlled release : official journal of the Controlled Release Society, 2016. **240**: p. 349-363.
435. Tomlinson, J.E., et al., *Temporal changes in macrophage phenotype after peripheral nerve injury.* J Neuroinflammation, 2018. **15**: p. 185.

436. Chen, P., X. Piao, and P. Bonaldo, *Role of macrophages in Wallerian degeneration and axonal regeneration after peripheral nerve injury.* Acta Neuropathologica, 2015. **130**(5): p. 605-618.
437. Stratton, J.A., et al., *Macrophages Regulate Schwann Cell Maturation after Nerve Injury.* Cell Reports, 2018. **24**(10): p. 2561-2572.e6.
438. Gomez-Sanchez, J.A., et al., *Schwann cell autophagy, myelinophagy, initiates myelin clearance from injured nerves.* J Cell Biol, 2015. **210**(1): p. 153-68.
439. Stratton, J.A. and P.T. Shah, *Macrophage polarization in nerve injury: do Schwann cells play a role?* Neural Regeneration Research, 2016. **11**(1): p. 53-57.
440. Taciak, B., et al., *Evaluation of phenotypic and functional stability of RAW 264.7 cell line through serial passages.* PLoS ONE, 2018. **13**(6): p. e0198943.
441. Hsieh, C.Y.C., et al., *Reducing the Foreign Body Reaction by Surface Modification with Collagen/Hyaluronic Acid Multilayered Films.* ISRN Biomaterials, 2014. **2014**: p. 8.
442. Swartzlander, M.D., et al., *Understanding the host response to cell-laden poly(ethylene glycol)-based hydrogels.* Biomaterials, 2013. **34**(4): p. 952-964.
443. Li, B., et al., *In vitro and in vivo responses of macrophages to magnesium-doped titanium.* Scientific Reports, 2017. **7**: p. 42707.
444. Ray, A. and B.N. Dittel, *Isolation of Mouse Peritoneal Cavity Cells.* Journal of Visualized Experiments : JoVE, 2010(35): p. 1488.
445. Rimmer, S., et al., *Cytocompatibility of poly(1,2 propandiol methacrylate) copolymer hydrogels and conetworks with or without alkyl amine functionality.* Biomaterials, 2009. **30**(13): p. 2468-78.
446. Damanik, F.F.R., et al., *Towards an in vitro model mimicking the foreign body response: tailoring the surface properties of biomaterials to modulate extracellular matrix.* Scientific Reports, 2014. **4**: p. 6325.
447. Du, L., et al., *Histological evaluation and biomechanical characterisation of an acellular porcine cornea scaffold.* Br J Ophthalmol, 2011. **95**(3): p. 410-4.
448. Wu, Q., et al., *Optimizing perfusion-decellularization methods of porcine livers for clinical-scale whole-organ bioengineering.* BioMed research international, 2015. **2015**: p. 785474-785474.
449. Baiguera, S., et al., *Long-term changes to in vitro preserved bioengineered human trachea and their implications for decellularized tissues.* Biomaterials, 2012. **33**(14): p. 3662-3672.
450. Duarte, A.S., A. Correia, and A.C. Esteves, *Bacterial collagenases - A review.* Crit Rev Microbiol, 2016. **42**(1): p. 106-26.
451. Herbert, A., et al., *The effects of irradiation dose and storage time following treatment on the viscoelastic properties of decellularised porcine super flexor tendon.* Journal of Biomechanics. **57**: p. 157-160.
452. Urbani, L., et al., *Long-term cryopreservation of decellularised oesophagi for tissue engineering clinical application.* PLoS ONE, 2017. **12**(6): p. e0179341.
453. Eagle, M.J., et al., *Validation of radiation dose received by frozen unprocessed and processed bone during terminal sterilisation.* Cell Tissue Bank, 2005. **6**(3): p. 221-30.

454. Hogg, P., et al., *Development of a terminally sterilised decellularised dermis.* Cell and Tissue Banking, 2015. **16**(3): p. 351-359.
455. Bottino, M.C., et al., *Freeze-dried acellular dermal matrix graft: Effects of rehydration on physical, chemical, and mechanical properties.* Dental Materials, 2009. **25**(9): p. 1109-1115.
456. Gabriel, A. and G.P. Maxwell, *AlloDerm RTU Integration and Clinical Outcomes When Used for Reconstructive Breast Surgery.* Plastic and reconstructive surgery. Global open, 2018. **6**(5): p. e1744-e1744.
457. NHSBT. *dCELL Human Dermis*. [cited 2019 2nd May]; Available from: https://www.nhsbt.nhs.uk/tissue-and-eye-services/products/skin/dcell-human-dermis/.
458. Axogen. *Avance Nerve Graft*. [cited 2019 2nd May]; Available from: https://www.axogeninc.com/avance-nerve-graft/.
459. He, B., et al., *Safety and efficacy evaluation of a human acellular nerve graft as a digital nerve scaffold: a prospective, multicentre controlled clinical trial.* J Tissue Eng Regen Med, 2015. **9**(3): p. 286-95.
460. Singh, R., et al., *Use of gamma-irradiated amniotic membrane for the healing of split skin graft donor site.* Tissue Engineering and Regenerative Medicine, 2013. **10**(3): p. 110-114.
461. Vargas, B. and J. Caton, *Acetabular revision with freeze-dried irradiated and chemically treated allograft: a minimum 5-year follow-up of 17 cases.* Int Orthop, 2009. **33**(1): p. 35-9.
462. Loty, B., et al., *Bone allografts sterilised by irradiation. Biological properties, procurement and results of 150 massive allografts.* Int Orthop, 1990. **14**(3): p. 237-42.
463. ISO, *BS EN ISO 14160 - Sterilization of health care products - Liquid chemical sterilizing agents for single-use medical devices utilizing animal tissues and their derivatives - Rquirements for characterization, development, validation and routine control of a sterilization process for medical devices.* 2011, ISO: International Organisation for Standardization. p. 46.
464. ISO, *BS EN ISO 11135 - Sterilization of health-care products. Ethylene oxide. Requirements for the development, validation and routine control of a sterilization process for medical devices* 2014, ISO: International Organization for Standardization. p. 94.
465. ISO, *BS EN ISO 11137 - Sterilization of health care products. Radiation. Requirements for development, validation and routine control of a sterilization process for medical devices.* 2015, ISO: International Organization for Standardization. p. 52.
466. Marsit, N., et al., *Substantiation of 25 kGy radiation sterilization dose for banked air dried amniotic membrane and evaluation of personnel skill in influencing finished product bioburden.* Cell and Tissue Banking, 2014. **15**(4): p. 603-611.
467. Setlow, B., et al., *Mechanism of Bacillus subtilis Spore Inactivation by and Resistance to Supercritical CO(2) plus Peracetic Acid.* Journal of Applied Microbiology, 2016. **120**(1): p. 57-69.
468. Binnet, M.S., B. Akan, and A. Kaya, *Lyophilised medial meniscus transplantations in ACL-deficient knees: a 19-year follow-up.* Knee Surg Sports Traumatol Arthrosc, 2012. **20**(1): p. 109-13.

469. Keselowsky, B.G., D.M. Collard, and A.J. García, *Surface chemistry modulates focal adhesion composition and signaling through changes in integrin binding.* Biomaterials, 2004. **25**(28): p. 5947-5954.
470. Gardin, C., et al., *Decellularization and Delipidation Protocols of Bovine Bone and Pericardium for Bone Grafting and Guided Bone Regeneration Procedures.* PLoS ONE, 2015. **10**(7): p. e0132344.
471. Cui, L., et al., *Preparation and characterization of IPN hydrogels composed of chitosan and gelatin cross-linked by genipin.* Carbohydr Polym, 2014. **99**: p. 31-8.
472. Singelyn, J.M. and K.L. Christman, *Modulation of material properties of a decellularized myocardial matrix scaffold().* Macromolecular Bioscience, 2011. **11**(6): p. 731-738.
473. Pinheiro, A., et al., *Comparison of natural crosslinking agents for the stabilization of xenogenic articular cartilage.* Journal of Orthopaedic Research, 2016. **34**(6): p. 1037-1046.
474. Kijeńska-Gawrońska, E., et al., *Alignment and bioactive molecule enrichment of bio-composite scaffolds towards peripheral nerve tissue engineering.* Journal of Materials Chemistry B, 2019. **7**(29): p. 4509-4519.
475. Prabhakaran, M.P., J.R. Venugopal, and S. Ramakrishna, *Mesenchymal stem cell differentiation to neuronal cells on electrospun nanofibrous substrates for nerve tissue engineering.* Biomaterials, 2009. **30**(28): p. 4996-5003.
476. Xu, D., et al., *Comparison of viscoelasticity between normal human sciatic nerve and amniotic membrane.* Neural Regen Res, 2013. **8**(14): p. 1269-75.
477. Ju, M.-S., C.-C. Lin, and C.-T. Chang, *Researches on biomechanical properties and models of peripheral nerves - A review.* Journal of Biomechanical Science and Engineering, 2017. **12**.
478. Zhang, X., et al., *Dynamic mechanical analysis to assess viscoelasticity of liver tissue in a rat model of nonalcoholic fatty liver disease.* Medical Engineering & Physics, 2017. **44**: p. 79-86.
479. Buckley, M.R., et al., *The dynamics of collagen uncrimping and lateral contraction in tendon and the effect of ionic concentration.* Journal of Biomechanics, 2013. **46**(13): p. 2242-2249.
480. Nagasawa, K., et al., *Static and dynamic biomechanical properties of the regenerating rabbit Achilles tendon.* Clinical Biomechanics, 2008. **23**(6): p. 832-838.
481. Edwards, J.H., E. Ingham, and A. Herbert, *Decellularisation affects the strain rate dependent and dynamic mechanical properties of a xenogeneic tendon intended for anterior cruciate ligament replacement.* Journal of the Mechanical Behavior of Biomedical Materials, 2019. **91**: p. 18-23.
482. Hoburg, A., et al., *Fractionation of high-dose electron beam irradiation of BPTB grafts provides significantly improved viscoelastic and structural properties compared to standard gamma irradiation.* Knee Surg Sports Traumatol Arthrosc, 2011. **19**(11): p. 1955-61.
483. Wei, W., et al., *Fractionation of 50 kGy electron beam irradiation: Effects on biomechanics of human flexor digitorum superficialis tendons treated with ascorbate.* Journal of Biomechanics, 2013. **46**(4): p. 658-661.

484. Kerecman Myers, D., et al., *From in vivo to in vitro: The medical device testing paradigm shift.* ALTEX, 2017. **34**(4): p. 479-500.
485. Junka, R. and X. Yu, *Novel Acellular Scaffold Made from Decellularized Schwann Cell Sheets for Peripheral Nerve Regeneration.* Regenerative engineering and translational medicine, 2015. **1**(1): p. 22-31.
486. Schira, J., et al., *Secretome analysis of nerve repair mediating Schwann cells reveals Smad-dependent trophism.* Faseb j, 2019. **33**(4): p. 4703-4715.
487. Chen, Z., et al., *Primary Neuron Culture for Nerve Growth and Axon Guidance Studies in Zebrafish (Danio rerio).* PLoS ONE, 2013. **8**(3): p. e57539.
488. Hai, M., et al., *Comparative analysis of Schwann cell lines as model systems for myelin gene transcription studies.* Journal of Neuroscience Research, 2002. **69**(4): p. 497-508.
489. Angius, D., et al., *A systematic review of animal models used to study nerve regeneration in tissue-engineered scaffolds.* Biomaterials, 2012. **33**(32): p. 8034-8039.
490. Choi, J., et al., *Decellularized sciatic nerve matrix as a biodegradable conduit for peripheral nerve regeneration*. Vol. 13. 2018. 1796.
491. Mohammadi, R., et al., *Improvement of peripheral nerve defects using a silicone conduit filled with hepatocyte growth factor.* Oral Surgery, Oral Medicine, Oral Pathology and Oral Radiology, 2013. **116**(6): p. 673-679.
492. Dayawansa, S., et al., *Allotransplanted DRG neurons or Schwann cells affect functional recovery in a rodent model of sciatic nerve injury.* Neurological research, 2014. **36**(11): p. 1020-1027.
493. Jeans, L., D. Healy, and T. Gilchrist, *An evaluation using techniques to assess muscle and nerve regeneration of a flexible glass wrap in the repair of peripheral nerves.* Acta Neurochir Suppl, 2007. **100**: p. 25-8.
494. Jeans, L.A., T. Gilchrist, and D. Healy, *Peripheral nerve repair by means of a flexible biodegradable glass fibre wrap: a comparison with microsurgical epineurial repair.* J Plast Reconstr Aesthet Surg, 2007. **60**(12): p. 1302-8.
495. Kelleher, M.O., et al., *Use of a static magnetic field to promote recovery after peripheral nerve injury.* J Neurosurg, 2006. **105**(4): p. 610-5.
496. Szynkaruk, M., et al., *Experimental and clinical evidence for use of decellularized nerve allografts in peripheral nerve gap reconstruction.* Tissue Eng Part B Rev, 2013. **19**(1): p. 83-96.

Appendix A: Equipment and Materials

Supplementary Table 1: Chemicals and Reagents

Chemical/Reagent	Company
Acetic Acid, glacial (17:4 mM)	Thermo Fisher Scientific Ltd.
AlamarBlue®	Thermo Fisher Scietific Ltd.
Aprotinin (50 ml; 10,000 KIU.ml^{-1})	Mayfair House
Bovine Serum Albumin	-
Benzonase nuclease hc, purity >99% (250 U.µl^{-1})	Merck
Calcium acetate 97+ % (Dried)	Thermo Fisher Scientific Ltd.
Chloramine T	Sigma-Aldrich
Citric acid	Sigma-Aldrich
Cyanoacrylate contact adhesive: Scotch® Super Glue Liquid	3M UK PLC
Dako fluorescence mounting medium	Agilent
DAPI (4',6-diamidino-2-phenylindole dihydrochloride)	Sigma-Aldrich
Dimethylene blue	Sigma-Aldrich
DMSO	-
DNAse I (10,000 U/ml)	-
DNeasy kit	Qiagen
Dulbecco's minimal essential medium	Sigma
PBS (without Ca/Mg, suitable for cell culture)	Sigma
Distyrene Plasticiser Xylene (DPX) mountant	Sigma-Aldrich
EDTA (disodium ethylenediaminetetraacetic acid)	Thermo Fisher Scientific Ltd.
Ehrlich’s Reagent	
Eosin Y	Merck Millipore
Eppendorf thermomixer	Eppendorf
Ethanol 190 % proof	Sigma-Aldrich
Foetal bovine serum	Sera Lab
Gentamycin sulphate	Sigma-Aldrich
Giemsa stain	-
Glasgow's minimal essential media	Sigma

Chemical/Reagent	Company
Haematoxylin (Mayer's)	Atom Scientific
Hydrochloric acid (6 M)	Fisher Scientific
Hydroxylamine hydrochloride	Sigma-Aldrich
Iron (III) chloride	Sigma-Aldrich
Isopropanol	-
L-glutamine (200 mM)	Sigma
Magnesium chloride hexahydrate	Thermo Fisher Scientific Ltd.
Molecular grade water	Sigma-Aldrich
Neutral Buffered Formalin (10 % v/v)	Biostains Ready Reagents
Oxalic acid	Sigma-Aldrich
Papain	Sigma-Aldrich
Paraffin wax	Raymond A Lamb Ltd
PBS tablets (Dulbecco's `A' PBS tablets, without Ca/Mg)	Oxoid
Penicillin (5000 U/ml)/streptomycin (5 mg/ml)	Sigma
Peracetic Acid, 32 % (v/v)	Sigma-Aldrich
Polymyxin B	Sigma-Aldrich
Potassium permanganate	Sigma-Aldrich
RNAse A (100 U/ml)	-
RNase A (17,000 U)	Qiagen
Roswell Park Memorial Institute Media	Sigma
Scott's tap water	-
SDS (sodium dodecyl sulphate)	Thermo Fisher Scientific Ltd.
Sirius Red	Sigma-Aldrich
SLS pH Buffer Coloured Red pH4	Scientific Laboratory Supplies
SLS pH Buffer Coloured Yellow pH7	Scientific Laboratory Supplies
SLS pH Buffer Coloured Blue pH10	Scientific Laboratory Supplies
Sodium acetate	Sigma Aldrich
Sodium chloride (NaCl)	Thermo Fisher Scientic Ltd.
Sodium di-orthophosphate	Sigma-Aldrich

Chemical/Reagent	Company
Sodium hydroxide (NaOH)	Scientific Laboratory Supplies
Trichloroacetic acid	Sigma-Aldrich
Tris (trizma base)	Sigma-Aldrich
Trypan blue solution, 0.4 % (v/v)	Sigma
Trypsin-EDTA solution	Sigma
Tryptone phosphate broth	Sigma
Vancomycin hydrochloride	Sigma-Aldrich
Virkon R Rely+OnTM	DuPont
Water, nuclease-free (R0582)	Fermentas
Weigert's Haematoxylin	Sigma-Aldrich
Xylene	Biostains Ready Reagents
Zinc acetate 99.9 %	Sigma-Aldrich
Zinc chloride	Fluka

Supplementary Table 2: Equipment

Equipment	Company
Accumax Pipette Controller	Fine Care Biosystems
Airone 1800R Fume hood	Safelab Systems Ltd
Bunsen burner	-
Camera, Olympus 450D	Camera, Olympus 450D
Camera stand	Manfrotto
CellB Microscope Software, v3.2	Olympus
Centrifuge, Harrier 15/80	Sanyo
Centrifuge, Evolution RC	Sorvall
Dissection kit	Dissection kit
DSC Q2000	TA Instruments
FastPetteTM V2 Pipette Controller	Labnet International, Inc.
Finnpipette Pipettes (0.2 {2 µl, 2 {20 µl, 20 {200 µl & 200 {1000 µl)	Scientific Laboratory Supplies
Forceps, blue plastic Spencer Wells	Fisher Scientific Ltd
Freezer, cell culture	-
Glass troughs E105	Raymond A Lamb
Haemacytometer, Neubauer Improved	-
Heraeus Hera Safe Class II biosafety cabinet	Thermo Electron Corporation, USA
Heraeus Incubator	Jencons PLC
Histology cassettes CMB-160-030R	Thermo Fisher Scientific Ltd.
Histology moulds E10.8/4161	Raymond A Lamb
Histology water bath MH8515	Barnstead Electrothermal

Equipment	Company
Hotplate Stirrer heat-stir CB162	Stuart Scientific
Hotplate E18/31	Raymond A Lamb
Hot wax oven E18/31	Raymond A Lamb
Incubator, cell culture	-
Instron 3365	Instron
Jenway 3510 pH Meter	Jenway Ltd
Lancer 810 LX undercounter glassware Washer	Lancer UK Ltd
Magnetic flea	-
Microcentaur centrifuge	MSE
Microscope, inverted: Olympus CK40	Olympus
Microtome, Leica RM2255	Leica
Modulyo Freeze Drier	Thermo Savant
Mr Frosty	-
Nanodrop ND-1000 spectrophotometer	Labtech
Olympus BX51 Microscope	Olympus
Pipe fittings	-
PIPETMAN ® Pipettes (0.2{2 µl, 2{20 µl, 20{200 µl & 200{1000 µl)	Gilson, Inc.
Precision Balance GR-200	A&D Instruments Ltd
Purelab OptionWater Purification System	ELGA
Refrigerator, cell culture	-
Ruler, 150 mm, stainless steel	Fisher Scientific Ltd
Ruler, 300 mm, stainless steel	Fisher Scientific Ltd

Equipment	Company
Slide holder E102	Raymond A Lamb
Spatulas	-
Table shaker KS 130	IKA
Table shaker PSU 10i	Grant
Table shaker POS 300	Grant
Tissue Processor TP1020	Leica
Water bath	-
Triplered SG Series Compact	Triple Red
Wax dispenser E66	Raymond A Lamb
Whiteley Fume hood	Whiteley
Whirli mixer CM-1 vortexer	Thermo Fisher Scientific
Zeiss AX10 Microscope	Carl Zeiss
Zeiss HXP 10	Carl Zeiss

Supplementary Table 3: Glassware

Glass/Plasticware	Company
Beaker, 3 L	Scientific Laboratory Supplies
Duran bottles (0.25 l, 0:5 l, 1 l and 2 l)	Scientific Laboratory Supplies
Funnel, small with long neck	Scientific Laboratory Supplies
Funnel, medium with short neck	Scientific Laboratory Supplies
Jar, polypropylene, wide neck with lid, 1 l	Thermo Scientific Nalgene
Measuring cylinders (50 mm, 100 mm, 250mm and 1000mm)	Scientific Laboratory Supplies
Mr Frosty	-
Petri Dish, glass, large (200 mm)	Smith Scientific Ltd

Supplementary Table 4: Consumables

Consumable	Company
Autoclave tape SLS1612	Scientific Laboratory Supplies
Bijous (sterile, 5 ml)	-
Cell scraper	ThermoFisher
Coverslips, glass, E105	Scientific Laboratory Supplies
Cryovials, 1 ml	-
Eppendorfs	Eppendorf
Foil	-
Histology cassettes	-
Measuring dishes	Scientific Laboratory Supplies
Microtube I, 1.5 ml, loop cap, Simport	VWR International
Minisart syringe filters, 0.2 µm pore size	Sartorius Stedim UK Ltd.
Needles, Neolus Hypodermic Terumo-Thin 25G 16 mm (NN-2516R)	Terumo UK Ltd.
Parafilm	-
Pipettes, Pasteur	-
Pipette Tips, TipOne® (10 µl, 20 µl, 200 µl, 1000 µl)	STARLAB
Serological Pipettes, sterile (5 ml, 10 ml, 25 ml)	Starstedty AG & Co.
Scalpel blades, No. 22, non-sterile	Swann-Morton Limited
Scalpel blades, No. 22, sterile	Swann-Morton Limited
Sterilin pots (150 ml and 250 ml)	-
Superfrost slides	Scientific Laboratory Supplies
Superfrost plus slides MIC3040	Scientific Laboratory Supplies
Syringes (1 ml, 2.5 ml, 5 ml, 10 ml)	Terumo UK Ltd.
Tissue culture flasks (T25, T75, T175)	Thermo Fisher Scientific
Tissue culture 6-well plates	Thermo Fisher Scientific
Universal containers (20 ml)	-

Supplementary Table 5: Antibodies

Antibody type	Antigen	Isotype	Supplier	Code
Primary	Laminin	Monoclonal Rabbit IgG1	Sigma Aldrich	L929
Primary	Fibronectin	Polyclonal rabbit IgG	Dako	A0245
Primary	Collagen type IV	Mouse monoclonal IgG1	Dako	M0785
Isotype control	Mouse IgG1	-	Dako	X0931
Isotype control	Rabbit polyclonal IgG	-	Genetex	GTX35035
Secondary	Goat anti-rabbit IgG AlexaFluor 488	-	Invitrogen	A11070

Supplementary Table 6: Cell Lines

Cell line	Source
BHK 21 (epithelial)	European Collection of Authenticated Cell Cultures
L929	European Collection of Authenticated Cell Cultures
RAW 264.7	European Collection of Authenticated Cell Cultures